β- and γ- Peptides:

Structural Investigations on Heterotypic Coiled-Coil Assemblies of an $\alpha/\beta/\gamma$-Chimera with all-α-Peptides

Inaugural-Dissertation
to obtain the academic degree
Doctor rerum naturalium (Dr. rer. nat.)

submitted to the Department of Biology, Chemistry, Pharmacy
of Freie Universität Berlin

by

Zeinab Mahfouz, M.Sc.

from Berlin, Germany

August 2023

The present work was carried out under the supervision of Prof. Dr. Beate Koksch from August 2019 to August 2023 at the Institute of Chemistry and Biochemistry in the Department of Chemistry, Biology, and Pharmacy at Freie Universität Berlin.

1st Reviewer: Prof. Dr. Beate Koksch (Freie Universität Berlin)

2nd Reviewer: Prof. Dr. Heiko M. Möller (Universität Potsdam)

Date of defense: 31.01.2024

Declaration of Authorship

I hereby declare that I have prepared the present dissertation entitled "β- and γ-Peptides: Structural Investigations on Heterotypic Coiled-Coil Assemblies of an $\alpha/\beta/\gamma$-Chimera with all-α-Peptides" autonomously and without impermissible assistance. All external sources and resources have been specified and properly cited or acknowledged. I further declare that this thesis has not been submitted, accepted, rated as insufficient, or rejected in any other doctorate degree procedure.

Berlin, August 2023 Zeinab Mahfouz

Oral Presentations

- "Bioactive β- and γ-Peptides"; 15th RTG seminar; Berlin, Germany; 23/09/**2022**.
- "Bioactive β- and γ-Peptides"; 2nd RTG Retreat; flash talk; Waren (Müritz), Germany; 18/11/**2021**.
- "Bioactive β- and γ-Peptides"; 10th RTG seminar; Berlin, Germany; 23/09/**2021**.
- "Bioactive Peptides"; Peptide Therapeutics Forum 2021; online; Basel, Switzerland; 19/08/**2021**.
- "Bioactive β- and γ-Peptides"; 6th RTG seminar; online; Berlin, Germany; 10/12/**2020**.
- "Bioactive β- and γ-Peptides"; 1st RTG Retreat; flash talk; Kremmen, Germany; 02/03/**2020**.

Poster Presentations

- "Bioactive β- and γ-Peptides"; 36th European Peptide Symposium and 12th International Peptide Symposium; Sitges, Spain; 28/08/ – 02/09/**2022**.
- "Bioactive β- and γ-Peptides"; 14th Australian Peptide Conference; online; Queensland, Australia; 08.05. – 13/05/**2022**.
- "Bioactive β- and γ-Peptides"; 1st RTG Retreat; Kremmen, Germany; 02/03/**2020**.

Acknowledgments

First, I would like to express my sincere gratitude to Prof. Dr. Beate Koksch for the opportunity to conduct my doctoral research in her working group. The freedom I was granted to do self-determined research and the trust I was given to realize my ideas and pursue self-initiated collaborations that made this work so valuable are greatly appreciated. Thank you for your encouraging and scientific support during the challenges I faced in this project.

Next, I would like to thank Prof. Dr. Heiko M. Möller, not only for being my second supervisor, but also for the time he spent on very helpful scientific discussions, thoughts, and advice during and after the RTG symposia and our meetings.

My special thanks go to all my collaboration partners who broadened my scientific horizon and let me benefit from their expertise or introduced me to new techniques. I would therefore like to thank Prof. Dr. Markus Wahl and M.Sc. Daniela Gjorgjevikj as well as Prof. Dr. Derek N. Woolfson and Dr. Bram Mylemans for our collaboration in crystallization. Many thanks to Prof. Dr. Björn Braunschweig and Dana Glikman for the SFG measurements. Dr. Marius Horch and M.Sc. Cornelius Constantin Maria Bernitzky is thanked for the IR measurements. Further, thanks go to Prof. Dr. Heiko M. Möller and M.Sc. Nikolai Klishin for the NMR measurements. Dr. Boris Schade and Dipl.-Ing. Jörg Bürger is sincerely thanked for the collaboration in cryo-TEM. Their efforts are greatly appreciated and have added tremendous value to this work.

I would also like to thank all my research internship students, B.Sc. Sinem Özcirpan, M.Sc. Paul Anton Albrecht, and M.Sc. Nianci Zhang, not only for their precious contributions to this work but also for the great time we had during the lab work. In addition, I like to thank M.Sc. Sian Catherine Allerton for the wonderful time we had while supervising her Master's thesis.

Furthermore, I am very grateful for the help of M.Sc. Michael Krummhaar, who helped me to take the crystal structure snapshots, and the scientific discourse that helped me deepen my knowledge on the crystallization of peptides.

I thank the Koksch group, for the pleasant, productive, and inspiring working atmosphere. Dr. Allison Berger, thank you for your caring support and precious

advice. Your helpful teaching in English scientific writing has increased my skills tremendously. Thank you M.Sc. Alexander Langhans for sharing the office with me during the years I worked on this thesis, for your encouraging words, and for the fruitful discussions.

Moreover, I would like to thank the graduate program “GRK-2473” not only for funding but also all doctoral researchers and professors for the enjoyable time and scientific discourse. I am also grateful for the connections that have developed and that go far beyond the scientific field.

Last, but not least, my deepest gratitude goes to my family and friends, on whom I could rely in difficult times and who provided me with emotional support. Many thanks to Jerome, Dana, Guilhem, and Franziska who challenged me to excel and always supported me. I thank my parents Mohamad and Wafaa for their loving and caring support in all my ways to achieve all my goals. I thank my siblings Mahmoud, Ibrahim, Houda, Mouna, Mariam, and Omar for cheering me up and giving me the love and relief I needed.

Abstract

Predicting the behavior of foldamer assemblies with all-α-peptides in higher-ordered arrangements remains a challenge. However, there is a strong interest and need to develop a deeper and more thorough knowledge to access foldamer designs that undergo interactions with natural peptide motifs. In this dissertation, the endeavors of investigating higher-ordered interactions between foldamers and all-α-peptides were continued in a well-defined tetrameric coiled-coil model system.

First, two Cys/Phe-motifs identified in previous work as complementary binding partners of an $\alpha/\beta/\gamma$-chimera were compared using CD-spectroscopy and cryogenic transmission electron microscopy (cryo-TEM). Systematic substitutions were performed on cysteine and analyzed by CD-spectroscopy to determine differences between the two different Cys/Phe-motif-containing complementary sequences in the formation of helical bundles with the $\alpha/\beta/\gamma$-chimeric sequence. High-resolution structural data were obtained using a variety of analytical methods to investigate the favored side chain packing in the higher-ordered helical fold. The analytical techniques applied are NMR spectroscopy, vibrational sum-frequency generation (SFG) spectroscopy, Fourier-transform infrared (FT-IR) spectroscopy, and X-ray crystallography. In the course of this thesis, the thiol region was examined for the first time by vibrational SFG-spectroscopy at the air/water interface for shifts due to H-bonding. In addition, the first crystal structure of a heterotypic coiled-coil assembly of an $\alpha/\beta/\gamma$-chimera with an all-α-peptide was generated, providing the first high-resolution packing information of the heterotypic helical bundle in a solid state.

Another part of this work deals with the construction of a library of chimeric peptides with iterative substitutions that increase the number of β/γ-modules. These chimeras were then evaluated for stability when complemented with corresponding all-α-peptide sequences involving the Cys/Phe-motifs. This investigation revealed a restriction of intermolecular interactions sensitive to a variation in the number of backbone residues. Finally, a β/γ-peptide consisting of five β/γ-modules was analyzed for structural features by CD-spectroscopy.

Kurzzusammenfassung

Die Vorhersage des Verhaltens von Foldamer-Assemblierungen mit α-Peptiden in höher strukturierten Anordnungen ist noch immer eine Hereausforderung. Aufgrund dessen besteht die Notwendigkeit ein tiefgründiges Verständnis zu entwickeln, um Zugang zu Foldamer-Designs zu erhalten, die den Wechselwirkungen in diesen Anordnungen unterliegen. In dieser Dissertation wurden die Wechselwirkungen zwischen Foldameren und α-Peptiden anhand eines bereits in der AG Koksch etablierten, wohldefinierten tetrameren Coiled-Coil-Modellsystems untersucht.

Zunächst wurden hierfür zwei Cys/Phe-Motive, die an eine $\alpha/\beta/\gamma$-Chimäre binden, mit Hilfe von CD-Spektroskopie und kryogener Transmissionselektronenmikroskopie (cryo-TEM) miteinander verglichen. Systematische Substitutionen an Cystein und anschließende CD-spektroskopische Untersuchungen wurden vorgenommen um Unterschiede in den beiden verschiedenen Cys/Phe-Motiv-haltigen komplementären Sequenzen des Helixbündels mit der $\alpha/\beta/\gamma$-Chimärsequenz zu ermitteln. Die bevorzugten Seitenkettenwechselwirkungen zwischen der $\alpha/\beta/\gamma$-Chimäre und den komplementären Sequenzen, welche Cys/Phe-Motive enthalten, werden in dieser Arbeit untersucht. Hierbei wurden hochauflösende Strukturdaten durch verschiedene analytische Methoden gewonnen, um die bevorzugte Seitenkettenpackung in der tetrameren Faltung zu erforschen. Bei den angewandten Analysetechniken handelte es sich um NMR-Spektroskopie, Schwingungssummenfrequenz-Spektroskopie (SFG), Fourier-Transform-Infrarot-Spektroskopie (FT-IR) und Röntgenkristallographie. Im Rahmen dieser Arbeit wurde die Thiol-Region demnach erstmals mit Hilfe der Schwingungs-SFG-Spektroskopie an der Luft/Wasser-Grenzfläche auf Verschiebungen aufgrund von Wasserstoffbrücken-Bindungen untersucht. Darüber hinaus wurde die erste Kristallstruktur einer heterotypischen Coiled-Coil-Anordnung einer $\alpha/\beta/\gamma$-Chimäre mit einem α-Peptid generiert, welche erste hochauflösende Packungsinformationen zum Helixbündel im festen Zustand liefert.

Ein weiterer Teil dieser Arbeit befasst sich mit dem Aufbau einer Bibliothek von chimären Peptiden mit iterativen Substitutionen, die die Anzahl der β/γ-Module

systematisch erhöhen. Diese Chimären wurden auf ihre Stabilität hin untersucht, wenn sie mit den α-Peptidsequenzen mit entsprechenden Cys/Phe-Motiven inkubiert wurden. Diese Untersuchung ergab eine Einschränkung der intermolekularen Wechselwirkungen, die empfindlich auf eine Variation in der Anzahl der Aminosäure-Reste reagieren. Schließlich wurde ein β/γ-Peptid, das aus fünf β/γ-Modulen besteht, mittels CD-Spektroskopie auf strukturelle Merkmale untersucht.

Table of Contents

Abstract ..... **xi**

Kurzzusammenfassung ..... **xii**

List of Abbreviations ..... **xvi**

1. Introduction **1**

1.1 The characteristics of α-helices *2*

1.2 The coiled-coil folding motif as a ubiquitous model system *4*

1.3 Foldamers *11*

1.3.1 Helical structures formed by β- and γ-peptides *14*

1.3.2 Foldamers in coiled-coil designs *18*

1.3.3 Bioactive foldamers *26*

1.4 The theory behind vibrational sum-frequency generation (SFG) spectroscopy *31*

2. Aim of this work **34**

3. Results and Discussion **35**

3.1 Structural investigation of the Cys/Phe-motifs of all-α-peptides and the α/β/γ-foldamer in heterotypic assemblies *35*

3.1.1 Substitutions on cysteine: comparative studies to the Cys/Phe-motifs *45*

3.1.2 NMR Spectroscopy of the α/β/γ-foldamer heterotypic assemblies with all-α-peptides *50*

3.1.3 Vibrational sum-frequency generation spectroscopy: investigating the thiol region of the Cys/Phe-motifs of all-α-peptides in assembly with B3β2γ *59*

3.1.4 Crystallization of the α/β/γ-foldamer heterotypic assemblies with all-α-peptides *68*

3.2 Iterative substitution library: systematic exploration of foldameric space by pushing the molecular interactions to the limit *81*

3.2.1 Structural studies on the β^3/γ^4-chimeric sequence using CD-spectroscopy *89*

4. Summary and Outlook **93**

5. Materials and Methods **97**

5.1 Reagents and solvents *97*

5.2 High-performance liquid chromatography (HPLC) devices *98*

5.2.1 Preparative HPLC *98*
5.2.2 Analytical HPLCs *99*
5.3 Microwave-assisted solid-phase peptide synthesis *100*
5.3.1 Determination of successful β-amino acid loading *102*
5.4 Peptide cleavage from the resin and purification *102*
5.4.1 Monitoring synthetic progress: Test cleavage *102*
5.4.2 Full cleavage of the peptides from the resin *104*
5.4.3 Purification and characterization by HPLC *105*
5.4.4 Peptide counterion exchange *107*
5.5 Synthesized peptides *107*
5.6 Analytical methods *136*
5.6.1 ESI-ToF Mass spectrometric measurements *136*
5.6.2 Determination of the peptide concentration by UV-spectroscopy *136*
5.6.3 Circular dichroism (CD)-spectroscopy *137*
5.6.4 Cryogenic-transmission electron microscopy (cryo-TEM) *138*
5.6.5 Nuclear magnetic resonance (NMR) spectroscopy *139*
5.6.6 Vibrational sum-frequency generation spectroscopy (SFG) *139*
5.6.7 Fourier-transform infrared spectroscopy (FT-IR) *141*
5.6.8 Crystallization *141*
5.7 Figures and Graphs *146*
6. Literature 147
7. Appendix 173

List of Abbreviations

Å	Angstrom
ACN	acetonitrile
AMPs	antimicrobial peptides
BIS-TRIS	bis(2-hydroxyethyl)-imino-tris(hydroxymethyl)-methane
$CaCl_2$	calcium chloride
CD	circular dichroism
CPPs	cell-penetrating peptides
cryo-TEM	cryogenic transmission electron microscopy
Da	Dalton
DAD	diode array detection
DBU	1,8-Diazabicyclo[5.4.0]undec-7-ene
DCM	dichloromethane
DIC	*N*, *N*′-Diisopropylcarbodiimid
DIEA	*N*, *N*-diisopropylethylamine
DMF	*N*, *N*-dimethylformamide
DNA	deoxyribonucleic acid
DSS	sodium 3-(trimethylsilyl)propane-1-sulfonate
DTT	dithiothreitol
e.g.	exempli gratia
EDT	ethane-1,2-dithiol
ESI	electron spray ionization
ESI-ToF	electron spray ionization – time of flight
ESR	electron spin resonance
EtOH	ethanol
FDA	U.S. Food and Drug Administration
FT-IR	Fourier-transform infrared spectroscopy
GndHCl	guanidine-hydrochloride
HCMV	human cytomegalovirus
HEPES	4-(2-hydroxyethyl)-1-piperazineethanesulfonic acid
HFIP	1,1,1,3,3,3-hexafluoro-propan-2-ol
HIV	human immunodeficiency virus
HOBt	*N*-hydroxybenzotriazole

HPLC	high-performance liquid chromatography
HSQC	heteronuclear single quantum correlation
i.e.	id est
IR	infrared
m/z	mass per charge
MD	molecular dynamic
min	minutes
MPD	2-methyl-2,4-pentanediol
mRNA	messenger ribonucleic acid
MS	mass spectrometry
NCL	native chemical ligation
NMP	*N*-methyl-2-pyrrolidone
NMR	nuclear magnetic resonance
NOE	nuclear Overhauser effect
NOESY	Nuclear Overhauser Enhancement Spectroscopy
NRPSs	Non-ribosomal peptide synthetases
Oxyma Pure	ethyl (2*Z*)-2-cyano-2-(hydroxyimino)acetate
PEG	polyethylene glycol
PEG-mme	polyethylene glycol monomethyl ether
PPI	protein-protein interaction
r.t.	retention time
RMSD	root-mean-square deviation of atomic positions
ROESY	Rotating-frame Overhauser Effect Spectroscopy
RT	room temperature
SAD	single-wavelength anomalous diffraction
SF	Sum-Frequency
SFG	Sum-Frequency Generation
SPPS	solid phase peptide synthesis
TEM	Transmission electron microscopy
TFA	trifluoroacetic acid
TFE	2,2,2-trifluoroethanol
TIS	triisopropylsilane
TOCSY	Total Correlation Spectroscopy

tRNA	transfer ribonucleic acid
v/v	volume per volume
w/v	weight per volume

The amino acids were abbreviated according to the one- and three-letter codes recommended by IUPAC-IUB Joint commission on Biochemistry Nomenclature (JCBN) [Eur. J. Biochem. **1984**, 138, 9-37].

Abbreviations of the non-canonical L-amino acids used in this work are enlisted below.

Abu	(2*S*)-2-aminobutanoic acid
β^3hA or β^3A	homologous β^3 alanine
β^3hG or βA	homologous β^3 glycine, β-L-alanine
β^3hK or β^3K	homologous β^3 lysine, β-L-homolysine
β^3hL or β^3L	homologous β^3 leucine, β-L-homoleucine
γ^4hD or γ^4D	homologous γ^4 aspartic acid, β-D-homoglutamic acid
γ^4hK or γ^4K	homologous γ^4 lysine, 4,8-diaminooctanoic acid
*m*C or *m*Cys	S-methyl-L-cysteine
o-Abz	*ortho*-aminobenzoic acid

1. Introduction

The α-helix is the most abundant secondary structure motif in proteins[1] and it is typically involved in intermolecular interactions. As a result, helix-helix mediated protein-protein interactions play a key role in various biological processes, e.g., transcriptional control, mediation of endocytosis and exocytosis, as well as virus entry into host cells, and they are emerging as an important target for drug discovery.[2–4] Basic research on coiled-coil model systems provides an excellent strategy to study the consequences of disruption between helical domains, providing a foundation for pharmaceutical research.

Peptides emerged as attractive candidates for drug discovery in the early 1920s when insulin was the first peptide to be used for the medical treatment of type I diabetes. Currently, about 80 peptides are available as drugs on the market and several hundred peptides are in clinical development or preclinical studies.[5] Nowadays, peptides are easy to generate due to continuous developments and improvements in the field of solid-phase peptide synthesis (SPPS) that enable efficient synthesis routes. Advances in purification by HPLC also facilitate the production process of peptides. Despite the many advantages offered by peptides composed of natural α-amino acids, e.g., low toxicity, high affinity, selectivity, as well as molecular and structural diversity, they also bring disadvantages such as poor oral bioavailability, membrane permeability, and short *in vivo* half-life due to protease degradation.[5–9]

However, to circumvent the protease susceptibility of natural peptides, strategies such as the replacement of α-amino acids with non-canonical residues, macrocyclization, and backbone modifications are used to stabilize and mimic helical secondary and higher-order structural motifs.[6,9–11] In general, the design of foldamers is considered a promising attempt to find clinically applicable drug candidates that selectively and specifically bind to helical domains with high affinity.[12,13]

In the present work, the focus is set on the incorporation of homologous β- and γ-amino acids into peptides.

1.1 The characteristics of α-helices

The peptide bond exhibits planar rigidity due to the partial double bond between the carbon and nitrogen atoms (Figure **1**a). Consequently, folding flexibility results from the two torsional angles implicating the α-carbon atom in the backbone. These preferred angles, denoted φ and ψ (Figure **1**b), are shown in the Ramachandran plot to depend greatly on the side chain and illustrate the energetically permissible local secondary structure. Repeating dihedral angles of φ -60° and ψ -45° throughout the backbone yield α-helical structures.[14,15]

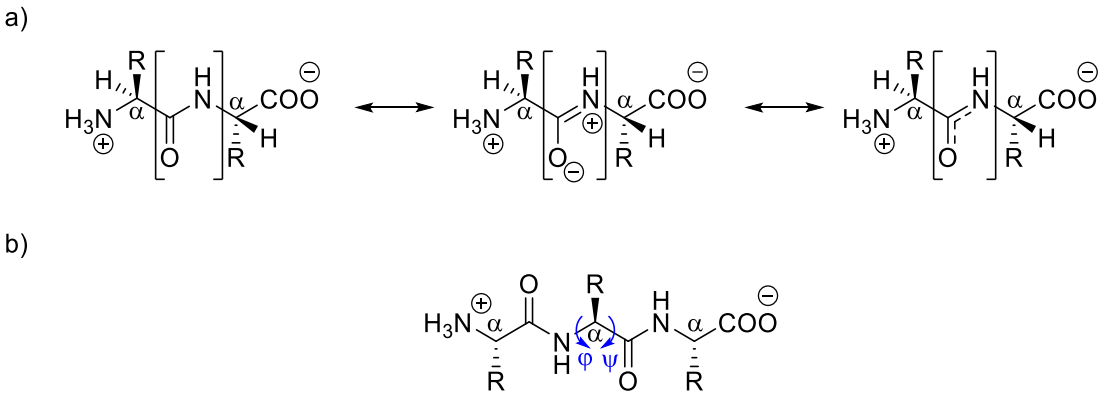

Figure 1: a) Planar rigidity of the peptide bond through the partial double bond formation (Modified according to Ramachandran and Sasisekharan, *Adv Protein Chem* **1968**, *23*, 283–437. Copyright © 1968 Academic Press Inc. Adapted with permission from Elsevier Inc.).[15] b) Torsional angles φ and ψ of the α-carbon atom in the backbone (Modified according to Boyle and Woolfson. Used with permission of Royal Society of Chemistry, from De Novo Designed Peptides for Biological Applications, Boyle and Woolfson, *Chem Soc Rev* **2011**, *40* (8), 4295–4306.; permission conveyed through Copyright Clearance Center, Inc.).[14]

Naturally occurring α-helices are right-handed and comprise 3.63 amino acid residues per helical turn, corresponding to a distance of about 5.4 Å along the axis. The formation of an α-helix structure results from the formation of intramolecular H-bonds in the backbone between the carbonyl groups (*i*) and the amides (*i+4*). The side chains are oriented toward the solvent (Figure 2).

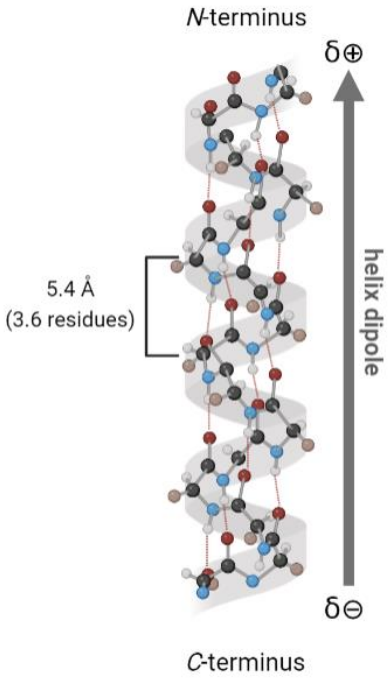

Figure 2: Schematic representation of a right-handed α-helix. The ball colors of the ball and stick model correspond to black-carbon, blue-nitrogen, white-hydrogen, red-oxygen, and brown-residue. The red dotted lines indicate backbone H-bonding (drawn with BioRender.com).

The formation of α-helical structures is accompanied by a loss of conformational side-chain entropy, which is compensated for in native folds by the enthalpic contribution of stabilizing interactions. Depending on the side chain, this compensation can vary, which is why some amino acids (e.g. Ala, Glu, Leu, and Lys) are more frequently incorporated into helical structures than others. This different tendency of individual amino acids to be incorporated into helical structures is also referred to as helical propensity. The helix propensity of certain amino acids indicates how the side chains influence the backbone conformation. It results from short-range interactions between the side chain and the peptide backbone and solvent, as well as from the interactions of the peptide backbone with itself and the solvent.

The stability of α-helices can be affected by various factors. For example, the electrostatic repulsion between successively charged side chains, or steric clashes can destabilize the helix. To avoid unfavorable Coulomb or hydrophobic interactions between consecutive residues, positively and negatively charged, or two non-polar residues, respectively, are positioned three to four residues apart.

As these side chains find each other spatially through this positioning, they contribute to the stabilization of the structure.

The intramolecular H-bond network in the α-helix leads to the formation of an electric dipole. Thereby, the carboxyl terminus is partially negatively charged, and the amino terminus is correspondingly partially positively charged (see Figure 2). The last four amino acids are usually not involved in the intramolecular H-bonding pattern. Negatively charged residues are positioned close to the *N*-terminus and accordingly, positively charged residues are located close to the *C*-terminus, stabilizing the helical structure.

An abundance of either glycine or proline can lead to the destabilization of the helical structure. While the absence of a side chain in Gly leads to high conformational flexibility, the rigid ring structure of Pro does not allow rotation between the nitrogen and the α-carbon bond, resulting in a destabilizing kink. In addition, the missing proton bound to the nitrogen of Pro also makes impossible its contribution to the hydrogen bonding pattern with other residues, representing another destabilizing factor.[16]

However, isolated α-helices are rarely stable in solution, and, due to their amphipathic nature, in most cases assemble into helical bundles, the so-called coiled coils, by hydrophobic collapse as the main driving force and attractive Coulomb interactions as a secondary contribution.[17,18]

1.2 The coiled-coil folding motif as a ubiquitous model system

Coiled coils are a well-understood structural system and were described around 70 years ago[19] by Francis Crick[20] and Linus Pauling, as well as Robert B. Corey,[21] based on the diffraction pattern of α-keratin by William T. Astbury.[22] They are composed of at least two α-helices intertwined to form supercoiled quaternary structures and exhibit a primary sequence periodicity of seven amino acid residues, designated positions *a* to *g*. They exhibit hydrophobic residues in the first (*a*) and fourth (*d*) positions that form “knobs-into-holes-packing” which provides the energy to distort the α-helices. This distortion results in a reduction of the periodicity by 0.13 residues per helical turn, i.e., 3.5 residues per helix turn in a left-handed coiled

coil instead of 3.63 residues for regular α-helices. As a result, the right-handed α-helices adopt left-handed supercoils (Figure 3).[14,19,23]

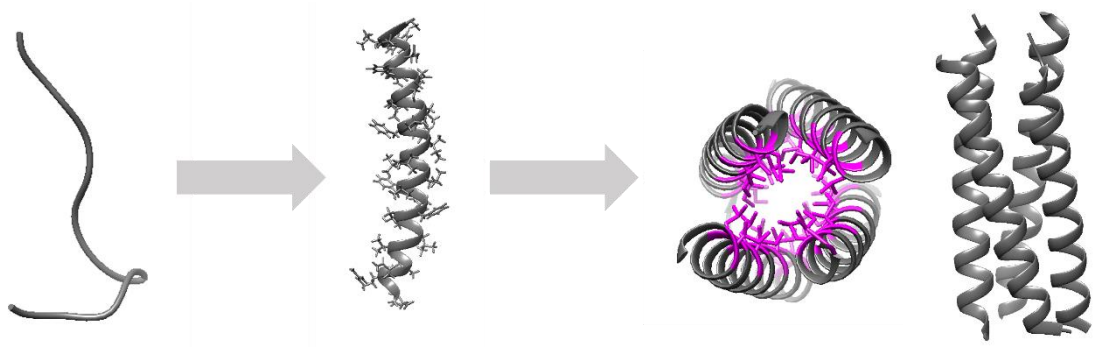

Figure 3: From polypeptide chain (PDB: 1BA6) to helix (PDB: 1XRD) to coiled coil (PDB: 3R4A). The aliphatic residues of the hydrophobic core of the coiled coil are highlighted in magenta (Modified according to Boyle and Woolfson. Used with permission of Boyle and Woolfson, from De Novo Designed Peptides for Biological Applications. *Chem Soc Rev* **2011**, *40* (8), 4295–4306.; permission conveyed through Copyright Clearance Center, Inc.).[14]

The thermodynamically strongest and thus most important driving force for the folding and assembly of coiled coils is the hydrophobic effect.[14,24] Hydrophobic canonical residues, denoted "*h*", are Ala, Phe, Ile, Leu, Met, Val, Trp, and Tyr. Polar canonical amino acids, referred to as "*p*", are Asp, Glu, His, Lys, Asn, Gln, Arg, Ser, and Thr. Macromolecules fold or assemble to minimize their hydrophobic surface area toward aqueous bulk solvents. Therefore, amphipathic polypeptide chains fold in such a way as to bury hydrophobic residues and expose polar residues to the physiological/buffer environment. The "knobs-into-holes"-pattern of the heptad repeats refers to the non-covalent arrangement of the residues as *hpphppp*, resulting in a side chain (knob) of one helix being surrounded by a space from four residues in a diamond-shaped arrangement (hole) of the other helix (Figure 4).[25] Overall, the stability of the coiled-coil assembly is predominately determined by the hydrophobic core.[26]

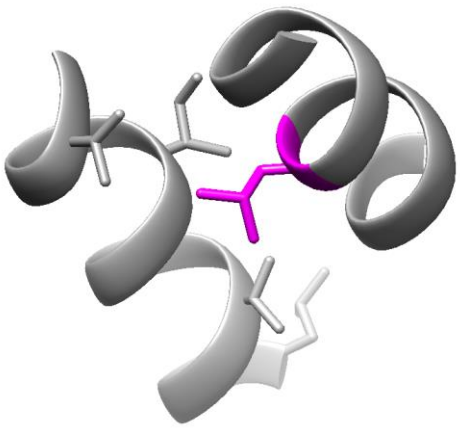

Figure 4: Knobs into-holes packing in GCN4-mutant (PDB: 1KDB8). The Leu residue (knob) colored in magenta is surrounded by a space (hole) from four residues in a diamond-shaped arrangement (according to Rhys et *al.*).[27]

The repetitive *hpphppp* heptad pattern characteristic for coiled coils is usually referred to as $(a\text{-}b\text{-}c\text{-}d\text{-}e\text{-}f\text{-}g)_n$ for one helix and $(a'\text{-}b'\text{-}c'\text{-}d'\text{-}e'\text{-}f'\text{-}g')_n$ for the opposing helix.[14,23–26] The number *n* of heptad repeats can vary from two, in designed coiled coils,[28] to 200, in natural fibrous proteins.[26,29] The helical-wheel model is a schematic representation commonly used to facilitate the illustration of the spatial arrangement of residues along the helical axis in coiled coils (Figure 5). While positions *a* and *d* form the interhelical hydrophobic core, the second molecular recognition motif is determined by the interhelical electrostatic interactions resulting from positions *e* and *g*.[30] Moreover, positions *b*, *c*, and *f* are occupied by residues exposed to the solvent.[23] These positions can be used for substitutions that introduce orthogonal functional properties.[14,31]

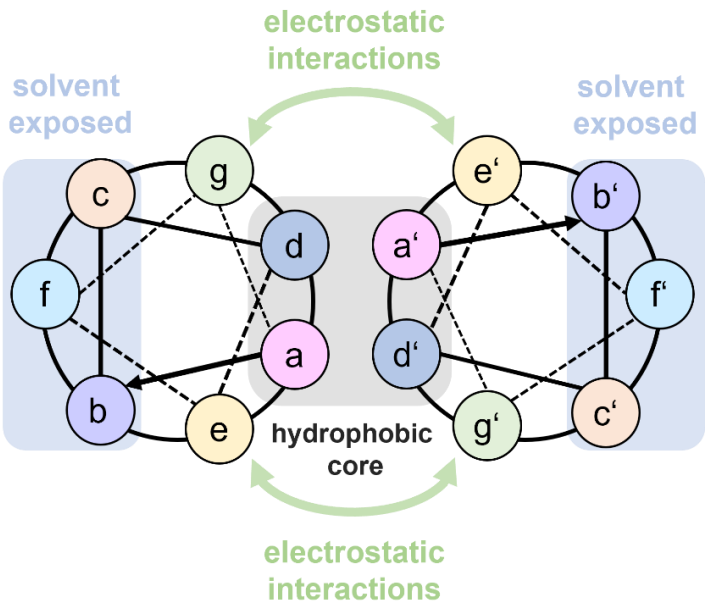

Figure 5: Helical wheel model of a parallel coiled-coil motif. Hydrophobic amino acid residues at *a* and *d* positions form the hydrophobic core, as indicated by the gray box. Coulomb interactions, indicated by green arrows from charged residues at positions *e* and *g*, contribute to the specificity of the pairing. The side chains of the amino acids in positions *b*, *c*, and *f* are exposed to the solvent and underlined by a blue box.

In addition to their dominant influence on stability, the *a* and *d* positions can also affect the oligomerization state. Variations in the *a* and/or *d* positions in GCN4-p1, a parallel homodimeric coiled-coil leucine zipper, were shown to alter the oligomerization state.[32–35] Mutation of the hydrophobic core to exclusively Leu, for instance, results in tetramer assembly.[26]

Electrostatic recognition by coiled-coil systems can be affected by the *e* and *g* positions, which are typically occupied by Lys and Glu. The charge pattern of the sequences influences pairing specificity between helices in the coiled-coil motif through the pairing of *g* and *e*' ($i \rightarrow i'+5$), and *e* and *g*', depending on attractive or repulsive Coulomb interactions. Here, the oligomerization of helices into coiled coils can occur either in a homotypic manner, when two identical helices oligomerize, or in a heterotypic manner, when different helices pair together (Figure 6a). The orientation of the helices in the assemblies can be directed in a parallel or antiparallel fashion, respectively, when the same termini (*C*-and *C*' termini and *N*-and *N*'-termini) or different termini (*C*-and *N*'-termini and *N*-and *C*'-

termini) are proximal to each other (Figure 6b). Furthermore, the association stoichiometry can also be influenced by the electrostatic interactions.[25,26]

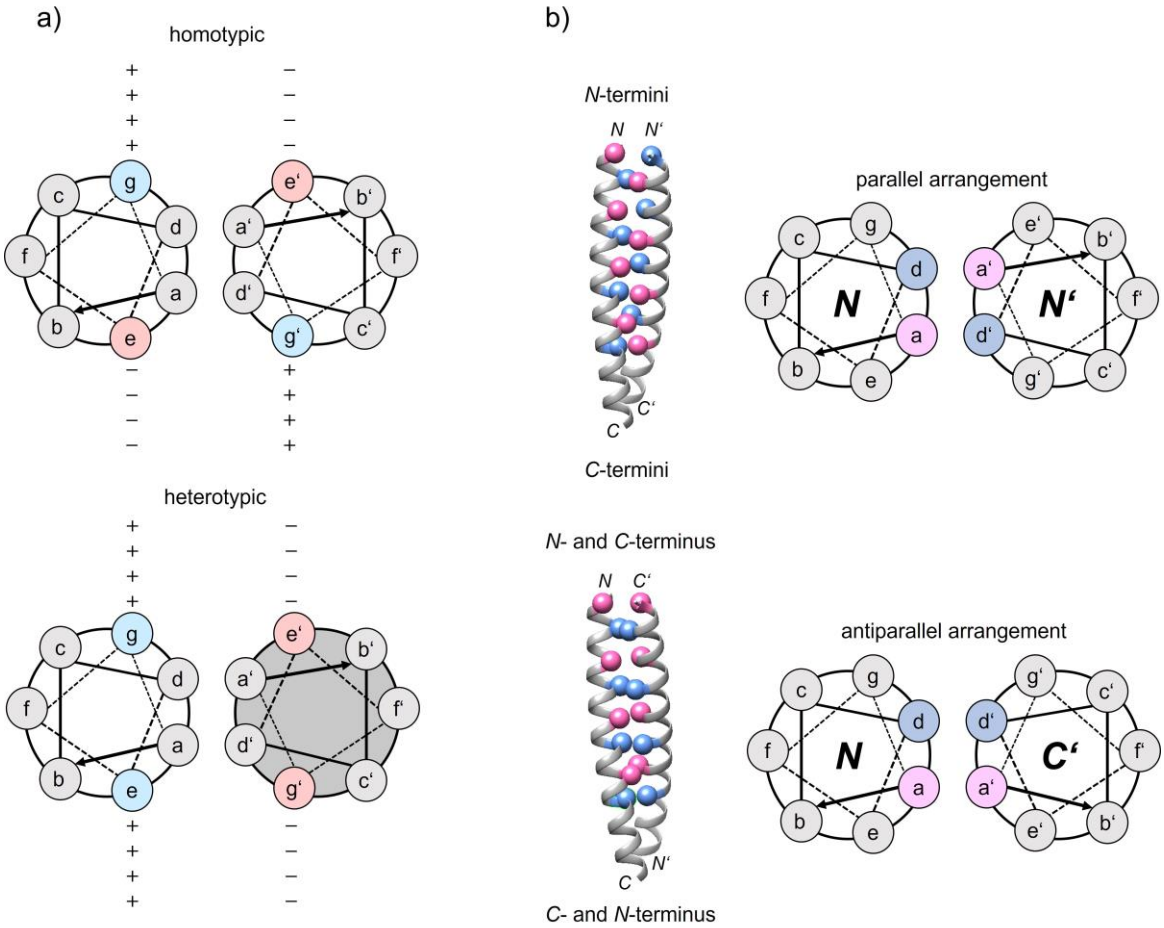

Figure 6: a) Homotypic and heterotypic pairing corresponding to charge complementarity of positions *e* and *g* (Modified according to Yu, *Drug Deliv Rev* **2002**, *54*, 1113–1129. Copyright © 2002 Elsevier Science B.V. Adapted with permission from Elsevier Inc.).[30] b) Parallel and antiparallel arrangement of a coiled-coil dimer. The gray-blue and pink spheres corresponding to residues in the *a* and *d* positions, respectively, represent the packing of side chains in a parallel and antiparallel aligned coiled coil. *C* and *N* in the helical wheel representation refer to the *N*-and *C*-termini of the peptide chain, respectively (according to Truebestein and Leonard).[36]

Modification of the classical *hpphppp* repeat pattern (Type N) by increasing the size of the hydrophobic core leads to higher oligomerization states. Type I comprises hydrophobic residues in *a*, *d*, and *e* positions leading to an *hpphhpp* repeat that forms tetramers. In this case, the side chains in the *g* position form the knobs. Pentamers and higher oligomeric states can be formed by Type II *hpphhph* repeating units, by including the residues in the *e* and *g* positions in the knobs-into-holes interactions. The largest known coiled-coil assembly is the dodecameric (12-

helix) barrel of the TolC membrane protein[37] with a Type III interface containing a *hhphphp* repeating motif (Figure 7).[25] The Alacoil, which introduces Ala into residues at *b* and *g* positions (*pAphhpA*) and forms α-sheets, also belongs to the Type III grouping.[19,25]

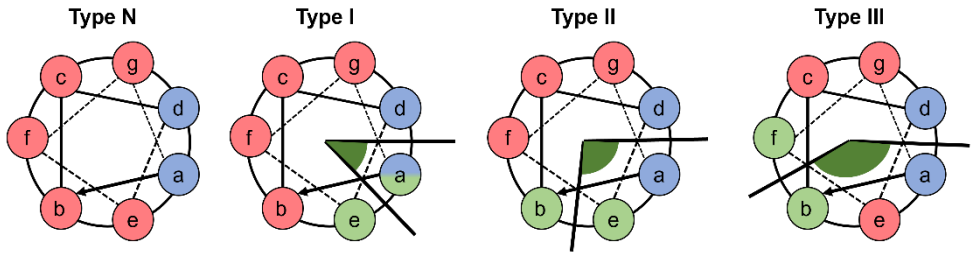

	Type N	Type I	Type II	Type III
Repeat	*hpphppp*	*hpphhpp*	*hhphhpp*	*hhphphp*
Angle		≈51°	≈103°	≈154°
Predominant oligomerization	dimer	trimer and tetramer	tetramer – heptamer	octamer and higher

Figure 7: Variants of heptad repeat patterns compared to the classical heptad repeat, referred to as Type N. The blue and green balls are occupied by hydrophobic amino acids and represent the knob-forming residues. The remaining residues, which are usually polar, are colored red. The dark green angles correspond to the angles between the two resulting hydrophobic seams (Modified according to Woolfson. In *Fibrous Proteins: Structures and Mechanisms. Subcellular Biochemistry*; Springer, **2017**; Vol. *82*, pp 35–61. Copyright © 2017, Springer International Publishing AG.).[25]

The insertion or deletion of residues in heptad repeats can interrupt the periodicity in coiled coils. Three types of these discontinuities can be distinguished, the “skip”, the “stutter”, and the “stammer” (Figure 8).[38–40] A skip denotes the insertion of one residue. The stutter is defined by a deletion of three residues or an insertion of four residues and is compensated by an underwinding of the supercoil and features a dextrorotatory section to preserve hydrophobic contacts. The stammer, on the other hand, leads to an overwinding of the supercoil. It comprises a deletion of four residues or an insertion of three residues. In general, these distortions are limited to two helical turns on either side of the deletion/insertion and can serve either to provide flexibility in the helical domains or to terminate the structure by causing local pertubations.[26,39,41]

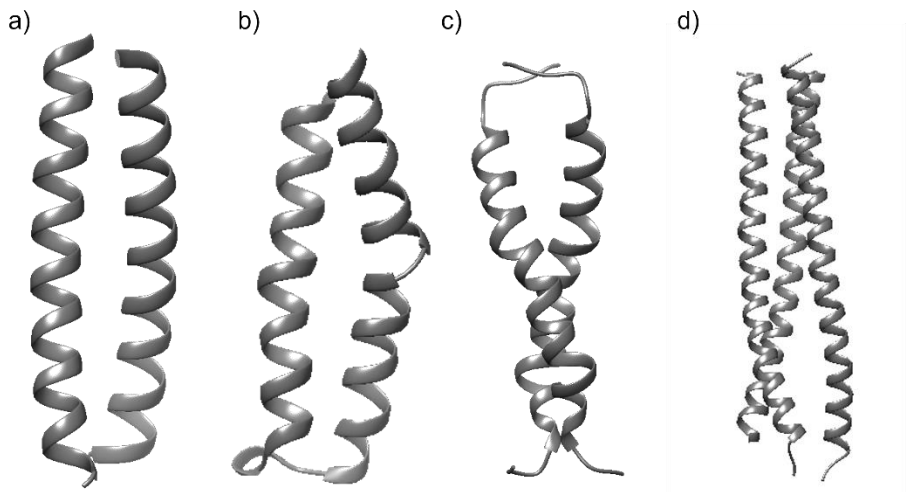

	a)	b)	c)	d)
Discontinuity	without	skip	stutter	stammer
Insertion	-	1 amino acid	3 amino acids	4 amino acids
Heptad	$(a\ b\ c\ d\ e\ f\ g)_n$	a b b c d e f g	a b c a b c d e f g	a b c d a b c d e f g
Example	GCN4	GreA	H-NS	Hemaglutinin
PDB code	2ZTA	1GRJ	1LR1	2HMG

Figure 8: Structural deformation of coiled coils through discontinuities (according to Truebestein and Leonard).[36]

α-Helical coiled-coil systems often terminate with non-helical segments, e.g., in tropomyosin in which the non-α-helical domain includes eight residues.[41] Hodges and co-workers studied a synthetic coiled-coil homodimer with 35 amino acid residues in each polypeptide chain containing Leu side chains in *a* and *d* positions. Mutation of the Leu residues to Ala demonstrated destabilizing properties. However, they found that hydrophobic interactions at both ends contribute less to stability than do those at the center of the sequence, and are more flexible and less buried since substitutions here do not greatly compromise the stability of the coiled coil.[42]

All in all, coiled-coil folding motifs are considered the best-studied structures in protein design.[14,24,43] They have evolved into a ubiquitous model system suitable for the design of novel structures and rationally designed functions.[19] In this work, a well-defined tetrameric coiled-coil model system was utilized to study the interactions and stabilities of $\alpha/\beta/\gamma$-foldameric helices when assembled with polypeptide sequences containing solely natural L-α-amino acids.

1.3 Foldamers

The term “foldamer” was first defined by Gellman and co-workers in 1966 for non-natural oligomers that can fold into higher-ordered structures resembling those of proteins.[44] Non-proteinogenic amino acids such as β-, γ-, δ-amino acids, α,α-disubstituted amino acids, peptoids, or oligourea variants (Figure 9) can be used as monomeric units for the design of foldameric peptides with bioactive properties, e.g., inhibition of protein-protein interactions (PPIs),[45,46] cell-penetrating peptides (CPPs),[47,48] antimicrobial peptides (AMPs),[49–51] or drug-delivery tools[48,52] for drug discovery.

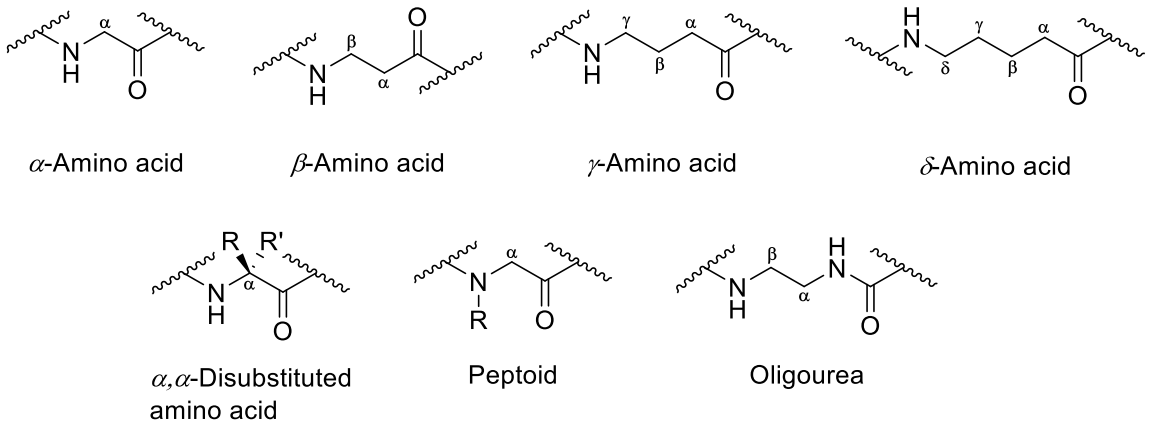

Figure 9: Selection of non-proteinogenic amino acid derivatives in comparison to α-amino acids (Modified according to Kato. In *Cell-penetrating peptides: Design, Development and Applications*; Wiley-VCH GmbH: Weinheim, Germany, **2022**; pp 79–107. Copyright © 2022, John Wiley and Sons.).[53]

The incorporation of unnatural amino acids into peptides is advantageous because they cannot be recognized and degraded by proteases.[54] They can form stable secondary structures and are well suited for designing helical structures with amphipathic character, which plays a key role in bioactive properties such as protein-protein interactions (PPI), cell permeability, and antimicrobial activity. Moreover, foldameric peptides composed of these non-proteinogenic amino acids are readily accessible by established synthetic methods.[53]

The design of helical foldamer peptides that acquire higher-ordered conformations, can be accomplished by two different approaches: “bottom-up” or “top-down”. In the former, foldamers are designed *de novo*; in the latter, foldamers are designed based on well-characterized α-amino acid sequences known to form distinct

higher-ordered structures.[55] One effective “top-down” method was described by Fortuna *et al.* as “foldamerization”, which describes the replacement of at least one natural α-amino acid of α-peptides by unnatural amino acids.[56]

Foldamers composed of β- and γ-amino acids not only provide stability against proteolytic degradation but also exhibit H-bonding patterns comparable to those of natural all-α-peptides. Therefore, they resemble the self-assembling properties of peptides composed of natural amino acids and facilitate peptide design by allowing for the predictable alignment of side-chain functional groups.[57]

The difference between β- and γ-amino acids and natural α-amino acids lies in additional methylene units in the backbone (Figure 10). Here, β-amino acids have one additional methylene unit in the backbone and the corresponding γ-variants have two. While the side chains of β-iso and γ-iso amino acid variants are shortened by a shift of the amine group by the methylene groups incorporated into the backbone, the homologated amino acids retain their side-chain length and exhibit additional methylene groups in the backbone.[58]

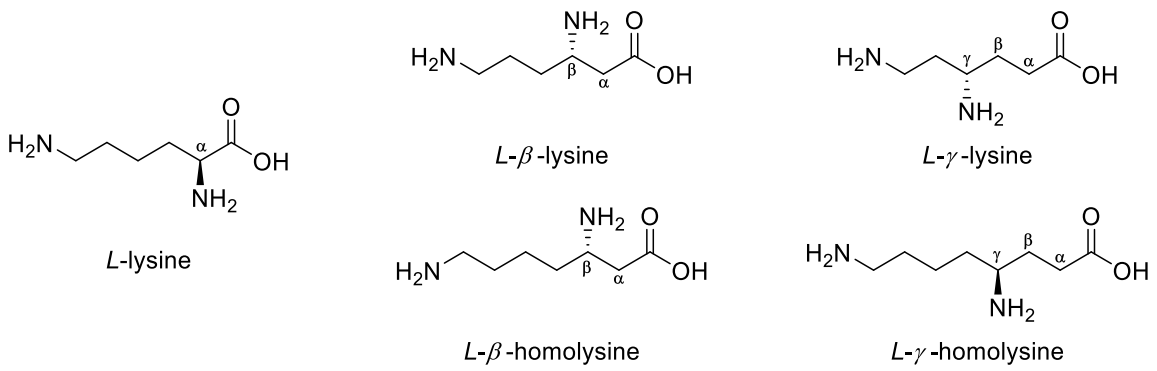

Figure 10: The difference between α-, β-, and γ-amino acids and their homo-variants using L-lysine as an example.

A variety of backbone extended β- and γ-amino acids can be accessed through chemical synthesis approaches[59–64] and homologated variants can be even accessed starting from their proteinogenic α-amino acids.[65] In natural compounds, β- and γ-amino acids are incorporated by non-ribosomal peptide synthetases (NRPSs). Biologically active compounds isolated from bacteria, fungi, plants, or marine organisms may contain β- and γ-amino acids derived from this biosynthetic pathway (Figure 11).[58,66,67] Until a few years ago, no ribosomally synthesized

peptides containing β- and γ-amino acids were amenable to screening methods such as mRNA display. Suga and co-workers were able to efficiently synthesize peptides bearing various non-proteinogenic amino acids, including β- and γ-amino acids, by ribosomal synthesis using tRNA engineering and thus manipulation of the genetic code.[68]

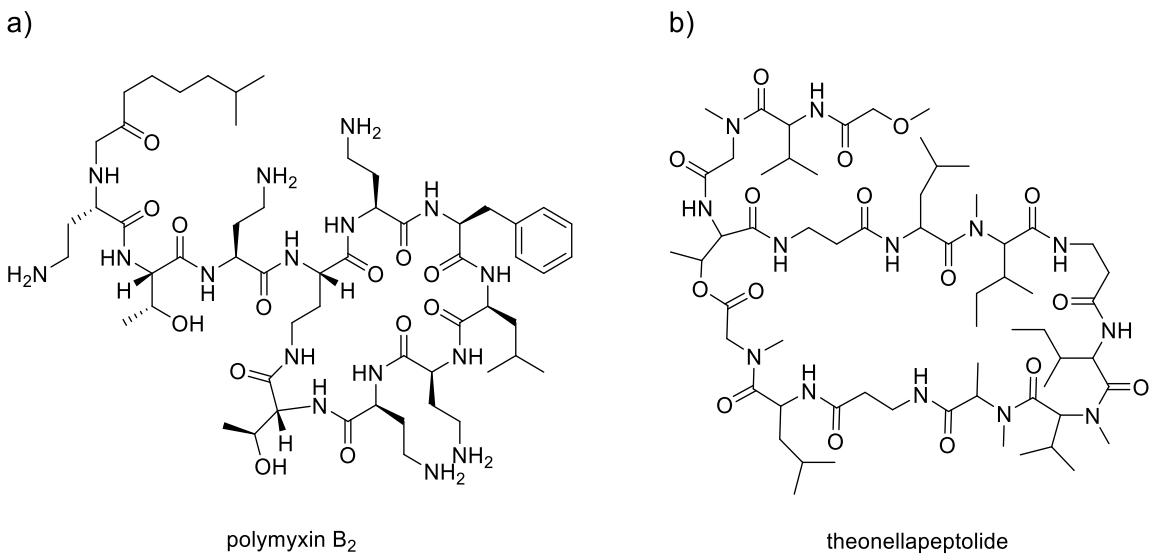

Figure 11: a) Structure of antibiotic polymyxin B_2 isolated from *Bacillus polymyxa*[69] involving six α,γ-diaminobutanoic acid building blocks. b) Structure of theonellapeptolide isolated from an Okinawan marine sponge pf Theonella sp.[70] containing three βAla/βhGly. (Adapted with permission from Seebach *et al*. *Chem Biodivers* **2004**, *1* (8), 1111–1239. Copyright © 2004 Verlag Helvetica Chimica Acta AG, Zürich.).[58]

Backbone extended β- and γ-amino acids offer a variety of design possibilities by either placing the residues into the different methylene groups of the backbone or varying the stereochemistry. The superscript numbering of the carbon atom after the Greek letter (Figure 12) indicates the position of the side chain in the backbone.[58]

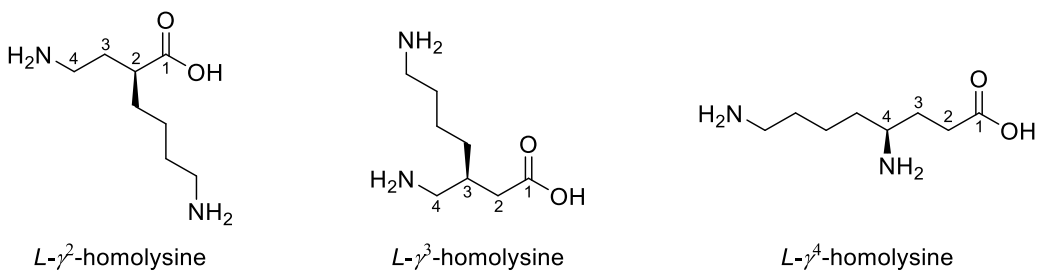

Figure 12: Nomenclature of the positioning of the side chains in the backbone using variants of L-γ-homolysine as an example.

Other variants of β- and γ-amino acids include multi-substituted backbones[59,61] and cyclic variants.[60,63]

This work deals with the incorporation of homologous β^3- and γ^4-amino acids into peptides. Their incorporation leads to greater torsional freedom and thus to an expansion of the energetically permissible conformational space. While α-amino acids have two torsional variables (φ,ψ), β- and γ-amino acids have three (φ,θ,ψ) or four ($\varphi,\theta_1,\theta_2,\psi$) of these variables, respectively, due to their additional backbone methyl units (Figure 13).[71]

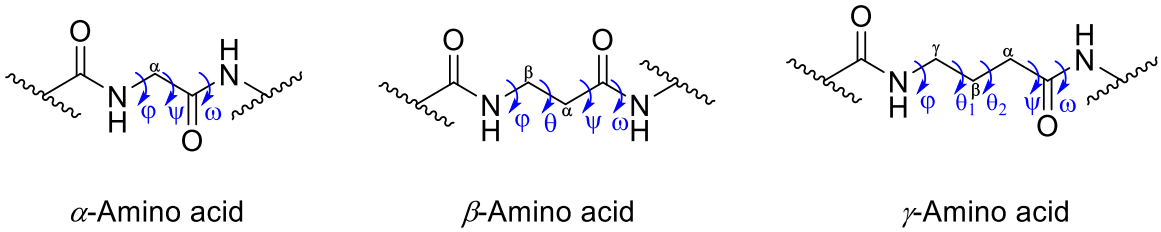

Figure 13: Backbone torsional angles of β- and γ-amino acids in comparison to α-amino acids (Adapted with permission from Vasudev *et al. Chem Rev* **2011**, *111* (2), 657–687. Copyright © 2011, American Chemical Society).[71]

However, the main challenge in replacing α-amino acids with homologated β- and γ-amino acids in a coiled-coil system is the reduced number of residues per helix-turn. Therefore, predicting the behavior of foldamers containing homologous β- and γ-amino acids in higher-ordered arrangements remains a difficult endeavor. There is tremendous interest and a strong need to develop a thorough and deeper knowledge to access foldamer designs that undergo these interactions.

1.3.1 Helical structures formed by β- and γ-peptides

Many different helical structures are known to be adopted by peptides incorporating β- and γ-amino acids.[53] These helices are classified according to the number of atoms in the intramolecular main chain H-bonds.[53,72,73] To characterize folding, 2D-NMR experiments such as NOESY (Nuclear Overhauser Enhancement Spectroscopy),[73,74] ROESY (Rotating-frame Overhauser Effect Spectroscopy),[75–78] and TOCSY (Total Correlation Spectroscopy)[75,76] were used to determine the patterns of the nuclear Overhauser effect (NOE). These were mostly

complemented by simulation methods[72,74], crystallization,[79] and CD-spectroscopy.[72,74]

While the classical α-helix formed by α-amino acids is classified as a 13-helix,[80] foldamers composed of β-amino acids can adopt a 14-helix,[72,74] a 12-helix,[73,79] or a 12/10-helix[75,81] as representative helical structures.[53] For example, the mixed 12- and 10-helix is favored by alternating monosubstituted β^2-amino acids *and* β^3-amino acids in β^2/β^3-peptides.[74,82] Moreover, it is noteworthy that in the 14-helix and 12-helix formed by the β-peptides, the helix dipoles point in opposite directions.[53] α/β-Peptides containing α-amino acids and β-amino acids were shown to adopt 11-helix[83] and 14/15-helix[76] structures. If the ratio of α-amino acid to β-amino acid is equal (α:β = 1:1), an 11/9-helix structure is formed.[77] Changes in this ratio lead to diverse other helical structures that can be adopted.[53] Foldamers composed of β- and γ-amino acids can adopt a 13-helix[78] or an 11/13-mixed helix[84] as two examples of the many different helical structures that can be obtained. γ-Peptides can form a 14-helix[85,86] or a 9-helix[87,88] as representative structures.[53] In the case of α/γ-peptides, 12-helix[89,90] or 12/10-helix[84,91] structures can be adopted. Table 1 shows the schematic representation of these helix structures:

Table 1: Schematic representation of selected helix types and their conformational properties composed of α-, β- and/or γ-amino acids. For clearer and simpler representation, only H-bonded parts of the peptide backbones are shown, and amino acid residues have been omitted (Adapted from Kato. In *Cell-penetrating peptides: Design, Development and Applications*; Wiley-VCH GmbH: Weinheim, Germany, **2022**; pp 79–107. Copyright © 2022, John Wiley and Sons. Modified according to Bouillère *et al*. *Amino Acids* **2011**, *41* (3), 687–707. Copyright © 2011, Springer-Verlag.).[53,92]

Incorporated amino acid variants	Helix type	Formed H-bonded ring(s)
α-amino acids	13-Helix	O=C(*i*) …. N(*i*+4)-H
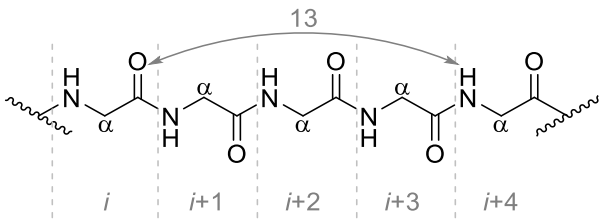		

β-amino acids	14-helix	N(i)-H …. O=C(i+2)

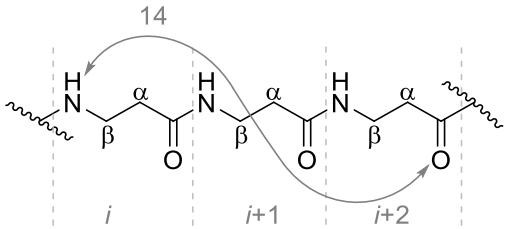

β-amino acids	12-helix	N(i+3)-H …. O=C(i)

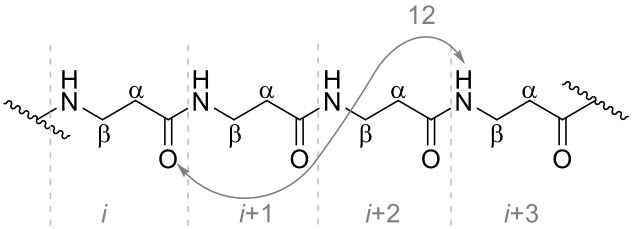

β-amino acids	12/10-helix	N(i+3)-H …. O=C(i) and N(i)-H …. O=C(i+1)

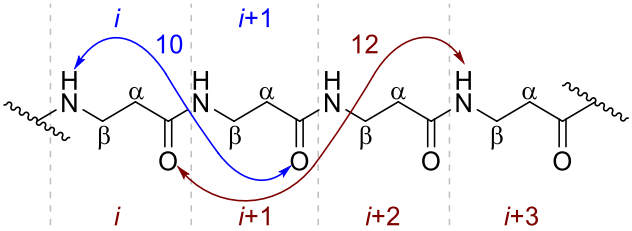

α- and β-amino acids	11-helix	N(i+3)-H …. O=C(i)

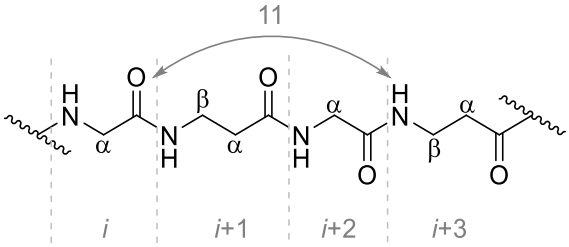

α- and β-amino acids	14/15-helix	N(i+4)-H …. O=C(i)

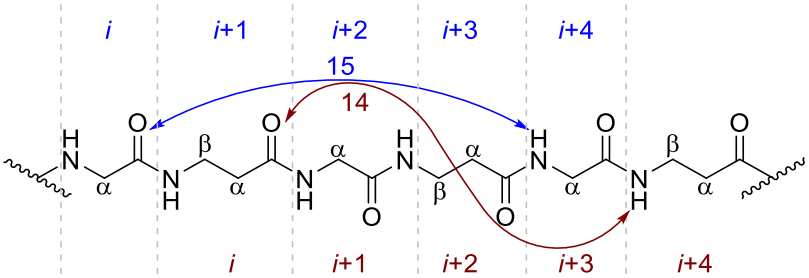

α- and β-amino acids (when 1:1 ratio)	11/9-helix	N(i)-H …. O=C(i+1) and N(i+3)-H …. O=C(i)

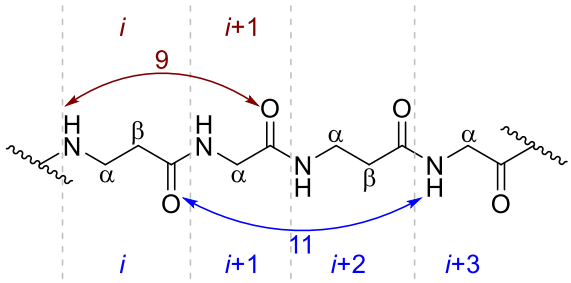

β- and γ-amino acids	13-helix	N(i+3)-H …. O=C(i)

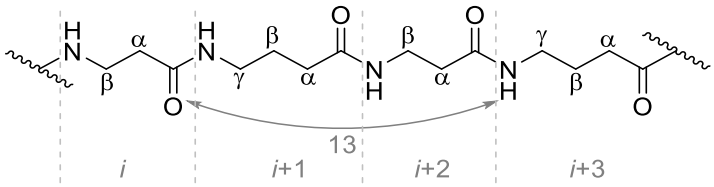

β- and γ-amino acids	11/13-helix	N(i)-H …. O=C(i+1) and N(i+3)-H …. O=C(i)

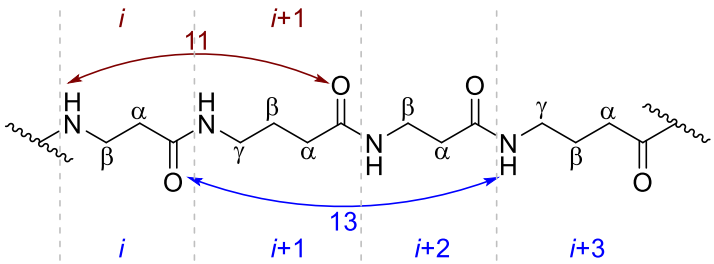

γ-amino acids	14-helix	N(i+3)-H …. O=C(i)

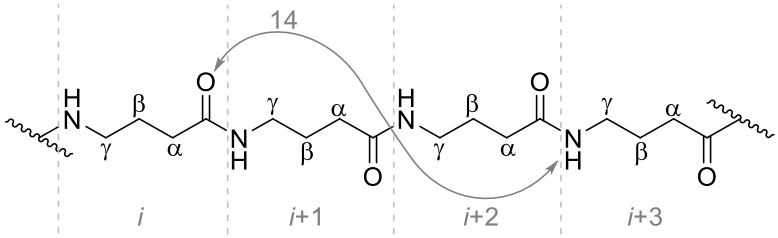

γ-amino acids	9-helix	N(i+2)-H …. O=C(i)

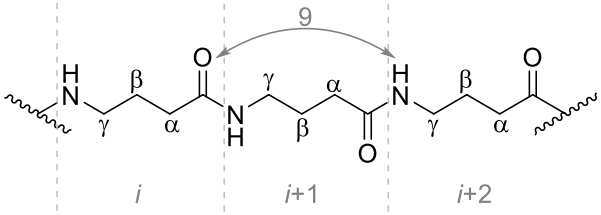

α- and γ-amino acids	12-helix	N(i+3)-H …. O=C(i)
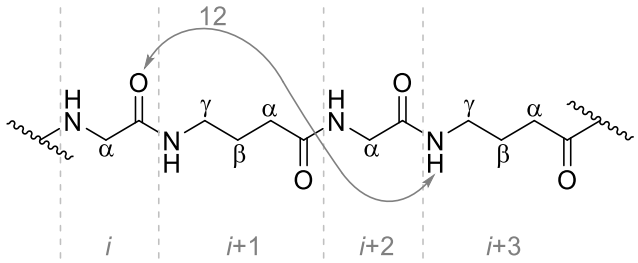		
α- and γ-amino acids	12/10-helix	N(i+3)-H …. O=C(i) and N(i)-H …. O=C(i+1)
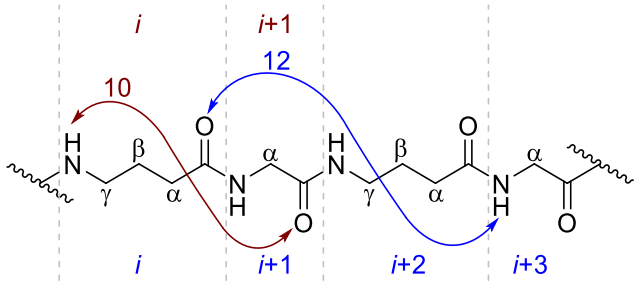		

1.3.2 Foldamers in coiled-coil designs

Designing foldameric sequences with modified backbones to study sequence-structure relationships requires elucidating the contribution of the backbone to protein folding behavior.[93] Therefore, the introduction of backbone-modified amino acids into coiled-coil folding motifs provides an excellent strategy to study their effects on tertiary and quaternary protein structures.

Gellman and co-workers provided the first insights into the consequences of replacing α-amino acids with homologous β^3-amino acids with their pioneering "top-down" approach to the coiled-coil systems of the parallel homo-dimeric GCN4-p1[94,95] and the parallel homo-tetrameric GCN4-pLI mutant.[35] In this approach, they altered all *b*- and *f*- positions in the coiled-coil systems by incorporating homologous β^3-amino acids, thereby varying the backbones and retaining the same residues (Figure 14). While the ability to form quaternary structures was preserved in both α/β-peptides, significant changes in stability and oligomerization state were observed for the α/β-analog of GCN4-p1, and changes in helix-association geometry were found for the α/β-analog of the parental GCN4-pLI.[55]

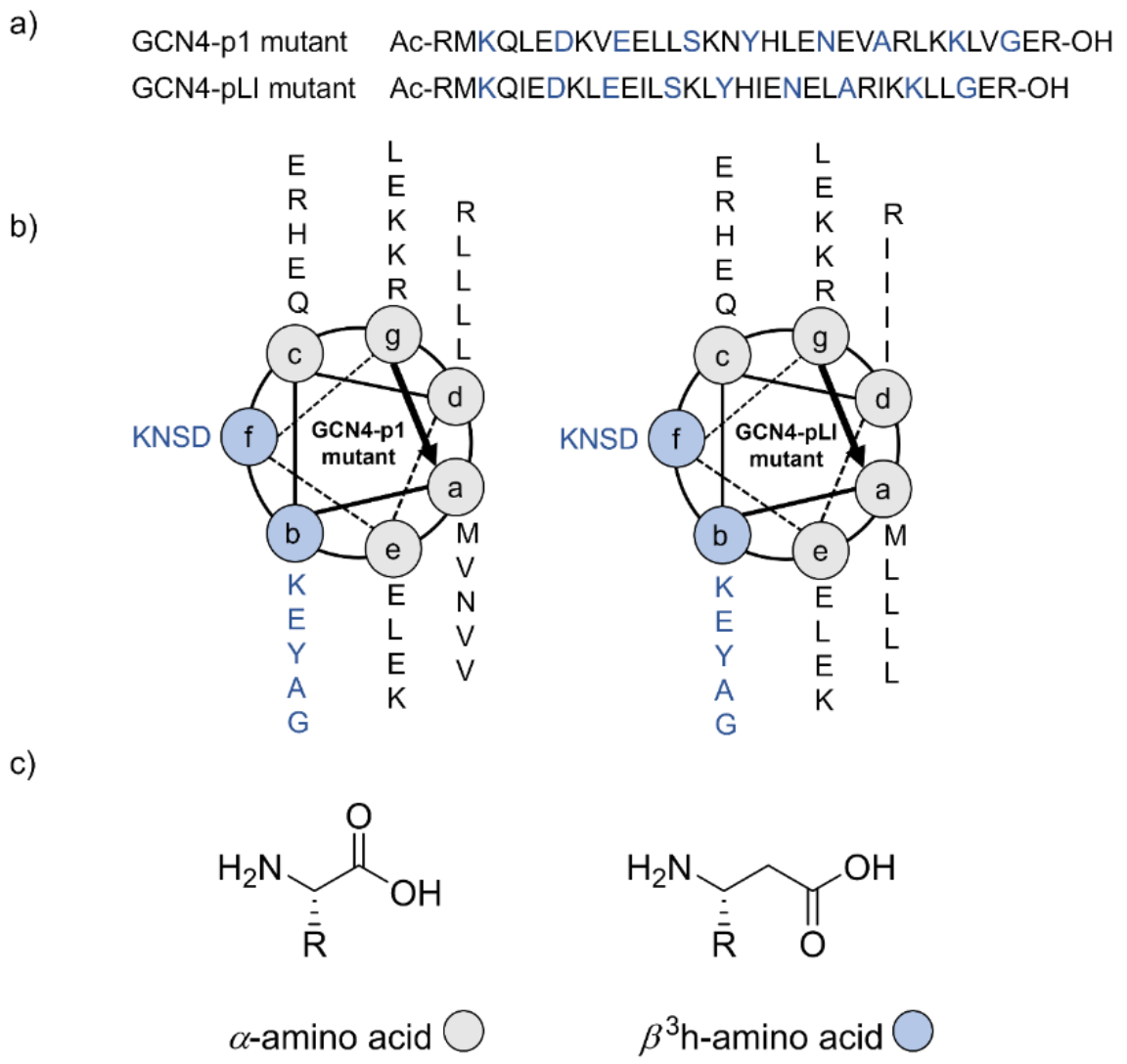

Figure 14: a) α/β-Peptide sequences of GCN4-p1 and GCN4-pLI replacing α-amino acid in positions *b* and *f* by homologous β^3-amino acids. b) Helical wheel representation. c) Structure of an α-amino acid in comparison to a homologous β^3-amino acid. Incorporated β^3h-amino acids are colored blue. Adapted with permission from Horne *et al.*, *J. Am. Chem. Soc*. **2007**, *129* (14), 4178-4180. Copyright © 2007 American Chemical Society. [55]

In a similar study using the parallel homo-tetrameric GCN4-pLI mutant, the incorporation of homologous β^3-amino acids in the hydrophobic core was studied. While the replacements of all *a*- and *d*- positions resulted in the preservation of tetrameric self-association with high thermal stability and C=O (*i*) → N-H (*i* +*4*) H-bonding patterns within the helical secondary structure, the features of the quaternary structure were significantly altered. The tetrameric quaternary structures exhibited antiparallel pairing, and the arrangement of the core side chains deviated from the classical “knobs-into-holes” arrangement, resulting in

“face-to-face” side-chain packing. This phenomenon was not observed when α-amino acids were substituted by homologous β^3-amino acids located in the peripheral positions of the coiled-coil system. Replacement of all *a*- and *e*-positions by homologous β^3-amino acids resulted in changes in stability and oligomerization state, similar to the first study. When all *d*- and *g*- positions were substituted by homologous β^3-amino acids, assembly was almost abolished.[96]

Two additional studies investigated the influence of torsional constraints required for homologous β^3-amino acids to form helical bundles. Therefore, cyclic β-amino acids that rigidify the secondary structure were incorporated into the GCN4-pLI sequence (Figure 15).

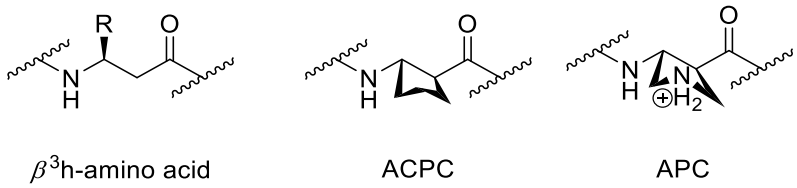

Figure 15: Structure of homologous β^3-amino acids compared to cyclically constrained uncharged (1*S*,2*S*)-2-aminocyclopentane-1-carboxylic acid (ACPC) and positively charged (3*S*,4*R*)-4-aminopyrrolidine-3-carboxylic acid (APC) when incorporated to a peptide sequence.

All in all, they stated that the incorporation of cyclic β-amino acids instead of the homologous β^3-amino acids can enhance the stability of the assembly but does not necessarily have to. Steric repulsions of the cyclic residue can limit the conformational benefits arising from backbone flexibility in the folded or assembled structure. Homologous β^3 to cyclic β-amino acid replacements were generally well-tolerated but led to variations in the self-association stoichiometry in some cases. Interestingly, they found one of the sequences to form a “stammer” discontinuity upon homologous β^3 to cyclic β-amino acid replacements leading to high-thermal stability through tighter binding. This stammer, however, appeared to be an anomaly.[93,97]

Nevertheless, these one-to-one substitutions of α-amino acids with β-amino acids lead to the insertion of additional atoms to the backbone compared to the parental α-peptides. Moreover, these α/β-peptide systems form coiled coils by self-association.

Aragahi *et al.* introduced a pentad of alternating homologous β^3- and γ^4-amino acids to mimic an α-helical turn based on the principle of “equal backbone atoms” in a designed coiled-coil motif. The designed parental coiled coil consists of a lysine-rich base strand (Base-pp) and a glutamic acid-rich acid strand (Acid-pp) that form a heterotypic tetramer assembly with a 1:1 stoichiometry. The central heptad of the base strand was substituted by a β^3/γ^4-pentad (Figure 16).[98] It has been previously reported that alternating β- and γ-amino acids are capable of forming a 13-helix (see Section 1.3.1). Thus, they provide an excellent opportunity to mimic the classical α-helix, which also forms a 13-helical network.[78,99]

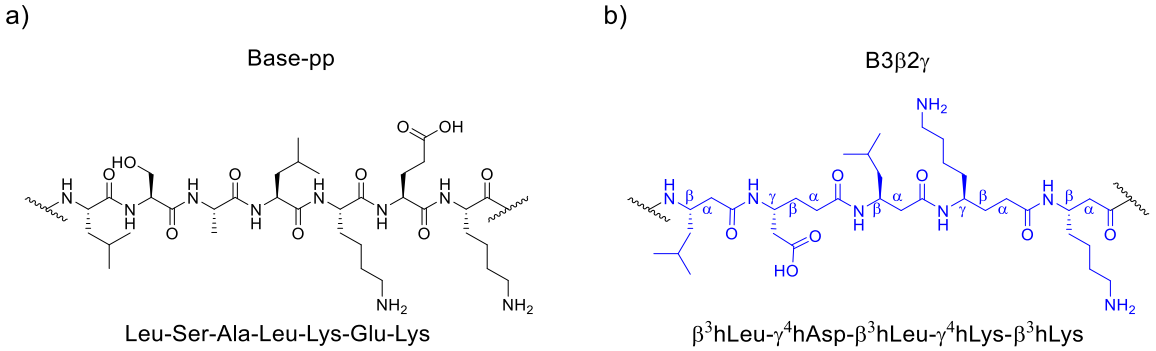

Figure 16: a) Central heptad of Base-pp comprising canonical α-amino acids and b) substituted central β^3/γ^4-pentad incorporating alternating homologous β^3- and γ^4-amino acids.

This $\alpha/\beta/\gamma$-chimeric base peptide, designated “B3β2γ”, was able to retain the propensity for tetrameric hetero-oligomerization with a 1:1 stoichiometry to the complementary acid strand comprising exclusively α-amino acids. Although this heterotypic helical bundle exhibited slightly less stability compared to the parental acid/base coiled coil, it was exceptionally stable to thermal denaturation and was not completely denatured even at 100 °C. Molecular dynamic (MD) simulations revealed that the hetero-oligomerized chimeric tetramer was equally stable in both parallel and antiparallel orientations. The spatial conformation of the α-peptide moieties of the helical quaternary structure and the α-helical secondary structure were not affected (Figure 17).[98]

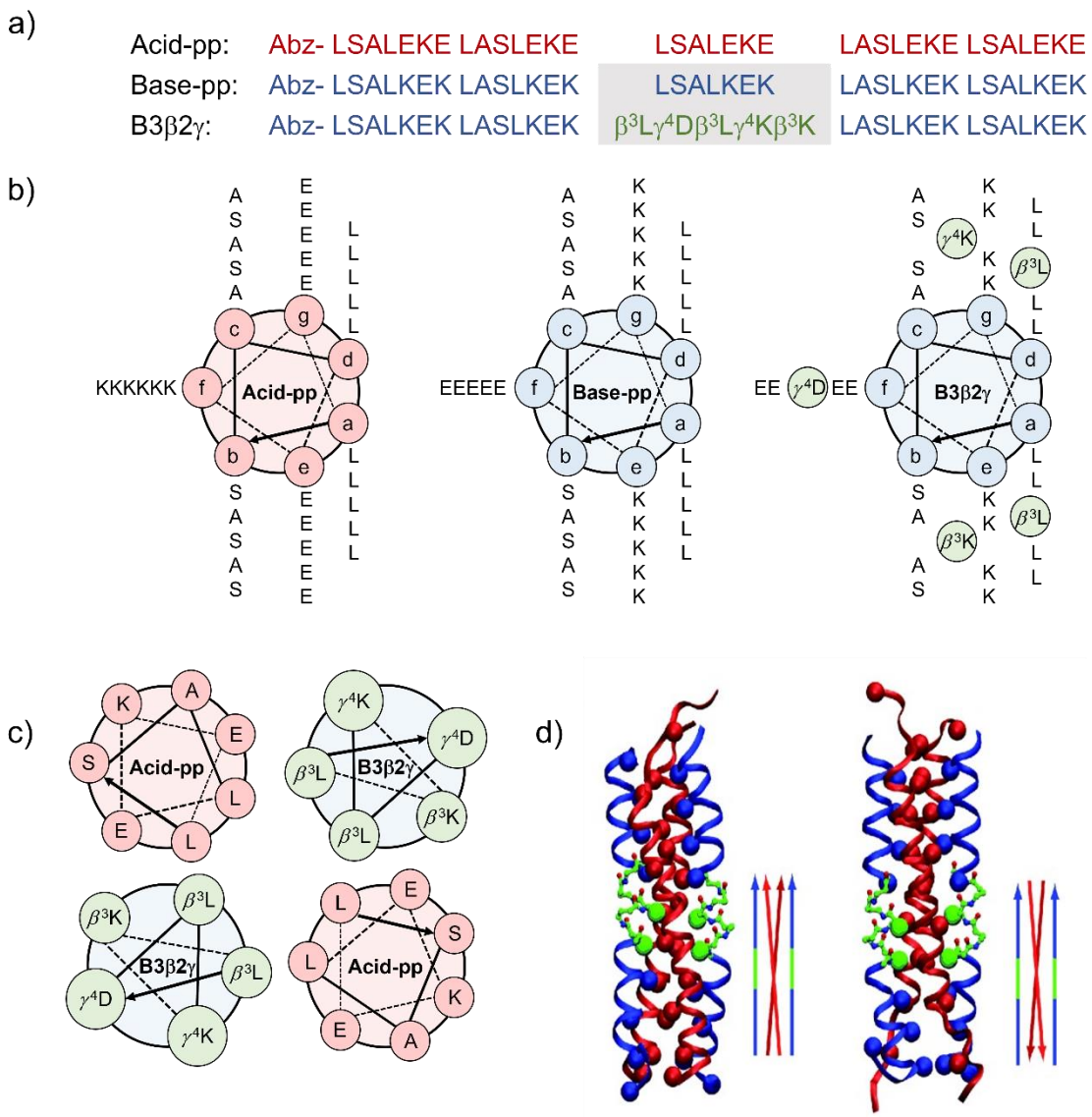

Figure 17: a) Peptide sequences of the parental peptides Acid-pp and Base-pp, as well as the $\alpha/\beta/\gamma$-chimera B3β2γ. The central heptad of Base-pp has been replaced by a pentad containing alternating homologous β^3- and γ^4-amino acids in B3β2γ (highlighted by a gray box). b) Helical wheel representation of Acid-pp, Base-pp, and B3β2γ. Green spheres indicate the central β^3/γ^4-pentad in B3β2γ. c) Helical wheel representation of the heterotypic tetrameric arrangement of central heptads of Acid-pp and pentads of B3β2γ. d) MD-simulation of Acid-pp/B3β2γ. The helix bundles are equally stable at both parallel and antiparallel alignment. In all illustrations, Acid-pp is red colored, Base-pp as well as the heptads of B3β2γ, which do not differ from Base-pp are blue colored, and the central β^3/γ^4-pentad in B3β2γ is green colored. Adapted from Araghi *et al.* *ChemBioChem* **2010**, *11* (3), 335-339 with permission. Copyright © 2010 WILEY-VCH Verlag GmbH & Co. KGaA, Weinheim.[98]

By replacing the hydrophobic or charged β^3/γ^4-amino acids with β-alanine variants (β-alanine or homologous β^3-alanine) in B3β2γ to determine the relative contributions of either the hydrophobic core or the charged interface to stability, they showed that the non-covalent interactions of hydrophobicity have a greater impact on the folding stability than the charged residues responsible for electrostatic recognition. Nevertheless, all variants of B3β2γ formed heterotypic helical bundles with the parental acid peptide, although the folding stability was significantly decreased.[98]

The replacement of one heptad formed by α-amino acids with the β^3/γ^4-pentad results on the one hand in a mimicry of the natural 13-helix H-bond network, but on the other hand in a loss of one intrahelical H-bond donor and one H-bond acceptor. Thus, the lack of one peptide bond may lead to disruptive structural consequences.[100] Therefore, spot array analysis[101] and phage display[57,102] were used to screen for high affinity binding partners to B3β2γ.

By replacing the *a/d*-, *e/g*-, and *a/d/e/g*-positions of the central heptad with glycine in Acid-pp, the properties responsible for hetero-oligomerization, hydrophobicity and electrostatic recognition to B3β2γ, were disrupted. All manipulations resulted in a loss of heterotypic bundle formation, demonstrating the necessity of interhelical interactions between the third heptad of the parental acid-strand and the central β^3/γ^4-pentad of the $\alpha/\beta/\gamma$-chimera. Subsequent spot-array analysis was used to screen these key positions for more efficient binding partners with various natural α-amino acids. Koksch and co-workers found that different hydrophobic amino acid residues were favored in *a*- and *d*-positions. Leucine was favored in the *a*-position, whereas the bulkier phenylalanine was more prevalent in the *d*-position. This suggests that, besides hydrophobicity, side-chain packing is involved in the selection of suitable binding partners to the β^3/γ^4-pentad. The flanking positions of the hydrophobic core, positions *e* and *g*, were found to be populated by hydrophobic residues, resulting in a more extensive hydrophobic core; thereby, the *e*-position was more sensitive towards replacements compared to the *g*-position.[101]

Further randomization of these *a/d/e/g*-positions was achieved by phage display. This method screens for high-affinity peptide-peptide, protein-protein, and protein-DNA interaction partners and was first described by George P. Smith in 1985,[103]

for which he was awarded the Nobel Prize in Chemistry 2018 jointly with Sir Gregory P. Winter.[104] Application of this method on *N*-terminally immobilized B3β2γ led to the identification of two variants of the Acid-pp sequence bearing a Cys/Phe-motif that selectively bind to the *α/β/γ*-chimera. The Acid-CFLE and Acid-ICEF sequences comprise a cysteine at either the *a*- or *d*-position and a phenylalanine in close proximity in the *d*- or *g*-position, respectively. Both sequences involve only one glutamic acid residue in the *e*- or *g*-position, and the other position flanking the core is occupied by a hydrophobic amino acid residue that extends the hydrophobic core. The heterotypic helical bundles formed with B3β2γ retain the tetrameric oligomerization state. The thermal stability of the Acid-ICEF/B3β2γ assembly is comparable to the parental Base-pp/Acid-pp coiled coil. MD-simulation revealed that the side-chain orientation of the thiol group in cysteine changes from an intramolecular H-bond to an intermolecular H-bond to the non-H-bonded backbone carbonyl of *β*-leucine (Figure 18c). This leads to improved packing of the extended hydrophobic core in the helical bundle. In addition, substitutions of cysteine by either serine or aminobutyric acid showed significantly reduced stability in solution when forming helical bundles with the *α/β/γ*-chimera.[102]

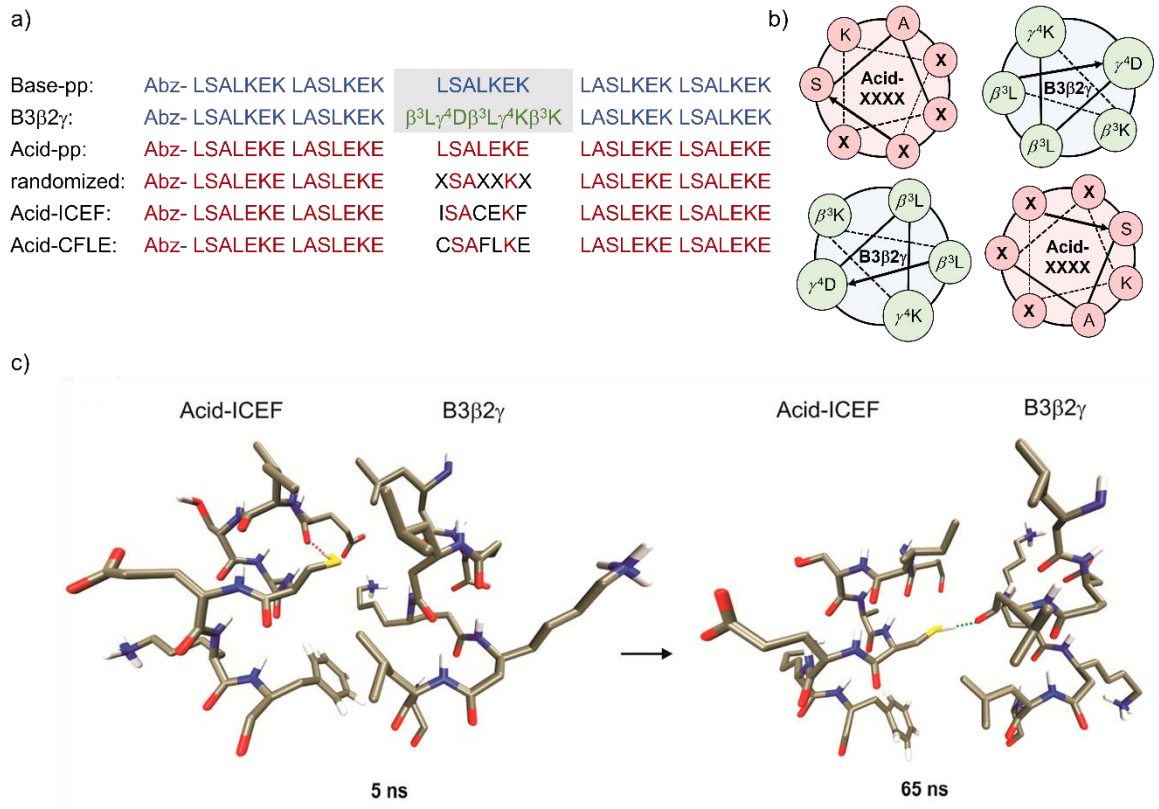

Figure 18: a) Peptide sequences. Randomized positions are shown in black letters. b) Helical wheel representation of the central heptad of Acid-pp variants with randomized *a*, *d*, *e,* and *g* positions and the central β^3/γ^4-pentad in B3β2γ incorporating homologous β^3- and γ^4-amino acids. c) MD-simulation of the change from intra- to intermolecular H-bond from the thiol of Cys. Adapted with permission from Nyakatura *et al.*, *ACS Chem. Biol*. **2014**, *9* (3), 613-616. Copyright © 2014 American Chemical Society.[102]

While the *N*-terminally immobilized $\alpha/\beta/\gamma$-chimera led to the selection of parallel-orientated opposing acid strands by phage display, the helical bundle of Acid-pp/B3β2γ exhibited a nonspecific orientation. Surprisingly, immobilization of the *C*-terminus of B3β2γ during phage display resulted in a nonspecific orientation comparable to the Acid-pp/B3β2γ assembly. In contrast to the spot array analysis and the *N*-terminal immobilized phage display approach, the two acid sequences that formed heterotetrameric assemblies with B3β2γ consisted exclusively of hydrophobic amino acids in *a/d/e/g*-positions, which exhibited high thermal stability. Two other sequences harboring charged amino-acid residues in most randomized positions, including the *a*- and *d*-positions that are typically occupied by hydrophobic residues, revealed dimeric oligomerization states. Thermal stabilities were significantly reduced, and both partial dissociation and unfolding

were observed. Interestingly, however, one of these two sequences contained a cysteine in the *d*-position.[57]

1.3.3 Bioactive foldamers

Research on foldamers is driven by the main motivation to incorporate non-natural scaffolds capable of adopting defined structures and imitating parts of biological protagonists in their function while providing resistance toward proteolytic degradation.[105,106] Therefore, the incorporation of unnatural amino acids into peptides is considered a promising strategy for the development of bioactive reagents such as PPI-inhibitors, AMPs, CPPs, and structures with enzymatic like-behavior. [53,107,108]

α-Helices are commonly found as recognition elements between proteins. Mimicking them to inhibit PPIs has already led to promising success in targeting apoptotic regulators or proteins involved in infectious diseases.[54] Kritzer *et al.* studied the disruption of hDM2-p53 interaction through β^3-peptides.[109] The inhibition of hDM2-p53 is an important target for oncologic research because the tumor suppressor protein p53, which can induce apoptosis in response to cell stress, is negatively regulated by hDM2.[110] The β^3-decapeptides were designed based on the trans-activation domain sequence of wild-type p53 to inhibit hDM2.[109] Later, Grison *et al.* used the cyclically constrained β-amino acid trans-2-amino cyclobutane carboxylic acid (tACBC) and γ^4-amino acids as key design elements in hexameric $\alpha/\beta/\gamma$-peptide sequences to mimic a segment of p53 (Figure 19). In addition to increased proteolytic stability compared with the parental α-peptide, the $\alpha/\beta/\gamma$-peptides were shown to exhibit selective inhibition of hDM2-p53 interaction.[111]

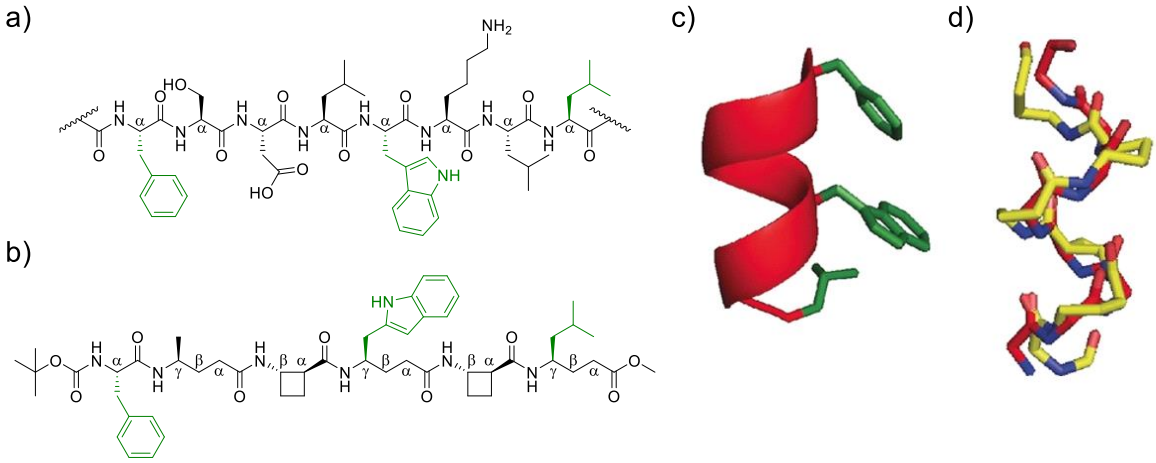

Figure 19: a) The segment of p53 including amino acids from position 19-26. b) Structure of one of the eight $\alpha/\beta/\gamma$-peptide helix mimetics used in the work of Grison *et al.* Key side chains are colored green and were retained in the $\alpha/\beta/\gamma$-peptide design. c) Crystal structure of the p53 segment from position 16-29 excised from its complex with hDM2. Key side chains are colored in green and the helical backbone is colored red. d) Superimposition of the backbones of the $\alpha/\beta/\gamma$-peptide from b) (yellow) and of the p53 segment (red). The root-mean-square deviation of atomic positions (RMSD) value is 0.89 Å (adapted from Grison *et al.*).[111]

A second target of key interest in cancer therapy is the mimicry of the α-helical BH3 domain of the pro-apoptotic protein Bim that strongly binds to the anti-apoptotic proteins Bcl-x_L and Mcl-1 by helical foldamers.[112] Intensive effort and research were dedicated by Gellman and co-workers to finding protease-resistant foldameric antagonists for the BH3 domain-Bcl-x_L recognition (Figure 20).[113] Starting with a "structure-based" design of chimeric ($\alpha/\beta+\alpha$) patterns[113–115] they found the "sequence-based design" with α-amino acids to homologated β^3-amino acid substitutions to be more efficient.[116–118] However, also in the BH3 domain studies, $\alpha/\beta/\gamma$-peptidomimetic sequences were later investigated by Shin and Yang. In addition to canonical α-amino acids, the designs included homologous β^3- and γ^4-amino acids as well as ring constrained β- and γ-amino acids.[46]

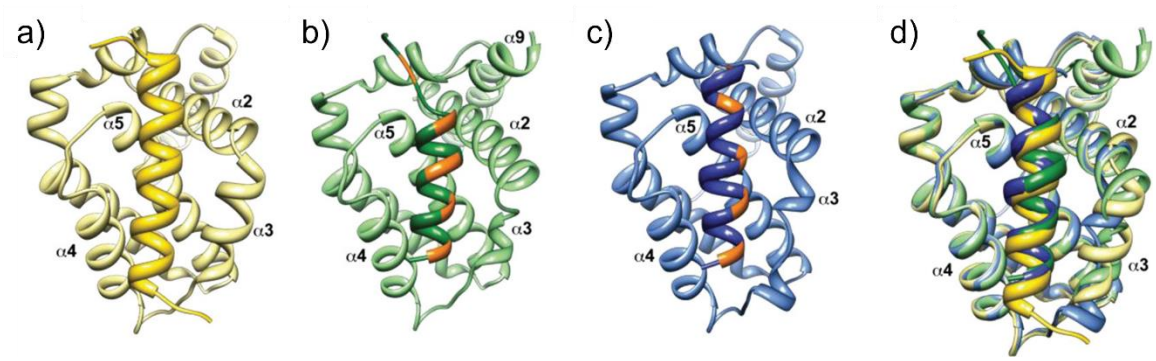

Figure 20: Crystal structures of BH3-derived a) α-peptide (yellow) and α/β-peptides incorporating homologous β^3-amino acids with b) ααβαaβ (green) and c) αααβ (blue) backbone patterns bound to Bcl-x_L. The darker-colored helix indicates the BH3 domain-derived peptides and the lighter-colored positions correspond to the Bcl-x_L of each co-crystal structure. The positions of the β^3h-amino acid residues are indicated by orange patches in b) and c). A superposition of the three structures a) to c) is shown in d). The overall structures show high similarity except for the α3 helix of Bcl-x_L, which differs significantly. Reprinted with permission from Boersma *et al.*, *J. Am. Chem. Soc*. **2012**, *134* (1), 315-323. Copyright © 2012 American Chemical Society.[116]

Targeting the inhibition of PPIs leading to virus entry in infectious diseases, helical foldameric binders to the virus entry protein gp41 of the human immunodeficiency virus (HIV) were investigated by Stephans *et al.* consisting exclusively of β^3-homoamino acids.[119] Contrarily, the Gellman group investigated blocking HIV fusion with α/β-sequence patterns.[120,121] Figure 21 shows 4α/β, an α/β-chimeric peptide, designed according to an ion-pair array containing negatively charged Glu and positively charged Arg homologous β^3 amino acids. Despite the disorder in the charged side chains during binding to gp41, this peptide exhibits high infectivity inhibition activity against several HIV-1 virus strains. This activity is comparable to or in some cases superior to that of T20 (enfuvirtide),[122] an FDA-approved drug.[120] Another example for examination on blocking virus entry through α/β-peptides was performed on human cytomegalovirus (HCMV).[123]

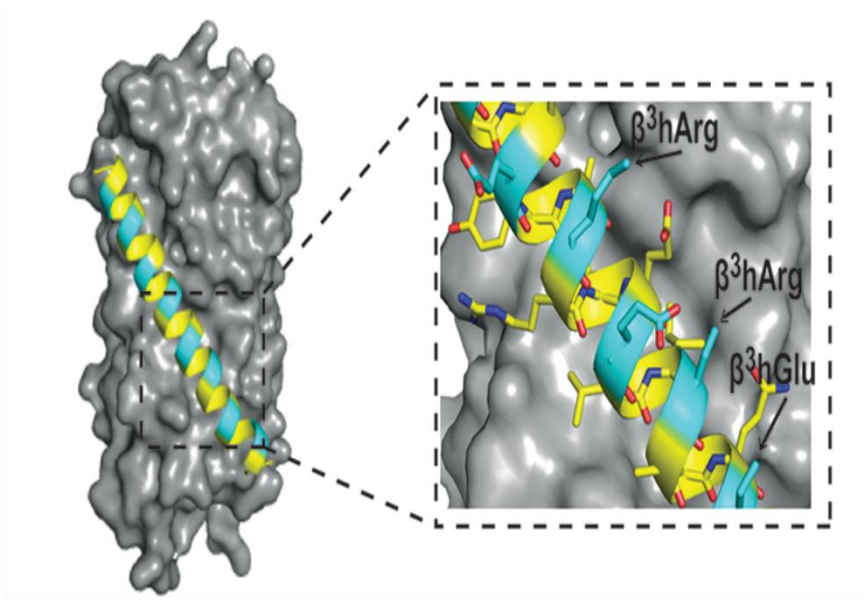

α/β-foldamer sequence

Ac – β³R T W E β³E W D β³R A I A β³E Y A β³R R I E β³E L I β³R A A Q β³E Q Q β³R K N E β³E A L β³R E L – NH_2

Figure 21: Crystal structure of gp41-5 and an *α/β*-peptide designated 4*α/β* (PDB 4DZV). The magnified view shows the disorder of ion pairing side chains. The gray area is gp41-5, the yellow ribbon indicates the *α*-residues and the cyan ribbon designates the homologous β^3-amino acid residues. Reprinted with permission from Johnson *et al.*, *J. Am. Chem. Soc*. **2012**, *134* (17), 7317-7320. Copyright © 2012 American Chemical Society.[120]

As a result of the dual control over monomer sequence and secondary structure, as well as the diversity of building blocks, foldamers often combine structure and function. The helical structure of designed foldamers is as important in AMP development as it is in PPI inhibitor development. Many foldamer AMP mimics are designed to form global amphiphilic helices by accumulating hydrophobic and cationic residues at the helix surface.[54] Here, the amphiphilic character facilitates penetration into microbial membranes resulting in cell lysis.[124] The groups of DeGrado,[50,125] Gellman,[126] and Seebach[127] independently showed that amphiphilic 14- or 12-helix forming *β*-peptides provided potent antimicrobial activity.[51] Moreover, the Gellman group found *β*-peptides composed of cyclic residues to be less hemolytic than that composed of acyclic residues.[126]

The helical coiled-coil motif is also involved in various catalytic processes.[128–131] Araghi and Koksch presented the first example of an *α/β/γ*-chimeric ligase. The *α/β/γ*-chimera B3β2γ described in the previous section (see Section 1.3.2) showed

catalytic activity in a template-directed peptide native chemical ligation (NCL) approach with two fragments of modified Acid-pp. Thus, the first fragment involved a *C*-terminal thioester and the second an *N*-terminal Cys (Figure 22).[108,132] The ligase activity of B3β2γ was slightly decreased compared to the parental peptide Base-pp. This indicates that the side-chain alignment of the homologous β^3- and γ^4-amino acids is compatible with the coiled-coil structure leading to function, even though the number of H-bonds from the backbone is reduced compared to Base-pp.[108]

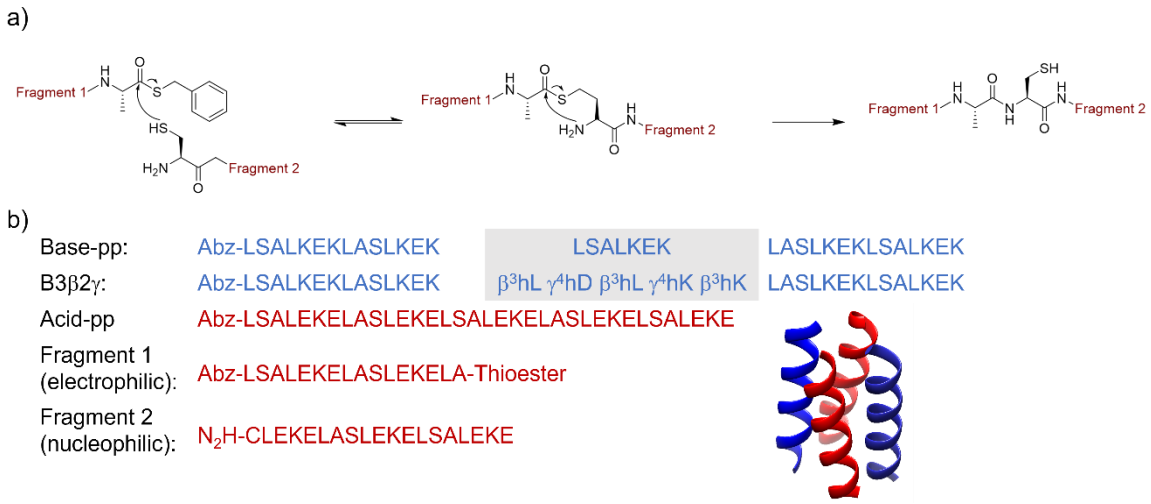

Figure 22: Template-directed NCL of Acid-pp by Base-pp or B3β2γ. a) Scheme of the ligation reaction between the thioester of fragment 1 and the Cys of fragment 2. b) Peptide sequences and schematic representation of the heterotypic tetramer helix bundle formed by red helices indicating Acid-pp and blue helices indicating Base-pp or B3β2γ (Used with permission of Royal Society of Chemistry, from A Helix-Forming αβγ-Chimeric Peptide with Catalytic Activity: A Hybrid Peptide Ligase, Araghi and Koksch, *Chem. Commun.* **2011**, *47* (12), 3544–3546.; permission conveyed through Copyright Clearance Center, Inc).[108]

All in all, helical foldamers incorporating β- and/ or γ-amino acids offer a mirage of potential bioactive functions. However, due to a large number of building blocks and diverse design possibilities, the prognosis of effectiveness and selectivity for desired bioactive applications is complicated. Prediction of preferable side-chain alignment of foldameric β- and γ-amino acid sequences in higher ordered structures can be aggravated by the high backbone flexibility, especially in terms of PPI inhibitory applications.

1.4 The theory behind vibrational sum-frequency generation (SFG) spectroscopy

Vibrational sum-frequency generation spectroscopy is a second-order nonlinear optical technique, which is inherently interface sensitive because symmetry breaking is required.[133,134] It involves two pulsed laser beams of fixed visible (ω_{VIS}) and tunable infrared (ω_{IR}) frequencies overlapping spatially and in time.[135] The resulting photons with sum-frequency (ω_{SF}) are detected in the visible frequency range (Figure 23).[136,137]

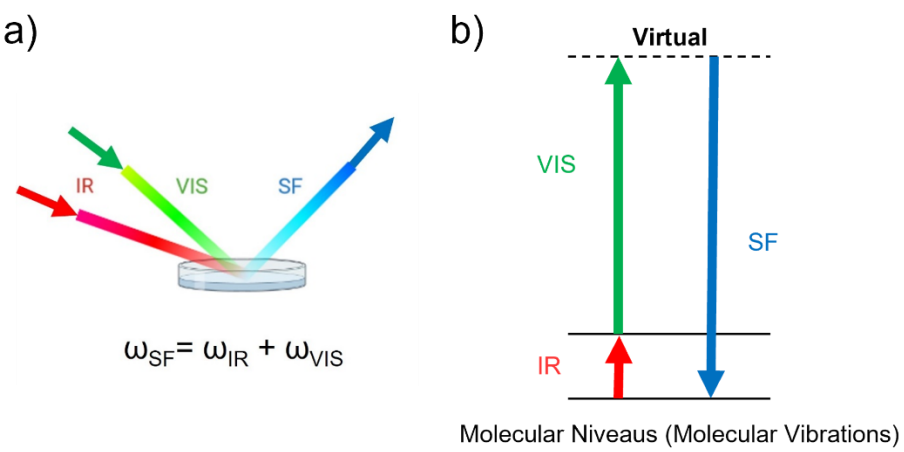

Figure 23: a) Schematic representation of pulsed Vis and IR beams overlapping in space and time at an air/water interface generating a third sum-frequency beam in reflection. b) Energy level diagram of SFG; continuous lines indicate a real state and the dotted lines a virtual state (according to Morsbach).[137]

Here, the vibrational sum-frequency (SF) signal can only be generated by vibrational modes that are both IR- and Raman-active.[138–140] Its intensity is hereby dependent on the beam intensities of the two incoming laser beams as well as the sum from resonant and non-resonant parts of the second-order electric susceptibility $\chi^{(2)}$.[141,142] The third-order electric susceptibility $\chi^{(3)}$ contribution can provide qualitative information on the charging state of charged interfaces:[141–143]

$$I(\omega_{SF}) \propto \left|\chi^{(2)}_{Nres} + \chi^{(2)}_{R} + \frac{\kappa}{\kappa + i\Delta k_z}\chi^{(3)}\phi_0\right|^2 \qquad (1)$$

κ corresponds to the inverse Debye length and Δk_z to the wave factor mismatch. The resonance component shown in the next equation depends on the resonance

frequency ω_q of the molecular vibration, its Lorentzian linewidth Γ_q and amplitude A_q.

$$\chi_R^{(1)} \propto \sum_q \frac{A_q}{\omega_q - \omega + i\Gamma_q} \tag{2}$$

Here, the amplitude depends on the number of molecules at the interface and the orientational average $\langle \ldots \rangle$ of the molecular hyperpolarizability β_q:

$$A_q \propto N\langle \beta_q \rangle \tag{3}$$

It can provide orientational information of the molecules in the interface by considering the phase of the *q*th vibrational mode.[135,144,145] Moreover, in isotropic bulk media such as liquids and gases, which are centrosymmetric, the orientational average of the molecular hyperpolarizability β_q becomes zero. From this, the SF intensity also becomes zero.[146] The required centrosymmetric breakage is applied at the phase boundary between two media (e.g., liquid/gas, gas/solid, solid/liquid). Consequently, the obtained molecular data are not perturbed by background signals from isotropic bulk media. Thus, highly interface-selective molecular vibrational data can be measured.[147,148]

Phase-resolved vibrational SFG measurements can provide information on how proteins are folded, their orientation at the surface, and which side chains interact with the surface. The amide regions are conformationally sensitive as in conventional Fourier-transform infrared spectroscopy (FT-IR) measurements. Secondary structural features can be measured by tuning the IR frequency to the amide I region. All amide regions have specific absorption patterns for α-helix. β-sheet, random coil, and loop structures, which in sum reflect the various protein substructures at the surface.[137]

The pioneering vibrational SFG studies of amino acids at the oil/water interface by Watry and Richmond[149] laid the foundation for label-free studies of protein structures and interfacial hydration of proteins. Hence, phase-resolved vibrational SFG measurements can be used to determine key effects of protein structures at the interface and thus assess side-chain structure,[150] orientation, and backbone folding.[137,151]

Nevertheless, the physicochemical environment of an interface is different from that of a homogeneous bulk phase. Therefore, the folding and molecular structure may differ from X-ray crystallography, cryo-EM, and NMR-spectroscopy.[148] The interpretation of measured vibrational SFG spectra for structure determination in this work must be complemented with data from other techniques and compared with structural data obtained in the bulk solvent.

2. Aim of this work

Developing a sophisticated understanding of how foldamers interact with canonical amino acids in higher-ordered structure systems is of great interest, as predicting these interactions still proves difficult. This work addresses the high-resolution structural investigation of B3β2γ,[98] an $\alpha/\beta/\gamma$-chimeric peptide when bound to all-α-peptides in a well-defined heterotypic coiled-coil model system.

Previous studies used phage display to screen for all-α-peptide sequences that selectively bind to this chimeric peptide in a parallel tetrameric coiled-coil arrangement. Here, two sequences were identified, each incorporating a Cys/Phe-motif and exhibiting high thermal stability when forming helical bundles with B3β2γ. MD-simulations revealed the formation of an interstrand H-bond between the thiol residue of Cys and the unbound backbone carbonyl of the β^3/γ^4-pentad of B3β2γ.[102] However, structural data analysis was evaluated using only MD-simulation.

Therefore, the preferential side-chain interactions between the complementary sequences incorporating the Cys/Phe-motifs and the $\alpha/\beta/\gamma$-chimeric sequence should be investigated experimentally in this work. Analytical methods such as NMR spectroscopy and X-ray crystallography should be applied to visualize the preferable packing of residues in the quaternary structure. In addition, the limits of intermolecular binding strength between foldamers and all-α-peptides should be examined in an iterative substitution design. For this purpose, a library with a systematically expanded number of β^3/γ^4-modules in the chimeric peptides should be constructed. This library will then be complemented with corresponding all-α-peptide sequences containing the Cys/Phe-motifs. The resulting structures will be analyzed by CD-spectroscopy.

3. Results and Discussion

3.1 Structural investigation of the Cys/Phe-motifs of all-α-peptides and the $\alpha/\beta/\gamma$-foldamer in heterotypic assemblies

Both the *C*- and *N*-terminal immobilized B3β2γ phage-display studies by Koksch and co-workers revealed a prevalence of cysteine for the complementary acid strands in the *a*- or *d*-position of the central heptad.[57,102] These positions are integrated into the hydrophobic core of the heterotypic coiled-coil assemblies with B3β2γ. While *N*-terminal immobilization identified two acid sequences with Cys/Phe-motifs that provide high thermal stability in the assembly, *C*-terminal immobilization also led to the identification of a Cys-containing acid sequence with cysteine in the *d*-position that exhibits decreased thermal stability. However, the prominence of cysteine in three different sequences identified by phage-display studies searching for interaction partners with high affinity,[103] suggests that cysteine provides selective recognition of the homologous β^3/γ^4-module of B3β2γ. The present work is therefore devoted to the structural investigation of the Cys/Phe-motifs in assembly with the $\alpha/\beta/\gamma$-chimera.

The peptides Base-pp, B3β2γ, Acid-pp, Acid-CFLE, and Acid-ICEF reported by Nyakatura *et al.*[102] were synthesized (Table 2). Subsequently, all heterotypic coiled-coil systems (Acid-pp/Base-pp, Acid-pp/B3β2γ, Acid-CFLE/B3β2γ, and Acid-ICEF/B3β2γ) were characterized thoroughly by CD-spectroscopic measurements. Moreover, the peptides Acid-CFLE and Acid-ICEF, which comprise the Cys/Phe-motifs, were analyzed for differences in the absence and presence of the reducing agent dithiothreitol (DTT) both as monomeric sequences and in the helical bundle with the $\alpha/\beta/\gamma$-chimera.

Table 2: Peptide sequences of the parental base- and acid-strands, B3β2γ, and the two acid sequences involving the Cys/Phe-motifs. All peptides were *N*-terminally labeled with *o*-aminobenzoic acid (*o*-Abz) for concentration determination. Substitutions were highlighted by gray boxes. Base strand variants are colored blue and acid strand variants are shown in red. Homologous β^3- and γ^4-amino acids are colored green and amino acids of the Cys/Phe-motifs in black.

	Peptide sequence					
Base-pp	*o*-Abz	L S A L K E K	L A S L K E K	L S A L K E K	L A S L K E K	L S A L K E K
B3β2γ	*o*-Abz	L S A L K E K	L A S L K E K	β^3L γ^4D β^3L γ^4K β^3K	L A S L K E K	L S A L K E K
Acid-pp	*o*-Abz	L S A L E K E	L A S L E K E	L S A L E K E	L A S L E K E	L S A L E K E
Acid-CFLE	*o*-Abz	L S A L E K E	L A S L E K E	C A S F L K E	L A S L E K E	L S A L E K E
Acid-ICEF	*o*-Abz	L S A L E K E	L A S L E K E	I A S C E K F	L A S L E K E	L S A L E K E

CD-spectroscopic measurements of the peptide sequences revealed no significant changes in the secondary structure of Acid-CFLE and Acid-ICEF in the presence and absence of the reducing agent (Figure 24). Base-pp exhibits a helical secondary structure characterized by two distinct minima at 208 nm and 222 nm. All acid-variants indicate disrupted helical structures with the first minimum shifted to a lower wavelength and a second minimum at 222 nm. B3β2γ has a random coil structure.

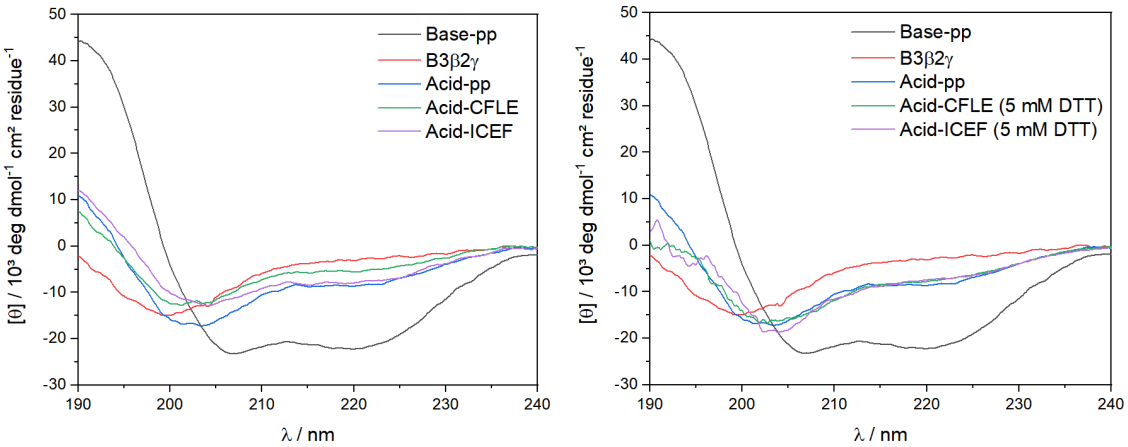

Figure 24: CD-spectra of monomeric peptide sequences with 20 µM peptide concentration in 10 mM phosphate buffer at pH 7.4 in the absence of DTT (left) and in the presence of 5 mM DTT (right).

Equimolar mixtures of Acid-pp/Base-pp, Acid-pp/B3β2γ, Acid-CFLE/B3β2γ, and Acid-ICEF/B3β2γ were then examined by CD-spectroscopy for successful formation of coiled-coil assemblies. As a result, all heteroassemblies demonstrate helical structure characteristics with minima at 208 nm and 222 nm, indicating coiled-coil formation (Figure 25):

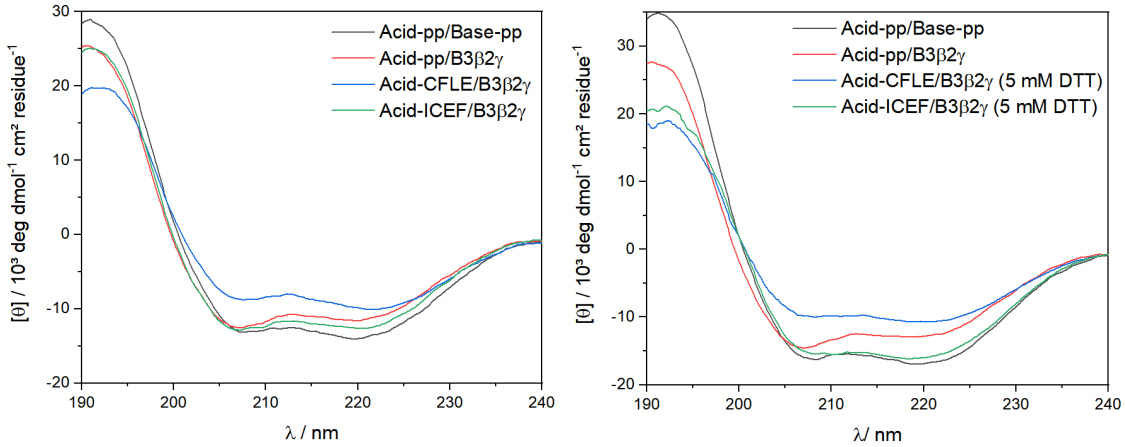

Figure 25: CD-spectra of 1:1 peptide mixtures with 20 µM total peptide concentration in 10 mM phosphate buffer at pH 7.4 in the absence of DTT (left) and in the presence of 5 mM DTT (right).

Again, Acid-CFLE/B3β2γ and Acid-ICEF/B3β2 show no significant differences in the absence and presence of DTT. Acid-CFLE/B3β2γ exhibits the lowest helical content (28%), and the Acid-ICEF/B3β2 assembly displays a similar helix content to the parental acid and base coiled-coil arrangement (40% and 38%, respectively). In addition, the coiled coil of Acid-pp/B3β2γ has a helical content of 32%. The same trends of helicity were maintained even at 3-fold concentrations (Figure 26). Less pronounced ellipticities at 208 nm suggest that molecular rearrangements are occurring.[152,153] The strongest decrease in ellipticity is observable for Acid-CFLE/B3β2γ.

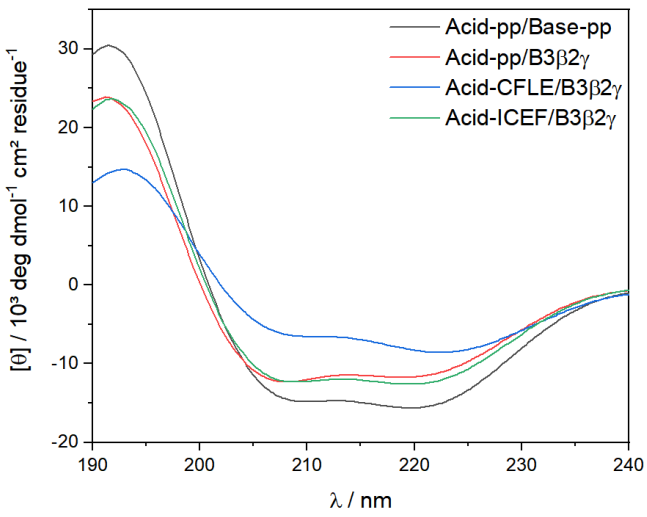

Figure 26: Equimolar peptide mixtures with 60 µM total peptide concentration in 10 mM phosphate buffer at pH 7.4.

At higher concentrations, precipitation of the helix bundles was also observed. This was more rapidly seen in the Acid-CFLE/B3β2γ and Acid-ICEF/B3β2γ systems. Transmission electron microscopy (TEM) studies performed by Araghi already revealed the formation of α-fibers for Acid-pp/Base-pp and Acid-pp/B3β2γ at higher concentrations.[154] This phenomenon was also validated by cryogenic-TEM (cryo-TEM) measurements of equimolar mixtures at 1 mg/mL total peptide concentration, performed in collaboration with Dr. Boris Schade and Dipl.-Ing. Jörg Bürger.

Long unbranched α-fibers with an average diameter of 3.4 ± 0.5 nm were formed for Acid-pp/Base-pp (Figure 27) and Acid-pp/B3β2γ (Figure 28) with 3.5 ± 0.4 nm. These diameters are consistent with the measured parameters of approximately 3 nm for the α-fibers reported by Araghi.[154] While the morphology of the formed α-fibers of Acid-pp/B3β2γ are not significantly different from the parental system, the assemblies of Acid-CFLE/B3β2γ (Figure 29) and Acid-ICEF/B3β2γ (Figure 30) form completely dissimilar supramolecular arrangements. The fibers formed by Acid-CFLE/B3β2γ are laterally organized and form partially stacked layers, creating a crossed-over pattern. Here, the triple zooms display crystalline layers. Average diameters of the crystalline parts were determined by plotting the light-to-dark distances, which yielded a highly uniform diameter of approximately 2.9 nm (see Appendix). The Acid-ICEF/B3β2γ fibers, on the other hand, have a strong tendency to twist into larger units and thus into thicker rope-like strands. Average diameters

of 5.2 ± 0.3 nm are formed. This mean diameter is thus broadened compared to the measured parameters of the other assemblies. However, it cannot be ruled out that two of the α-fibers are tightly wrapped around each other, nearly doubling the diameters. Nevertheless, widened diameters could form due to an enlarged hydrophobic surface of the residues from the Cys/Phe-motif, which increase this surface area by involving the phenylalanine in *g*-position in the Acid-ICEF peptide sequence. Szefcyzyk *et al.* previously reported the formation of larger aggregates caused by the introduced hydrophobic surface of the cyclopentane side chains of trans-ACPC during the formation of α-fibers in homotypic β/γ-chimeric coiled coils.[155] Thus, the formation of supramolecular structures could explain the faster precipitation of the Acid-CFLE/B3β2γ and Acid-ICEF/B3β2γ helical bundles.

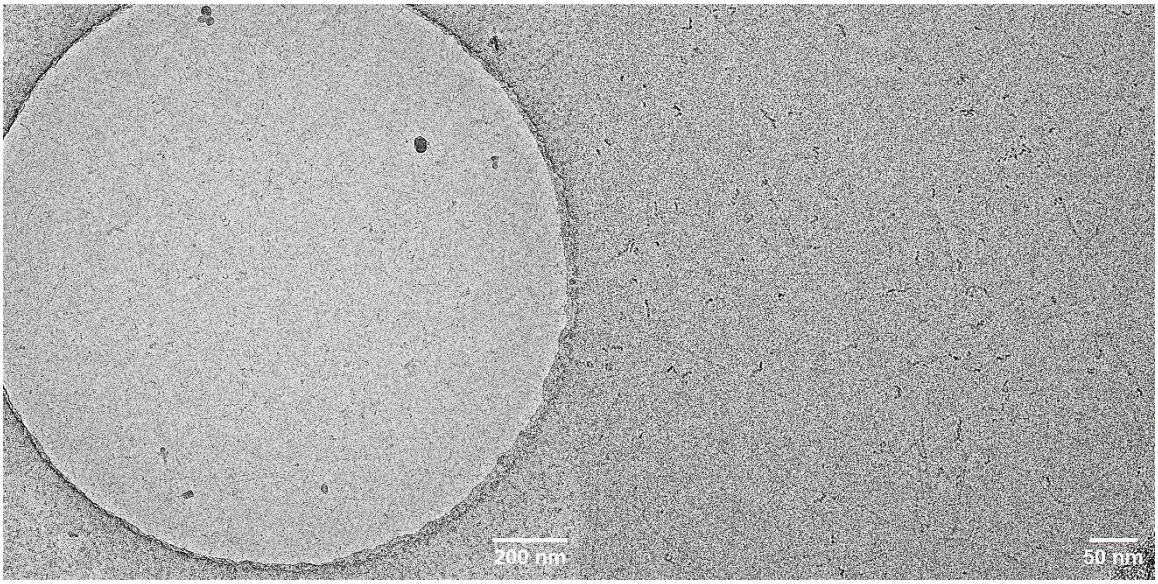

Figure 27: Cryo-TEM images of Acid-pp/Base-pp assembly at 1 mg/mL total peptide concentration in 10 mM phosphate buffer at pH 7.4.

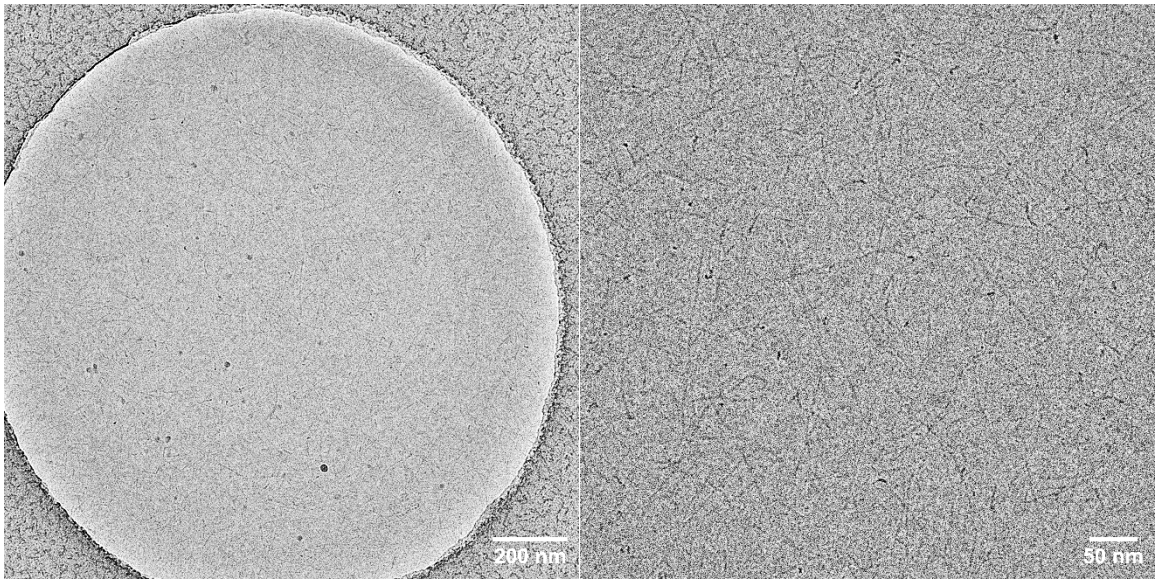

Figure 28: Cryo-TEM images of Acid-pp/B3β2 assembly at 1 mg/mL total peptide concentration in 10 mM phosphate buffer at pH 7.4.

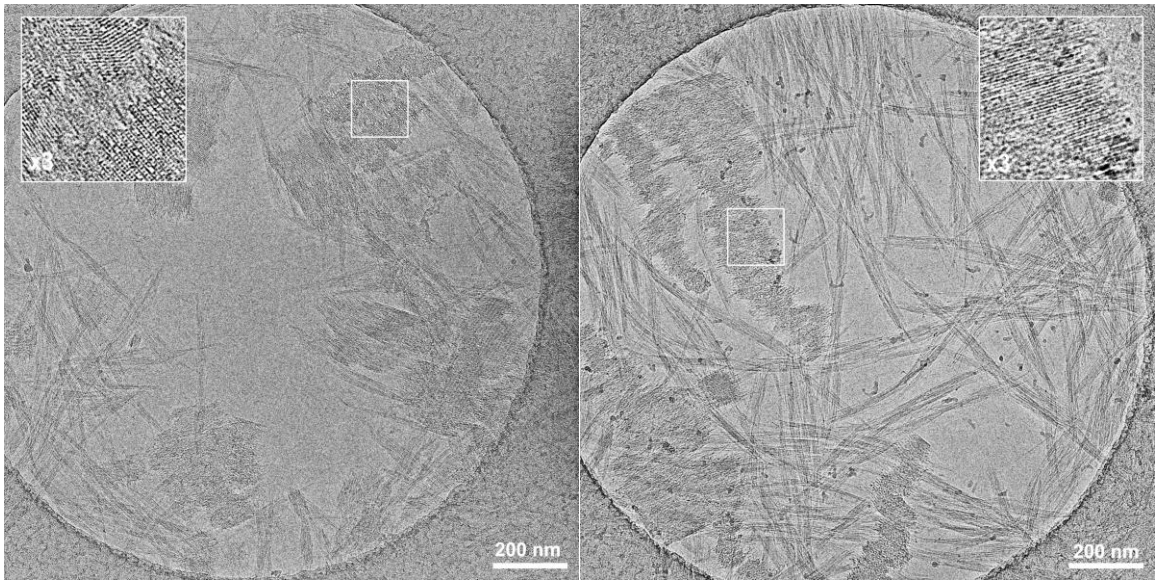

Figure 29: Cryo-TEM images of Acid-CFLE/B3β2 assembly at 1 mg/mL total peptide concentration in 10 mM phosphate buffer at pH 7.4.

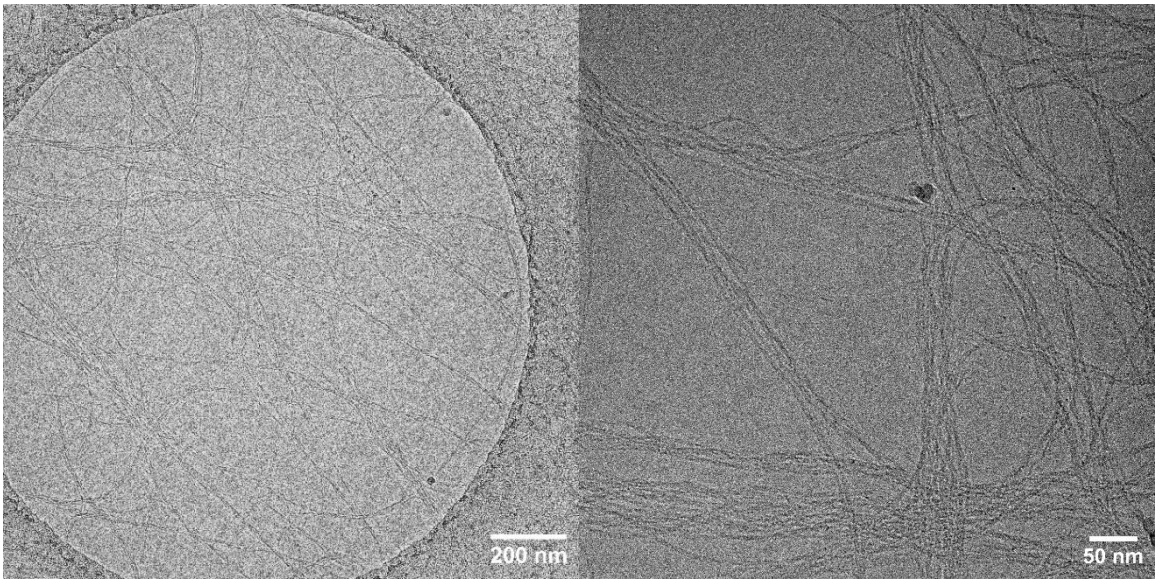

Figure 30: Cryo-TEM images of Acid-ICEF/B3β2 assembly at 1 mg/mL total peptide concentration in 10 mM phosphate buffer at pH 7.4.

All helix bundles were additionally tested for their heat stability, chemical stability to guanidinium hydrochloride (GndHCl), which acts as a chemical denaturant, and stability over time.

Thermal denaturation (Figure 31) at a wavelength of 222 nm, which is characteristic for α-helices, shows melting temperatures of >80 °C for Acid-pp/Base-pp, 76 °C for Acid-pp/B3β2γ, 63 °C for Acid-CFLE/B3β2γ, and 72 °C for Acid-ICEF/B3β2γ. Thus, the thermal stability of Acid-ICEF/B3β2γ is comparable to that of the parental acid sequence with the $\alpha/\beta/\gamma$-chimera (Acid-pp/B3β2γ), but significantly different from that of the Acid-CFLE/B3β2γ assembly. Moreover, the melting curves in the absence and presence of DTT of the two assemblies, Acid-CFLE/B3β2γ and Acid-ICEF/B3β2γ, containing the Cys/Phe-motifs were almost identical. This indicates that no oxidation of the cysteines occurred (Figure 32).

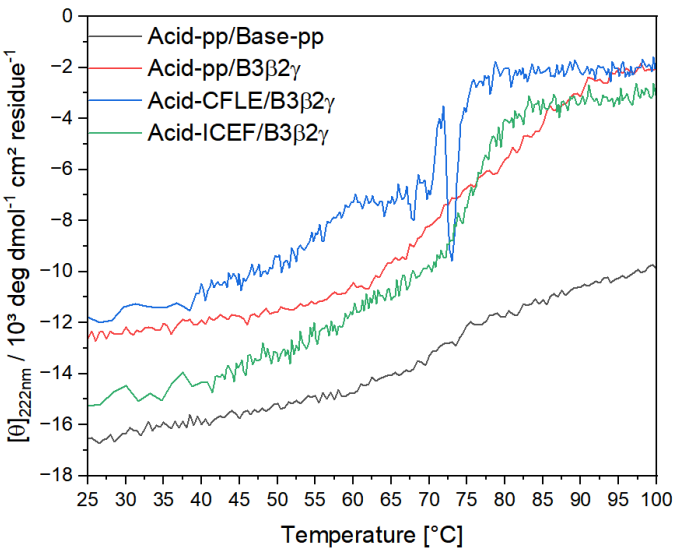

Figure 31: Melting curves of equimolar mixtures with 20 µM total peptide concentration in 10 mM phosphate buffer at pH 7.4.

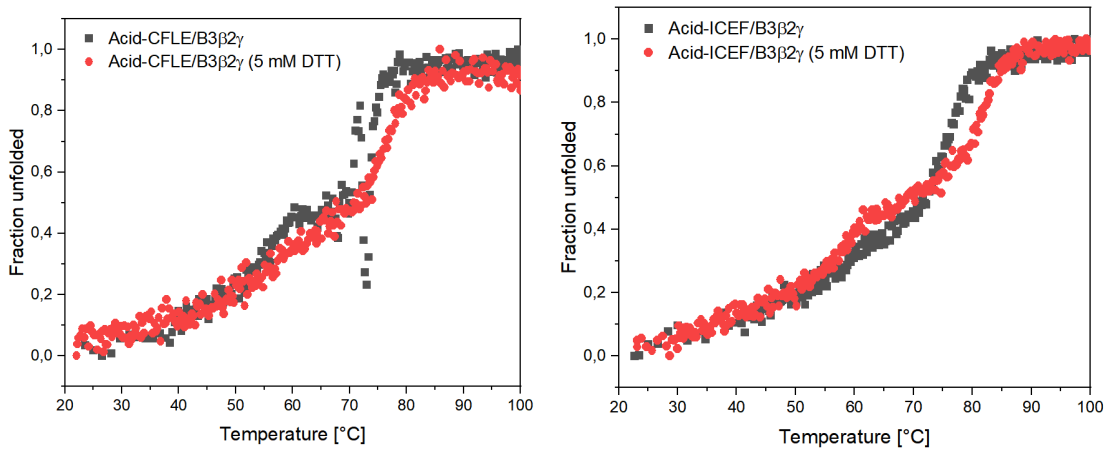

Figure 32: Thermal denaturation of Acid-CFLE/B3β2γ (left) and Acid-ICEF/B3β2 (right) in the absence of DTT and the presence of 5 mM DTT. Measurements were carried out in 10 mM phosphate buffer at pH 7.4 with 20 µM total peptide concentration of 1:1 mixtures.

Chemical denaturation varying GndHCl concentrations revealed that all helix bundles formed involving the *α/β/γ*-chimeric sequence are less stable than the parental Acid-pp/Base-pp assembly (Figure 33). Similar to the thermal stability, the Acid-CFLE/B3β2γ arrangement also exhibits the least stability. The two helix bundles of Acid-pp/B3β2γ and Acid-ICEF/B3β2γ show similar stabilities in the chemical denaturation studies, which is also comparable to the thermal denaturation experiments.

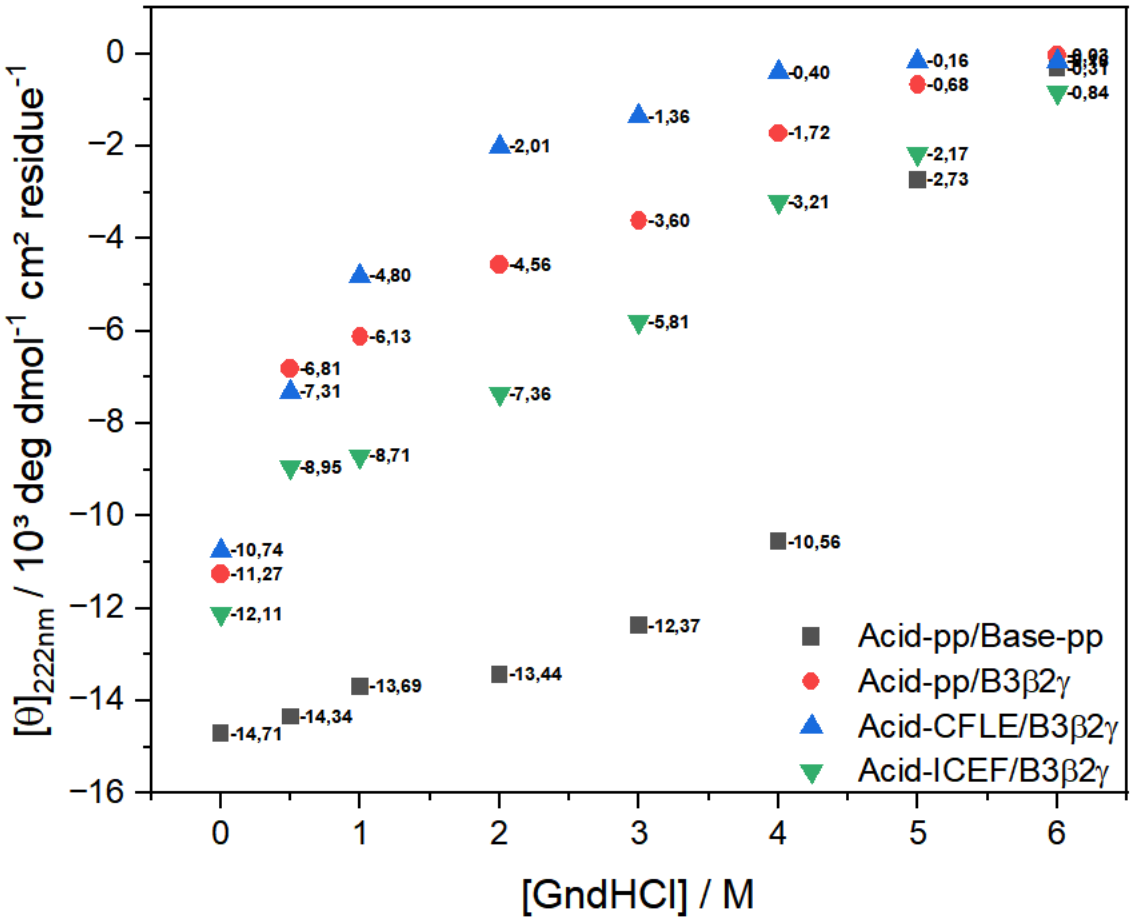

Figure 33: Chemical denaturation of all 1:1 helix bundles (20 µM total peptide concentration) with varying GndHCl concentrations in 10 mM phosphate buffer at pH 7.4.

Regarding temporal stability, all helix bundles exhibited exceptional stability for up to one week (Figure 34):

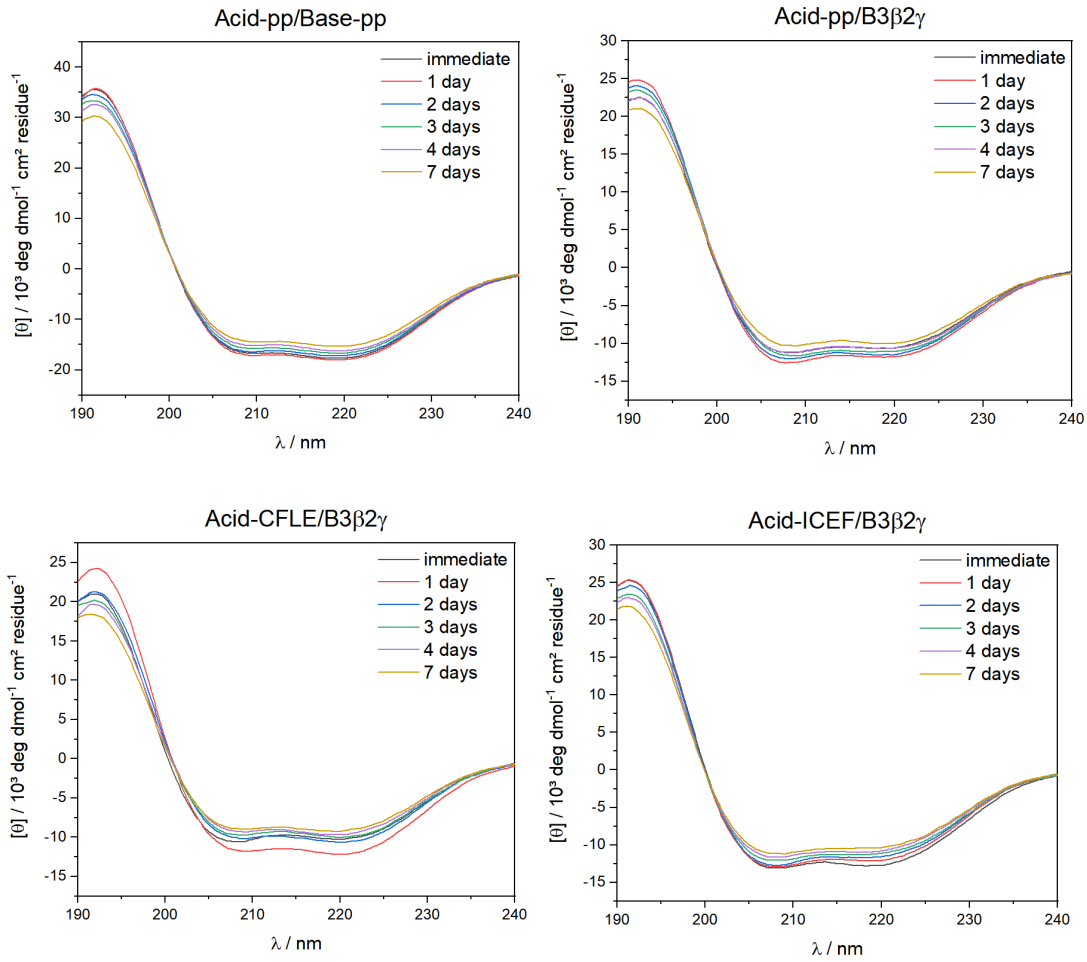

Figure 34: Stability over time when stored at room-temperature for all heterotypic assemblies at 20 µM total peptide concentration (1:1 mixtures) in 10 mM phosphate buffer at pH 7.4.

The temporal stability of the Cys/Phe-motif containing helical assemblies of Acid-CFLE/B3β2γ and Acid-ICEF/B3β2γ was tested in the absence of the reducing agent. However, after one day, a more significant increase in helicity can be observed for the Acid-CFLE/B3β2γ assembly, indicating different dynamics within this system. The same could not be observed for the Acid-ICEF/B3β2γ helix bundles.

In conclusion, the two acid sequences with the Cys/Phe-motifs differ in their properties and thermal and chemical stability when combined with B3β2γ. The formed supramolecular structures also suggest significant differences between the two helical assemblies of Acid-CFLE/B3β2γ and Acid-ICEF/B3β2γ. The quaternary

structures of both systems differ substantially from the combination of the parental acid strand with B3β2γ, as the Acid-pp/B3β2γ system shows high similarity to the parental combination of Acid-pp/Base-pp in the cryo-TEM measurements. Substitutions were performed on the cysteine to investigate its influence on stability and to further compare the properties of the two Cys/Phe-motifs with each other.

3.1.1 Substitutions on cysteine: comparative studies to the Cys/Phe-motifs

For the two Cys/Phe-motifs, the effects of incorporating cysteine in the acid strands at the *a*-position (Acid-CFLE) or *d*-position (Acid-ICEF) were explored. Cysteine in these positions was therefore replaced with either serine, aminobutyric acid (Abu), or S-methyl cysteine (*m*Cys, *m*C). The selection of these amino acids was based on the similar length of the residues but different polarity. Ser represents a polar residue and Abu involves a nonpolar side chain, both with the same side chain length as cysteine. The S-methylated cysteine variant was chosen to cap the functional thiol group of the cysteine side chain (Figure 35). Resulting properties were then compared in terms of helicity as well as thermal and chemical stability.

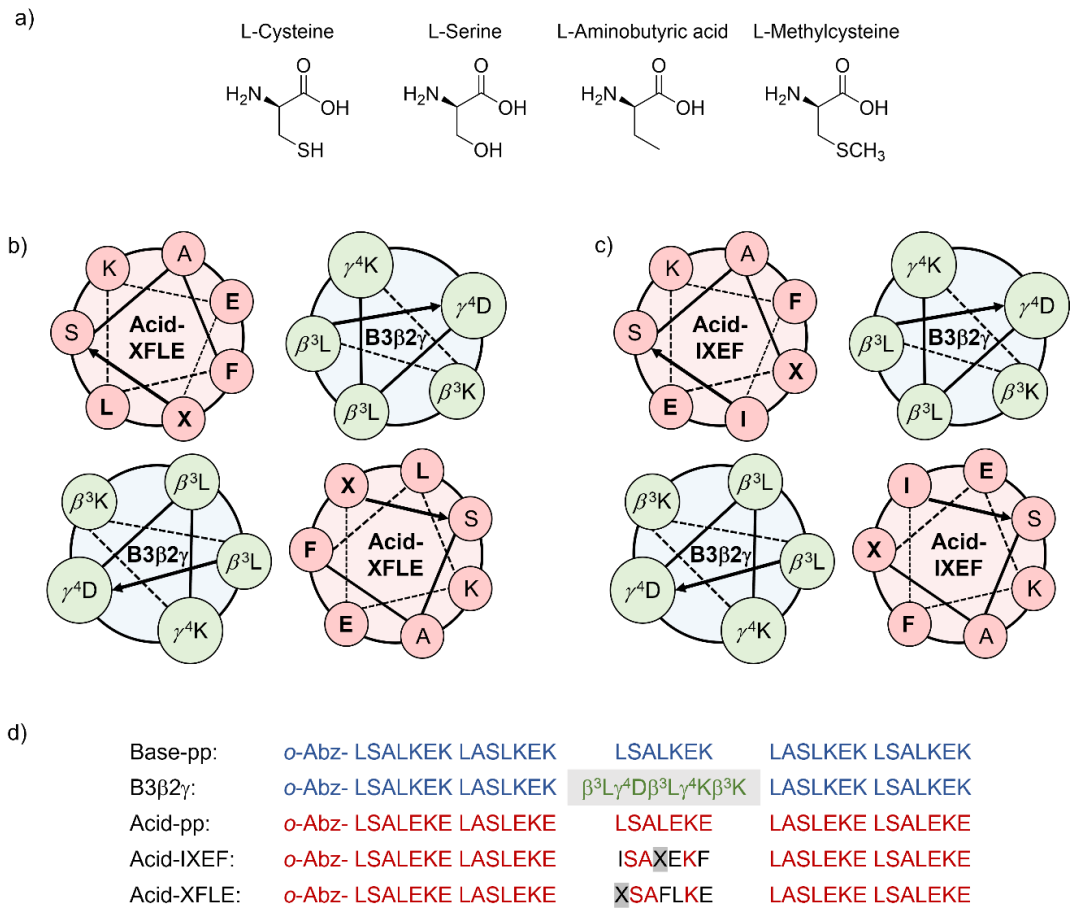

d)

Base-pp:	*o*-Abz- LSALKEK LASLKEK	LSALKEK	LASLKEK LSALKEK
B3β2γ:	*o*-Abz- LSALKEK LASLKEK	β^3Lγ^4Dβ^3Lγ^4Kβ^3K	LASLKEK LSALKEK
Acid-pp:	*o*-Abz- LSALEKE LASLEKE	LSALEKE	LASLEKE LSALEKE
Acid-IXEF:	*o*-Abz- LSALEKE LASLEKE	ISAXEKF	LASLEKE LSALEKE
Acid-XFLE:	*o*-Abz- LSALEKE LASLEKE	XSAFLKE	LASLEKE LSALEKE

Figure 35: a) Amino acid structures of cysteine and its substituents. b) Helical wheel model displaying the central heptad of Acid-CFLE in which cysteine was replaced and the central pentad of B3β2γ involving homologous β^3- and γ^4-amino acids. c) Helical wheel model of the central heptad of Acid-ICEF in which cysteine was replaced and the central β^3/γ^4-pentad of B3β2γ. d) Peptide sequences for the cysteine replacements. X represents either Cys, Ser, Abu, or *m*Cys. All peptides were *N*-terminally labeled with *o*-aminobenzoic acid (*o*-Abz) for concentration determination.

CD-spectroscopic measurements (Figure 36) of all monomer sequences in which the cysteines were replaced indicate disrupted helical structures with a more pronounced and shifted minimum at 202 nm and a second minimum at 222 nm, comparable to the original cysteine sequences. In all cases, the equimolar mixtures show assembly to the $\alpha/\beta/\gamma$-chimeric peptide B3β2γ by exhibiting α-helical features with two distinct minima at 208 and 222 nm. Helical bundles with B3β2γ of the three variants of Acid-XFLE incorporating either cysteine, serine, or S-methyl cysteine display similar helical content. In Acid-IXEF, however, the assembly of the serine variant with B3β2γ exhibits the lowest helical content. The most pronounced helical pattern was observed when cysteine was replaced by aminobutyric acid for both

the Acid-XFLE and Acid-IXEF variants, which resembled the properties of the parental peptide assembly (Base-pp/ Acid-pp) that only consisted of α-amino acids.

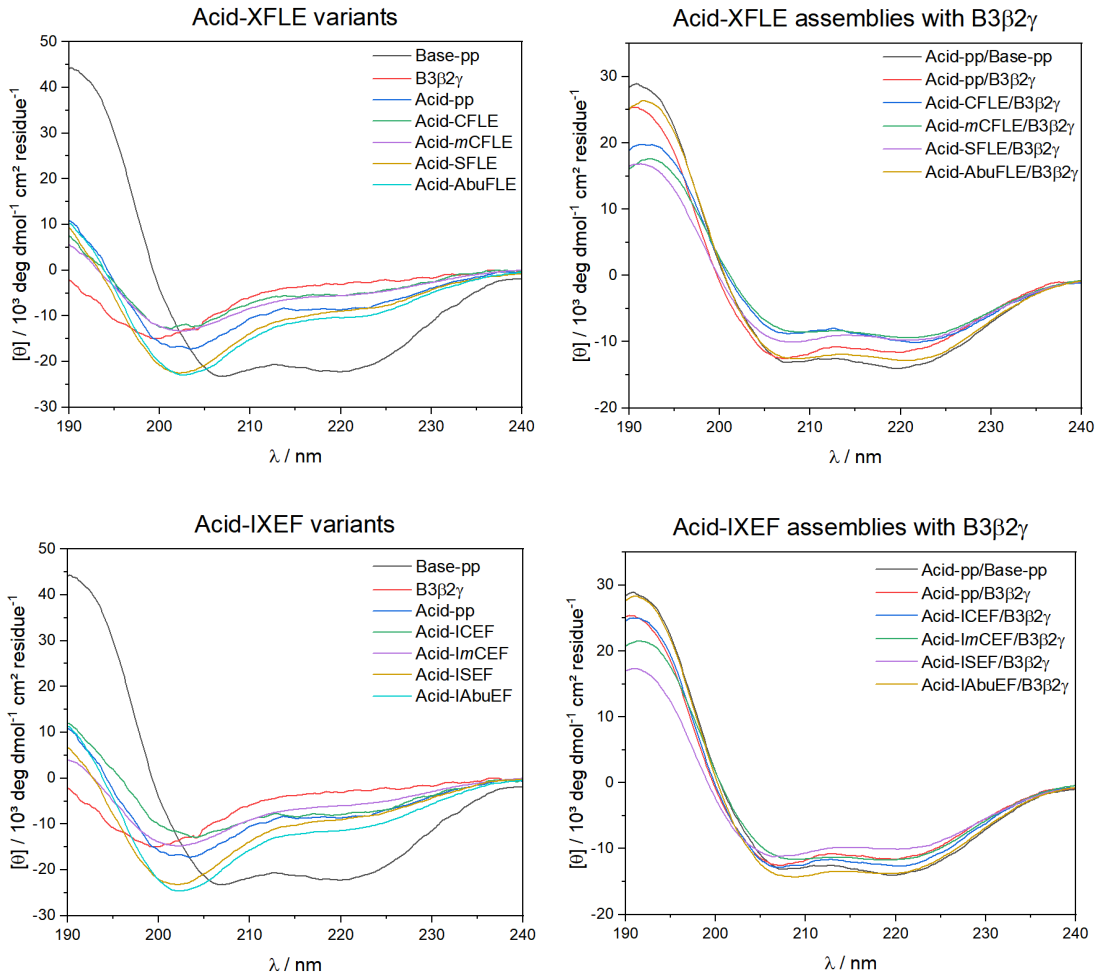

Figure 36: CD-spectroscopic measurements of the Acid-XFLE and Acid-IXEF variants (20 µM) and as a 1:1 mixture with B3β2γ (20 µM total peptide concentration) in 10 mM phosphate buffer at pH 7.4. X represents either Cys, Ser, Abu, or *m*Cys.

A decrease in thermal stability is observed for both the XFLE- and IXEF-motifs as assembled systems with the $\alpha/\beta/\gamma$-chimera when a serine mutation is made (Figure 37). The incorporation of a polar residue into both systems appears to disrupt hydrophobic core packing but does not prevent assembly with the chimera. In fact, Woolfson and co-workers previously reported that the structural properties of coiled coils do not necessarily change when a certain quantity of hydrophilic residues is introduced into the hydrophobic core, but their stability may still be altered.[156]

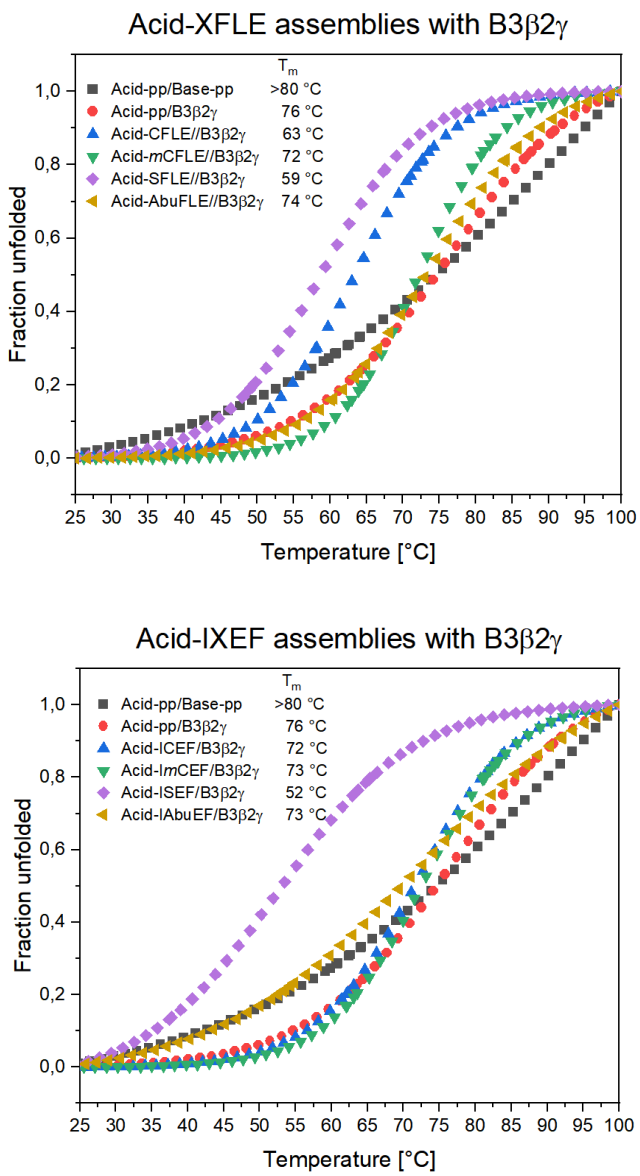

Figure 37: Comparison of normalized thermal denaturation curves of Acid-XFLE/B3β2γ (top) and Acid-IXEF/B3β2γ (bottom) at 20 µM total peptide concentration of 1:1 mixtures in 10 mM phosphate buffer at pH 7.4. The Acid-pp/Base-pp assembly does not show sigmoidal behavior, as it was not denatured at 100 °C. X represents either Cys, Ser, Abu, or *m*Cys.

Substitution of aminobutyric acid for the cysteine leads to an increase in thermal stability in the case of the heterotypic assemblies with B3β2γ involving the Acid-XFLE sequence. For the helical bundles with B3β2γ incorporating an Acid-IXEF sequence, this leads to similar stability to heat. The same applies when S-methyl cysteine is incorporated into the acid strands. Substitution of the cysteine in Acid-CFLE/B3β2γ with either aminobutyric acid or S-methyl cysteine might therefore increase the thermal stability by further increasing hydrophobicity in the

hydrophobic core with residues that do not lead to steric hindrance. Spot array analysis in previous studies from Araghi *et al.* already demonstrated the importance of hydrophobicity in assemblies with B3β2γ and that the side-chain packing was influenced by specificity toward preferred hydrophobic side chains in the *a*- and *d*-positions.[101]

Lastly, all Acid variants were also examined as equimolar mixtures with the parental base sequence (Figure 38). The assemblies Acid-CFLE/Base-pp and Acid-AbuFLE/Base-pp exhibited less pronounced minima at 208 nm and 222 nm compared to Acid-pp/Base-pp. In contrast, all heterotypic helical bundles of Base-pp with the Acid-IXEF variants, Acid-*m*CFLE/Base-pp, and Acid-SFLE/Base-pp showed no differences from the parental acid/base helix bundle.

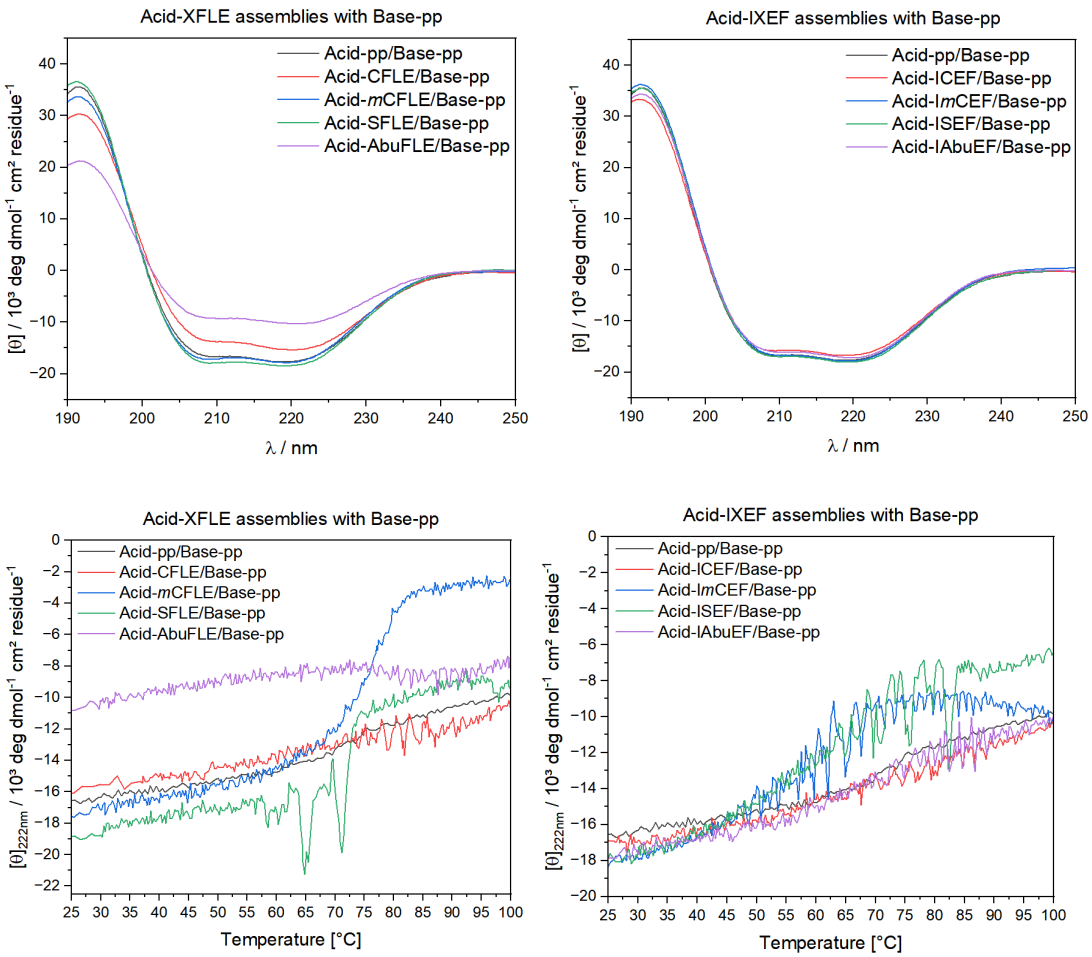

Figure 38: CD-spectroscopic measurements of the Acid-XFLE and Acid-IXEF variants as an equimolar mixture with Base-pp (20 µM total peptide concentration) in 10 mM phosphate buffer at pH 7.4 and their thermal denaturation. X represents either Cys, Ser, Abu, or *m*Cys.

All helical bundles in combination with Base-pp display high thermal stability and are not completely denatured at 100 °C, except for the Acid-*m*CFLE/Base-pp combination, which, however, has a high melting temperature of approximately 75 °C. Accordingly, in contrast to the $\alpha/\beta/\gamma$-chimera, the parental base sequence appears to be less sensitive to changes in the complementary acid strand in the central heptad.

After comparing both Cys/Phe-motifs by experimental approaches and thus substitutions on the cysteine, a variety of methods were applied in the following to obtain high-resolution structural information about these motifs.

3.1.2 NMR Spectroscopy of the $\alpha/\beta/\gamma$-foldamer heterotypic assemblies with all-α-peptides

The study of coiled-coil motifs using NMR spectroscopic methods has been extensively used to obtain high-resolution structural information about the oligomerization interface formed in the core of the complex.[157] This would allow the investigation of the molecular interactions that drive the formation of helical bundles and contribute to the structural integrity of the $\alpha/\beta/\gamma$-chimera in assembly with all-α-complementary sequences in solution. In this way, a structural understanding of the quaternary structure formation could be acquired.

Due to the large number of charged residues serving the high solubility and the stable conformation of coiled coils over a wide pH range, it is advantageous to pursue structural studies through NMR spectroscopy. However, the repetitive nature of the primary sequence may lead to aggregation at concentrations required for structural elucidation by NMR in solution, which is about 1 mM. Acquisition of high-frequency spectra is, therefore, necessary to maximize the resolution of coiled coils in solution and to enable a high number of ^{1}H-NMR assignments required for structural elucidation. Lindhout *et al.* have listed several factors that must be considered for heterotypic coiled coil designs to be suitable for structure determination by NMR in solution: 1) they must have a binding constant of suitable strength so that only one species can be detected in solution, 2) the system must have adequate stability in solution, and 3) the associated system must be of a

suitable size, i.e., molecular weight, to allow sufficiently narrow linewidths for unambiguous assignment of NMR spectral data sets.[158]

Solution NMR spectroscopic measurements were carried out in collaboration with Prof. Dr. Heiko M. Möller from the Universität Potsdam by M.Sc. Nikolai Klishin.

^{1}H 1D-NMR as well as ^{1}H-^{1}H TOCSY, ^{1}H-^{15}N- and ^{1}H-^{13}C heteronuclear single quantum correlation (HSQC) 2D-NMR spectroscopic measurements were performed.

Figure 39 shows the solvent-suppressed ^{1}H-NMR spectra of the monomeric peptide sequences. The ^{H}N-backbone region of Base-pp in the low-field exhibits a different chemical shift that appears upshifted compared to the other peptides. This can be attributed to the different secondary structure of Base-pp in which the amides of the backbone and the amine groups of lysine are involved in H-bonding networks. In section 3.1, the CD-spectroscopic measurements showed that the Base-pp sequence forms an α-helical secondary structure. Conversely, the other monomeric peptide sequences displayed either distorted α-helices or random coil for B3β2γ. Significant broadening of the amide region is observed for Base-pp, and the same is valid for Acid-pp, Acid-CFLE, and Acid-ICEF. B3β2γ has sharper peaks that could originate from the backbone amides of the central β^3/γ^4-pentad. Furthermore, Acid-CFLE and Acid-ICEF indicate additional aromatic peaks for phenylalanine present in the sequence. Considering the upfield region, this is also markedly broadened in all cases. However, the methyl region of B3β2γ also reveals sharper peaks, which could be due to the additional methyl groups in the backbone of the homologous β^3-and γ^4-amino acids.

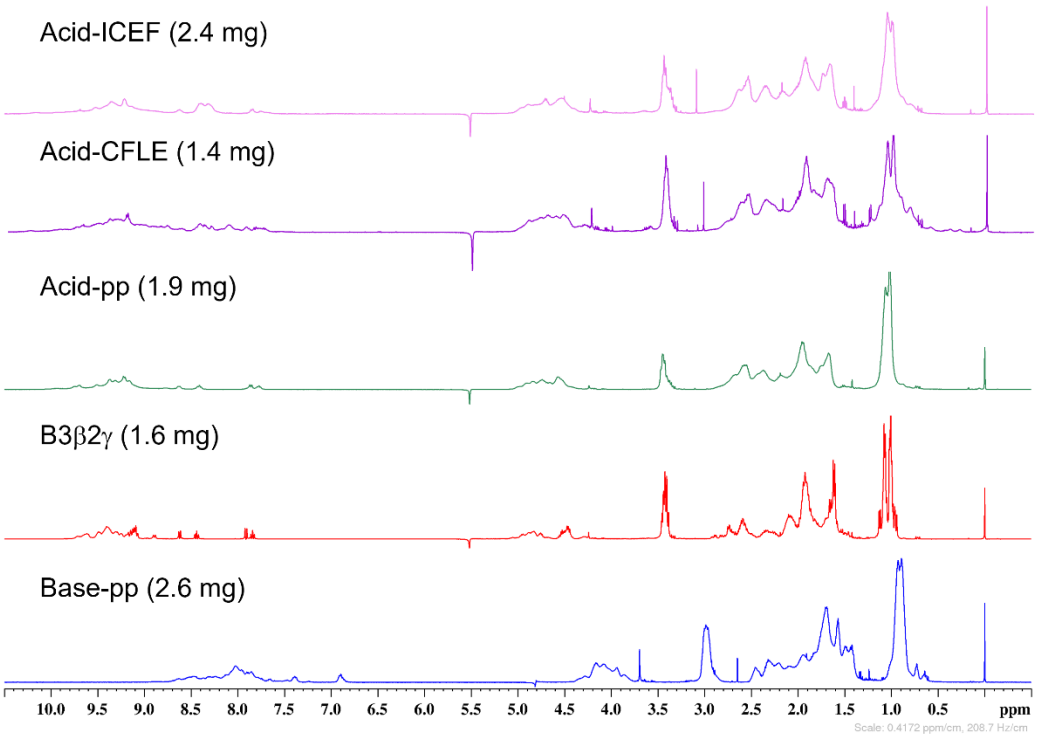

Figure 39: ^{1}H-NMR spectra of the monomeric peptide sequences in NMR buffer containing 100 mM phosphate buffer at pH 7.4, 20 mM potassium fluoride (KF), 0.1 mM sodium trimethylsilylpropanesulfonate (DSS), 4 mM sodium azide (NaN_3) and 5% deuterated water (D_2O). Measurements were performed at 298 K and referenced to DSS.

^{1}H-^{15}N-HSQC with a natural abundance of ^{15}N isotopes within Base-pp revealed a chemical shift dispersion of 1 ppm (Figure 40). This limited dispersion presumably reflects the aforementioned α-helical secondary structure of the peptide. While partial assignment of some amino acids was possible using natural abundance ^{1}H-^{13}C-HSQC spectra, as shown in Figure 41, most spectral regions were highly crowded, complicating data assignment without double-labeled ^{15}N and ^{13}C peptide samples. The study of highly repetitive peptide sequences presents a particular challenge for NMR spectroscopy, even when isotopically labeled peptides are used. This can be attributed to the highly overlapping signals arising from the similar environments of the nuclei. Therefore, assigning these signals and determining the structure of unlabeled monomeric heptad-repeat sequences with natural ^{15}N and ^{13}C abundance is extremely difficult.

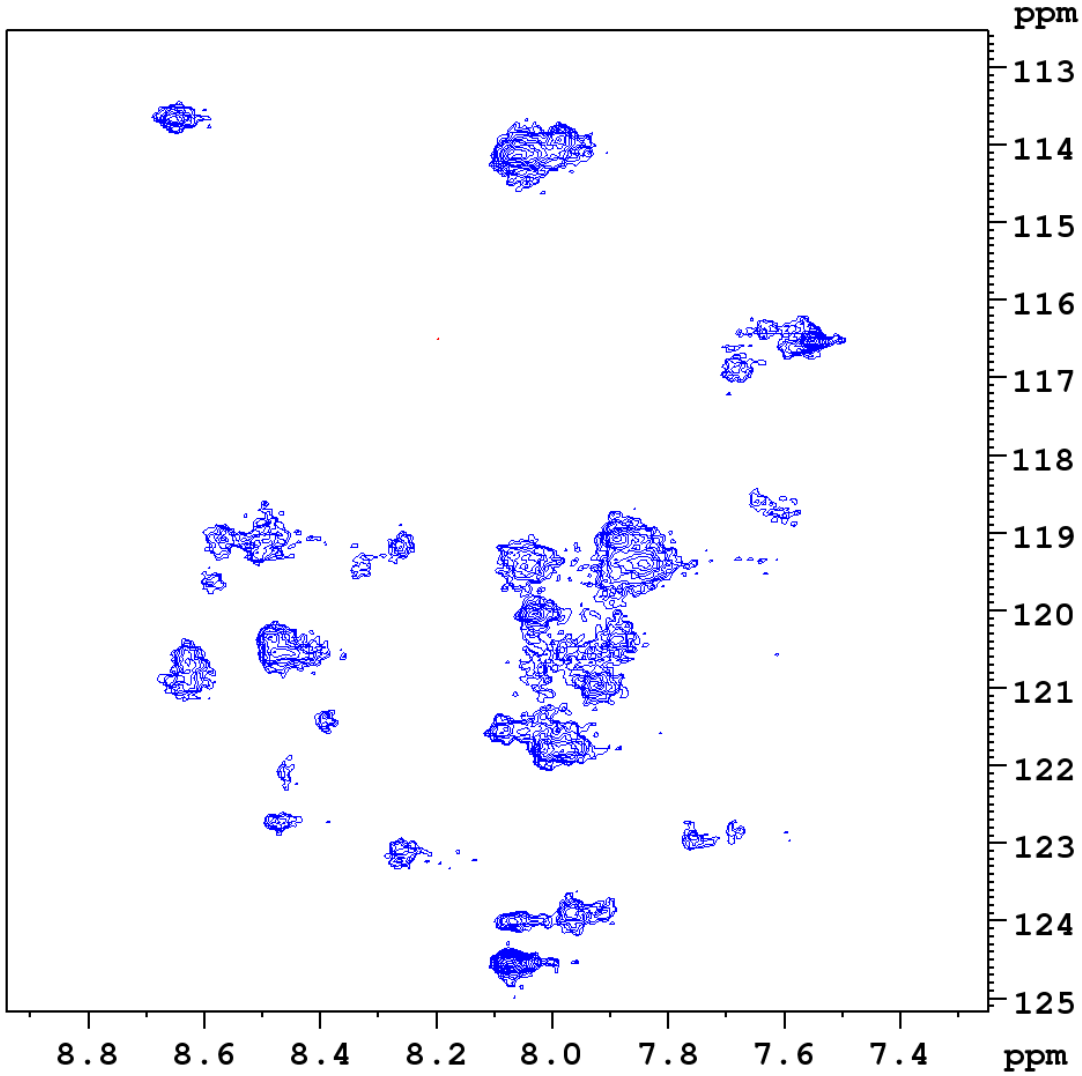

Figure 40: ^{1}H-^{15}N-HSQC spectrum of Base-pp (2.4 mg) in NMR buffer containing 100 mM phosphate buffer at pH 7.4, 20 mM potassium fluoride (KF), 0.1 mM sodium trimethylsilylpropanesulfonate (DSS), 4 mM sodium azide (NaN_3) and 5% deuterated water (D_2O). Measurements were performed at 298 K and referenced to DSS.

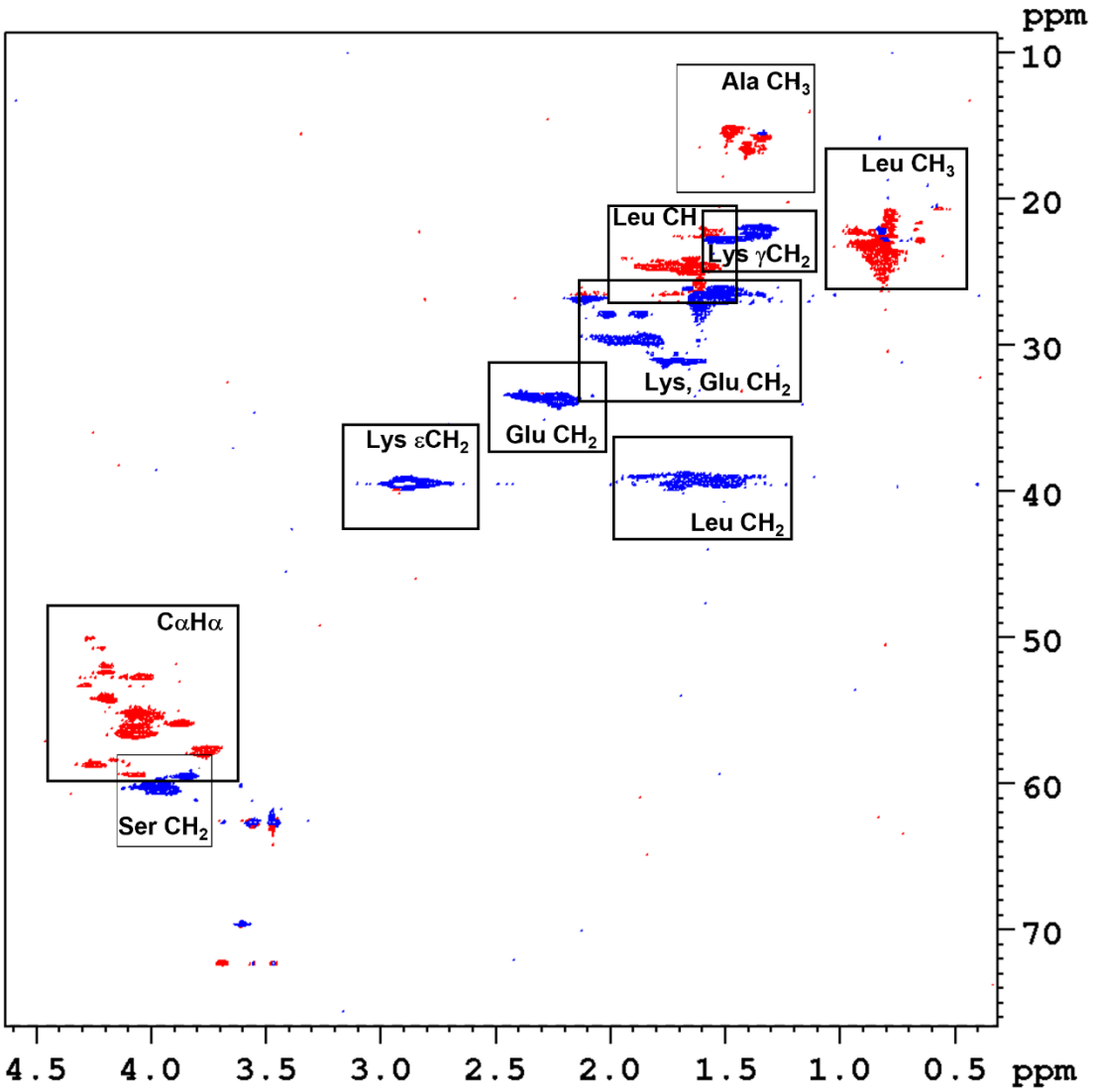

Figure 41: ^{1}H-^{13}C-HSQC spectrum of Base-pp (2.4 mg) in NMR buffer containing 100 mM phosphate buffer at pH 7.4, 20 mM potassium fluoride (KF), 0.1 mM sodium trimethylsilylpropanesulfonate (DSS), 4 mM sodium azide (NaN_3) and 5% deuterated water (D_2O). Measurements were performed at 298 K and referenced to DSS.

^{1}H-NMR spectra of the heteroassemblies Acid-pp/Base-pp, Acid-pp/B3β2γ, Acid-CFLE/B3β2γ, and Acid-ICEF/B3β2γ are shown in Figure 42. However, line broadening, most likely attributed to nonspecific quaternary interactions of different species and fast dynamics, resulted in insufficiently resolved spectra of the associated systems and greatly impeded assignment. Precipitation was observed, due to the formation of α-fibers, supporting the assumption of high dynamics and the presence of different associative species. The cryo-TEM measurements in section 3.1 already revealed not only the formation of α-fibers, but also the

tendency of the α-fibers to form supramolecular structures in the case of the Acid-CFLE/B3β2γ and the Acid-ICEF/B3β2γ assemblies. The addition of 2,2,2-trifluoroethanol (TFE) could be used to break all these higher molecular weight dynamics and allow the abundance of discrete tetramer species in solution,[158] but this would require finding suitable conditions that do not affect heterotypic tetramer association, and desirable studies under physiological conditions would need to be varied.

In addition, potentially repulsive electrostatic interactions of similarly charged residues may lead to further dynamics, especially during the investigation of the monomeric peptide sequences of Base-pp, B3β2γ, Acid-pp, Acid-CFLE or Acid-ICEF. Acetylation of the *N*-termini and uncharged amide *C*-termini could attenuate these effects to some extent.[158]

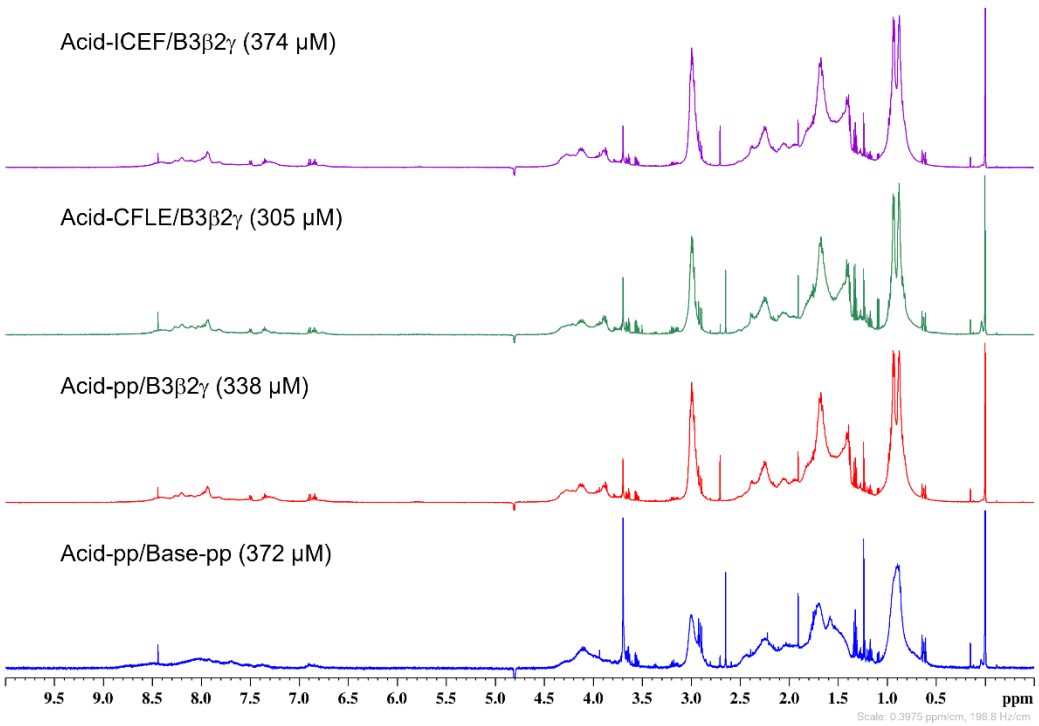

Figure 42: ^{1}H-NMR spectra of the equimolar peptide mixtures in NMR buffer containing 100 mM phosphate buffer at pH 7.4, 20 mM potassium fluoride (KF), 0.1 mM sodium trimethylsilylpropanesulfonate (DSS), 4 mM sodium azide (NaN_3) and 5% deuterated water (D_2O). Measurements were performed at 298 K and referenced to DSS.

To gain deeper insight into the behavior of the Acid-CFLE/B3β2γ bundle, ^{1}H-NMR spectra were acquired at different temperatures (277 K, 298 K, and 340 K), as depicted in Figure 43. While the aromatic and aliphatic regions of the spectra exhibited uniform patterns, the amide region displayed a temperature-dependent behavior, as shown in Figure 44. In particular, at 277 K, the amide signals possessed a broader range when compared to higher temperatures, indicating that the assembly is more rigid at this temperature. At 340 K, a significant signal broadening is observed, which could be attributed to a chemical exchange between the amide protons and water molecules.

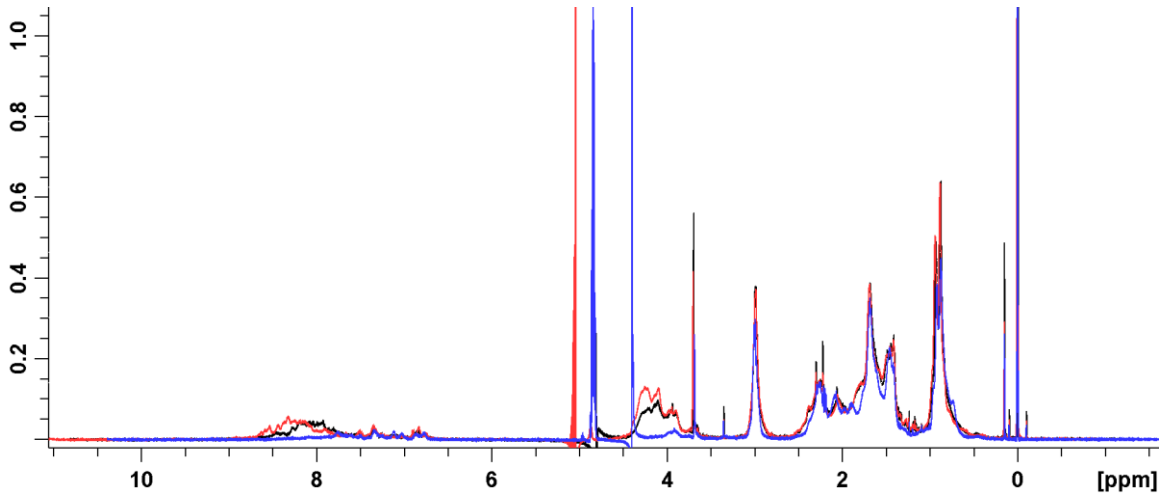

Figure 43: ^{1}H-NMR spectra at different temperatures of the equimolar peptide mixture Acid-CFLE/B3β2γ (305 µM) in NMR buffer containing 100 mM phosphate buffer at pH 7.4, 20 mM potassium fluoride (KF), 0.1 mM sodium trimethylsilylpropanesulfonate (DSS), 4 mM sodium azide (NaN_3) and 5% deuterated water (D_2O). Measurements were referenced to DSS. The red curve corresponds to a temperature of 277 K, black to 298 K, and blue to 340 K.

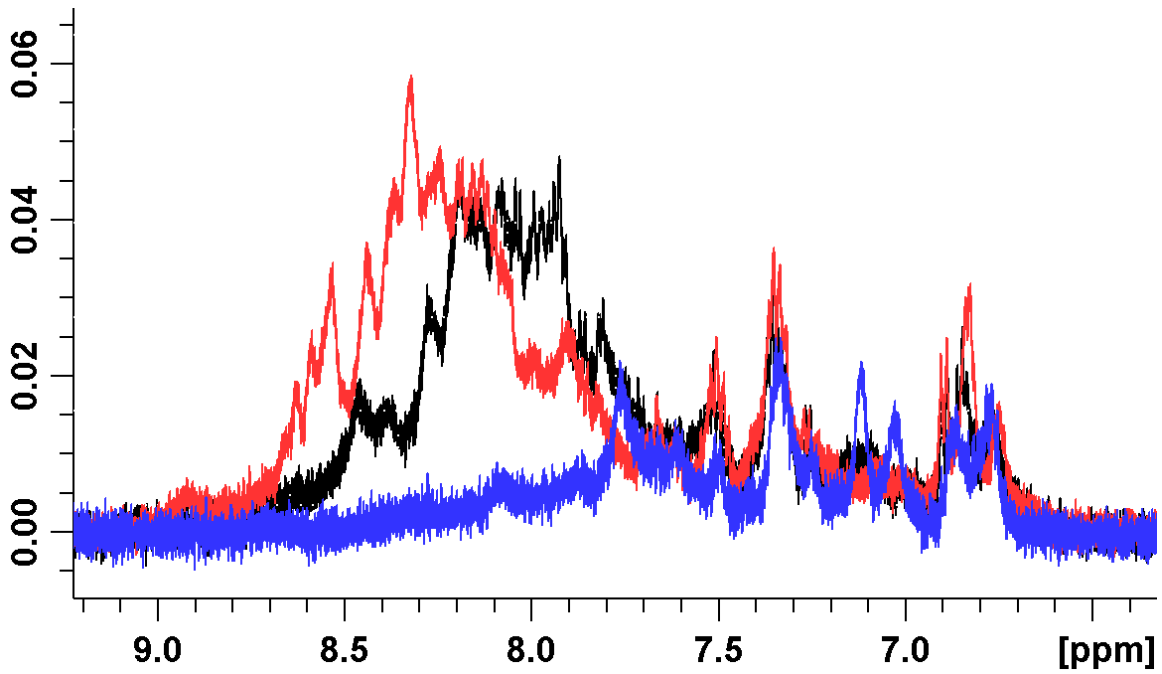

Figure 44: Amide region of the ^{1}H-NMR spectra at different temperatures of Acid-CFLE/B3β2γ (305 µM) in NMR buffer containing 100 mM phosphate buffer at pH 7.4, 20 mM potassium fluoride (KF), 0.1 mM sodium trimethylsilylpropanesulfonate (DSS), 4 mM sodium azide (NaN_3) and 5% deuterated water (D_2O). Measurements were referenced to DSS. The red curve corresponds to a temperature of 277 K, black to 298 K, and blue to 340 K.

In general, a high degree of chemical shift redundancy was observed in the ^{1}H- and 2D-spectra as a result of the highly repetitive primary sequences. Figure 45 shows the ^{1}H-^{1}H-TOCSY of Acid-ICEF/B3β2γ as a representative example (additional ^{1}H-^{1}H-TOCSY spectra of the heteroassemblies are included in the Appendix). It can be clearly seen that the high-field region, which includes the methyl- and aliphatic groups as well as the H^{α}-atoms, exhibits no separation of the signals. Hence, the identification of the cysteine side chain, for example, was not possible. In general, the chemical shift degeneracy rendered the assignment and determination of intra- or intermolecular NOE contacts emanating from the cross peaks impossible. Therefore, the chemical shift environment within the four subunits is relatively equal, leading to the observed overlapping pattern. Chemical shift degeneracy is not an atypical phenomenon in the structural analysis of coiled coils.[159] However, most of the structurally studied coiled-coil structures previously investigated by NMR spectroscopy are biologically active and thereby exhibit variations in the heptad repeats.[158,160] In addition, secondary structure determination and characterization of helical structures formed by foldameric

sequences comprising β- and γ-amino acids has been performed for relatively short peptide sequences using 2D-NMR spectroscopy. The sequences used to determine the NOE patterns involved approximately ten residues or less.[73–78,161]

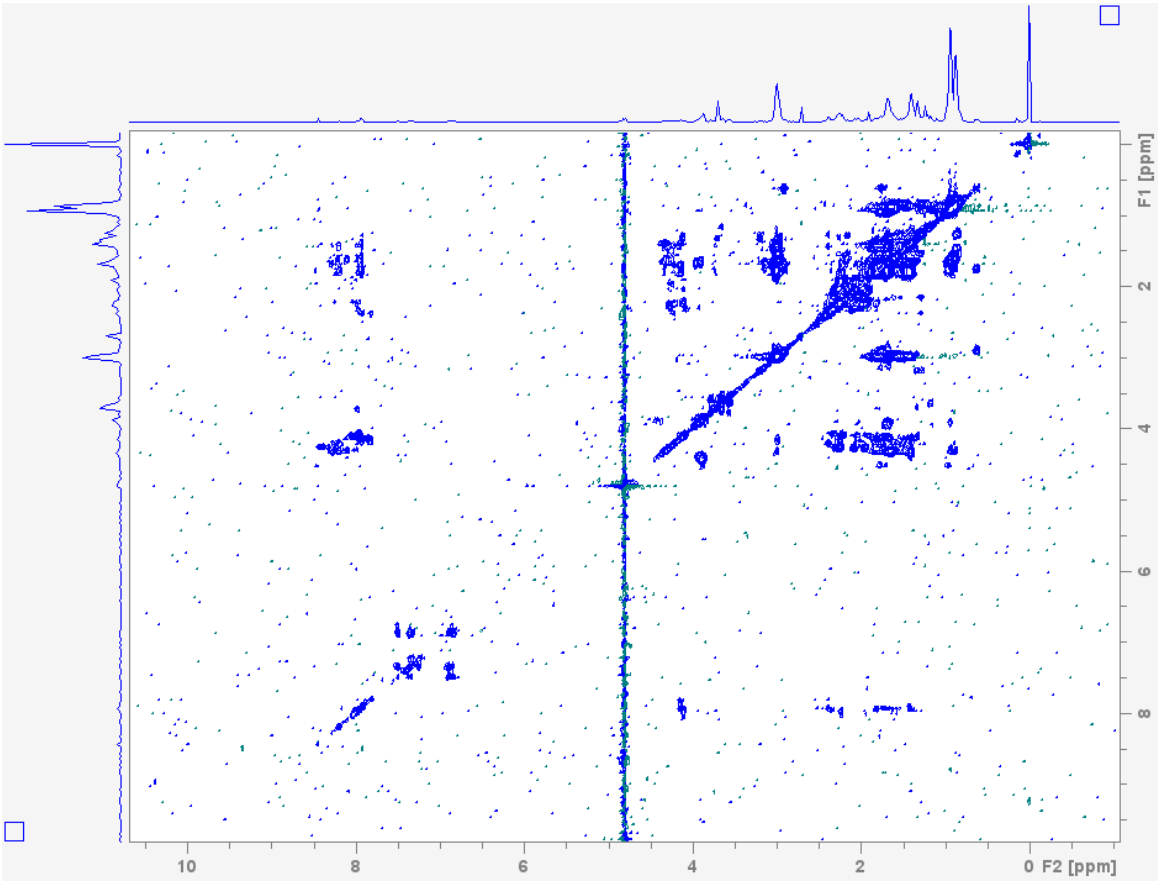

Figure 45: ^{1}H-^{1}H-TOCSY of Acid-ICEF/B3β2γ (374 µM, total peptide concentration of 1:1 mixture) in NMR buffer containing 100 mM phosphate buffer at pH 7.4, 20 mM potassium fluoride (KF), 0.1 mM sodium trimethylsilylpropanesulfonate (DSS), 4 mM sodium azide (NaN_3) and 5% deuterated water (D_2O). Measurement was performed at 298 K and referenced to DSS.

The measured heterotypic tetrameric coiled-coil designs incorporate five heptad repeats for each sequence and are comparatively too large to allow for sufficiently narrow line widths and consist largely of invariant sequence designs. A truncation to three heptads involving the central β^3/γ^4-pentad substitution of B3β2γ may have led to adequate linewidth. However, it is not known whether these truncated peptide sequences would associate and acquire appropriate stability. It has been already shown that the chemical stabilities (based on GndHCl denaturation experiments) are significantly diminished (see Section 3.1) for the assemblies involving B3β2γ in the original primary sequence when compared to the parental

Acid-pp/Base-pp system. In addition, the peptide sequences were not isotopically labeled, which further aggravated resolution due to the low natural abundance of ^{13}C and ^{15}N isotopes of 1.11%[162] and 0.366%,[163] respectively. This could not be improved through HSQC measurements with more than 100 scans. Labeling of peptide sequences for NMR spectroscopic measurements can be achieved by bacterial expression involving isotope-labeled media. However, expression of the $\alpha/\beta/\gamma$-chimeric sequence is not straightforward because manipulation of genetic code[68] would be required to incorporate the central β^3/γ^4-module of B3β2γ. Moreover, the introduction of isotopically labeled amino acids through the solid-phase peptide synthesis methodology involves escalating costs and relatively low yields, which proves to be an unviable option.[164] Searching the PDB database for coiled-coil structures yields mainly data based on crystal structures. In contrast, NMR data are rarely found. This indicates the immense difficulties associated with the study of coiled coils in solution by NMR spectroscopy.

All in all, the current designs of the heterotypic tetrameric coiled coils do not appear to be suitable for NMR spectroscopic investigation in order to obtain structural data information. Therefore, further methods were applied to obtain structural information on the two Cys/Phe-motifs in assembly with B3β2γ.

3.1.3 Vibrational sum-frequency generation spectroscopy: investigating the thiol region of the Cys/Phe-motifs of all-α-peptides in assembly with B3β2γ

The tendency of heterotypic coiled-coil systems to form α-fibers greatly complicates the structural investigation of the Cys/Phe-motifs in assembly with B3β2γ. Vibrational SFG can provide structural information (see Section 1.4) on coiled-coil systems at the air/water interface at a concentration range equivalent to that used for CD-spectroscopy. The synthesized peptides exhibit surface activity and are thus well-suited for this type of measurement. In addition, the molecular data that are generated are not perturbed by the solvent.[147,148] Hence, the study of the thiol absorption of the assemblies that incorporate the Cys/Phe-motifs was aimed at using this method. However, the physiochemical environment of the

air/water interface that differs from the bulk phase may alter their molecular structure.[148] To exclude these changes, the preservation of helical structures at the amide I region was investigated and complemented by FT-IR measurements of the bulk phase. Classical FT-IR measurements proved to be unsuitable to study the thiol band in our experiments because very high concentrations are required, and the background signals of the bulk medium significantly interfered with the measurements. In addition, the strong bending vibration of water near 1640 cm^{-1} correlated with the amide I region and led to problems with solvent subtraction in the first measurement trials.[165] Therefore, on the one hand, deuterated buffer solution was used, and on the other hand, 10-fold higher concentrations were used to measure the FT-IR amide I region than those used for the vibrational SFG measurements. Moreover, the 10-fold higher concentrations led to precipitation and thus the measurement of assemblies that had formed α-fibers and/or supramolecular structures.

Vibrational SFG data were generated in collaboration with Prof. Dr. Björn Braunschweig from the Westfälische Wilhelms-Universität Münster by M.Sc. Dana Glikman and FT-IR measurements were performed in collaboration with Dr. Marius Horch from the Freie Universität Berlin by M.Sc. Cornelius Constantin Maria Bernitzky.

The amide I region is the most sensitive spectral region to protein and peptide secondary structure and arises mainly from the C=O stretching vibration of the amide group with minor contributions from the out-of-phase stretching vibration of the C-N bond, CCN deformation, along with in-phase bending of the N-H bond. These amide I vibrations in the region between 1700-1600 cm^{-1} are directly correlated with the backbone conformation, and certain secondary structural features are associated with each frequency. Therefore, the amide I region is most commonly used for secondary structure analysis. The corresponding band positions for α-helices can be found in the region between 1648-1657 cm^{-1} and in D_2O between 1642-1660 cm^{-1}.[166–168]

In both measurements, the vibrational SFG spectroscopic measurement (Figure 46, top) and the FT-IR measurements (Figure 47), the helical secondary structural features of the heterotypic assemblies are preserved. The vibrational

SFG spectra show a maximum at approximately 1649 cm^{-1} and the FT-IR measurements show a broad absorption around 1643 cm^{-1}. In the FT-IR spectra, absorption contributions are seen over a comparatively wide frequency range; depending on the sample, the maximum is found somewhat below what is usually reported for typical α-helices. Band shifts in the spectra might result from the change in chemical bond weights as the hydrogen atom is replaced by deuterium in H-N and H-O bonds.[167] Minor differences could be attributed to differences in the helical packing of amino acid side chains.[155] In addition, H-bonding to solvent molecules may decrease the absorption frequency.[166] The additional Raman contribution arising from the visible laser pulses during the SFG measurements may also marginally affect the differences in the shifts compared to the FT-IR measurements. However, the changes in the amide I absorption of the monomeric peptide sequences compared to the helical bundles are better seen in the vibrational SFG spectra (Figure 46, bottom). Here, Base-pp shows a maximum at around 1646 cm^{-1}, corresponding to an α-helical secondary structure. The acidic monomeric sequences display a slightly broader absorption with a red-shifted maximum at approximately 1644 cm^{-1} and some contributions in the α-helical region. B3β2γ, however, exhibits a broad absorption that differs from that of all other monomers. Comparison of these absorption patterns in the amide I region with the CD-spectroscopic measurements performed for the monomeric peptide sequences, the secondary structure features to be in good agreement. While Base-pp displayed α-helical secondary structure in the CD-measurements, the acid sequences exhibited distorted α-helical structures and B3β2γ random coil formation (see Section 3.1).

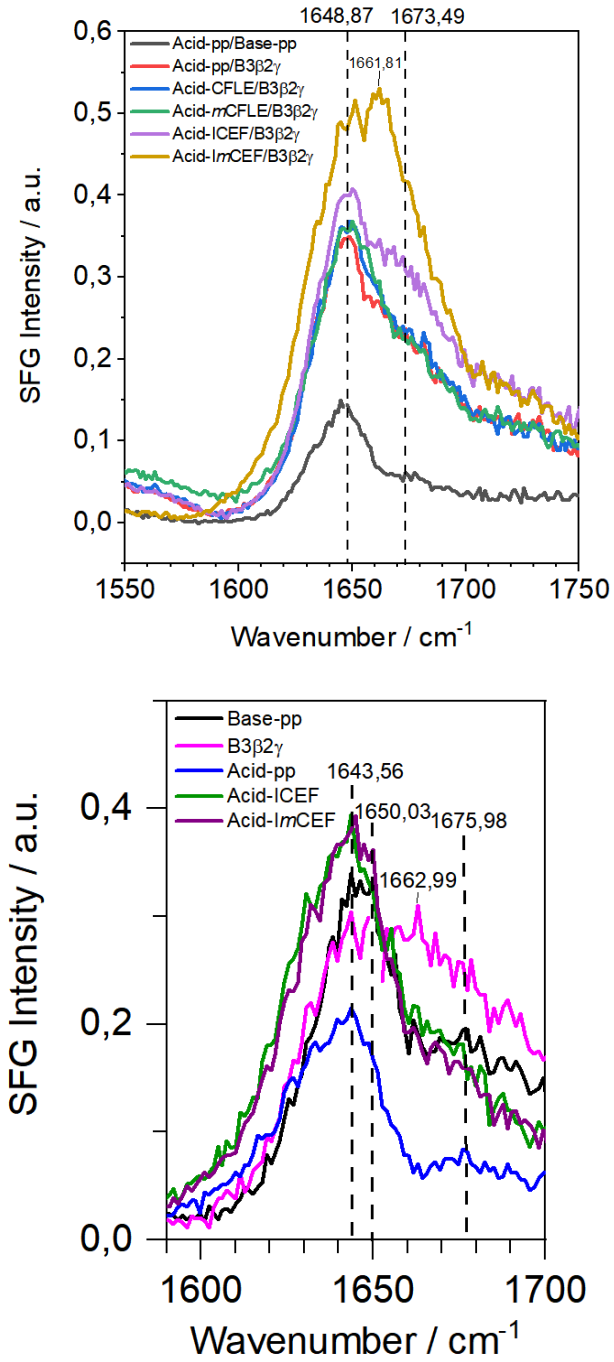

Figure 46: Vibrational SFG spectroscopic measurements at the air/water interface of the amide I region of the equimolar mixtures with 20 µM total peptide concentration (top) and the monomeric peptide sequences at 20 µM concentration (bottom) in phosphate buffer pH 7.4.

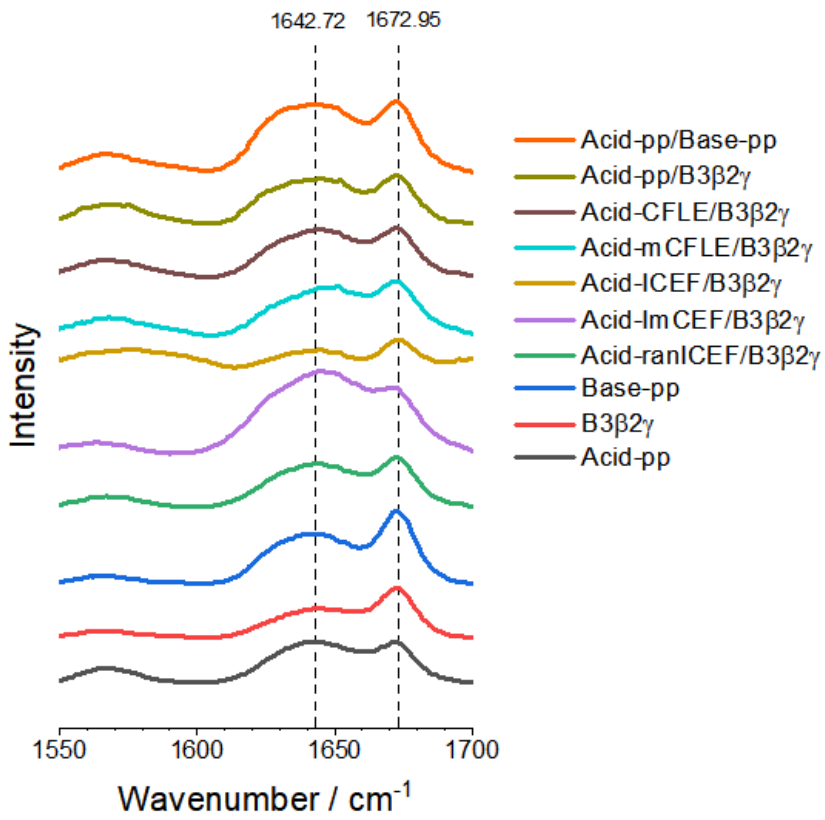

Figure 47: FT-IR spectroscopic measurements of the equimolar peptide mixtures at 200 µM peptide concentration and the monomeric peptide sequences at 100 µM peptide concentration in deuterated phosphate buffer at pH 7.4.

The FT-IR spectra exhibit a pronounced absorption at 1673 cm^{-1}, and this absorption is also evident in the vibrational SFG spectra, but less pronounced and broadened. This absorption at higher wavenumber is usually attributed to β-sheet structures. However, the strong COO^- vibration of trifluoroacetic acid (TFA) was found to contribute as an impurity to the amide region at 1673 cm^{-1} and should not be erroneously assigned to the amide I region.[169,170] The peptides used were synthesized and contain TFA counterions due to HPLC purification in which 0.1% TFA was added to the eluents (see Section 5.4). To prevent TFA from interfering with the amide I region, re-salting with HCl would have been beneficial.[170] The absence of β-sheet structure formation due to higher concentrations required for the FT-IR measurements was also confirmed by the cryo-TEM measurements (see Section 3.1), which showed α-fiber formation at higher concentrations. The α-fiber FT-IR measurements, only displaying α-helical structure and disregarding the 1673 cm^{-1} absorption originating from TFA, would be concordant with Szefczyk *et*

al. They reported on α/β-chimeric peptides forming homotypic coiled coils and subsequently α-nanofibers. The maxima of their attenuated total reflectance-FT-IR measurements of the peptide powders in the amide I region were also assigned to α-helical structures.[155]

Having shown that the amide I region retains the α-helical features of the coiled-coil systems at the air/water interface and that the complemented FT-IR spectra show similar features, the thiol region could be investigated by vibrational SFG spectroscopy.

The thiol region was investigated for the first time using vibrational SFG measurements. The S-H stretching vibration band, which can be observed in the range between 2500-2600 cm^{-1}, is of low intensity in IR spectroscopy. Nevertheless, this stretching vibration is known to directly reflect the nature of interactions, such as hydrogen bonding, of the S-H group with the environment of the protein/peptide and/or the medium by shifts ranging from one wavenumber to several dozen wavenumbers.[171–174] Accordingly, attempts were made to determine these shifts through vibrational SFG spectroscopy. Indeed, weak bands could be identified for the thiol region. In order to analyze the shifts of the thiol bands, the spectra were fitted considering the resonant and non-resonant part of the second-order electric susceptibility $\chi^{(2)}$.[175] The parameters for the fitting are included in the Appendix.

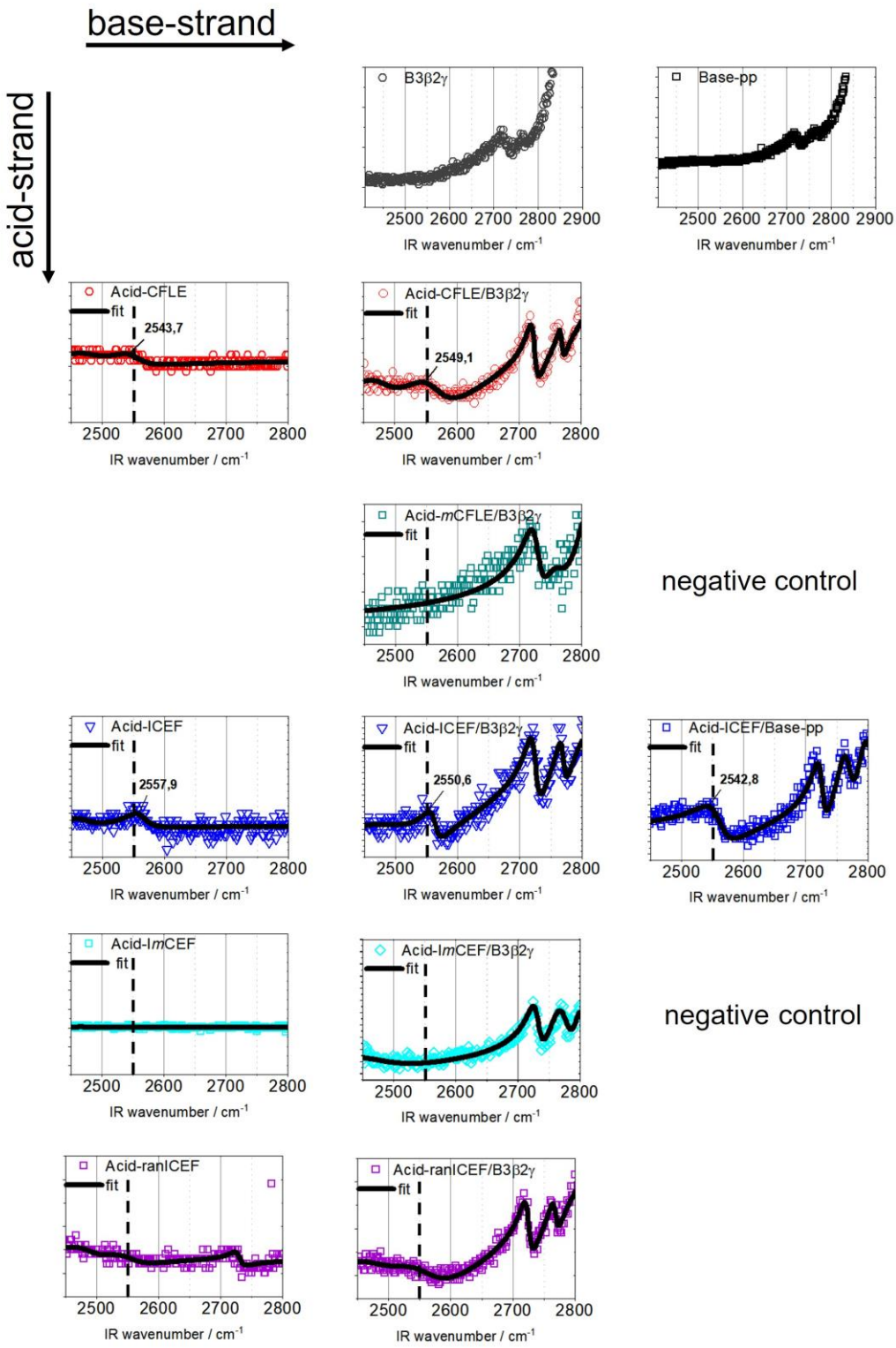

Figure 48: Vibrational SFG spectroscopic measurements at the air/water interface in the thiol region in 10 mM phosphate buffer at pH 7.4 with 20 µM monomeric peptide concentration or 20 µM total peptide concentration for equimolar peptide mixtures. The vertical column on the left includes the acidic peptide sequences and the top row lists the monomeric basic peptides. The mixtures are shown in the row as a cross to the corresponding acid sequence and the base peptide. Negative controls are highlighted with a label on the right for the corresponding row.

Figure 48 shows the vibrational SFG spectroscopic measurements in the thiol region. Both base strands, the parental base strand and the $\alpha/\beta/\gamma$-chimera show no absorption in the thiol region, as expected. However, the three absorption bands in the region above 2700 cm^{-1} appear to be characteristic for both base strands, since they are preserved in the measurements of the mixtures but are not present for the acid sequences. They could originate from C-H stretches that are highly red-shifted due to conformational constraints. The thiol bands are found for all cysteine-containing sequences, but for the randomized ICEF sequence (Acid-ranICEF) it is barely visible. This can be attributed to several possible reasons: It could be partly oxidized, or disulfide formation or NOS-bridging to the highly abundant lysine side chains[176] in the sequences might have occurred, or it could be due to weak saturation of the air/water interface. The methylated variants of the Cys/Phe-motifs served as negative controls either as monomers or as mixtures with B3β2γ and showed no absorption in the thiol region. The Acid-CFLE/B3β2γ combination displays a blue-shift of the thiol band compared to its monomer. In contrast, the Acid-ICEF/B3β2γ mixture is red-shifted by approximately seven wavenumbers compared to the Acid-ICEF. This downshift in wavenumber indicates H-bonding in Acid-ICEF/B3β2γ. However, the combination of Acid-ICEF and Base-pp leads to a stronger red-shift of about 15 wavenumbers and thus stronger H-bonding. Here, the red-shifts are also associated with a higher absorption, which is a characteristic phenomenon for the thiol band. Thus, the observation of shifts in the S-H vibration correlates with structural changes in the vicinity of the thiol group (Figure 49).[177]

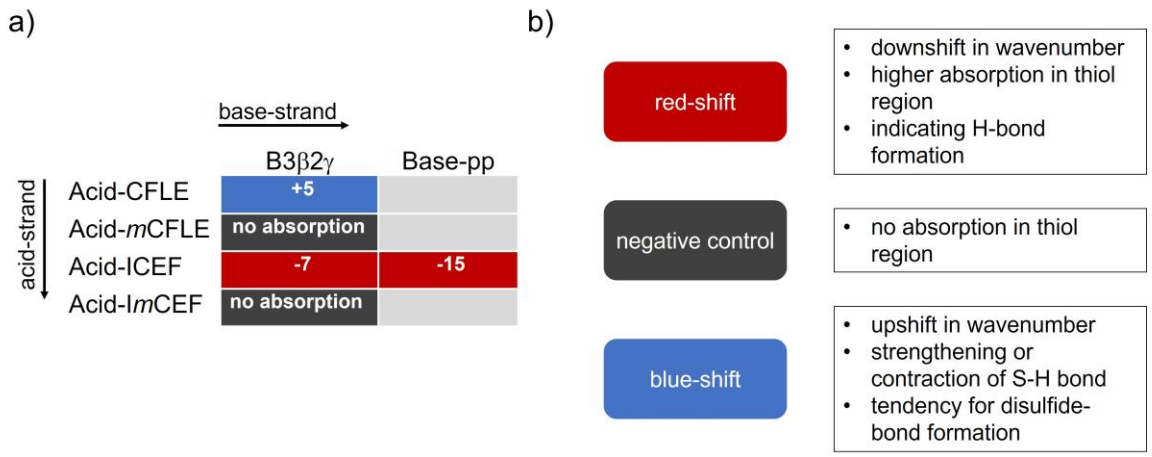

Figure 49: a) Schematic summary of the shifts in the thiol region of the peptide mixtures during the vibrational SFG measurements at the air/water interface. The vertical column on the left includes the acidic peptide sequences and the top row lists the monomeric basic peptides. The mixtures are shown in the row as a cross to the corresponding acid sequence and base peptide. b) Color code for the shifts in the thiol region and their corresponding characteristics.

The observation that the thiol bond is involved in H-bond formation in the Acid-ICEF/B3β2γ assembly is thus in agreement with the MD-simulation performed by Nyakatura *et al.*[102] CD-spectroscopic investigations in the presence and absence of DTT for both Acid-CFLE and Acid-ICEF showed no significant differences for the monomers, the mixtures, and the thermal denaturation of the mixtures with the *α/β/γ*-chimeric sequence (see Section 3.1). This indicates that the thiol groups in the hydrophobic core of the assemblies are not disulfide-bonded. The Woolfson group reported on two hexameric peptide coiled-coil assemblies involving cysteine in different *a*-positions that are not disulfide-linked in their crystal structures.[178] Tamogami *et al*. recently reported the involvement of cysteine in the interhelical H-bond interaction with aspartic acid in Acetabularia rhodopsin II.[179] In addition, hydrogen bonding involving cysteine has been shown to promote structural stability.[180,181] Nevertheless, Acid-CFLE/B3β2γ and Acid-ICEF/B3β2γ differ substantially in their thermal stability and in terms of substitutions to cysteine (see Section 3.1.1). Here, the thiol band shifts showed a red-shift and hence H-bond formation for Acid-ICEF/B3β2γ. This was not evident for the Acid-CFLE/B3β2γ mixture that displayed a blue-shift and hence a strengthening or contraction of the S-H bond. Furthermore, incubation for several hours resulted in the disappearance of the thiol absorption for the Acid-CFLE/B3β2γ system indicating a tendency for

disulfide formation. For Acid-ICEF/B3β2γ, thiol absorption was still detected. Temporal CD spectroscopic measurements in the absence of the reducing agent already revealed an increase in helicity for Acid-CFLE/B3β2γ after only one day, indicating the presumed different dynamics due to a thiol-bond formation of the cysteines. Acid-ICEF/B3β2γ, on the other hand, showed no differences in its helicity (see Section 3.1). Thus, stabilization by interhelical thiol H-bonding may be present for Acid-ICEF/B3β2γ in contrast to Acid-CFLE, which is consistent with the previous results of this thesis. Nonetheless, the influence of the increased hydrophobic core due to phenylalanine in position *g* of the Acid-ICEF sequence could also have a stabilizing effect that should not be underestimated, since hydrophobicity is known to play a key role in coiled-coil stability.[26,168] Furthermore, in the SPOT array analysis Araghi *et al.* reported a significantly higher sensitivity to changes in the *e*-position compared to the *g*-position.[101] Increasing the hydrophobic core with a bulky hydrophobic phenylalanine side chain in the *g*-position may therefore be beneficial and also further influence the higher thermal stability of the helical bundle of Acid-ICEF/B3β2γ compared to Acid-CFLE/B3β2γ.

In the following, crystallization attempts were carried out to gain further insight into the structures formed by the different heterotypic helical bundles.

3.1.4 Crystallization of the *α*/*β*/*γ*-foldamer heterotypic assemblies with all-*α*-peptides

Macromolecular crystals such as the crystals of peptides and proteins differ substantially in their properties from crystals of small molecules. Crystal structures of small molecules offer intense X-ray diffraction patterns due to their highly ordered structures and fixed lattice forces. They exhibit a hard and brittle morphology and are often insensitive to air exposure. Crystallized macromolecular systems, in contrast, provide poor diffraction properties. Because of their weak diffraction, they are measured with highly convergent X-ray sources such as a synchrotron. The crystals are very sensitive to environmental changes such as humidity and temperature and are damaged by prolonged irradiation. In addition, they are limited in size, soft, and easily crushed. The different morphology and passable diffraction properties of peptide and protein crystals can be attributed to

the high solvent content, averaging about 50%, and the numerous conformational changes that can arise. Nevertheless, this high solvent content ensures structures that do not differ greatly from those in the solution. This is what makes the crystal structure analysis of peptides and proteins so valuable.[182] Growing crystals suitable for structure determination can be a difficult and time-consuming endeavor for any protein and peptide. Coiled-coil peptides and proteins, however, have traditionally been considered particularly difficult to crystallize due to their physical properties and tendency to aggregate.[183]

Initial crystallization attempts were carried out in collaboration with Prof. Dr. Markus Wahl from the Freie Universität Berlin by M.Sc. Daniela Gjorgjevikj and as part of a joint research internship by M.Sc. Paul Anton Albrecht.

The four different hetero-assemblies Acid-pp/Base-pp, Acid-pp/B3β2γ, Acid-CFLE/B3β2γ, and Acid-ICEF/B3β2γ were crystallized using the sitting drop vapor diffusion method. An examination of the crystal structures should serve to elucidate the structural differences between the Cys/Phe-motif-containing assemblies of the acidic peptide strands with the chimeric base strand compared to the parental acidic strand and the parental assembly. For visualizing side chain positioning, we would acquire a resolution of 3 Å or higher.

For each hetero-assembly 384 different crystallization conditions were screened. The crystallization conditions of the initial hits are enlisted in Table 3.

Table 3: Original hits – crystallization conditions of different initial screenings in 96-well plates.

Screening plate	Position	Condition	Sample
The Classic Suite	B3	0.02 M $CaCl_2$, 0.1 M sodium acetate pH 4.6, 30% (v/v) MPD	Acid-CFLE/B3β2γ
The Classic Suite	D2	0.1 M imidazole pH 6.5, 1.0 M sodium acetate	Acid-pp/B3β2γ
The Classic Suite	G2	0.02 M $CaCl_2$, 0.1 M HEPES sodium salt pH 7.5, 28% (v/v) PEG400	Acid-pp/B3β2γ, Acid-CFLE/B3β2γ
Core S26	C1	0.05 M calcium acetate, 0.1 M imidazole pH 8.0, 35% 2-ethoxyethanol	Acid-pp/B3β2γ
Core S26	F3	0.1 M sodium/ potassium phosphate pH 6.5, 35% (v/v) MPD	Acid-pp/B3β2γ
Core S26	H7	0.1 M citric acid pH 2.5, 40% (v/v) MPD, (final pH 4.0)	Acid-CFLE/B3β2γ
Index HR2-144	A6	0.1 M sodium acetate trihydrate pH 4.5, 25% (w/v) PEG3350	Acid-pp/Base-pp
Index HR2-144	B7	0.2 M ammonium acetate, 0.1 M BIS-TRIS pH 5.5, 45% (v/v) MPD	Acid-ICEF/B3β2γ
Index HR2-144	F7	0.05 M $CaCl_2$, 0.1 M 0.1 M BIS-TRIS pH 6.5, 30% PEG-mme 550	Acid-ICEF/B3β2γ
Index HR2-144	H5	0.1 M citric acid pH 3.5, 25% (w/v) PEG3350	Acid-pp/Base-pp

Optimization screens were performed on multiple hits to grow crystals of sufficient quality for X-ray data collection. Most of the assemblies produced either microcrystals or irregularly shaped or twinned crystals (see Appendix). Subsequent optimization rounds focused on slowing down nucleation and crystal growth.

All in all, optimizations of the initial screenings resulted in increased crystal size and slightly improved the apparent crystal morphology (Figure 50) but did not provide sufficient resolution for structure determination.

System	Initial screening	Optimization
Acid-pp/Base-pp	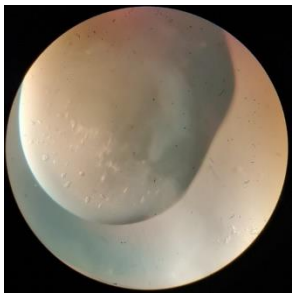	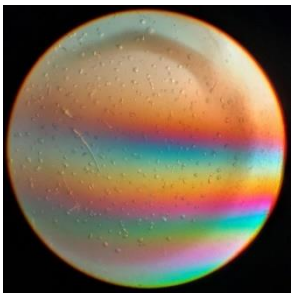
	0.1 M citric acid pH 3.5, 25% (w/v) PEG3350	0.12 M citric acid pH 3.5, 29% (w/v) PEG3350, 15 mg/mL total peptide concentration
Acid-pp/ B3β2γ		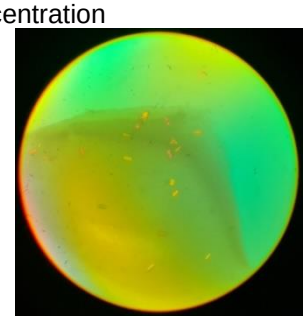
	0.05 M calcium acetate, 0.1 M imidazole pH 8.0, 35% 2-ethoxyethanol	0.08 M calcium acetate hydrate, 0.1 M imidazole, 20% 2-ethoxyethanol, 15 mg/mL total peptide concentration
Acid-CFLE/ B3β2γ	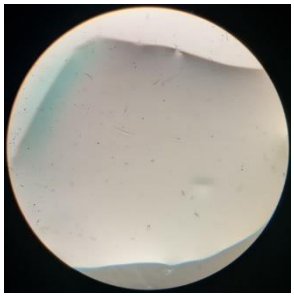	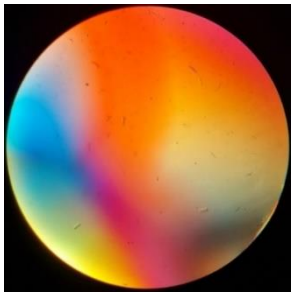
	0.02 M $CaCl_2$, 0.1 M sodium acetate pH 4.6, 30% (v/v) MPD	0.02 M $CaCl_2$ dihydrate, 0.1 M sodium acetate trihydrate pH 4.6, 25% (v/v) MPD, 10 mg/mL total peptide concentration
Acid-ICEF/B3β2γ	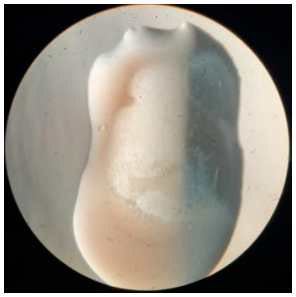	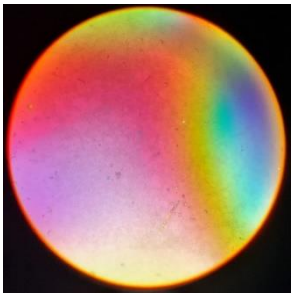
	0.05 M $CaCl_2$, 0.1 M BIS-TRIS buffer pH 6.5, 30% PEG-mme 550	0.04 M $CaCl_2$ dihydrate, 0.1 M BIS-TRIS buffer pH 6.5, 20% PEG-mme 550, 13 mg/mL total peptide concentration

Figure 50: Crystals grown by initial screenings in comparison to those grown under optimized conditions.

Diffraction varied from 10 Å to 3 Å. Furthermore, most of the measured crystals displayed high diffraction anisotropy and were not suitable for structure determination (Table 4).

Table 4: Selection of some crystals measured at the BESSY-synchrotron and information about their diffraction data.

System	Crystallization condition	Cryoprotectant	Diffraction data information
Acid-pp/Base-pp	0.11 M citric acid pH 3.5, 25% (w/v) PEG3350	30% glycerol	7.0 Å
	0.11 M citric acid pH 3.5, 25% (w/v) PEG3350	30% PEG400	5.0 Å
	0.11 M citric acid pH 3.5, 25% (w/v) PEG3350	20% PEG400	3.0 Å, anisotropic
	0.11 M citric acid pH 3.5, 26% (w/v) PEG3350	30% PEG400	5.0 and 5.5 Å
Acid-pp/B3β2γ	0.3 M $CaCl_2$, 0.1 M HEPES pH 7.5, 15% PEG400	15% PEG400	salt
	0.1 M imidazole, 0.05 M calcium acetate, 28% 2-ethoxyethanol	10% glycerol	salt
Acid-CFLE/B3β2γ	0.1 M sodium acetate trihydrate pH 4.6, 0.02 M $CaCl_2$, 25% MPD	25% MPD	10 Å
	0.1 M sodium acetate trihydrate pH 4.6, 0.02 M $CaCl_2$, 30% MPD	30% MPD	3.5 and 4.0 Å
Acid-ICEF/B3β2γ	0.04 M $CaCl_2$, 0.1 M BIS-TRIS pH 6.5, 24% PEG-mme 550		no diffraction

Further crystallization experiments based on the first attempts were performed in collaboration with Prof. Dr. Derek N. Woolfson from the University of Bristol by Dr. Bram Mylemans.

Here, 576 crystallization conditions were screened for each hetero-assembly by using the sitting drop vapor diffusion technique.

The crystallization conditions of the hits are enlisted in Table 5.

Table 5: Original hits – crystallization conditions of different screenings in 96-well plates.

Screening plate	Position	Condition	Sample
Structure Screen 1 + 2	C3	1.5 M lithium sulfate, 0.1 M sodium HEPES pH 7.5	Acid-CFLE/B3β2γ, Acid-ICEF/B3β2γ
Structure Screen 1 + 2	H2	0.1 M cadmium chloride hemi(pentahydrate), 0.1 M sodium acetate pH 4.6, 30% (v/v) PEG400	Acid-pp/Base-pp
JCSG Plus™	D8	0.1 M Tris pH 8.0, 40% (v/v) MPD	Acid-CFLE/B3β2γ
JCSG Plus™	G5	0.2 M cobalt(II) chloride hexahydrate, 0.005 M cadmium chloride hemi(pentahydrate), 0.005 M magnesium chloride hexahydrate, 0.005 M nickel(II) chloride hexahydrate	Acid-CFLE/B3β2γ
JCSG Plus™	H12	0.2 M ammonium acetate, 0.1 M HEPES pH 7.5, 45% (v/v) MPD	Acid-CFLE/B3β2γ
ProPlex	A12	0.2 M sodium acetate trihydrate, 0.1 M sodium citrate pH 5.5, 5% (w/v) PEG4000	Acid-CFLE/B3β2γ

In the course of these screens, the previous screens, and all additional optimizations, we found that MPD appears to be favorably involved in crystal growth of the Cys/Phe-motif containing heterotypic helix bundles of Acid-CFLE/B3β2γ and Acid-ICEF/B3β2γ. Moreover, Acid-pp/Base-pp, Acid-pp/B3β2γ, and Acid-ICEF/B3β2γ require higher concentrations than Acid-CFLE/B3β2γ to crystallize.

The crystal of Acid-CFLE/B3β2γ grown in well H12 of the JCSG Plus™ screen provided sufficient diffraction of 2.5 Å suitable for preliminary structural investigations (Figure 51).

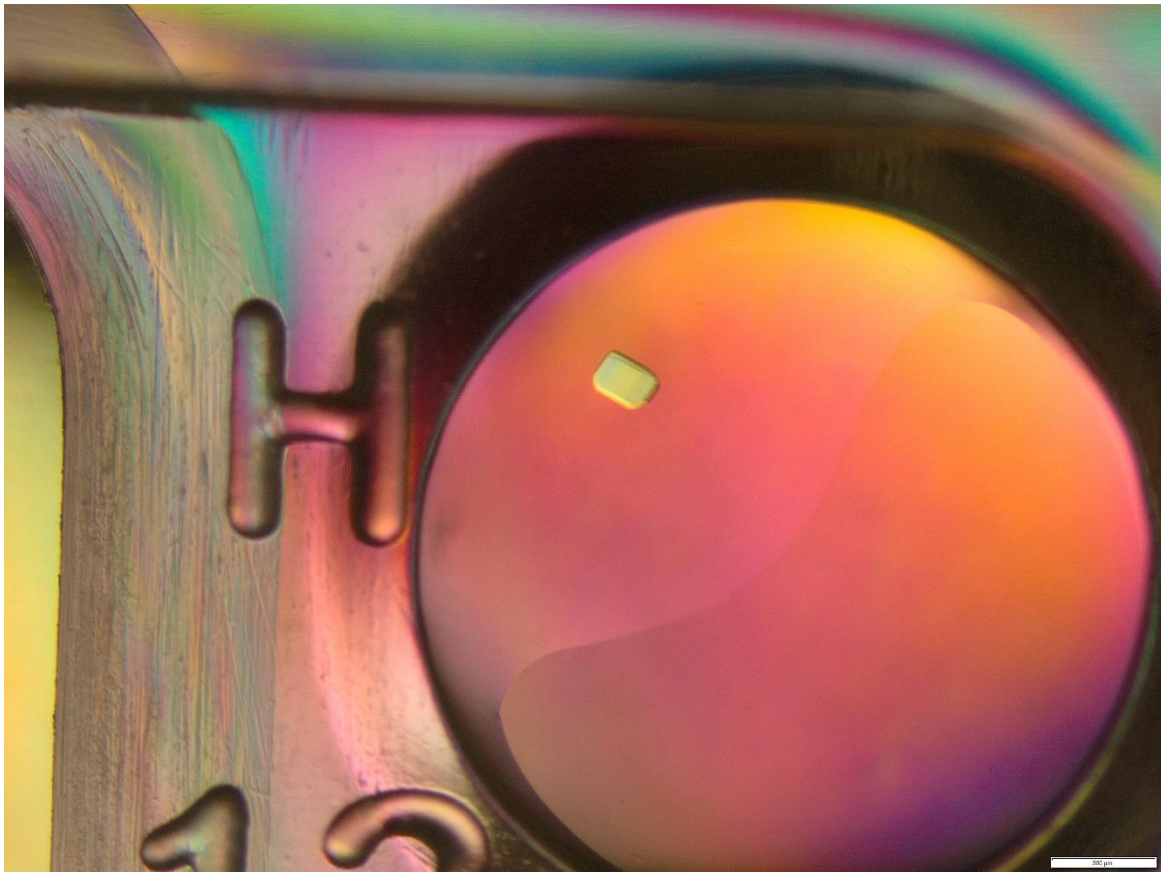

Figure 51: Acid-CFLE/B3β2γ; hit for the crystal that diffracted and was used for structure determination. H12 from JCSG Plus™ screen: 0.2 M ammonium acetate, 0.1 M HEPES pH 7.5, 45% (v/v) MPD. The scale bar in the bottom right corner corresponds to 500 µm.

Although not yet perfectly refined, it gives some indication of the H-bonding network in the helices. During refinement, it proved difficult to find good restraints for the β^3- and γ^4-amino acids. Nevertheless, this is the first crystal structure ever obtained for the chimeric peptide B3β2γ, which forms a heterotypic assembly with an all-α complementary peptide strand. The Acid-CFLE peptide here includes the Cys/Phe-motif which is of interest for our structural investigations.

The Acid-CFLE/B3β2γ crystal has the trigonal space group $P3_221$. In contrast to the tetrameric stoichiometry in solution,[102] we observe two trimeric helical bundles in the unit cell of the crystal structure (Figure 52). These helix bundles consist of two Acid-CFLE strands and the $\alpha/\beta/\gamma$-chimeric sequence. In addition, the two Acid-CFLE peptides display a different association geometry to B3β2γ; one is oriented antiparallel, and the other parallel.

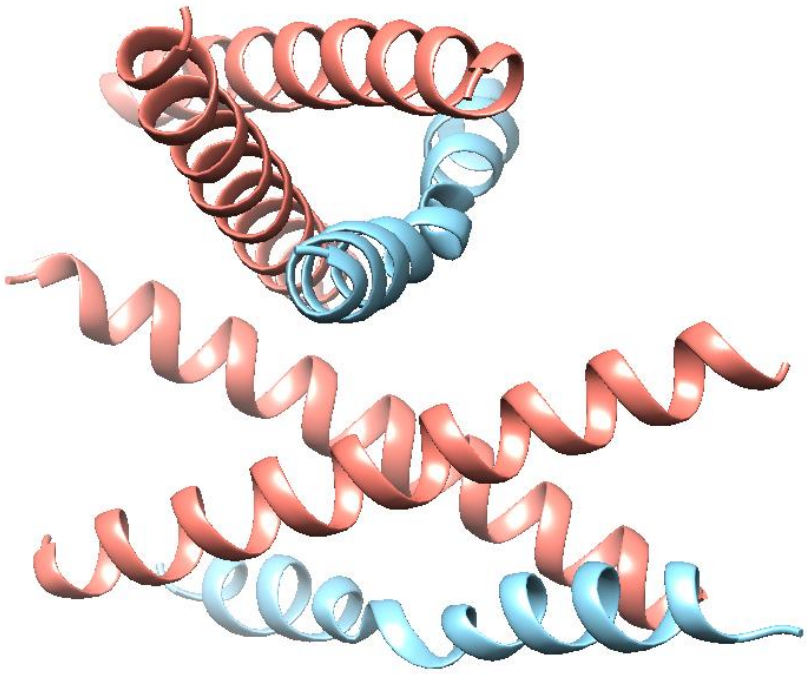

Figure 52: Two heterotypic trimeric helix bundles, each consisting of two Acid-CFLE strands (salmon color) and B3β2γ (light blue colored).

Changes in association stoichiometry between solution behavior and crystal structure were previously reported by Gellman and co-workers for their $\alpha \rightarrow \beta^3$ amino acid replacements in GCN4-p1 (see Section 1.3.2).[55] This phenomenon applies to our current observations.

Surprisingly, it is most likely that the cysteines have formed a disulfide bond (Figure 53). The sulfur atoms have a close distance of 2.04 Å, and due to the high nucleophilicity of the thiol groups in the Cys residues, the probability of disulfide bond formation is high. In addition, this distance corresponds to an expected disulfide bond length.[178] However, the electron density of the difference map exhibits a negative density, which may have resulted from X-ray radiation damage to the macromolecule. Disulfides are susceptible to this damage and form sulfur radicals and subsequently, thiol groups, as previously shown by electron spin resonance (ESR) measurements.[184,185] Anyhow, it cannot be ruled out that this structure is a crystal artifact. The added reducing agent, dithiothreitol (DTT), may have been oxidized before crystals could form, as it took nearly one month for the crystal to grow. It could also be that disulfide formation is necessary to initiate crystallization, or that crystal packing forces the proximity of the cysteines, which

can then form the disulfide bonds. Nonetheless, we only detected a weak blue-shifted thiol absorption of the Acid-CFLE/B3β2γ mixture compared to the monomeric Acid-CFLE peptide sequence in the vibrational SFG-measurements. In addition, longer incubation led to a disappearance of the thiol absorption (see Section 3.1.3). Therefore, the intramolecular S-H vibration, which is stronger than that to the environment, may indicate that the Acid-CFLE sequence in the Acid-CFLE/B3β2γ assembly is prone to disulfide linkage. Moreover, compared to the Acid-ICEF peptides, the Acid-CFLE peptides showed significant differences in their thermal stability and in the cysteine substitution experiments upon assembly to B3β2γ (see Section 3.1.1). Thus, the disulfide formation might reflect the most stable conformation of the Acid-CFLE/B3β2γ assembly.

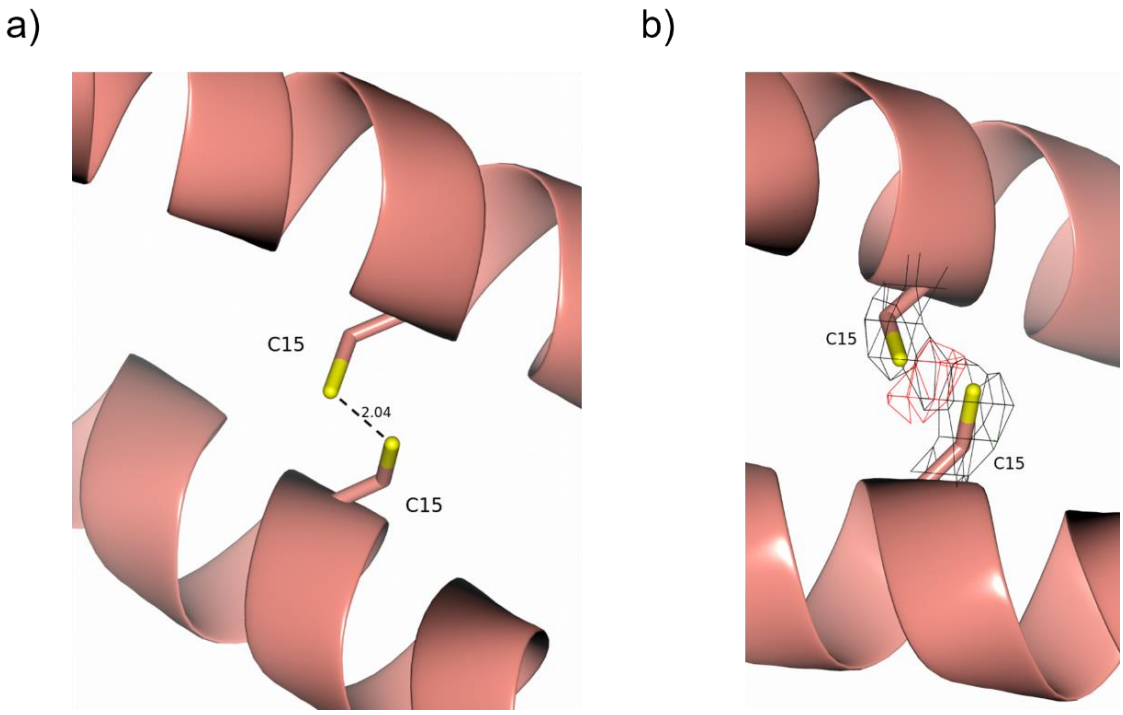

Figure 53: a) Distance of the two cysteine side chains from the Acid-CFLE sequences in the crystal structure. b) Electron density map of the cysteine residues. The electron density parameter of the normal map is 0.4 e/A³ (black) and -0.2 e/A³ for the difference map (red).

In the overall crystal structure, we detected only two intermolecular H-bonds within a radius of 4 Å: 1) between the Glu at position 28 of the antiparallelly aligned Acid-CFLE peptide and 2) Lys at position 7 of B3β2γ and between Glu21 of the same Acid-CFLE strand and Ser10 of the $\alpha/\beta/\gamma$-chimeric sequence (Figure 54a). Neither of these interhelical H-bonds is located near the homologous β^3- and γ^4-amino

acids of the central β^3/γ^4-pentad of the $\alpha/\beta/\gamma$-chimera. We observe many hydrophobic interactions between the parallel-oriented Acid-CFLE strand and B3β2γ within the 4 Å radius (Figure 54b). Here, the Leu residues at positions 4, 8, and 11, as well as Phe18 of Acid-CFLE are involved in the hydrophobic interactions. In contrast, the antiparallel Acid-CFLE sequence exhibits only two hydrophobic interactions originating from Leu4 and Phe18. The β^3hLeu15 of the $\alpha/\beta/\gamma$-chimera appears to be well stabilized in the environment by the bulky side chain, i.e., the proximal Phe18, of the antiparallel acid strand through favorable hydrophobic interactions (Figure 54c). This phenomenon is in agreement with the SPOT array analysis by Araghi *et al.* who reported a preference for phenylalanine in *d*-position.[101]

The crystal structure implies that the assembly of Acid-CFLE/B3β2γ is very different from the original classical coiled-coil design and thus to the parental peptide system Acid-pp/Base-pp. First, the two acid strands display different association geometry than expected, as the same orientation would be expected for both acid strands and second, electrostatic recognition seems to play a subordinate role and be almost absent. In general, throughout the experimental studies and cryo-TEM measurements, the helical bundle of Acid-CFLE/B3β2γ exhibited different characteristics and decreased stability when compared to the other Cys/Phe-motif-bearing Acid-ICEF/B3β2γ assembly, as well as to Acid-pp/B3β2γ and Acid-pp/Base-pp (see Section 3.1 and 3.1.1).

All in all, it seems that hydrophobicity is of paramount importance in the formation of the Acid-CFLE/B3β2γ helix bundles. Indeed, substitutions of Cys to Abu or S-methyl cysteine resulted in a significant increase in thermal stability of about 10 °C in our comparative studies with the two Cys/Phe-motifs (see Section 3.1.1). In addition, Nyakatura *et al.* showed in their *C*-terminal immobilized phage display studies that the extension of the hydrophobic core of the acid strands and the occupation of the central *a/d/e*-, and *g*-positions with at least three hydrophobic amino acid residues provides high thermal stability when assembled to B3β2γ. Moreover, the Acid-LLLL/B3β2γ helix bundle incorporating Leu in the *a/d/e/g*-positions in the central heptad of the acid strand exhibits thermal stability of >90 °C.[57]

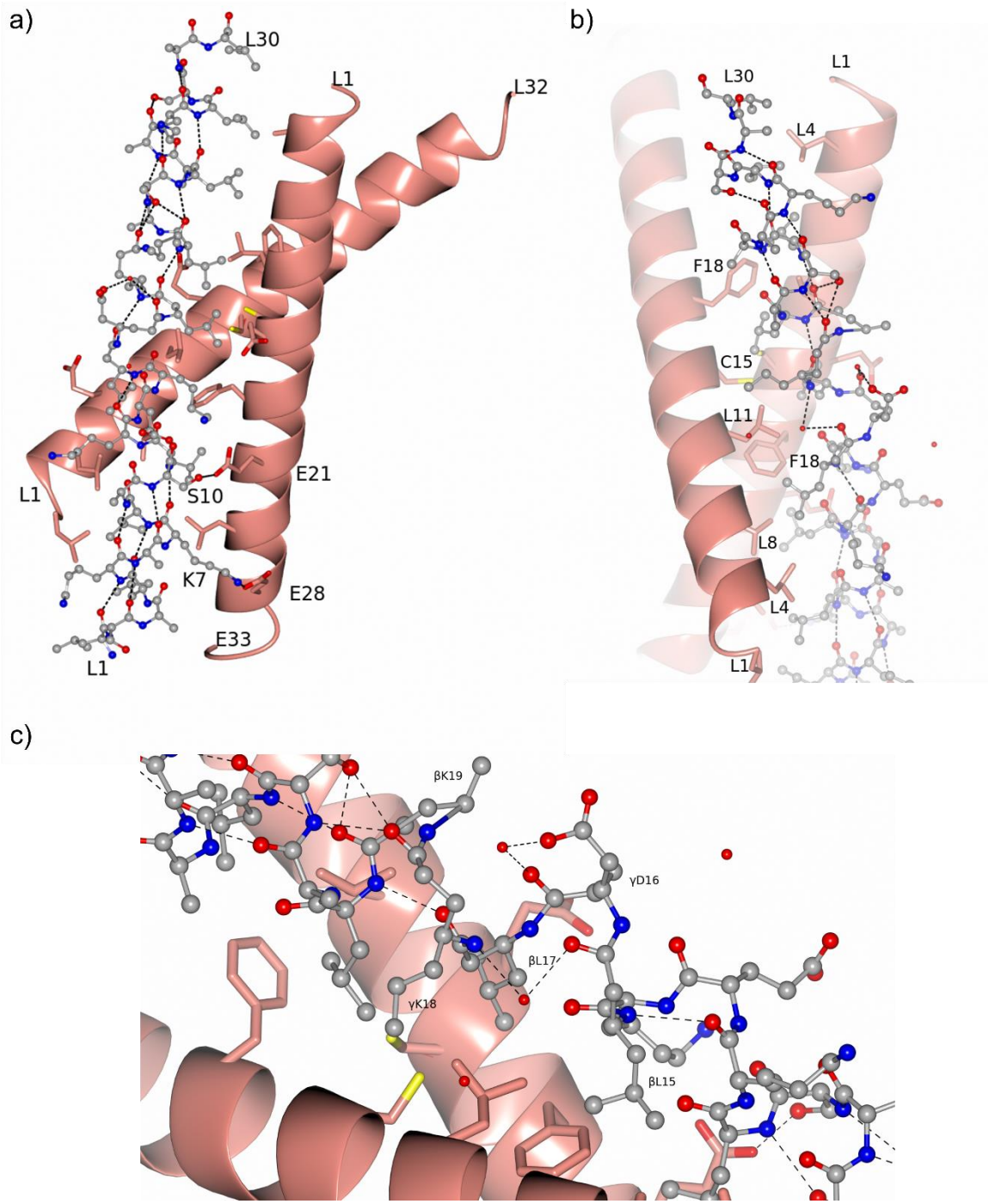

Figure 54: Crystal structure of the Acid-CFLE/B3β2γ trimer. a) Interhelical H-bonds (solid lines) between B3β2γ and the antiparallel-oriented Acid-CFLE strand within a radius of 4 Å. b) Hydrophobic interactions of both acid strands to B3β2γ in the 4 Å radius. c) Close-up of the central β^3/γ^4-pentad of the α/β/γ-chimera. In all images, the Acid-CFLE helices are displayed in salmon color, and B3β2γ as a ball and stick model. Sulfur atoms are shown in yellow, oxygen atoms in red, nitrogen atoms in blue, and carbon atoms of B3β2γ in gray. The dashed lines illustrate the H-bonding pattern of the backbone of the α/β/γ-chimera.

The Cys/Phe-motifs might thus induce selective binding to the $\alpha/\beta/\gamma$-chimeric base strand, as they were selected by phage display, but do not necessarily form the same classical coiled-coil arrangement of the original design, which would be comparable to the assembly with the parental peptide Acid-pp. The quaternary structural features of the Cys/Phe-motif incorporating assemblies with B3β2γ significantly differ from their cryo-TEM measurements (see Section 3.1) compared to Acid-pp/B3β2γ and Acid-pp/Base-pp. Here, the crystal structure of Acid-CFLE/B3β2γ shows the formation of a heterotypic antiparallel triple-helical coiled coil. The two antiparallelly oriented Acid-CFLE peptides appear to form a disulfide bond and therefore provide a template for association with the $\alpha/\beta/\gamma$-chimeric base strand to bury its hydrophobic residues by forming the helical bundle. All in all, the triple-helical coiled-coil structure of Acid-CFLE/B3β2γ provides a resemblance to spectrin repeats, from cytoskeletal proteins, which form an antiparallel helical bundle consisting of three helices that are separated by two small loops.[186–191]

A linear arrangement of several triple helical bundles formed by Acid-CFLE/B3β2γ similar to the observed supramolecular structures obtained through the cryo-TEM measurements (see Section 3.1) was also observed upon crystallization. The proximity of the successive linearly organized helical bundles seems to compensate for the almost V-shaped open conformation of the disulfide-linked Acid-CFLE strands (Figure 55).

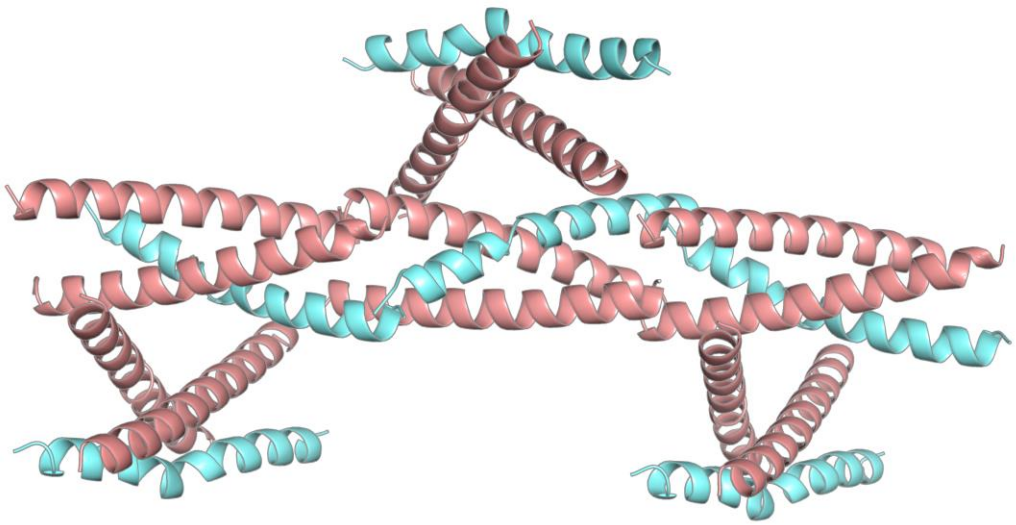

Figure 55: Linear arrangement of three triple helical bundles formed by Acid-CFLE/B3β2γ. The Acid-CFLE helices are displayed in salmon color, and B3β2γ helices are colored in light blue.

However, crystallographic structural elucidation of the Acid-ICEF/B3β2γ system has not been possible so far. The structural investigation of the helical assemblies of Acid-ICEF/B3β2γ would be of utmost importance to analyze the possible conservation of the originally designed coiled-coil assembly characteristics, since the experimental features are closer to those of Acid-pp/B3β2γ and therefore Acid-pp/Base-pp.

Additional hits were obtained for Acid-CFLE/B3β2γ from seeding experiments that have yet to be measured. Higher-resolution data from the new crystals could facilitate the refinement or enable additional single-wavelength anomalous diffraction (SAD) measurements. Acid-ICEF/B3β2γ also produced a hit during microseeding when cross-seeded with Acid-CFLE/B3β2γ crystals.

Hits from seeding screens of Acid-CFLE/B3β2γ and Acid-ICEF/B3β2γ are shown in Table 6:

Table 6: Screening hits of Acid-CFLE/B3β2γ obtained through microseeding.

Screening plate	Position	Condition	Sample
Structure Screen 1 + 2	B9	0.2 M sodium citrate tribasic dihydrate, 0.1 M sodium HEPES pH 7.5, 30% (v/v) MPD	Acid-CFLE/B3β2γ
Structure Screen 1 + 2	C12	0.2 M ammonium acetate, 0.1 M Tris pH 8.5, 30% (v/v) 2-Propanol	Acid-CFLE/B3β2γ
Structure Screen 1 + 2	E9	0.1 M Tris pH 8.5, 20% (v/v) Ethanol	Acid-CFLE/B3β2γ
JCSG Plus™	A4	0.02 M $CaCl_2$ dihydrate, 0.1 M sodium acetate pH 4.6, 30% (v/v) MPD	Acid-CFLE/B3β2γ
JCSG Plus™	D5	0.1 M HEPES pH 7.5, 70% (v/v) MPD	Acid-CFLE/B3β2γ
Structure Screen 1 + 2	A1	0.02 M $CaCl_2$ dihydrate, 0.1 M sodium acetate pH 4.6, 30% (v/v) MPD	Acid-ICEF/B3β2γ

3.2 Iterative substitution library: systematic exploration of foldameric space by pushing the molecular interactions to the limit

Aiming to examine the intermolecular binding strength in the quaternary structure system, a library of chimeric peptides that systematically increases the number of β^3/γ^4-modules was designed. These chimeric peptides were subsequently evaluated for stability when complemented with the corresponding Cys/Phe-motifs or the parental acid strand (Acid-pp).

The synthesis of peptide variants incorporating multiple substitutions to β^3/γ^4-stretches represented the first attempt to assess the stability of folding with an increased number of β^3/γ^4-modules. Each substitution of α-amino acid containing heptads to β^3/γ^4-pentads in the $\alpha/\beta/\gamma$-chimeric base strand shortens the peptide by one residue per helical turn owing to the additional backbone methylene groups of the β^3- and γ^4-amino acids.[98] Thus, the lack of peptide bonds and hence the loss of intrahelical H-bond donors and H-bond acceptors may lead to disruptive structural consequences.[100] Substitutions of the corresponding acid strands

comprising the Cys/Phe-motifs should reveal whether these motifs can maintain stability through their specificity, although the new $\alpha/\beta/\gamma$-chimeric strands are shortened by at least one additional peptide bond compared to B3β2γ. A library of systematic multiple substitutions in different heptad positions should show whether possible conservation of stability depends on the positions of the substitutions.

The proposed stabilizing effect of the Cys/Phe-motifs for the heteroassemblies was therefore exploited for five designs involving expansion of the β^3/γ^4-module moieties (Table 7). For this purpose, several heptad-repeats in Base-pp were replaced stepwise by β^3/γ^4-pentads, while the corresponding heptad of the complementary all-α-peptide was substituted by the Cys/Phe-motif (Table 7). An alternating system (B3β2γ-2,4), a variant with *C*- and *N*-terminal substitution (B3β2γ-1,5), a consecutive *N*-terminal (B3β2γ-1,2) and a consecutive *C*-terminal (B3β2γ-4,5) variant, as well as a triple centrally substituted system (B3β2γ-2,3,4), were investigated. Finally, a chimeric base strand consisting exclusively of β^3/γ^4-pentads (B3β2γ-1,2,3,4,5) was tested for its ability to bind to Acid-pp.

The numbers denote the heptad positions where the replacements to β^3/γ^4-pentads or to the Cys/Phe-motifs occurred:

Table 7: Peptide sequences of the multiply substituted variants. All peptides were *N*-terminally labeled with *o*-aminobenzoic acid (*o*-Abz) for concentration determination. For each chimeric peptide variant, the corresponding Cys/Phe-motifs were substituted accordingly at the same heptad position of Acid-pp. Substitutions were highlighted by gray boxes. Base strand variants are colored blue and acid strand variants are shown in red. Homologous β^3- and γ^4-amino acids are colored green and amino acids of the Cys/Phe-motifs in black.

	Peptide sequence					
Base-pp	*o*-Abz	L S A L K E K	L A S L K E K	L S A L K E K	L A S L K E K	L S A L K E K
Acid-pp	*o*-Abz	L S A L E K E	L A S L E K E	L S A L E K E	L A S L E K E	L S A L E K E
B3β2γ-2,4	*o*-Abz	L S A L K E K	β^3L γ^4D β^3L γ^4K β^3K	L S A L K E K	β^3L γ^4D β^3L γ^4K β^3K	L S A L K E K
Acid-CFLE-2,4	*o*-Abz	L S A L E K E	C A S F L K E	L S A L E K E	C A S F L K E	L S A L E K E
Acid-ICEF-2,4	*o*-Abz	L S A L E K E	I A S C E K F	L S A L E K E	I A S C E K F	L S A L E K E
B3β2γ-1,5	*o*-Abz	β^3L γ^4D β^3L γ^4K β^3K	L A S L K E K	L S A L K E K	L A S L K E K	β^3L γ^4D β^3L γ^4K β^3K
Acid-CFLE-1,5	*o*-Abz	C S A F L K E	L A S L E K E	L S A L E K E	L A S L E K E	C S A F L K E
Acid-ICEF-1,5	*o*-Abz	I S A C E K F	L A S L E K E	L S A L E K E	L A S L E K E	I S A C E K F
B3β2γ-1,2	*o*-Abz	β^3L γ^4D β^3L γ^4K β^3K	β^3L γ^4D β^3L γ^4K β^3K	L S A L K E K	L A S L K E K	L S A L K E K
Acid-CFLE-1,2	*o*-Abz	C S A F L K E	C A S F L K E	L S A L E K E	L A S L E K E	L S A L E K E
Acid-ICEF-1,2	*o*-Abz	I S A C E K F	I A S C E K F	L S A L E K E	L A S L E K E	L S A L E K E
B3β2γ-4,5	*o*-Abz	L S A L K E K	L A S L K E K	L S A L K E K	β^3L γ^4D β^3L γ^4K β^3K	β^3L γ^4D β^3L γ^4K β^3K
Acid-CFLE-4,5	*o*-Abz	L S A L E K E	L A S L E K E	L S A L E K E	C A S F L K E	C S A F L K E
Acid-ICEF-4,5	*o*-Abz	L S A L E K E	L A S L E K E	L S A L E K E	I A S C E K F	I S A C E K F
B3β2γ-2,3,4	*o*-Abz	L S A L K E K	β^3L γ^4D β^3L γ^4K β^3K	β^3L γ^4D β^3L γ^4K β^3K	β^3L γ^4D β^3L γ^4K β^3K	L S A L K E K
Acid-CFLE-2,3,4	*o*-Abz	L S A L E K E	C A S F L K E	C S A F L K E	C A S F L K E	L S A L E K E
Acid-ICEF-2,3,4	*o*-Abz	L S A L E K E	I A S C E K F	I S A C E K F	I A S C E K F	L S A L E K E
B3β2γ-1,2,3,4,5	*o*-Abz	β^3L γ^4D β^3L γ^4K β^3K	β^3L γ^4D β^3L γ^4K β^3K	β^3L γ^4D β^3L γ^4K β^3K	β^3L γ^4D β^3L γ^4K β^3K	β^3L γ^4D β^3L γ^4K β^3K

To prevent intramolecular disulfide formation or oxidation on the multiple inserted Cys/Phe-motifs, CD-measurements were performed with the addition of 5 mM DTT as a reducing agent. CD-spectroscopic measurements of the peptide sequences show that multiple substitutions incorporating the Cys/Phe-motifs can lead to the formation of α-helical structures of the acid sequences (Figure 56). Thus, the peptides Acid-CFLE-2,4, the consecutive *N*-terminal substituents, and the triple central substituents indicate the formation of α-helix structures. All other acid-variants indicate disrupted helical structures with the first minimum shifted to a lower wavelength and a second minimum at 222 nm.

Incubation of the equimolar mixtures shows that neither the alternating and the triple consecutive substitutions nor the full β/γ-chimeric sequence assembled to their corresponding acidic counter strands. In contrast, the consecutive *C*- and the consecutive *N*-terminal substituted heptads as well as the variant with *C*-and *N*-terminal substitution indicate assembly through α-helix formation. Except for Acid-CFLE-1,2/B3β2γ-1,2 and Acid-ICEF-1,2/B3β2γ-1,2, which display less pronounced minima at 208 and 222 nm, the systems exhibit helix contents that are comparable to or even higher than those of the parental system (Figure 57).

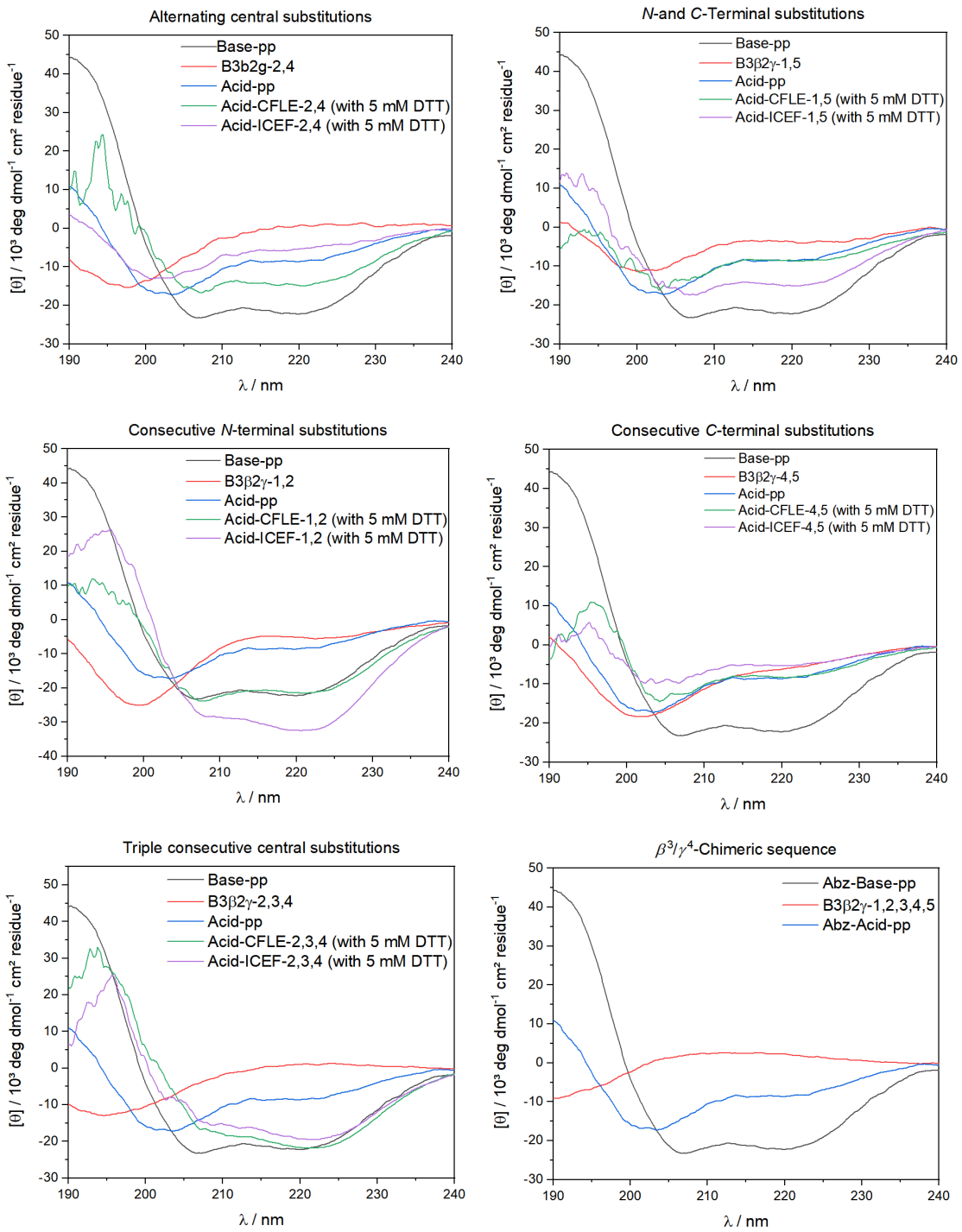

Figure 56: CD-spectra of multiple substituted peptides (20 µM) in 10 mM phosphate buffer at pH 7.4.

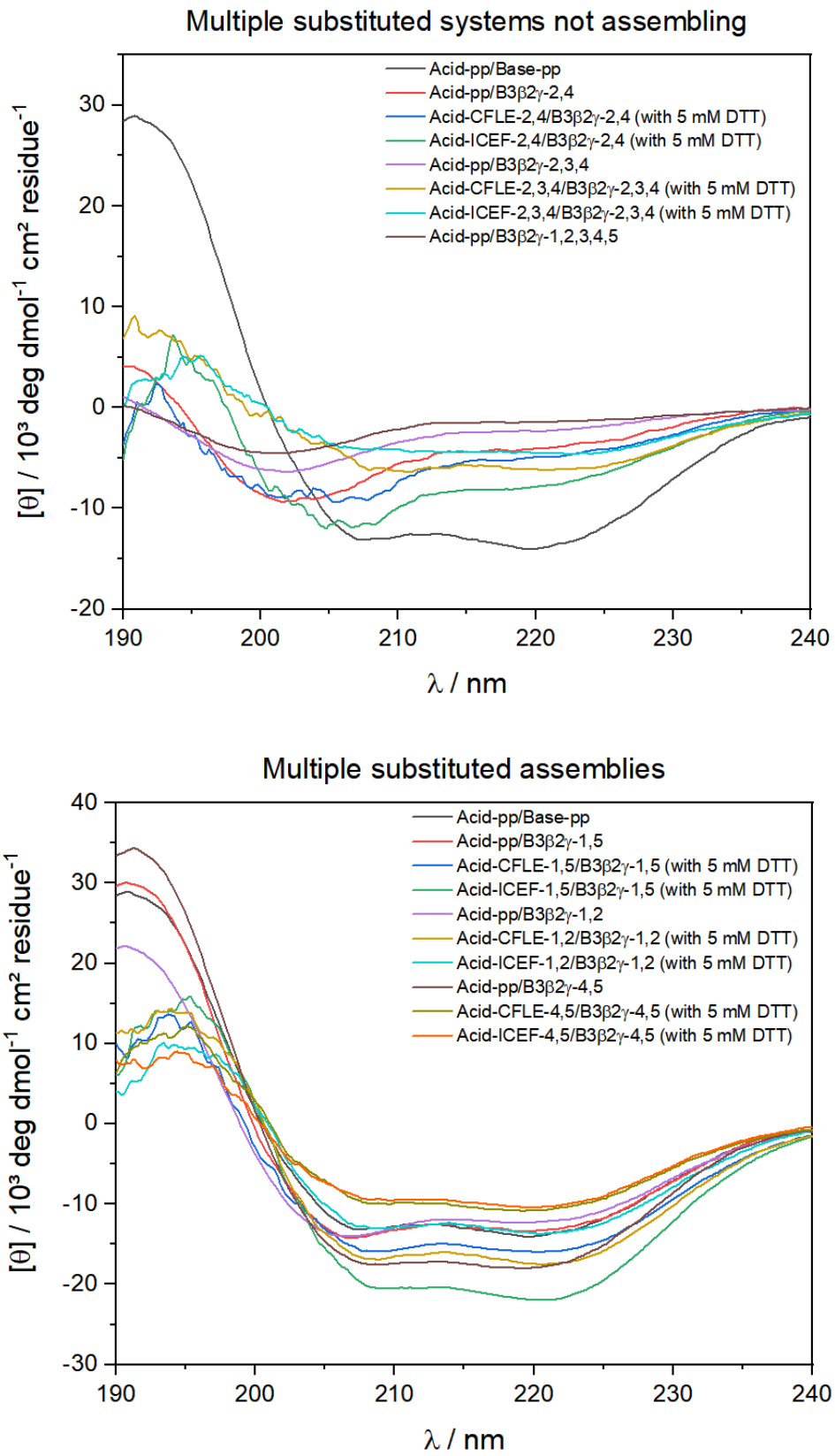

Figure 57: Multiple substituted peptide sequences that did not lead to assembly (top) and that form helical bundles (bottom). Measurements were conducted as 1:1 mixtures with 20 µM total peptide concentration in 10 mM phosphate buffer at pH 7.4 and their thermal denaturation.

All multiple substituted assemblies exhibit very high thermal stabilities of approximately 75 °C or higher in phosphate buffer at pH 7.4. The most thermally stable helix bundle was obtained with Acid-pp/B3β2γ-4,5, which has similar thermal stability compared to the parental Acid-pp/Base-pp peptide system (Figure 58).

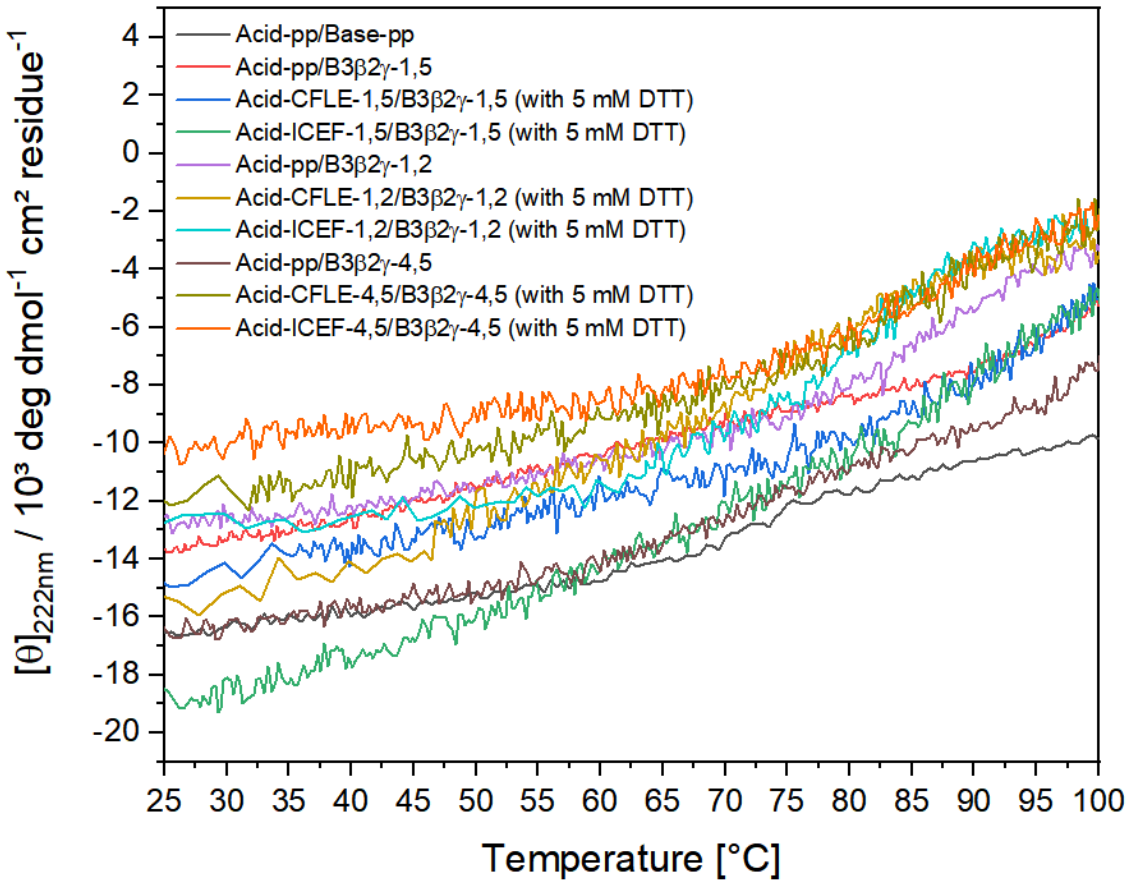

Figure 58: Thermal denaturation of multiply substituted variants forming helical bundles (20 µM total peptide concentration of equimolar mixtures, 10 mM phosphate buffer, pH 7.4).

All multiple substituted helical bundles were chemically less stable to denaturation induced by guanidinium hydrochloride compared to that of the parental combination (Figure 59).

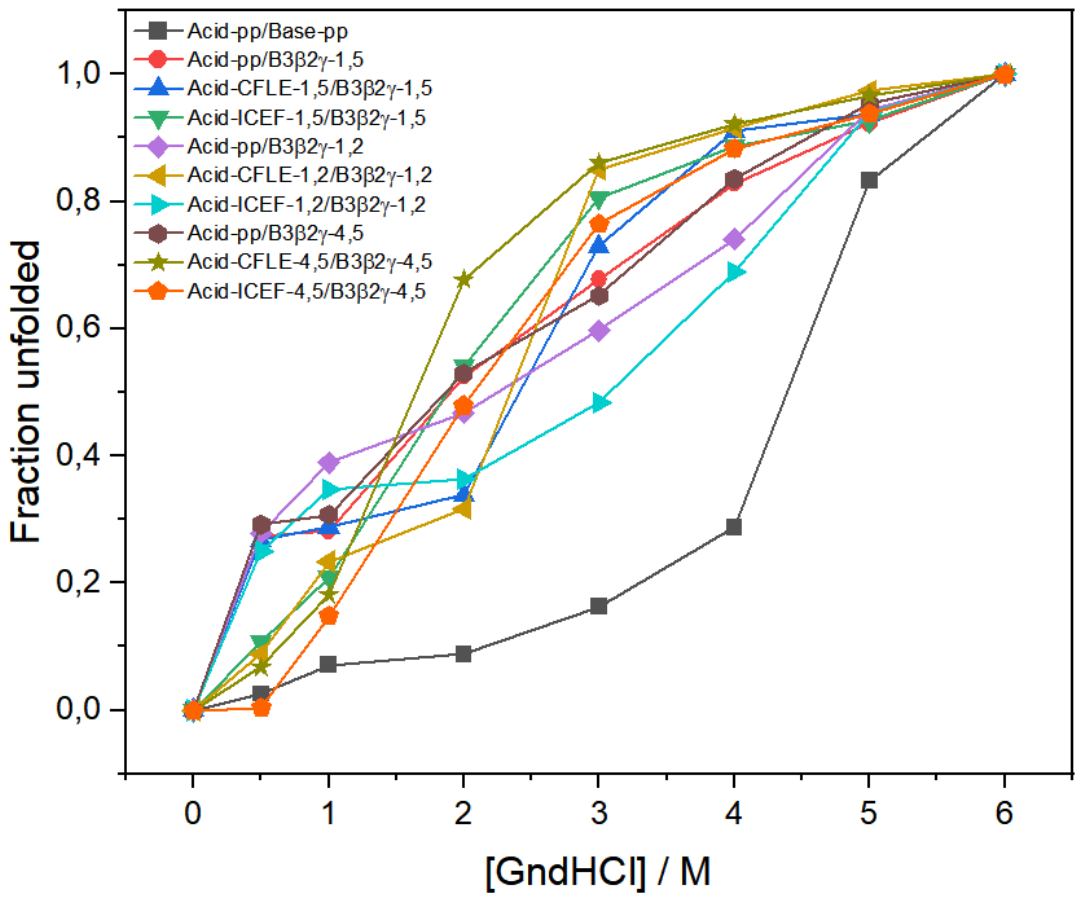

Figure 59: Chemical denaturation of multiply substituted variants forming helical bundles (20 µM total peptide concentration of equimolar mixtures, 10 mM phosphate buffer, pH 7.4).

Overall, multiple substitutions in the center of the chimeric base strand alter the number of backbone residues of the chimera in such a manner that the stability of the helical bundle cannot be maintained. The incorporation of the multiple Cys/Phe-motifs substitutions, surprisingly, shows no significant differences in assembly properties to the parental peptide acid strand. Whenever the complementary acid strands incorporating the Cys/Phe-motifs lead to the formation of helical bundles, so also does the parental acid strand (Figure 60).

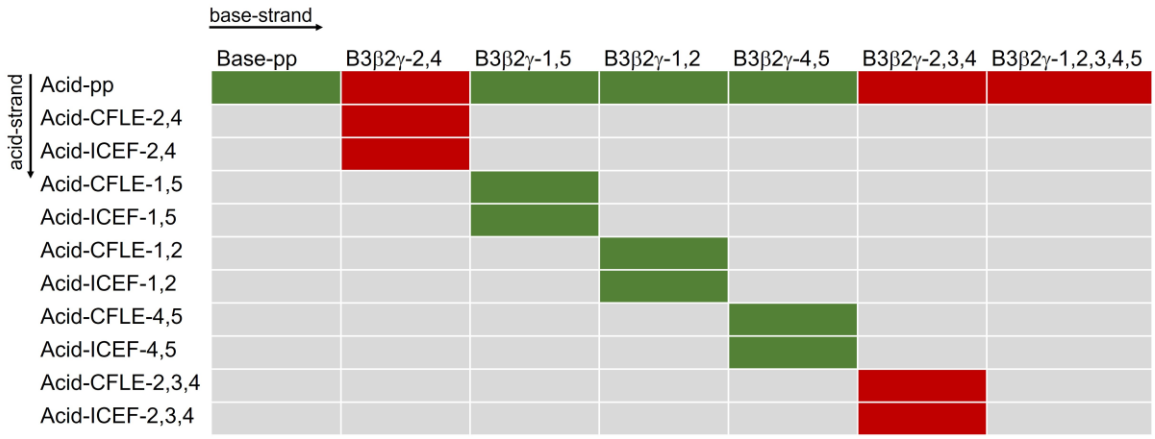

Figure 60: Schematic summary of the assembling and non-assembling combinations of the multiply substituted variants. The vertical column on the left includes the acidic peptide sequences and the top row lists the monomeric basic peptides. The mixtures are shown in the row as a cross to the corresponding acid sequence and base peptide. Red boxes indicate no assembly occurred, and green boxes represent the assembled mixtures. Peptide sequences that have not been combined are displayed by gray boxes.

However, substitutions at both termini are well tolerated and provide high thermal stability. Hodges and co-workers proposed that the hydrophobic interactions between leucines in a two-stranded coiled-coil system should be more flexible at the ends and less buried compared with the positions of the center by performing systematic substitutions of the leucine residues with alanine.[42] This phenomenon applies to our current observations regarding the assembly properties of natural peptide strands with foldameric peptide strands.

3.2.1 Structural studies on the β^3/γ^4-chimeric sequence using CD-spectroscopy

The β^3/γ^4-chimeric sequence, comprising solely five repeating β^3/γ^4-pentads of alternating homologous β^3 and γ^4-amino acids, has lost the ability to associate with the parental acidic counterstrand, but was nevertheless further studied as an isolated system by CD-spectroscopy. It exhibits a minimum at 190 nm and a weak positive band at around 213 nm that resembles a polyproline-like helical structure.[192] None of the other $\alpha/\beta/\gamma$-chimeric base strands display this positive band. Except for B3β2γ-2,3,4 which exhibits a minimum at 195 nm, almost all $\alpha/\beta/\gamma$-chimeric base strands display a pronounced minimum at approximately 200 nm.

The weak positive band, however, is found exclusively for B3β2γ-1,2,3,4,5 (Figure 61).

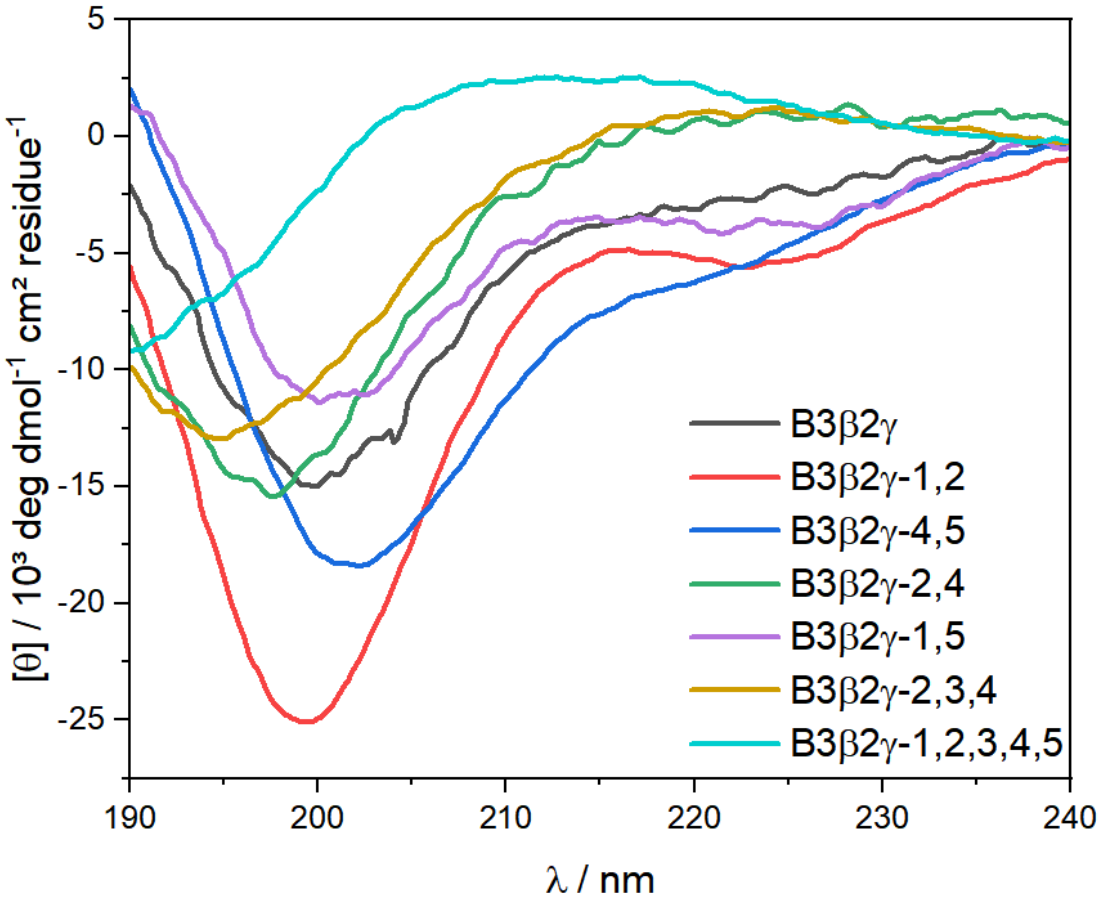

Figure 61: The β^3/γ^4-chimeric sequence in comparison to all other $\alpha/\beta/\gamma$-chimeric base strands; 20 µM peptide concentration in phosphate buffer pH 7.4.

The structure was insensitive to heat, and measurements up to 100 °C did not significantly alter the structure of the β^3/γ^4-chimeric sequence (Figure 62). Furthermore, higher concentrations and different pH values did not markedly change the structure.

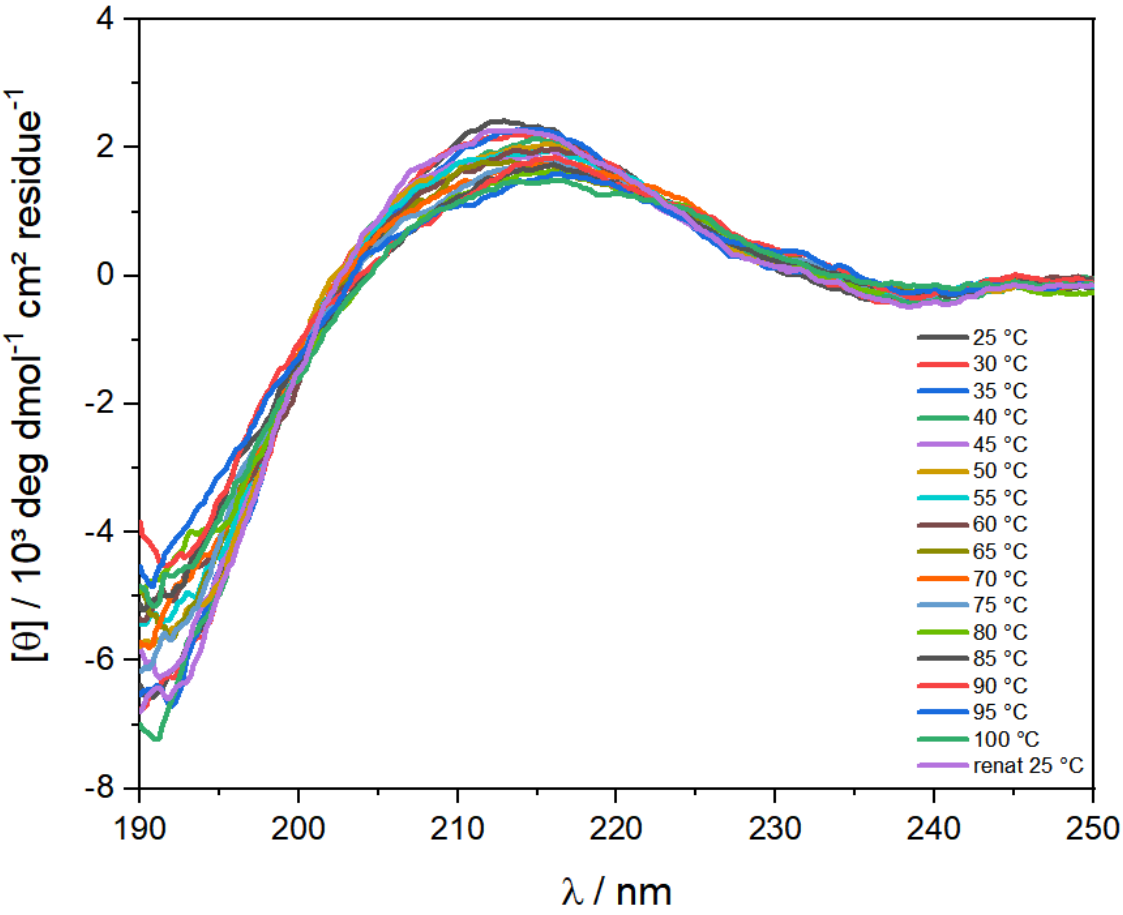

Figure 62: The β^3/γ^4-chimeric sequence at different temperatures; 60 µM peptide concentration in phosphate buffer pH 7.4.

Lastly, B3β2γ-1,2,3,4,5 was measured in various organic solvents (Figure 63). 2,2,2-Trifluoroethanol (TFE) and 1,1,1,3,3,3-hexafluoro-propan-2-ol (HFIP) resulted in a shift of the positive band to about 200 nm. TFE titration with up to 60% TFE, which is known to induce helical structures, also did not lead to major differences in the secondary structure pattern. Methanol did not change the structure significantly and is comparable to the structure in phosphate buffer. For ethanol, the minimum shifts to around 195 nm and the positive band to 220 nm. Isopropanol and octan-1-ol display a minimum at 204 nm, which is more pronounced in isopropanol. In addition, the positive band is extinguished in both solvents. None of the organic solvents triggered classical α-helical structure formation with the two distinct minima at 208 and 222 nm.

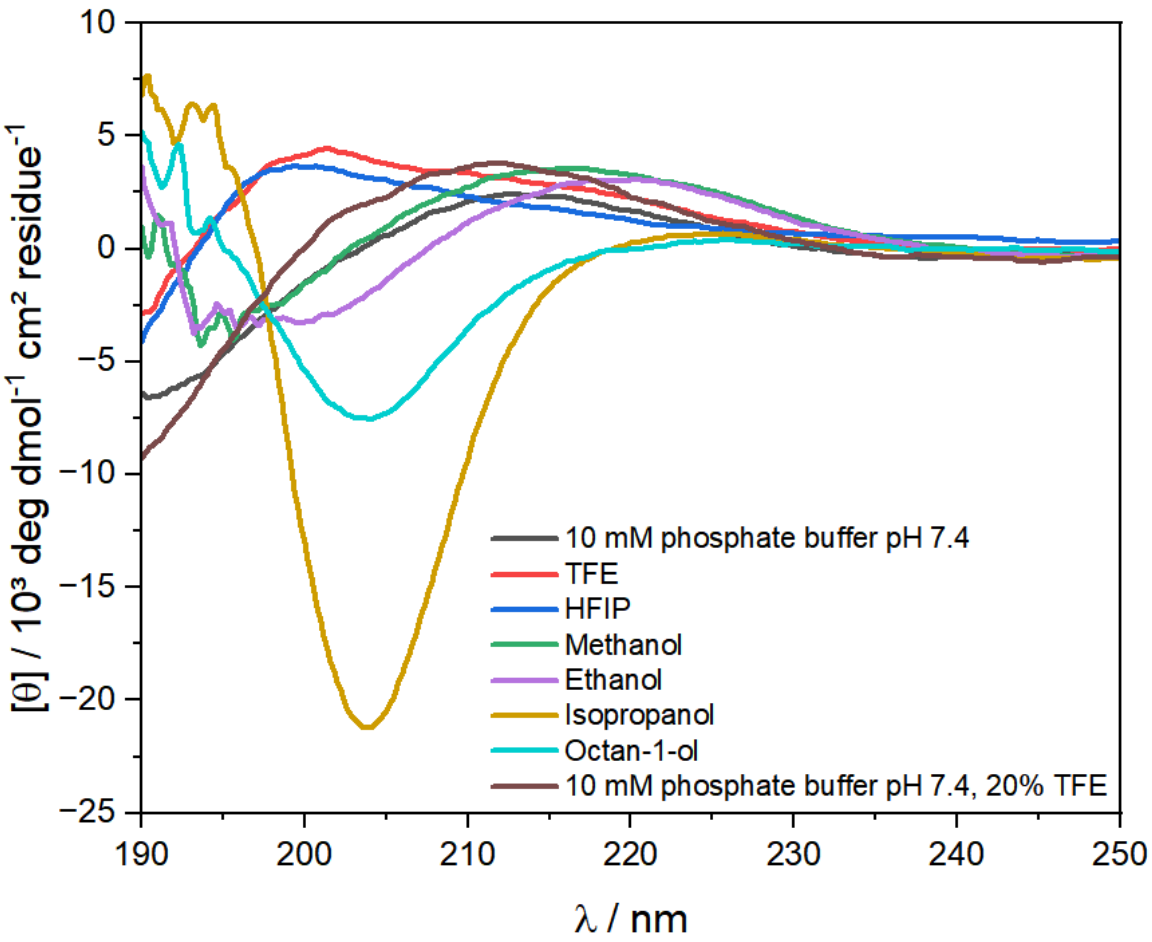

Figure 63: CD-spectroscopic measurements of the β^3/γ^4-chimeric sequence (60 µM) in various organic solvents.

4. Summary and Outlook

The importance of cysteine in the selective identification and binding of the $\alpha/\beta/\gamma$-chimera, denoted B3β2γ, was suspected based on its prevalence in the hydrophobic core positions when screening for high-affinity interaction partners by phage display[57,102] and was extensively investigated in this dissertation. Here, initial insights were gained from high-resolution structural analyses of the higher-ordered assemblies, which involve an $\alpha/\beta/\gamma$-chimera and all-α-peptides. This work contributes to developing a deeper and more sophisticated knowledge to access foldamer designs that engage in these interactions with natural peptides.

The two Cys/Phe-motif variants of the acidic parental peptide Acid-pp selectively binding to B3β2γ presented by Nyakatura *et al.*[102] were thoroughly examined in the presence and absence of DTT and showed significant differences in their characteristic features, such as helicity, quaternary structure properties, as well as stability. Cryo-TEM studies revealed that both systems incorporating the Cys/Phe-motifs exhibit markedly different quaternary structures compared to the heterotypic assemblies of Acid-pp/B3β2γ and Acid-pp/Base-pp. The parental peptide assembly (Acid-pp/Base-pp) and Acid-pp/B3β2γ form long unbranched α-fibers that do not form superordinate structures. The supramolecular structures formed by Acid-CFLE/B3β2γ show laterally organized α-fibers that create a crossed pattern by partially stacked layers. In contrast, the Acid-ICEF/B3β2γ fibers, have a strong tendency to twist into thicker rope-like strands. Moreover, substitutions to cysteine for additional comparison of the two Cys/Phe-motifs revealed further distinct dissimilarities between them. Substitutions of cysteine by nonpolar amino acids with similar side-chain length, i.e., S-methyl cysteine and aminobutyric acid, resulted in comparable thermal stability to the Acid-ICEF helix bundles with the $\alpha/\beta/\gamma$-chimeric base strand. However, these substitutions in the XFLE-sequence increased thermal stability compared to Acid-CFLE in the heterotypic helix bundles with B3β2γ. The introduction of serine as a polar residue decreased thermal stability for both Cys/Phe-motifs, but more significantly for the Acid-ISEF/B3β2γ assembly. Cryo-TEM examination of the substituted assemblies containing S-methyl cysteine may reveal whether capping of the cysteine leads to the formation of quaternary structures similar to those of the parental system and Acid-pp/B3β2γ,

or whether the enlargement of the side chain leads to larger hydrophobic contacts and thus the formation of new supramolecular structures.

Within the scope of this thesis, various analytical methods were applied to obtain high-resolution structural data on the preferential residue packing between the central β^3/γ^4-pentad of the $\alpha/\beta/\gamma$-chimera and the complementary central heptad of the all-α-peptides.

Structural elucidation of the coiled-coil assemblies using NMR-spectroscopy proved unsuccessful. The assignment was impeded due to line broadening resulting from nonspecific quaternary interactions and the rapid dynamics involved in the formation of the α-fibers. In addition, the assignment was greatly complicated by a high degree of chemical shift redundancy due to the highly repetitive nature of the coiled-coil design. Therefore, for future NMR structural analysis, a modification of the design should be made in which the sequences are truncated. Modifications to the *C*- and *N*-termini that reduce electrostatic repulsion and an appropriate TFE addition to suppress the high dynamics as well as the nonspecific quaternary interactions could further address these difficulties.[158] Expression of the all-α-peptides introducing ^{15}N- and ^{13}C-isotopes might further facilitate the assignment for future structural investigations.[164]

While classical FT-IR spectroscopy did not provide structural information in the thiol region, vibrational SFG-spectroscopic measurements gave first insights into the shifts of the S-H stretching vibration. The thiol region was investigated for the first time by vibrational SFG spectroscopy. In contrast to the Acid-CFLE/B3β2γ mixture, which was blue-shifted, a red-shift was observed for the Acid-ICEF/B3β2 system compared to their monomeric acid-sequences. These results suggest that the stabilization of the heterotypic assembly involving B3β2γ by interhelical thiol H-bonding proposed by Nyakatura *et al.*[102] might be present for Acid-ICEF/B3β2γ but not for Acid-CFLE. Moreover, prolonged incubation of Acid-CFLE/B3β2γ resulted in the disappearance of thiol absorption. To exclude the possibility of significant changes in the assemblies due to the different physicochemical properties at the air/water interface during SFG spectroscopic measurements, the amide I region was elucidated for secondary structural features and compared to FT-IR. When

comparing the amide I region, both measurements revealed mainly α-helical features for the mixtures with minor differences.

Crystallization approaches led to the investigation of the first crystal structure involving an $\alpha/\beta/\gamma$-chimera and all-α-peptides in a helix bundle arrangement. The crystal structure of the helical bundle of Acid-CFLE/B3β2γ showed differences in the degree of association and orientation of the acidic sequence containing the Cys/Phe-motif compared with the solution.[102] The trimer comprised two Acid-CFLE peptide strands aligned either parallel or antiparallel to B3β2γ and were disulfide-linked. In addition, hydrophobicity was of paramount importance for interhelical interactions. However, the overall originally designed coiled-coil features including electrostatic recognition do not apply to this association. Further promising single crystals could be obtained, which have not been measured to this date. These might lead to additional structure dissolution of the other assemblies and higher resolution crystal structure of Acid-CFLE/B3β2γ to facilitate its refinement process. Furthermore, structural elucidation of Acid-ICEF/B3β2γ could shed light on whether this assembly is subordinate to the conventional coiled-coil design. Otherwise, the incorporation of Cys/Phe motifs would mean that different assembly properties would form with the $\alpha/\beta/\gamma$-chimera, fundamentally different from the original design and driven only by the most effective shielding of the hydrophobic residues from the aqueous environment, disregarding the secondary recognition motif of the planned electrostatic interactions. Preferred conditions for the crystallization of the different assemblies were found, which could aid future optimizations and crystal growth.

As an outlook, preferred selective binding of the β/γ-module via cysteine could be further explored by proteomic affinity assays towards cysteine-rich proteins or by target immobilization and NMR screening.[193–196]

The second part of this work dealt with the construction of a library of $\alpha/\beta/\gamma$-chimeric peptides involving systematic, iterative substitutions. The number of β/γ-modules was systematically increased in the $\alpha/\beta/\gamma$-chimera and introduced to different positions, while the Cys/Phe-motifs of the complementary all-α-peptides were introduced to the corresponding positions of the complementary acid sequences. These chimeras were then evaluated for assembly properties when complemented

with corresponding all-α-peptide sequences involving the Cys/Phe-motifs. Restriction of intermolecular interactions was observed for the multiple modular replacements in the center towards a variation in the number of backbone residues. However, the incorporation of multiple β/γ-modules at both ends did not affect assembly and provided high thermal stability. It is highly desirable to further investigate these assemblies by size-exclusion chromatography and fluorescence resonance energy transfer to determine probable differences in the degree or orientation of the associated systems. Paramagnetic NMR measurements, which have been shown to be useful in obtaining this information could also be tried.[197]

Finally, the β/γ-peptide fully substituted with β/γ-modules was analyzed for structural features by CD-spectroscopy. The proposed polyproline-like helical structure should be further investigated by 2D-NMR spectroscopy to verify the finding of this structural conformation. Since the β^3/γ^4-chimeric sequence was shown to lose its ability to bind to all-α-peptides, rational design approaches using molecular dynamic calculations could be helpful to find β/γ-peptide sequences that bind to all-α-peptides. Another highly interesting method would be to perform phage-display screens with immobilized all-α-peptides to screen for suitable β- and γ-amino acids. This may be possible thanks to genetic code manipulation strategies.[68]

5. Materials and Methods

5.1 Reagents and solvents

Cl-MPA ProTide resins for performing solid-phase peptide synthesis (SPPS) were purchased from CEM Corporation (Matthews, NC, USA). Standard Fmoc-protected canonical L-amino acids with acid-labile orthogonal side-chain protection were obtained from ORPEGEN Peptide Chemicals GmbH (Heidelberg, Germany) and Carbolution Chemicals GmbH (St. Ingbert, Germany). Homologous Fmoc-protected β- and γ-L-amino acids with acid-labile orthogonal side chain protection used were Fmoc-γ-Homoasp(OtBu)-OH (Fmoc-β-D-HomoGlu-OtBu, Santa Cruz Biotechnology, Dallas, Texas, USA), Fmoc-γ-Homolys(Boc)-OH ((*S*)-N-4-Fmoc-N-8-Boc-diaminooctanoic acid, CHEMIMPEX GmbH, Berlin, Germany), Fmoc-β-Homoleu-OH (Merck KGaA, Darmstadt, Germany or abcr GmbH, Karlsruhe, Germany), and Fmoc-β-Homolys(Boc)-OH (Merck KGaA, Darmstadt, Germany).

Fmoc-2-Abz-OH was utilized by Fluorochem Ltd (Derbyshire, UK) as an *N*-terminal label for concentration determination with *o*-Abz-Gly-OH x HCl by Bachem Holding AG (Bubendorf, Switzerland).

The coupling reagent *N*, *N'*-Diisopropylcarbodiimid (DIC) was bought from either Iris Biotech GmbH (Marktredwitz, Germany) or Carbolution Chemicals GmbH (St. Ingbert, Germany) and the activator base Oxyma Pure either from Merck KGaA (Darmstadt, Germany) or Carbolution Chemicals GmbH (St. Ingbert, Germany). Piperazine was obtained from Merck KGaA (Darmstadt, Germany) and *N*-hydroxybenzotriazole (HOBt) from Carbolution Chemicals GmbH (St. Ingbert, Germany) for the deprotection of the fluorenylmethyloxycarbonyl (Fmoc)-protecting group during SPPS. In addition, *N*-methyl-2-pyrrolidone (NMP) from Carl Roth GmbH + Co. KG (Karlsruhe, Germany) and Ethanol (EtOH) from Thermo Fisher Scientific (Schwerte, Germany) were used as solvents for deprotection purposes. *N*, *N*-dimethylformamide (DMF) was purchased from Thermo Fisher Scientific (Schwerte, Germany) and *N*, *N*-diisopropylethylamine (DIEA) from Carl Roth GmbH + Co. KG (Karlsruhe, Germany) for the SPPS.

Trifluoroacetic acid (TFA) for peptide cleavage from the resin was from Thermo Fisher Scientific (Schwerte, Germany). Further for resin cleavage purposes 1-2-

ethanedithiol (EDT) from Acros Organics B.V.B.A. (Thermo Fisher Scientific, Geel, Belgium) and triisopropylsilane (TIS) from TCI Deutschland GmbH (Eschborn, Germany) were used.

High-performance liquid chromatography (HPLC)- or spectroscopy-grade solvents were utilized for the purification of the peptides. Acetonitrile (ACN) was therefore purchased from Thermo Fisher Scientific (Schwerte, Germany) and trifluoroacetic acid (TFA) from Merck KGaA (Darmstadt, Germany).

Deionized water (Millipore) for HPLC usage or buffer preparation was obtained with Milli-Q® Reference A+ Ultrapure Water System (Merck KGaA, Darmstadt, Germany).

Guanidine-hydrochloride (GndHCl) as denaturant from Carl Roth GmbH + Co. KG (Karlsruhe, Germany) and dithiothreitol (DTT) as reducing agent from Fisher Scientific (Waltham, Massachusetts, USA) were used during the analysis of the systems.

Further chemicals and solvents were purchased at the highest commercially available purity from Acros Organics (Thermo Fisher Scientific, Geel, Belgium), abcr GmbH (Karlsruhe, Germany), chemPUR (Karlsruhe, Germany), Fluorochem (Hadfield, UK), VWR (Darmstadt, Germany), Merck KGaA (Darmstadt, Germany), Alfa Aesar (Thermo Fisher (Kandel) GmbH, Karlsruhe, Germany), Novabiochem® (Merck KGaA, Darmstadt, Germany), or Roth (Carl Roth GmbH + Co. KG, Karlsruhe, Germany).

All reagents and solvents were used without further purification.

5.2 High-performance liquid chromatography (HPLC) devices

5.2.1 Preparative HPLC

The synthesized peptides were purified using a LaPrepΣ low-pressure semi-preparative HPLC system from VWR International GmbH (Darmstadt, Germany). This system is equipped with a LaPrepΣ LP 1200 preparative solvent pump with a 100 mL titanium pump head, a ternary low-pressure gradient, a dynamic mixing chamber, a 6-port-3-channel injection valve with an automated preparative 10 mL sample loop, a LaPrepΣ LP 3101 1-channel UV-detector, a LaPrepΣ semi-preparative flow cell with 0.5 mm path length, and a LaPrepΣ LP2016 17-port/1-

channel fractionation valve. A Kinetex® RP-C18 end-capped LC column (5 µm, 100 Å, 250 x 21.2 mm; Phenomenex, Torrance, CA, USA) with SecurityGuard™ PREP Cartridge Holder pre-column (21.2 mm; Phenomenex, Torrance, CA, USA) were installed providing the stationary phase for the purification processes. Used eluents were H_2O (Millipore) as solvent A and ACN (HPLC grade) as solvent B, both containing 0.1% (v/v) TFA. UV detection occurred at 220 nm. Obtained data were analyzed using EZChrom Elite software (Version 3.3.2 SP2, Agilent Technologies, Santa Clara, CA; USA).

5.2.2 Analytical HPLCs

5.2.2.1 LaChrom ELITE®

One of the analytical HPLC systems used for the analysis of synthetic progress and purity of the synthesized peptides was the LaChrom ELITE®-HPLC-System from VWR-Hitachi (VWR International GmbH, Darmstadt, Germany). This system comprises an organizer, two L-2130 HPLC pumps with solvent degasser, an L-2200 autosampler with a 100 µL sample loop, an L-2455 diode array flow detector, as well as a high-pressure gradient mixer. The stationary phase was served from a Kinetex® C18 column (5 µm, 100 Å, 250 x 4.6 mm, Phenomenx®, Torrance, CA; USA) equipped with a SecurityGuard™ Cartridge Kit (Ea, Phenomenex®, Torrance, CA, USA) and a C18 SecurityGuard™ cartridge (4 x 3.0 mm; Phenomenex®, Torrance, CA, USA) pre-column. The eluents used were H_2O (Millipore) as solvent A and ACN (HPLC grade) as solvent B, both containing 0.1% (v/v) TFA. UV detection occurred at 220 nm. Data analysis was performed with EZChrom Elite software (Version 3.3.2 SP2, Agilent Technologies, Santa Clara, CA; USA). Depicted chromatograms were generated with OriginPro 2023 (OriginLab Corporation, Northampton, MA, USA).

5.2.2.2 Chromaster HPLC 600 bar DAD

Another analytical HPLC system used for the analysis of synthetic progress and purity of the synthesized peptides was Chromaster HPLC 600 bar DAD by VWR-Hitachi (VWR International GmbH, Darmstadt, Germany). This system is equipped with an organizer, a 5160 pump with a 6-channel solvent degasser, a 5260 autosampler with a 100 µL sample loop, a 5310 column oven, and a 5430 diode array detector with a standard flow cell (1 mm optical path length). A Kinetex® C18 column (5 µm, 100 Å, 250 x 4.6 mm, Phenomenex®, Torrance, CA, USA), with a

SecurityGuard™ Cartridge Kit (Ea, Phenomenex®, Torrance, CA, USA) with C18 SecurityGuard™ cartridge as pre-column (4 x 3.0 mm, Phenomenex®, Torrance, CA, USA) provided the stationary phase. This HPLC system works with a low-pressure gradient with H_2O (Millipore) as solvent A and ACN (HPLC grade) as solvent B, both containing 0.1% (v/v) TFA, as eluents. UV detection was performed at 220 nm. Analysis of the data occurred with EZChrom Elite software (version 3.3.2, Agilent Technologies, Santa Clara, CA, USA) and the depiction of the chromatograms was generated with OriginPro 2023 (OriginLab Corporation, Northampton, MA, USA).

5.2.2.3 Primaide™

A further analytical HPLC system used for the analysis of synthetic progress and purity of the synthesized peptides was the Primaide™ purchased from VWR-Hitachi (VWR International GmbH, Darmstadt, Germany). This system involves an organizer, an 1110 pump with a low-pressure gradient and degasser, a 1210 autosampler with a 100 µL sample loop, a 1310 column oven, and a 1430 diode array detector. The stationary phase was provided by a Kinetex® C18 column (5 µm, 100 Å, 250 x 4.6 mm, Phenomenx®, Torrance, CA; USA) equipped with a SecurityGuard™ Cartridge Kit (Ea, Phenomenex®, Torrance, CA, USA) and a C18 SecurityGuard™ cartridge (4 x 3.0 mm; Phenomenex®, Torrance, CA, USA) pre-column. Eluents used were H_2O (Millipore) as solvent A and ACN (HPLC grade) as solvent B, both containing 0.1% (v/v) TFA. EZChrom Elite software (version 3.3.2, Agilent Technologies, Santa Clara, CA, USA) was used for data analysis. OriginPro 2023 (OriginLab Corporation, Northampton, MA, USA) was used to generate the depicted chromatograms.

5.3 Microwave-assisted solid-phase peptide synthesis

All peptides were synthesized from the *C*- to the *N*-terminus on a solid support, contrary to the biological direction of synthesis, using the Fmoc-SPPS strategy with acid-labile, side-chain-protected amino acids.

Fmoc protected canonical amino acids:

Fmoc-L-Ala-OH x H_2O, Fmoc-L-Cys(Trt)-OH, Fmoc-L-Glu(O^{t}Bu)-OH x H_2O, Fmoc-L-Ile-OH, Fmoc-L-Leu-OH, Fmoc-L-Lys(Boc)-OH, Fmoc-L-Phe-OH, Fmoc-L-Ser(^{t}Bu)-OH x H_2O.

Fmoc protected non-canonical amino acids:

Fmoc-L-Abu-OH, Fmoc-2-Abz-OH, Fmoc-γ-L-Homoasp(O^{t}Bu)-OH (Fmoc-β-D-Homoglu-O^{t}Bu), Fmoc-β-L-Homoleu-OH, Fmoc-β-L-Homolys(Boc)-OH, Fmoc-γ-L-Homolys(Boc)-OH ((*S*)-N-4-Fmoc-N-8-Boc-diaminooctanoic acid), Fmoc-S-methyl-L-Cys-OH.

Automated microwave-assisted SPPS was performed on CEM Liberty Blue™ (CEM Corporation, Matthews, NC, USA) using the CarboMAX™ approach. The approach size was 0.1 mmol using the Cl-MPA ProTide resin (resin substitution: 0.16 mmol g^{-1}).

The microwave settings (Table 8) were programmed for the different synthesis steps, which were performed in two phases. The first phase ensures a fast temperature rise with high power, the second involves low microwave power to avoid overshooting of the temperature during the reaction time.

Table 8: Microwave settings.

Process	**Temperature [°C]**	**Power [W]**	**Hold time [s]**	**Δ T [°C]**
DCA loading	80 90	75 20	60 540	2 1
Coupling 10 min at 90°C	75 90	217 40	15 585	1 1
Coupling 2 min	75 90	175 35	20 120	2 1
Coupling 4 min	75 90	217 43	15 225	2 2
Deprotection	75 90	155 35	15 120	2 1

Standard chloride loading of the desired 0.2 M (5 equiv) Fmoc-protected amino acid on the dry Cl-MPA ProTide resin was performed by Finkelstein reaction[198] with 1.0 M DIEA and 0.125 M potassium iodide in DMF. A standard deprotection time of 1 min was used for the deprotection of Fmoc with 10% (w/v) piperazine and

0.1 M HOBt in NMP/EtOH (9/1, v/v). Single coupling steps of 0.2 M (5 equiv) Fmoc-protected canonical amino acids, Fmoc-S-methyl-L-Cys-OH, and Fmoc-2-Abz-OH were executed with 1.0 M DIC and 1.0 M Oxyma Pure with 0.1 M DIEA in DMF for 4 min at 90 °C. Starting from the 21st amino acid, double coupling was performed for 2 min at 90 °C. The Fmoc-protected homologous β- and γ-amino acids (1.2 equiv) were coupled using a special coupling cycle for 10 min at 90 °C, followed by an additional washing step.

5.3.1 Determination of successful β-amino acid loading

Successful loading of the Cl-MPA resin with Fmoc-β-L-Homolys(Boc)-OH by the Finkelstein reaction[198] was determined through Fmoc-cleavage with 1,8-Diazabicyclo[5.4.0]undec-7-ene (DBU), following the procedure of Gude *et al.*[199] which was modified by Sigma Aldrich[200] for smaller scale approaches. Measurement of the UV absorbance of the dibenzofluvene provided an estimate of the resin loading. For this purpose, about 10 mg of the dried Fmoc-β-amino acid resin was weighed into a 10 mL graduated flask. Then, 2 mL of 2% (v/v) DBU in DMF was added and shaken for 30 min. Subsequently, the solution was diluted to 10 mL with ACN. 2 mL of this solution was transferred to a 25 mL graduated flask and further diluted to 25 mL with ACN. Three times 3 mL of this test solution were then analyzed by measuring the absorbance by UV/Vis spectroscopy at 304 nm on a Varian Cary 50 UV/Vis spectrophotometer (Varian Medical Systems, Palo Alto, CA, USA) in a quartz SUPRASIL® cuvette (10 mm path length, Hellma® Analytics, Müllheim, Germany). The reference solution was prepared using the same procedure as the test solution but without the addition of the resin.

The estimated amino acid loading was calculated from the equation:

$$loading_{Fmoc}\left[\frac{mmol}{g}\right] = \left(Abs_{sample} - Abs_{reference}\right) \times \frac{16.4}{mg\ of\ resin} \qquad (4)$$

5.4 Peptide cleavage from the resin and purification

5.4.1 Monitoring synthetic progress: Test cleavage

Test cleavages from the resin were carried out to confirm successful peptide synthesis. For this purpose, a small amount of peptide resin was treated in an

Eppendorf tube with a 100 µL cleavage cocktail for 2.5 – 3 h with shaking. The cleavage cocktail of all Cys-containing peptides consisted of 94% (v/v) TFA, 2.5% (v/v) EDT, 2.5% (v/v) H_2O (Millipore), and 1% (v/v) TIS. All other peptides were cleaved with a mixture containing 95% (v/v) TFA, 2.5% (v/v) H_2O (Millipore), and 2.5% (v/v) TIS. The corresponding cleavage cocktail was evaporated by a gentle N_2 stream. The crude peptide was then precipitated with 1.5 mL ice-cold diethyl ether. After centrifugation (MICRO CENTRIFUGE; Carl Roth GmbH + Co. KG; Karlsruhe, Germany), the diethyl ether was decanted, and the precipitate was dissolved in H_2O and ACN containing 0.1% (v/v) TFA according to the starting conditions of the reversed-phase analytical HPLC. Prior to injection into the analytical HPLC to monitor the synthetic progress, the resin beads were separated from the peptide solution by centrifugation.

Initial screening of the peptides occurred with a linear solvent gradient of 5 – 100% ACN/H_2O and 0.1% (v/v) TFA for 18 min. Detailed gradient information is given in Table 9:

Table 9: Gradient information for initial runs used for screening synthesized peptides on an analytical HPLC. Eluents: Solvent A = 0.1% (v/v) TFA in water, Solvent B = 0.1% (v/v) TFA in ACN.

Time [min]	**Solvent A [%]**	**Solvent B [%]**	**Flow rate [mL/min]**
0.0	95.0	5.0	1.00
18.0	0.0	100.0	1.00
20.0	0.0	100.0	1.00
21.0	95.0	5.0	1.00
26.0	95.0	5.0	1.00

Later, a linear solvent gradient of 10 – 80% ACN/H_2O and 0.1% (v/v) TFA (Table 10) for 18 min was applied for the basic peptide variants and a gradient of 30 – 100 ACN/H_2O and 0.1% (v/v) TFA (Table 11) for the acidic peptide variants.

Table 10: Gradient information for investigating purity of synthesized base peptide variants on an analytical HPLC. Eluents: Solvent A = 0.1% (v/v) TFA in water, Solvent B = 0.1% (v/v) TFA in ACN.

Time [min]	Solvent A [%]	Solvent B [%]	Flow rate [mL/min]
0.0	90.0	10.0	1.00
18.0	20.0	80.0	1.00
19.0	0.0	100.0	1.00
21.0	0.0	100.0	1.00
22.0	90.0	10.0	1.00
25.0	90.0	10.0	1.00

Table 11: Gradient information for investigating purity of synthesized acid peptide variants on an analytical HPLC. Eluents: Solvent A = 0.1% (v/v) TFA in water, Solvent B = 0.1% (v/v) TFA in ACN.

Time [min]	Solvent A [%]	Solvent B [%]	Flow rate [mL/min]
0.0	70.0	30.0	1.00
18.0	0.0	100.0	1.00
20.0	0.0	100.0	1.00
22.0	70.0	30.0	1.00
26.0	70.0	30.0	1.00

5.4.2 Full cleavage of the peptides from the resin

A full cleavage procedure was conducted to obtain side-chain deprotected peptides that are free from the resin. Deprotection of the side chains and resin cleavage occurred with shaking for 2.5 – 3 h in the cleavage cocktail (2.0 mL per 150 mg resin). The cleavage cocktail for all Cys-containing peptides consisted of 94% (v/v) TFA, 2.5% (v/v) EDT, 2.5% (v/v) H_2O (Millipore), and 1% (v/v) TIS, while the mixture for all other peptides contained 95% (v/v) TFA, 2.5% (v/v) H_2O (Millipore), and 2.5% (v/v) TIS. After completion of the shaking time, the solution was filtered into a 100 mL flask. The resin was then washed three times with dichloromethane (DCM). DCM was also collected into the 100 mL flask during this process. Excess solvents were then removed under reduced pressure. After precipitation of the

crude peptide with ice-cold diethyl ether, centrifugation was performed for 6 min at 4 °C and 4.4 rpm using Eppendorf® Centrifuge 5702 R (Merck KGaA; Darmstadt, Germany). After discarding the supernatant, the peptide pellets were diluted in H_2O (Millipore) using ultrasonication, frozen with liquid nitrogen, and subsequently lyophilized overnight using an ALPHA 1-2 LD dryer (Christ Gefriertrocknungsanlagen GmbH, Osterode am Harz, Germany) connected to a CHEMISTRY HYBRID PUMP RC 6 (Vacuubrand GmbH + Co KG, Wertheim, Germany). The dried crude peptides were dissolved in a solvent mixture corresponding to the starting conditions of the HPLC, filtered, and purified by reversed-phase preparative HPLC.

5.4.3 Purification and characterization by HPLC

The dried crude peptides dissolved in ACN/H_2O containing 0.1% (v/v) TFA (1.0 mL per 10 mg) according to the starting conditions of the preparative reversed-phase HPLC were filtered using a 0.45 µm Acrodisc® syringe filter with GHP membrane (Pall Corporation, Port Washington, NY, USA) before injection. Each injection contained a maximum of 4.0 mL of crude peptide solution. The purification was performed using a preparative reversed-phase HPLC (LaPrepΣ low-pressure HPLC; VWR, Darmstadt, Germany) equipped with a Kinetex® RP-C18 end-capped LC column (5 µm, 100 Å, 250 x 21.2 mm; Phenomenex, Torrance, CA, USA) and SecurityGuard PREP Cartridge Holder pre-column (21.2 mm; Phenomenex, Torrance, CA, USA). The preparative HPLC runs were executed at a flow rate of 15.0 mL/min for 18 minutes, and UV detection occurred at 220 nm. A linear solvent gradient of 10 – 80% ACN/H_2O and 0.1% (v/v) TFA was applied for all base peptide and chimeric peptide variants (Table 12). For all acid peptide variants, a linear solvent gradient of 30 – 100% ACN/H_2O and 0.1% (v/v) TFA was used (Table 13). Primaide™ or Chromaster 600 bar DAD analytical HPLC systems were used to analyze the collected fractions. After combining the fractions containing the desired and pure peptide, ACN was removed under reduced pressure. The remaining aqueous peptide solution was frozen with liquid nitrogen and then lyophilized using an ALPHA 1-2 LD dryer (Christ Gefriertrocknungsanlagen GmbH, Osterode am Harz, Germany) connected to a CHEMISTRY HYBRID PUMP RC 6 (Vacuubrand GmbH + Co KG, Wertheim, Germany) to obtain the dry and white peptide powder. Finally, the purity of the

obtained dry peptides was verified by analytical HPLC (either LaChrom ELITE®, Primaide™, or Chromaster 600 bar DAD) and high-resolution ESI-ToF-MS. All ICEF-peptide variants and Acid-pp had to be purified a second time by preparative reversed-phase HPLC since a single purification resulted in insufficient purity.

Table 12: Gradient information for purification of synthesized base peptide variants using a preparative HPLC. Eluents: Solvent A = 0.1% (v/v) TFA in water, Solvent B = 0.1% (v/v) TFA in ACN.

Time [min]	Solvent A [%]	Solvent B [%]	Flow rate [mL/min]
0.0	90.0	10.0	15.00
18.0	20.0	80.0	15.00
19.0	0.0	100.0	15.00
22.0	0.0	100.0	15.00
23.0	90.0	10.0	15.00
26.0	90.0	10.0	15.00

Table 13: Gradient information for purification of synthesized acid peptide variants using a preparative HPLC. Eluents: Solvent A = 0.1% (v/v) TFA in water, Solvent B = 0.1% (v/v) TFA in ACN.

Time [min]	Solvent A [%]	Solvent B [%]	Flow rate [mL/min]
0.0	70.0	30.0	15.00
18.0	0.0	100.0	15.00
21.0	0.0	100.0	15.00
22.0	70.0	30.0	15.00
25.0	70.0	30.0	15.00

5.4.4 Peptide counterion exchange

The synthesized peptides are obtained as salts with TFA as counterions by exposing them to TFA both during the full cleavage procedure to cleave the peptide from the solid support after synthesis and during the reverse-phase HPLC purification, where TFA is used as an ion-pairing reagent. The TFA ions are most likely to bind to the positively charged free amino groups of the residues such as Lys, Arg, and His, as well as to the free *N*-terminus.

The exchange of the TFA counterions to chloride counterions was used for crystallization purposes. Therefore, the dry peptides (approximately 10 mg) were dissolved in 2 mL water (Millipore) containing 1% (v/v) concentrated HCl. The peptides were vortexed for 1 min and lyophilized after freezing with liquid nitrogen using an ALPHA 1-2 LD dryer (Christ Gefriertrocknungsanlagen GmbH, Osterode am Harz, Germany) connected to a CHEMISTRY HYBRID PUMP RC 6 (Vacuubrand GmbH + Co KG, Wertheim, Germany). The procedure of dissolving the peptides in 2 mL water (Millipore) containing 1% (v/v) concentrated HCl and lyophilization was repeated five times.

5.5 Synthesized peptides

All peptides synthesized in this thesis are listed with their name, corresponding sequences, analytical HPLC, and high-resolution ESI-ToF-MS parameters. They offered a purity higher than 95%.

Table 14: Base-pp; peptide sequence, analytical HPLC- and ESI-MS data.

Base-pp

Peptide sequence:

o-Abz L S A L K E K L A S L K E K L S A L K E K L A S L K E K L S A L K E K - OH

Analytical HPLC:

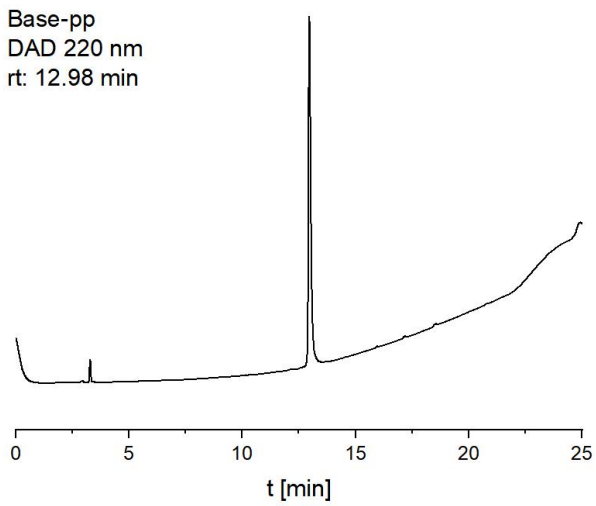

HPLC-system: Primaide™

Column: Kinetex® C18

Eluents: A = 0.1% (v/v) TFA in water, B = 0.1% (v/v) TFA in ACN

Gradient: 10 % eluent B in eluent A to 80 % eluent B over 18 min

ESI-ToF MS:

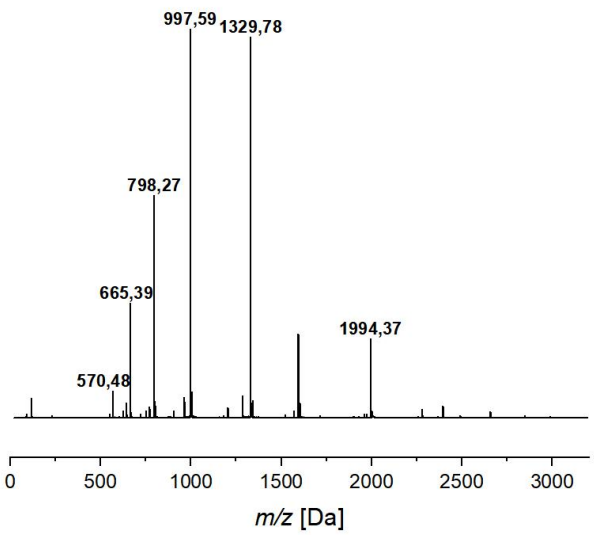

charge	*m/z* [Da] calculated (average)	*m/z* [Da] measured
$[M+2H]^{2+}$	1994.402	1994.374
$[M+3H]^{3+}$	1329.937	1329.782
$[M+4H]^{4+}$	997.705	997.586
$[M+5H]^{5+}$	798.366	798.269
$[M+6H]^{6+}$	665.473	665.392

Table 15: B3β2γ; peptide sequence, analytical HPLC- and ESI-MS data.

B3β2γ

Peptide sequence:

o-Abz L S A L K E K L A S L K E K β³hL γ⁴hD β³hL γ⁴hK β³hK L A S L K E K L S A L K E K - OH

Analytical HPLC:

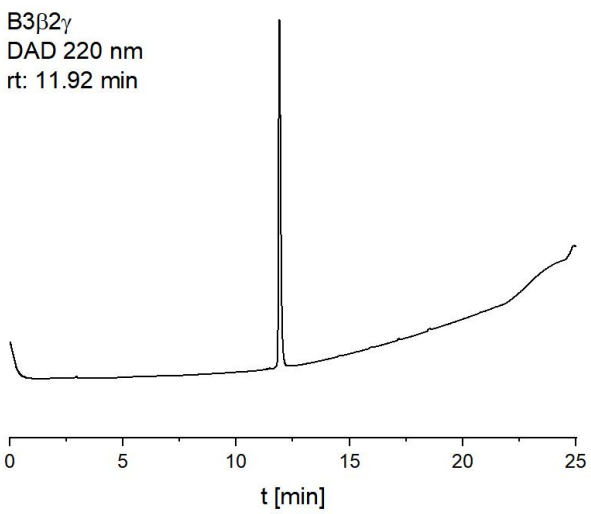

HPLC-system: Primaide™

Column: Kinetex® C18

Eluents: A = 0.1% (v/v) TFA in water, B = 0.1% (v/v) TFA in ACN

Gradient: 10 % eluent B in eluent A to 80 % eluent B over 18 min

ESI-ToF MS:

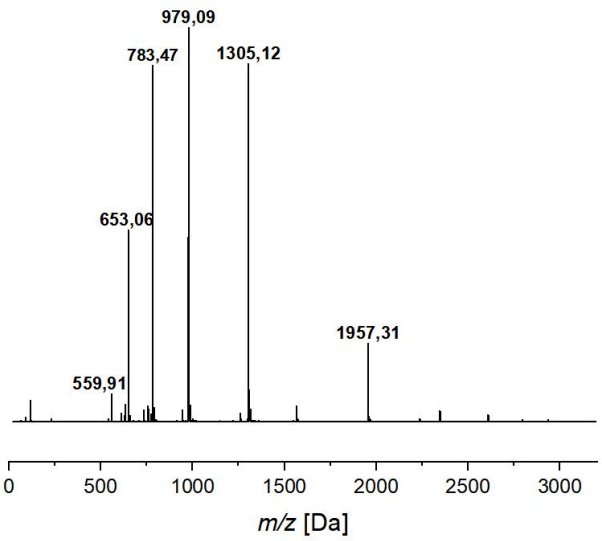

charge	*m/z* [Da] calculated (average)	*m/z* [Da] measured
$[M+2H]^{2+}$	1957.404	1957.305
$[M+3H]^{3+}$	1305.272	1305.122
$[M+4H]^{4+}$	979.206	979.090
$[M+5H]^{5+}$	783.566	783.473
$[M+6H]^{6+}$	653.140	653.062
$[M+7H]^{7+}$	559.978	559.913

Table 16: Acid-pp; peptide sequence, analytical HPLC- and ESI-MS data.

Acid-pp

Peptide sequence:

o-Abz L S A L E K E L A S L E K E L S A L E K E L A S L E K E L S A L E K E - OH

Analytical HPLC:

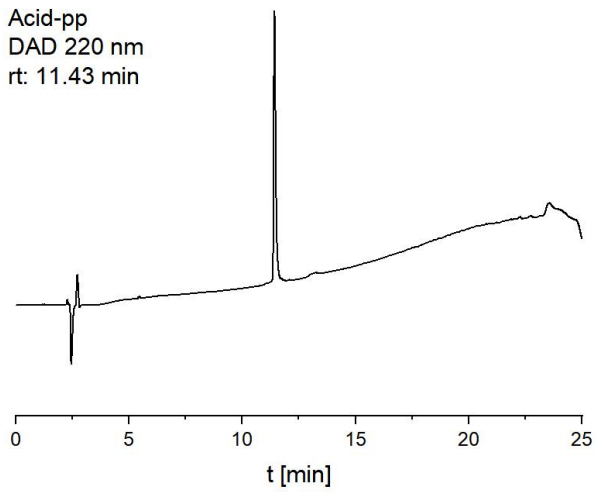

HPLC-system: Chromaster 600 bar DAD

Column: Kinetex® C18

Eluents: A = 0.1% (v/v) TFA in water, B = 0.1% (v/v) TFA in ACN

Gradient: 30 % eluent B in eluent A to 100 % eluent B over 18 min

ESI-ToF MS:

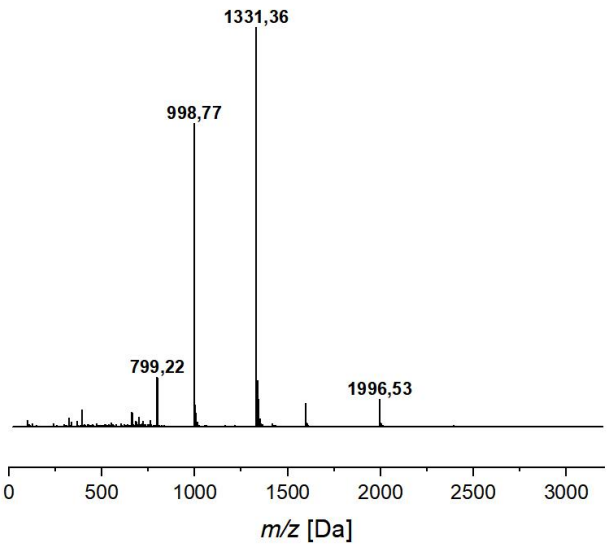

charge	*m/z* [Da] calculated (average)	*m/z* [Da] measured
$[M+2H]^{2+}$	1996.756	1996.535
$[M+3H]^{3+}$	1331.507	1331.363
$[M+4H]^{4+}$	998.882	998.774
$[M+5H]^{5+}$	799.307	799.221

Table 17: Acid-CFLE; peptide sequence, analytical HPLC- and ESI-MS data.

Acid-CFLE

Peptide sequence:

o-Abz L S A L E K E L A S L E K E C S A F L K E L A S L E K E L S A L E K E - OH

Analytical HPLC:

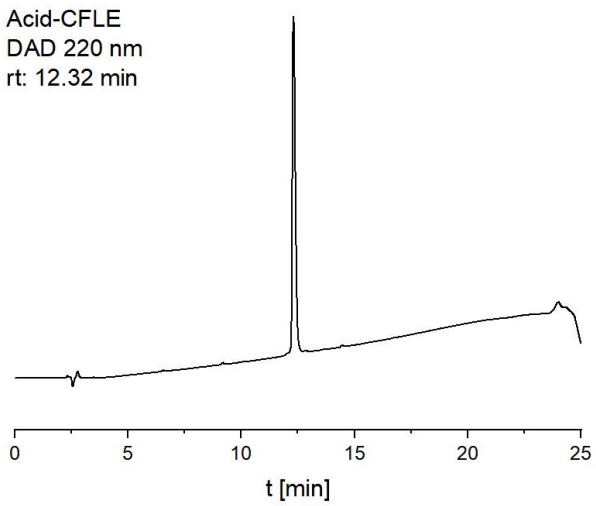

HPLC-system: Primaide™

Column: Kinetex® C18

Eluents: A = 0.1% (v/v) TFA in water, B = 0.1% (v/v) TFA in ACN

Gradient: 30 % eluent B in eluent A to 100 % eluent B over 18 min

ESI-ToF MS:

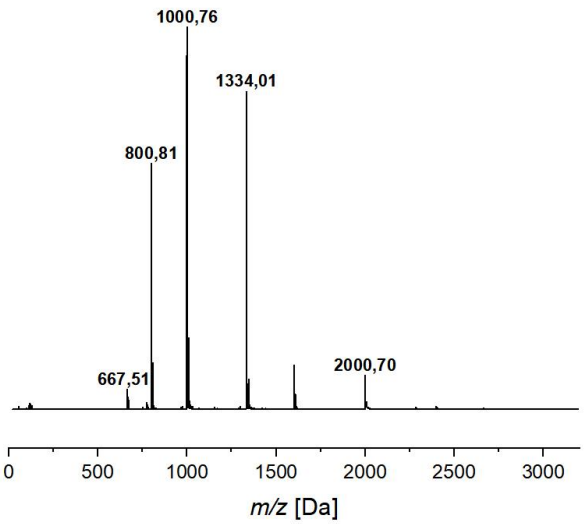

charge	*m/z* [Da] calculated (average)	*m/z* [Da] measured
$[M+2H]^{2+}$	2000.779	2000.701
$[M+3H]^{3+}$	1334.188	1334.014
$[M+4H]^{4+}$	1000.893	1000.759
$[M+5H]^{5+}$	800.916	800.809
$[M+6H]^{6+}$	667.598	667.511

Table 18: Acid-ICEF; peptide sequence, analytical HPLC- and ESI-MS data.

Acid-ICEF

Peptide sequence:

o-Abz L S A L E K E L A S L E K E I S A C E K F L A S L E K E L S A L E K E - OH

Analytical HPLC:

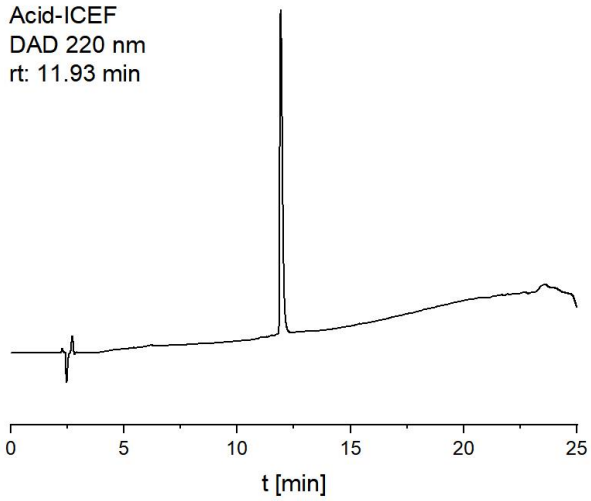

HPLC-system: Chromaster 600 bar DAD

Column: Kinetex® C18

Eluents: A = 0.1% (v/v) TFA in water, B = 0.1% (v/v) TFA in ACN

Gradient: 30 % eluent B in eluent A to 100 % eluent B over 18 min

ESI-ToF MS:

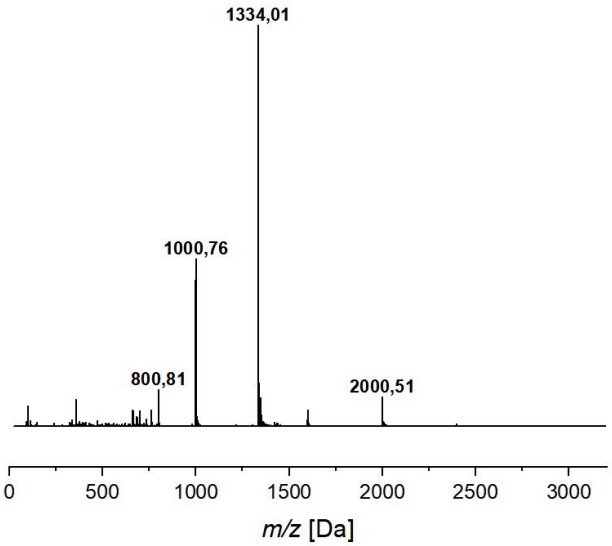

charge	*m/z* [Da] calculated (average)	*m/z* [Da] measured
$[M+2H]^{2+}$	2000.779	2000.510
$[M+3H]^{3+}$	1334.188	1334.010
$[M+4H]^{4+}$	1000.893	1000.759
$[M+5H]^{5+}$	800.916	800.809

Table 19: Acid-AbuFLE; peptide sequence, analytical HPLC- and ESI-MS data.

Acid-AbuFLE

Peptide sequence:

o-Abz L S A L E K E L A S L E K E Abu S A F L K E L A S L E K E L S A L E K E - OH

Analytical HPLC:

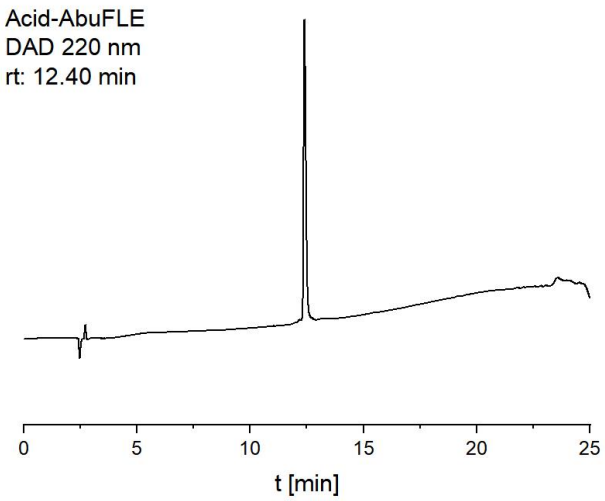

HPLC-system: Chromaster 600 bar DAD

Column: Kinetex® C18

Eluents: A = 0.1% (v/v) TFA in water, B = 0.1% (v/v) TFA in ACN

Gradient: 30 % eluent B in eluent A to 100 % eluent B over 18 min

ESI-ToF MS:

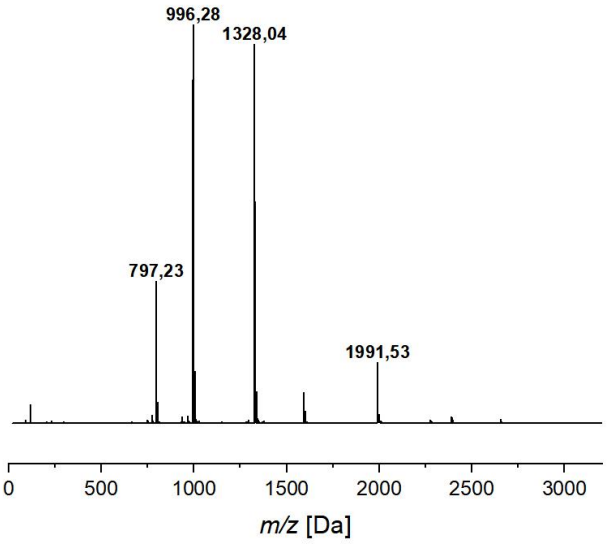

charge	*m/z* [Da] calculated (average)	*m/z* [Da] measured
$[M+2H]^{2+}$	1991.760	1991.531
$[M+3H]^{3+}$	1328.176	1328.041
$[M+4H]^{4+}$	996.384	996.279
$[M+5H]^{5+}$	797.309	797.225

Table 20: Acid-SFLE; peptide sequence, analytical HPLC- and ESI-MS data.

Acid-SFLE

Peptide sequence:

o-Abz L S A L E K E L A S L E K E S S A F L K E L A S L E K E L S A L E K E - OH

Analytical HPLC:

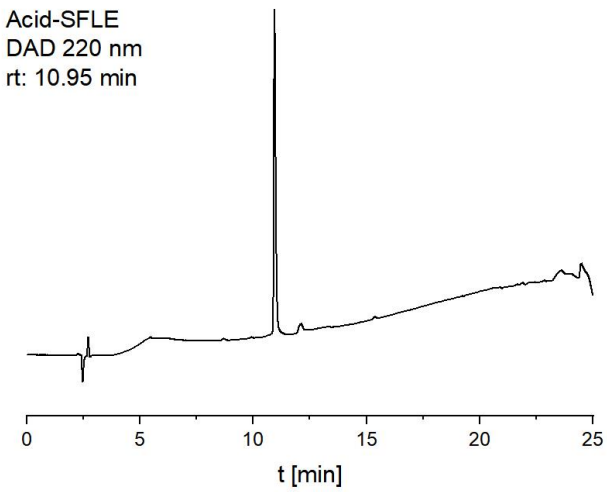

HPLC-system: Chromaster 600 bar DAD

Column: Kinetex® C18

Eluents: A = 0.1% (v/v) TFA in water, B = 0.1% (v/v) TFA in ACN

Gradient: 30 % eluent B in eluent A to 100 % eluent B over 18 min

ESI-ToF MS:

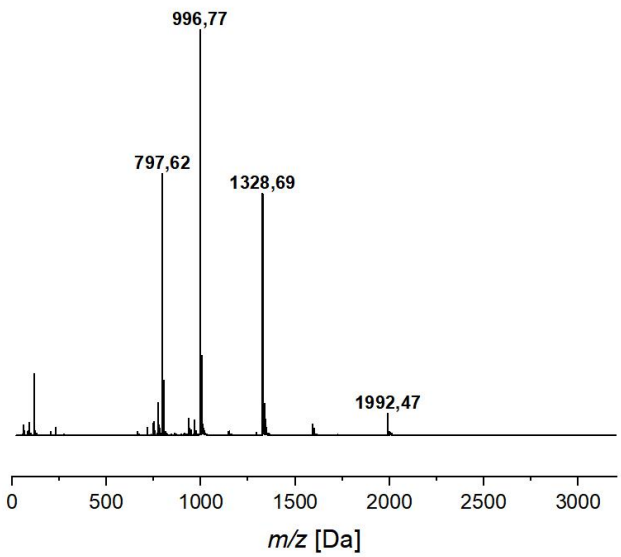

charge	*m/z* [Da] calculated (average)	*m/z* [Da] measured
$[M+2H]^{2+}$	1992.746	1992.466
$[M+3H]^{3+}$	1328.833	1328.694
$[M+4H]^{4+}$	996.877	996.771
$[M+5H]^{5+}$	797.703	797.618

Table 21: Acid-*m*CFLE; peptide sequence, analytical HPLC- and ESI-MS data.

Acid-*m*CFLE

Peptide sequence:

o-Abz L S A L E K E L A S L E K E C(Me) S A F L K E L A S L E K E L S A L E K E - OH

Analytical HPLC:

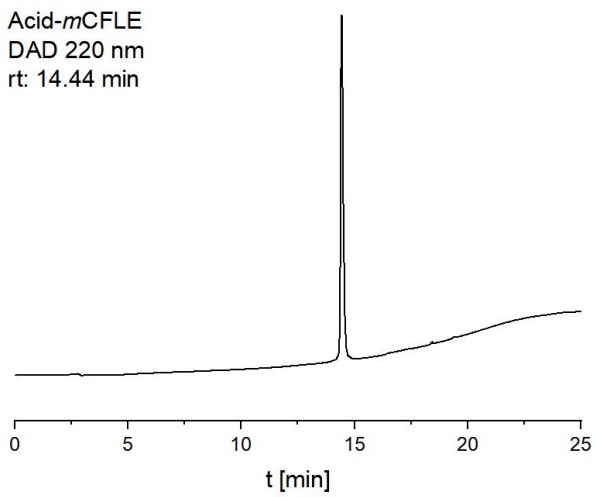

HPLC-system: LaChrom ELITE®

Column: Kinetex® C18

Eluents: A = 0.1% (v/v) TFA in water, B = 0.1% (v/v) TFA in ACN

Gradient: 30 % eluent B in eluent A to 100 % eluent B over 18 min

ESI-ToF MS:

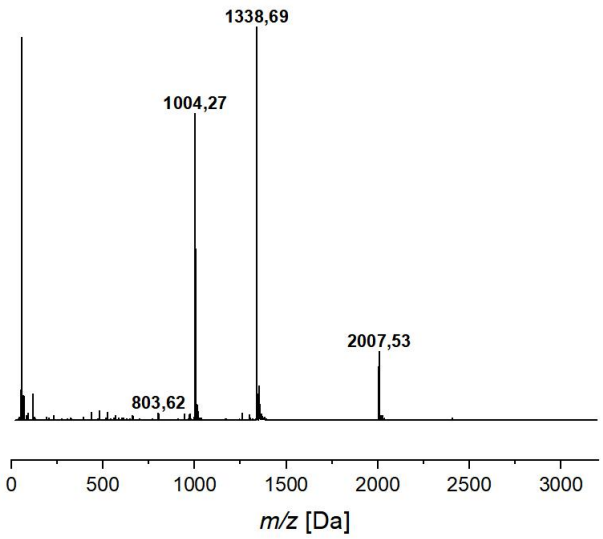

charge	*m/z* [Da] calculated (average)	*m/z* [Da] measured
$[M+2H]^{2+}$	2007.792	2007.532
$[M+3H]^{3+}$	1338.864	1338.698
$[M+4H]^{4+}$	1004.400	1004.267
$[M+5H]^{5+}$	803.722	803.616

Table 22: Acid-IAbuEF; peptide sequence, analytical HPLC- and ESI-MS data.

Acid-IAbuEF

Peptide sequence:

o-Abz L S A L E K E L A S L E K E I S A Abu E K F L A S L E K E L S A L E K E - OH

Analytical HPLC:

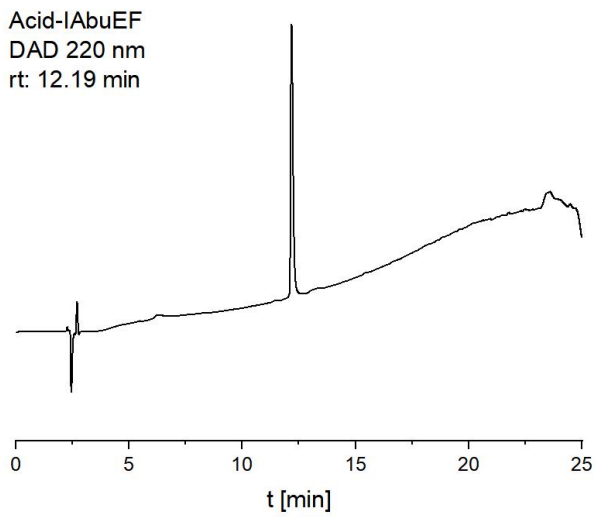

HPLC-system: Chromaster 600 bar DAD

Column: Kinetex® C18

Eluents: A = 0.1% (v/v) TFA in water, B = 0.1% (v/v) TFA in ACN

Gradient: 30 % eluent B in eluent A to 100 % eluent B over 18 min

ESI-ToF MS:

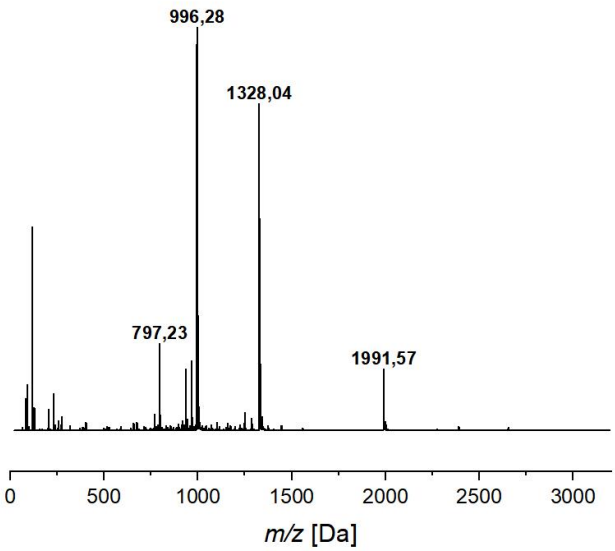

charge	*m/z* [Da] calculated (average)	*m/z* [Da] measured
$[M+2H]^{2+}$	1991.760	1991.566
$[M+3H]^{3+}$	1328.176	1328.041
$[M+4H]^{4+}$	996.384	996.279
$[M+5H]^{5+}$	797.309	797.226

Table 23: Acid-ISEF; peptide sequence, analytical HPLC- and ESI-MS data.

Acid-ISEF

Peptide sequence:

o-Abz L S A L E K E L A S L E K E I S A S E K F L A S L E K E L S A L E K E - OH

Analytical HPLC:

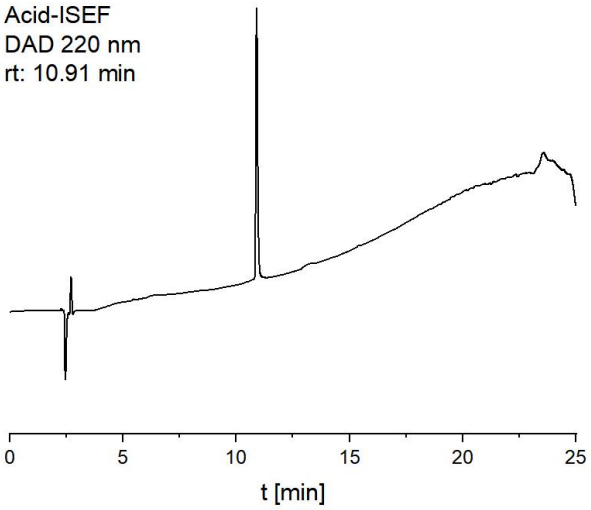

HPLC-system: Chromaster 600 bar DAD

Column: Kinetex® C18

Eluents: A = 0.1% (v/v) TFA in water, B = 0.1% (v/v) TFA in ACN

Gradient: 30 % eluent B in eluent A to 100 % eluent B over 18 min

ESI-ToF MS:

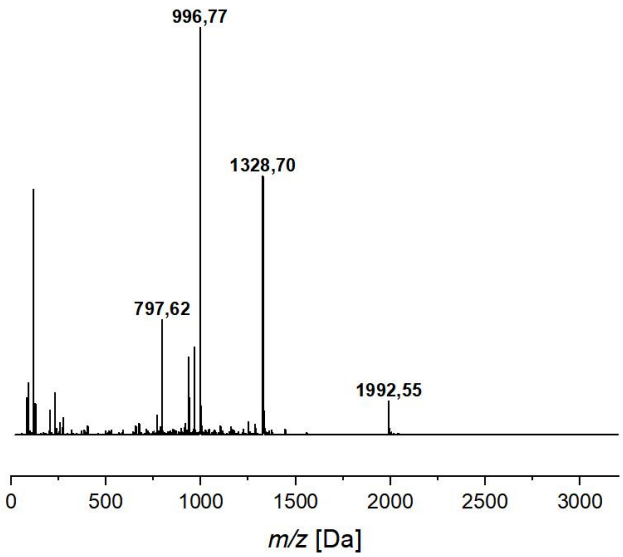

charge	*m/z* [Da] calculated (average)	*m/z* [Da] measured
$[M+2H]^{2+}$	1992.746	1992.552
$[M+3H]^{3+}$	1328.833	1328.698
$[M+4H]^{4+}$	996.877	996.774
$[M+5H]^{5+}$	797.703	797.622

Table 24: Acid-I*m*CEF; peptide sequence, analytical HPLC- and ESI-MS data.

Acid-I*m*CEF

Peptide sequence:

o-Abz L S A L E K E L A S L E K E I S A C(Me) E K F L A S L E K E L S A L E K E - OH

Analytical HPLC:

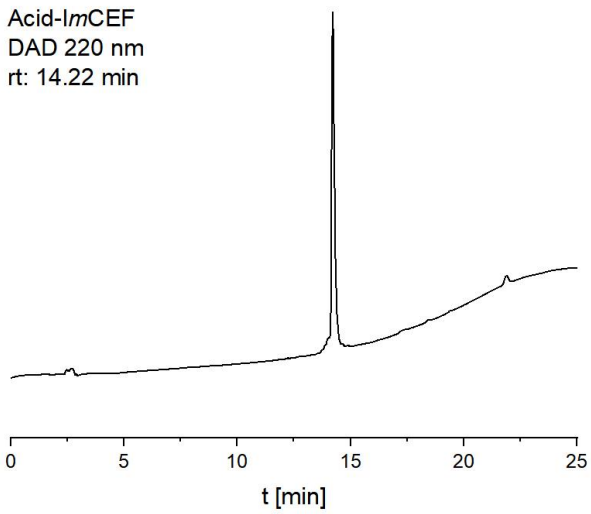

HPLC-system: LaChrom ELITE®

Column: Kinetex® C18

Eluents: A = 0.1% (v/v) TFA in water, B = 0.1% (v/v) TFA in ACN

Gradient: 30 % eluent B in eluent A to 100 % eluent B over 18 min

ESI-ToF MS:

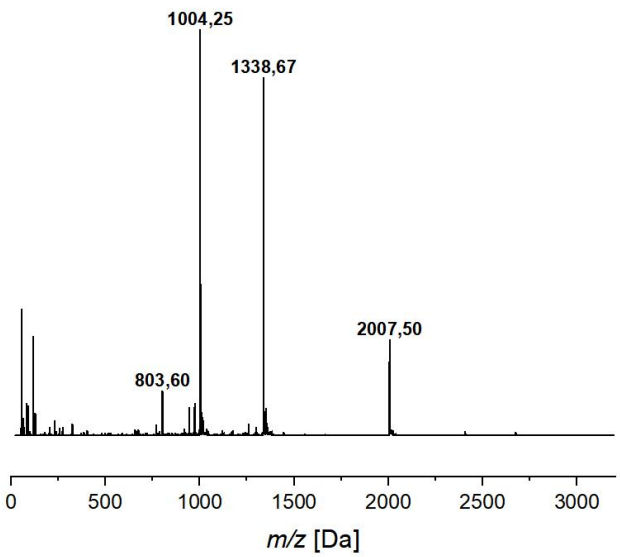

charge	*m/z* [Da] calculated (average)	*m/z* [Da] measured
$[M+2H]^{2+}$	2007.792	2007.503
$[M+3H]^{3+}$	1338.864	1338.670
$[M+4H]^{4+}$	1004.400	1004.254
$[M+5H]^{5+}$	803.722	803.604

Table 25: B3β2γ-2,4; peptide sequence, analytical HPLC- and ESI-MS data.

B3β2γ-2,4

Peptide sequence:

o-Abz L S A L K E K β³hL γ⁴hD β³hL γ⁴hK β³hK L S A L K E K β³hL γ⁴hD β³hL γ⁴hK β³hK L S A L K E K - OH

Analytical HPLC:

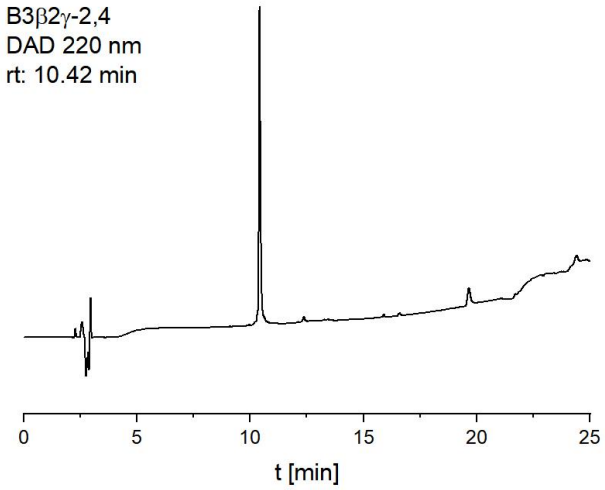

HPLC-system: Chromaster 600 bar DAD

Column: Kinetex® C18

Eluents: A = 0.1% (v/v) TFA in water, B = 0.1% (v/v) TFA in ACN

Gradient: 10 % eluent B in eluent A to 80 % eluent B over 18 min

ESI-ToF MS:

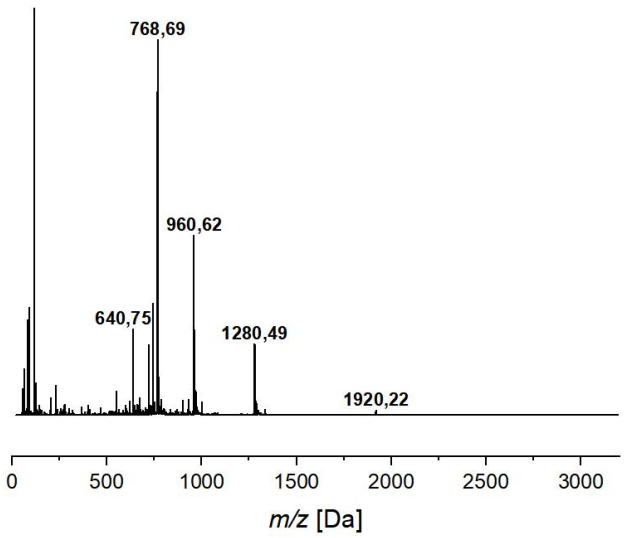

charge	*m/z* [Da] calculated (average)	*m/z* [Da] measured
$[M+2H]^{2+}$	1920.406	1920.219
$[M+3H]^{3+}$	1280.607	1280.486
$[M+4H]^{4+}$	960.707	960.615
$[M+5H]^{5+}$	768.767	768.693
$[M+6H]^{6+}$	640.807	640.746

Table 26: Acid-CFLE-2,4; peptide sequence, analytical HPLC- and ESI-MS data.

Acid-CFLE-2,4

Peptide sequence:

o-Abz L S A L E K E C A S F L K E L S A L E K E C A S F L K E L S A L E K E - OH

Analytical HPLC:

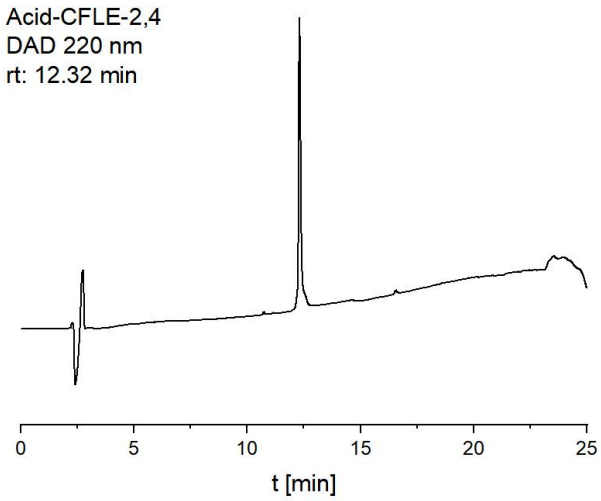

HPLC-system: Chromaster 600 bar DAD

Column: Kinetex® C18

Eluents: A = 0.1% (v/v) TFA in water, B = 0.1% (v/v) TFA in ACN

Gradient: 30 % eluent B in eluent A to 100 % eluent B over 18 min

ESI-ToF MS:

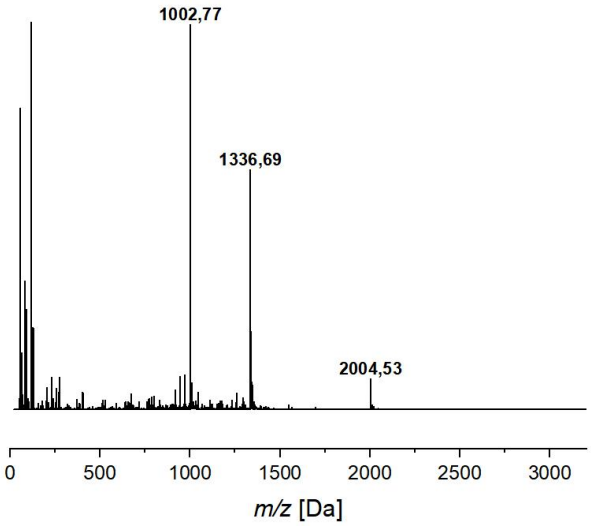

charge	*m/z* [Da] calculated (average)	*m/z* [Da] measured
$[M+2H]^{2+}$	2004.801	2004.526
$[M+3H]^{3+}$	1336.870	1336.688
$[M+4H]^{4+}$	1002.905	1002.768

Table 27: Acid-ICEF-2,4; peptide sequence, analytical HPLC- and ESI-MS data.

Acid-ICEF-2,4

Peptide sequence:

o-Abz L S A L E K E I A S C E K F L S A L E K E I A S C E K F L S A L E K E - OH

Analytical HPLC:

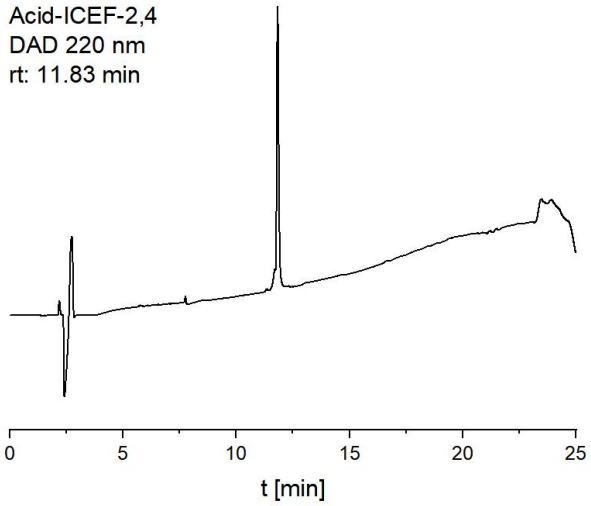

HPLC-system: Chromaster 600 bar DAD

Column: Kinetex® C18

Eluents: A = 0.1% (v/v) TFA in water, B = 0.1% (v/v) TFA in ACN

Gradient: 30 % eluent B in eluent A to 100 % eluent B over 18 min

ESI-ToF MS:

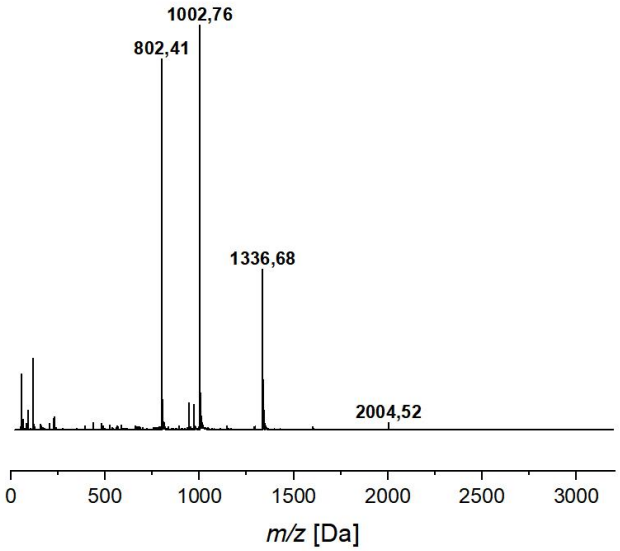

charge	*m/z* [Da] calculated (average)	*m/z* [Da] measured
$[M+2H]^{2+}$	2004.801	2004.516
$[M+3H]^{3+}$	1336.870	1336.684
$[M+4H]^{4+}$	1002.905	1002.764
$[M+5H]^{5+}$	802.525	802.412

Table 28: B3β2γ-1,5; peptide sequence, analytical HPLC- and ESI-MS data.

B3β2γ-1,5

Peptide sequence:

o-Abz β³hL γ⁴hD β³hL γ⁴hK β³hK L A S L K E K L S A L K E K L A S L K E K β³hL γ⁴hD β³hL γ⁴hK β³hK - OH

Analytical HPLC:

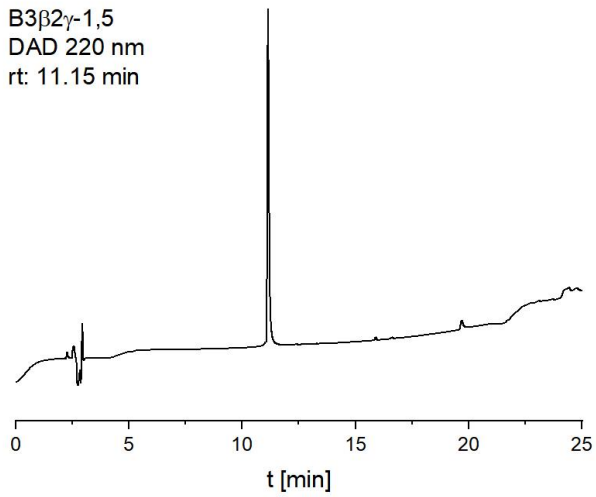

HPLC-system: Chromaster 600 bar DAD

Column: Kinetex® C18

Eluents: A = 0.1% (v/v) TFA in water, B = 0.1% (v/v) TFA in ACN

Gradient: 10 % eluent B in eluent A to 80 % eluent B over 18 min

ESI-ToF MS:

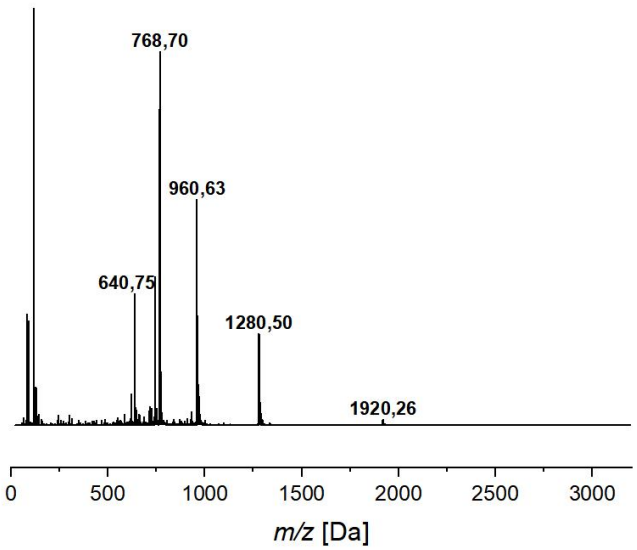

charge	*m/z* [Da] calculated (average)	*m/z* [Da] measured
$[M+2H]^{2+}$	1920.406	1920.255
$[M+3H]^{3+}$	1280.607	1280.499
$[M+4H]^{4+}$	960.707	960.625
$[M+5H]^{5+}$	768.767	768.699
$[M+6H]^{6+}$	640.807	640.749

Table 29: Acid-CFLE-1,5; peptide sequence, analytical HPLC- and ESI-MS data.

Acid-CFLE-1,5

Peptide sequence:

o-Abz C S A F L K E L A S L E K E L S A L E K E L A S L E K E C S A F L K E - OH

Analytical HPLC:

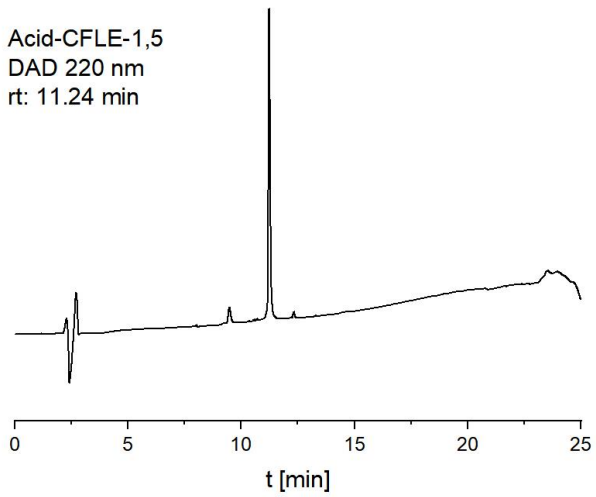

HPLC-system: Chromaster 600 bar DAD

Column: Kinetex® C18

Eluents: A = 0.1% (v/v) TFA in water, B = 0.1% (v/v) TFA in ACN

Gradient: 30 % eluent B in eluent A to 100 % eluent B over 18 min

ESI-ToF MS:

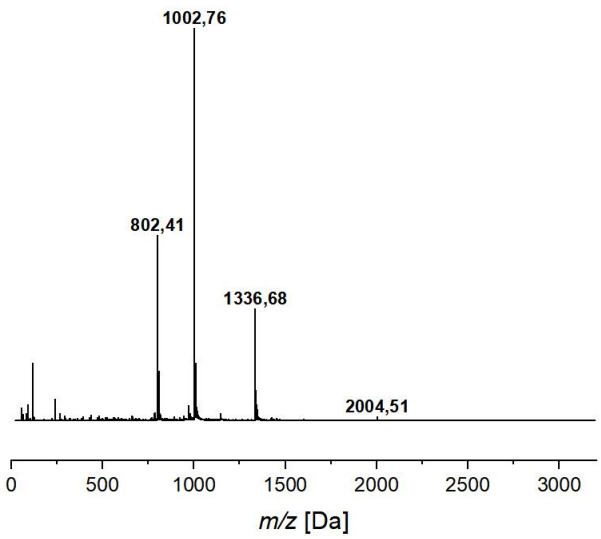

charge	*m/z* [Da] calculated (average)	*m/z* [Da] measured
$[M+2H]^{2+}$	2004.801	2004.514
$[M+3H]^{3+}$	1336.870	1336.678
$[M+4H]^{4+}$	1002.905	1002.759
$[M+5H]^{5+}$	802.525	802.408

Table 30: Acid-ICEF-1,5; peptide sequence, analytical HPLC- and ESI-MS data.

Acid-ICEF-1,5

Peptide sequence:

o-Abz I S A C E K F L A S L E K E L S A L E K E L A S L E K E I S A C E K F - OH

Analytical HPLC:

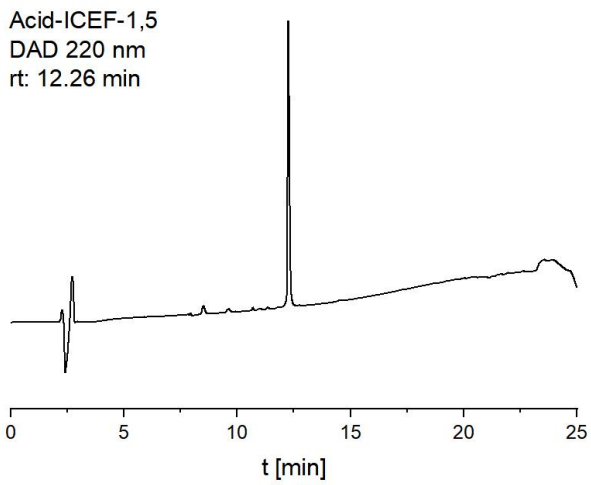

HPLC-system: Chromaster 600 bar DAD

Column: Kinetex® C18

Eluents: A = 0.1% (v/v) TFA in water, B = 0.1% (v/v) TFA in ACN

Gradient: 30 % eluent B in eluent A to 100 % eluent B over 18 min

ESI-ToF MS:

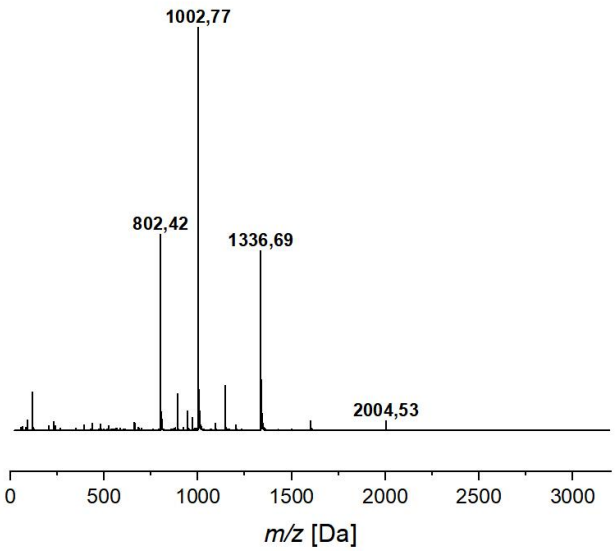

charge	*m/z* [Da] calculated (average)	*m/z* [Da] measured
$[M+2H]^{2+}$	2004.801	2004.531
$[M+3H]^{3+}$	1336.870	1336.692
$[M+4H]^{4+}$	1002.905	1002.769
$[M+5H]^{5+}$	802.525	802.418

Table 31: B3β2γ-1,2; peptide sequence, analytical HPLC- and ESI-MS data.

B3β2γ-1,2

Peptide sequence:

o-Abz β³hL γ⁴hD β³hL γ⁴hK β³hK β³hL γ⁴hD β³hL γ⁴hK β³hK L S A L K E K L A S L K E K L S A L K E K - OH

Analytical HPLC:

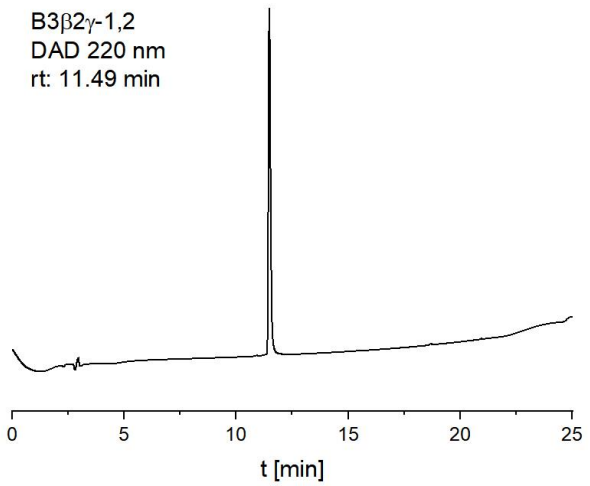

HPLC-system: Primaide™

Column: Kinetex® C18

Eluents: A = 0.1% (v/v) TFA in water, B = 0.1% (v/v) TFA in ACN

Gradient: 10 % eluent B in eluent A to 80 % eluent B over 18 min

ESI-ToF MS:

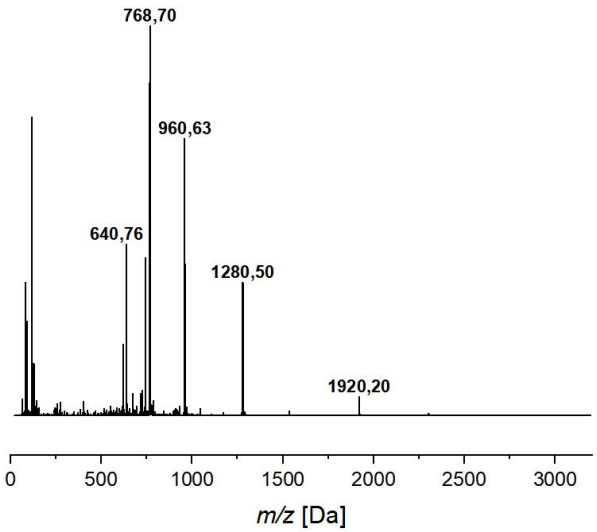

charge	*m/z* [Da] calculated (average)	*m/z* [Da] measured
$[M+2H]^{2+}$	1920.406	1920.203
$[M+3H]^{3+}$	1280.607	1280.503
$[M+4H]^{4+}$	960.707	960.629
$[M+5H]^{5+}$	768.767	768.704
$[M+6H]^{6+}$	640.807	640.755

Table 32: Acid-CFLE-1,2; peptide sequence, analytical HPLC- and ESI-MS data.

Acid-CFLE-1,2

Peptide sequence:

o-Abz C S A F L K E C A S F L K E L S A L E K E L A S L E K E L S A L E K E - OH

Analytical HPLC:

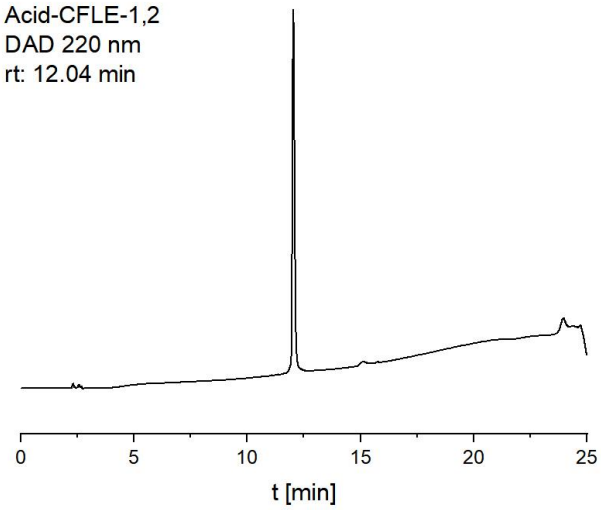

HPLC-system: Primaide™

Column: Kinetex® C18

Eluents: A = 0.1% (v/v) TFA in water, B = 0.1% (v/v) TFA in ACN

Gradient: 30 % eluent B in eluent A to 100 % eluent B over 18 min

ESI-ToF MS:

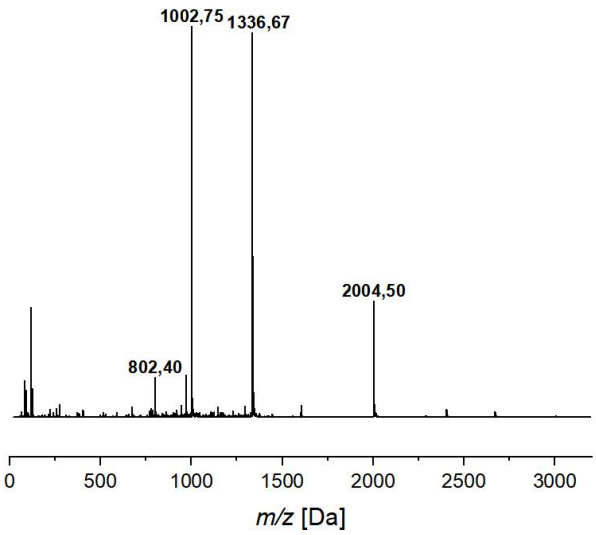

charge	*m/z* [Da] calculated (average)	*m/z* [Da] measured
$[M+2H]^{2+}$	2004.801	2004.501
$[M+3H]^{3+}$	1336.870	1336.665
$[M+4H]^{4+}$	1002.905	1002.748
$[M+5H]^{5+}$	802.525	802.397

Table 33: Acid-ICEF-1,2; peptide sequence, analytical HPLC- and ESI-MS data.

Acid-ICEF-1,2

Peptide sequence:

o-Abz I S A C E K F I A S C E K F L S A L E K E L A S L E K E L S A L E K E - OH

Analytical HPLC:

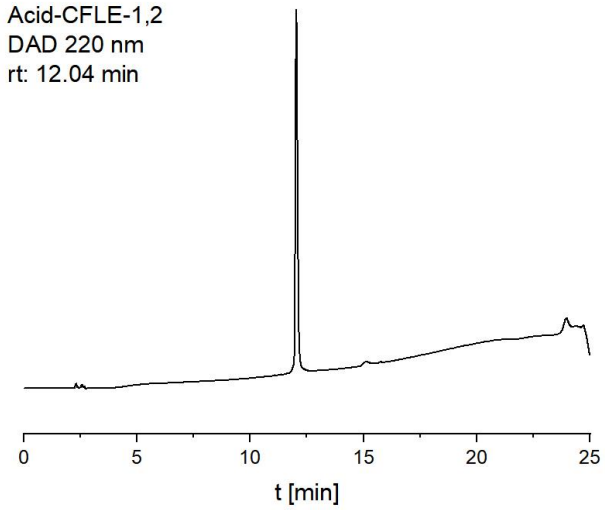

HPLC-system: Primaide™

Column: Kinetex® C18

Eluents: A = 0.1% (v/v) TFA in water, B = 0.1% (v/v) TFA in ACN

Gradient: 30 % eluent B in eluent A to 100 % eluent B over 18 min

ESI-ToF MS:

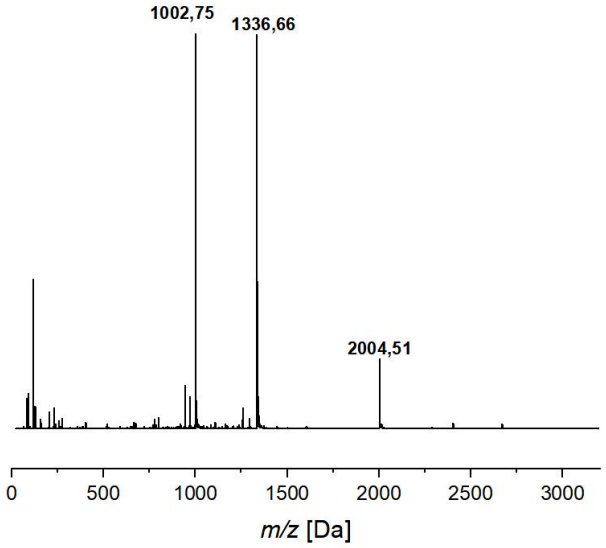

charge	*m/z* [Da] calculated (average)	*m/z* [Da] measured
$[M+2H]^{2+}$	2004.801	2004.501
$[M+3H]^{3+}$	1336.870	1336.665
$[M+4H]^{4+}$	1002.905	1002.748

Table 34: B3β2γ-4,5; peptide sequence, analytical HPLC- and ESI-MS data.

B3β2γ-4,5

Peptide sequence:

o-Abz L S A L K E K L A S L K E K L S A L K E K β^3hL γ^4hD β^3hL γ^4hK β^3hK β^3hL γ^4hD β^3hL γ^4hK β^3hK – OH

Analytical HPLC:

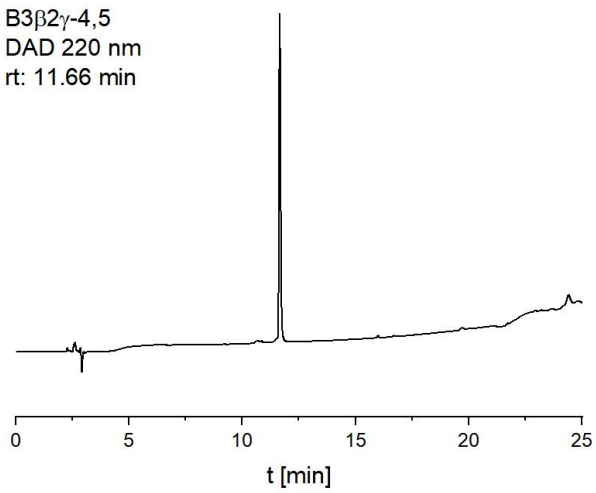

HPLC-system: Chromaster 600 bar DAD

Column: Kinetex® C18

Eluents: A = 0.1% (v/v) TFA in water, B = 0.1% (v/v) TFA in ACN

Gradient: 10 % eluent B in eluent A to 80 % eluent B over 18 min

ESI-ToF MS:

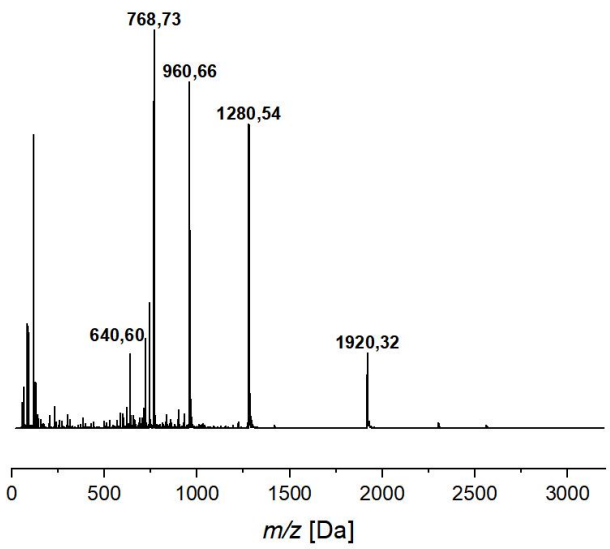

charge	*m/z* [Da] calculated (average)	*m/z* [Da] measured
$[M+2H]^{2+}$	1920.406	1920.319
$[M+3H]^{3+}$	1280.607	1280.541
$[M+4H]^{4+}$	960.707	960.655
$[M+5H]^{5+}$	768.767	768.725
$[M+6H]^{6+}$	640.807	640.601

Table 35: Acid-CFLE-4,5; peptide sequence, analytical HPLC- and ESI-MS data.

Acid-CFLE-4,5

Peptide sequence:

o-Abz L S A L E K E L A S L E K E L S A L E K E C A S F L K E C S A F L K E - OH

Analytical HPLC:

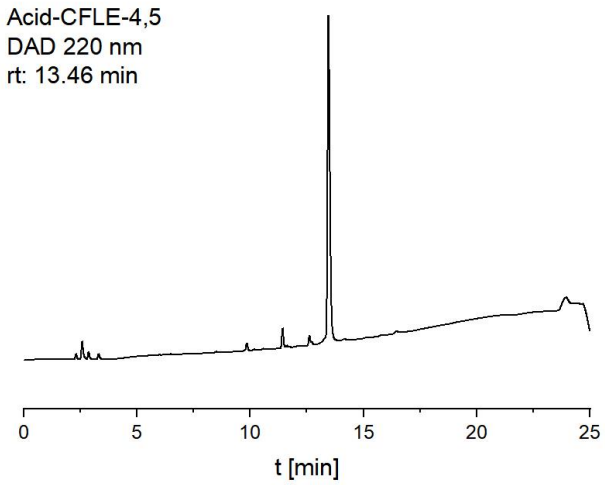

HPLC-system: Primaide™

Column: Kinetex® C18

Eluents: A = 0.1% (v/v) TFA in water, B = 0.1% (v/v) TFA in ACN

Gradient: 30 % eluent B in eluent A to 100 % eluent B over 18 min

ESI-ToF MS:

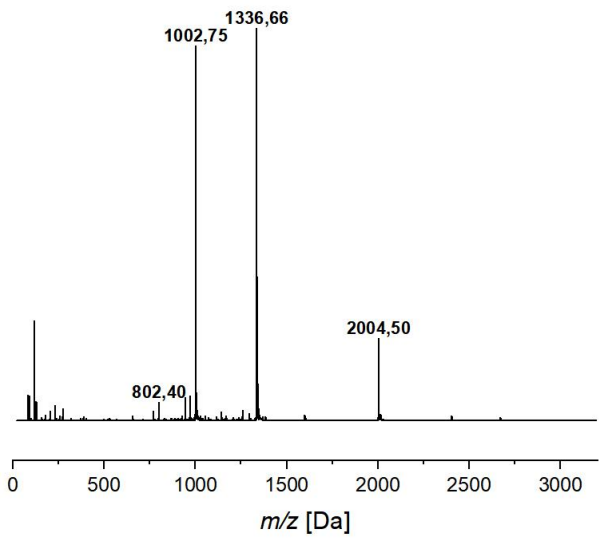

charge	*m/z* [Da] calculated (average)	*m/z* [Da] measured
$[M+2H]^{2+}$	2004.801	2004.501
$[M+3H]^{3+}$	1336.870	1336.662
$[M+4H]^{4+}$	1002.905	1002.746
$[M+5H]^{5+}$	802.525	802.396

Table 36: Acid-ICEF-4,5; peptide sequence, analytical HPLC- and ESI-MS data.

Acid-ICEF-4,5

Peptide sequence:

o-Abz L S A L E K E L A S L E K E L S A L E K E I A S C E K F I S A C E K F - OH

Analytical HPLC:

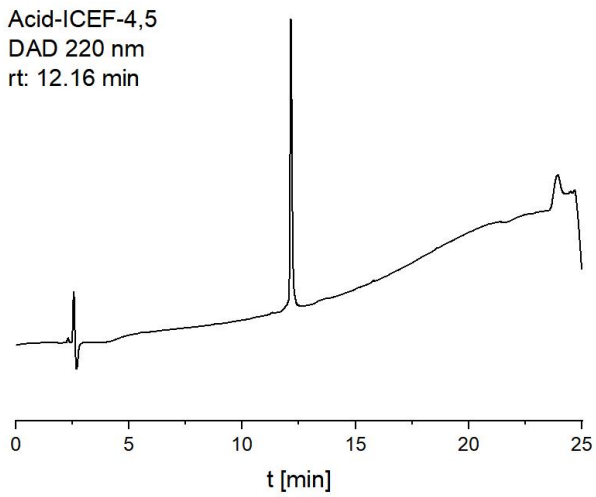

HPLC-system: Primaide™

Column: Kinetex® C18

Eluents: A = 0.1% (v/v) TFA in water, B = 0.1% (v/v) TFA in ACN

Gradient: 30 % eluent B in eluent A to 100 % eluent B over 18 min

ESI-ToF MS:

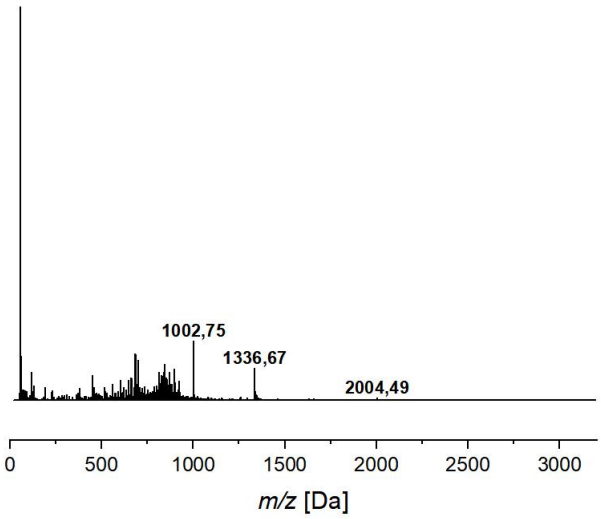

charge	*m/z* [Da] calculated (average)	*m/z* [Da] measured
$[M+2H]^{2+}$	2004.801	2004.494
$[M+3H]^{3+}$	1336.870	1336.669
$[M+4H]^{4+}$	1002.905	1002.753

Table 37: B3β2γ-2,3,4; peptide sequence, analytical HPLC- and ESI-MS data.

B3β2γ-2,3,4

Peptide sequence:

o-Abz L S A L K E K β^3hL γ^4hD β^3hL γ^4hK β^3hK β^3hL γ^4hD β^3hL γ^4hK β^3hK β^3hL γ^4hD β^3hL γ^4hK β^3hK L S A L K E K - OH

Analytical HPLC:

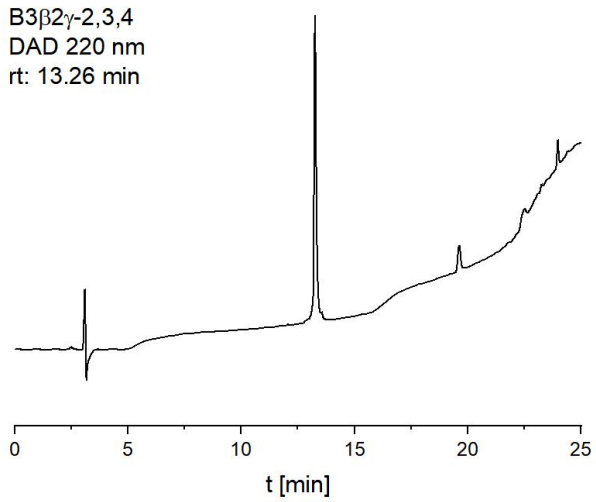

HPLC-system: LaChrom ELITE®

Column: Kinetex® C18

Eluents: A = 0.1% (v/v) TFA in water, B = 0.1% (v/v) TFA in ACN

Gradient: 10 % eluent B in eluent A to 80 % eluent B over 18 min

ESI-ToF MS:

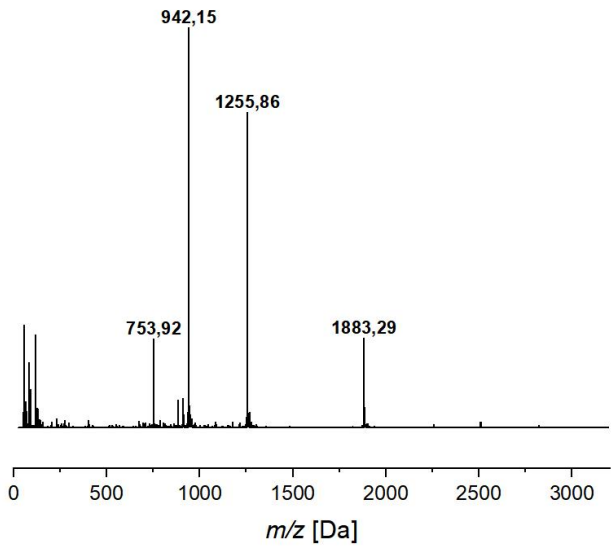

charge	*m/z* [Da] calculated (average)	*m/z* [Da] measured
$[M+2H]^{2+}$	1883.408	1883.286
$[M+3H]^{3+}$	1255.942	1255.859
$[M+4H]^{4+}$	942.208	942.145
$[M+5H]^{5+}$	753.968	753.917

Table 38: Acid-CFLE-2,3,4; peptide sequence, analytical HPLC- and ESI-MS data.

Acid-CFLE-2,3,4

Peptide sequence:

o-Abz L S A L E K E C A S F L K E C S A F L K E C A S F L K E L S A L E K E - OH

Analytical HPLC:

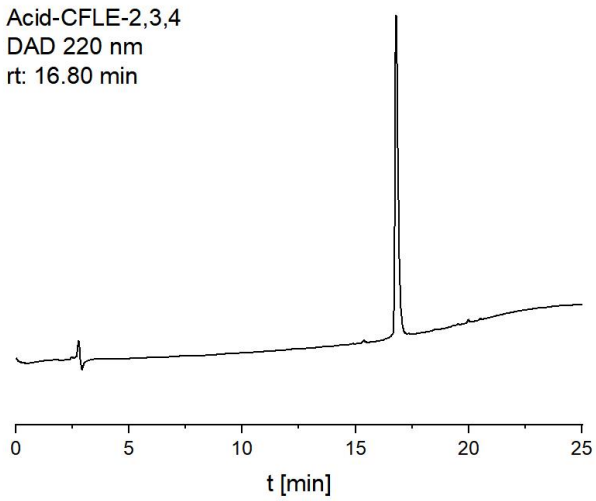

HPLC-system: LaChrom ELITE®

Column: Kinetex® C18

Eluents: A = 0.1% (v/v) TFA in water, B = 0.1% (v/v) TFA in ACN

Gradient: 30 % eluent B in eluent A to 100 % eluent B over 18 min

ESI-ToF MS:

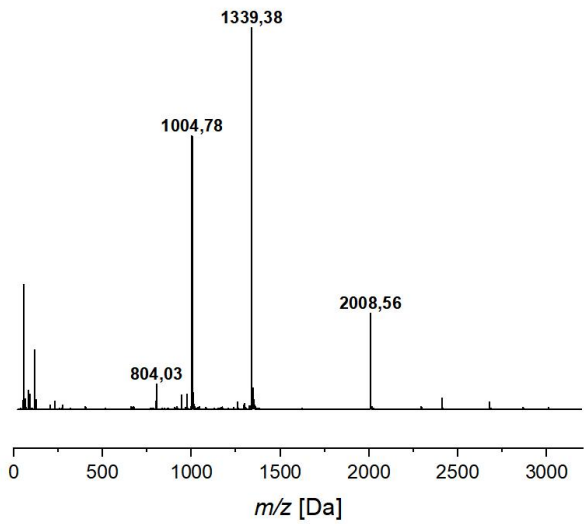

charge	*m/z* [Da] calculated (average)	*m/z* [Da] measured
$[M+2H]^{2+}$	2008.824	2008.559
$[M+3H]^{3+}$	1339.552	1339.379
$[M+4H]^{4+}$	1004.916	1004.783
$[M+5H]^{5+}$	804.134	804.026

Table 39: Acid-ICEF-2,3,4; peptide sequence, analytical HPLC- and ESI-MS data.

Acid-ICEF-2,3,4

Peptide sequence:

o-Abz L S A L E K E I A S C E K F I S A C E K F I A S C E K F L S A L E K E - OH

Analytical HPLC:

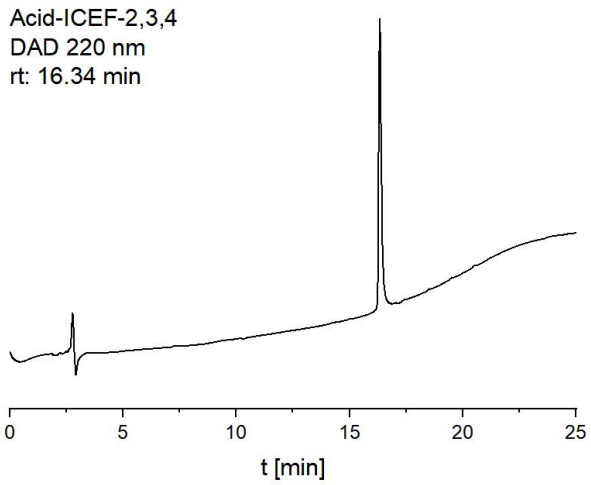

HPLC-system: LaChrom ELITE®

Column: Kinetex® C18

Eluents: A = 0.1% (v/v) TFA in water, B = 0.1% (v/v) TFA in ACN

Gradient: 30 % eluent B in eluent A to 100 % eluent B over 18 min

ESI-ToF MS:

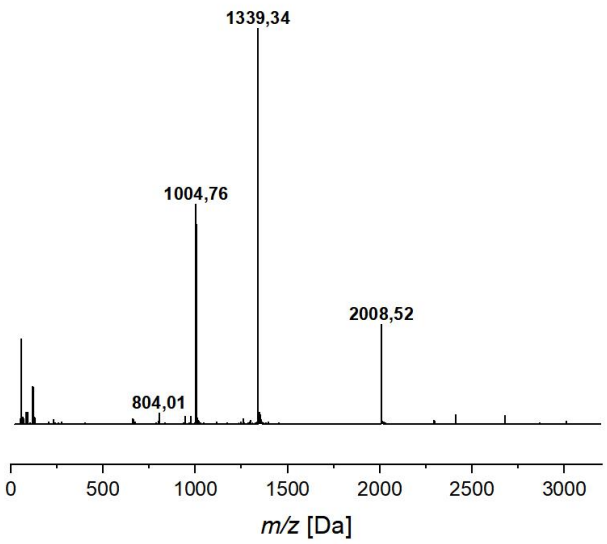

charge	*m/z* [Da] calculated (average)	*m/z* [Da] measured
$[M+2H]^{2+}$	2008.824	2008.515
$[M+3H]^{3+}$	1339.552	1339.343
$[M+4H]^{4+}$	1004.916	1004.758
$[M+5H]^{5+}$	804.134	804.008

Table 40: B3β2γ-1,2,3,4,5; peptide sequence, analytical HPLC- and ESI-MS data.

B3β2γ-1,2,3,4,5

Peptide sequence:

o-Abz β^{3}hL γ^{4}hD β^{3}hL γ^{4}hK β^{3}hK β^{3}hL γ^{4}hD β^{3}hL γ^{4}hK β^{3}hK β^{3}hL γ^{4}hD β^{3}hL γ^{4}hK β^{3}hK β^{3}hL γ^{4}hD β^{3}hL γ^{4}hK β^{3}hK β^{3}hL γ^{4}hD β^{3}hL γ^{4}hK β^{3}hK - OH

Analytical HPLC:

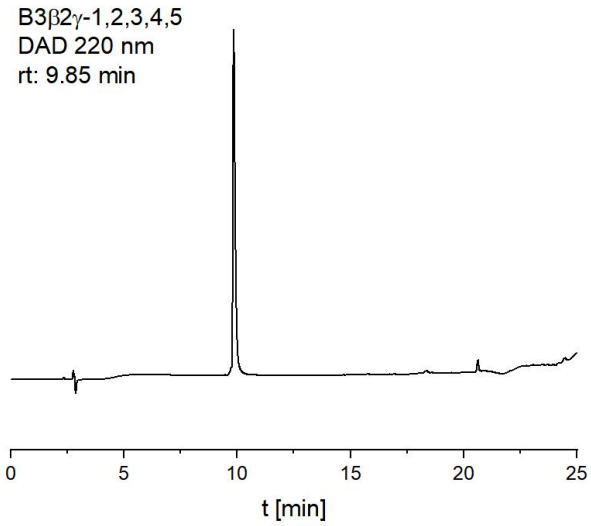

HPLC-system: Chromaster 600 bar DAD

Column: Kinetex® C18

Eluents: A = 0.1% (v/v) TFA in water, B = 0.1% (v/v) TFA in ACN

Gradient: 10 % eluent B in eluent A to 80 % eluent B over 18 min

ESI-ToF MS:

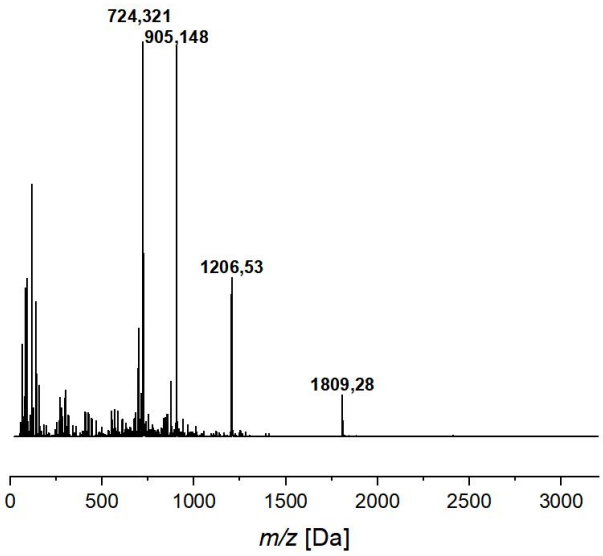

charge	*m/z* [Da] calculated (average)	*m/z* [Da] measured
$[M+2H]^{2+}$	1809.413	1809.284
$[M+3H]^{3+}$	1206.611	1206.528
$[M+4H]^{4+}$	905.210	905.148
$[M+5H]^{5+}$	724.370	724.321

Table 41: Acid-ranICEF; peptide sequence, analytical HPLC- and ESI-MS data.

Acid-ranICEF

Peptide sequence:

o-Abz L S K E A L E A L E S A K S E F C L I A E K L K E S L E A E L E K S L - OH

Analytical HPLC:

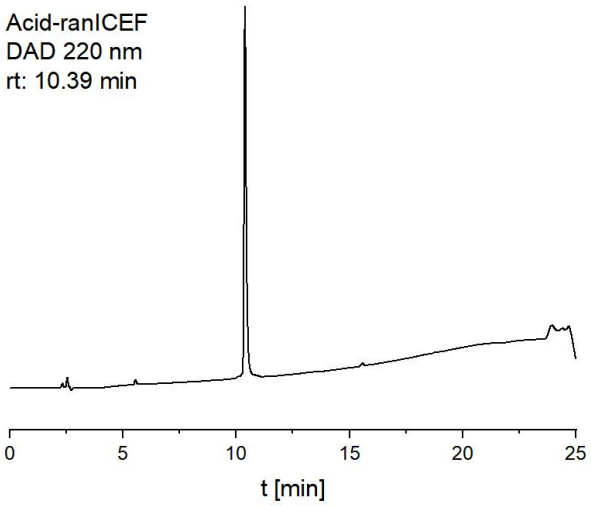

HPLC-system: Primaide™

Column: Kinetex® C18

Eluents: A = 0.1% (v/v) TFA in water, B = 0.1% (v/v) TFA in ACN

Gradient: 30 % eluent B in eluent A to 100 % eluent B over 18 min

ESI-ToF MS:

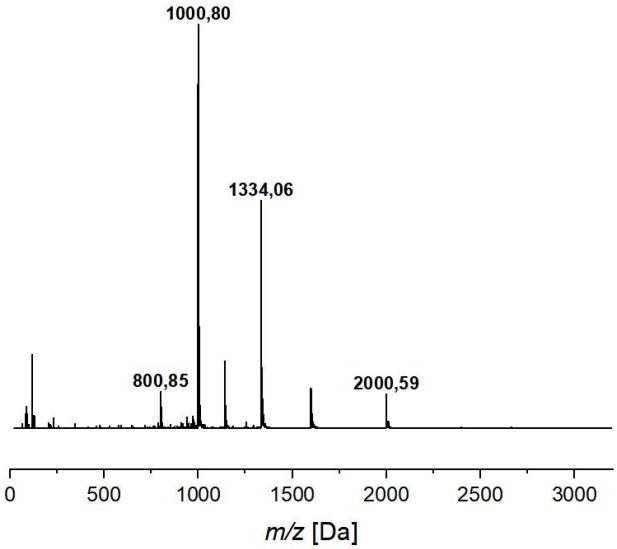

charge	*m/z* [Da] calculated (average)	*m/z* [Da] measured
$[M+2H]^{2+}$	2000.779	2000.590
$[M+3H]^{3+}$	1334.188	1334.060
$[M+4H]^{4+}$	1000.893	1000.800
$[M+5H]^{5+}$	800.916	800.845

5.6 Analytical methods

5.6.1 ESI-ToF Mass spectrometric measurements

High-resolution mass spectra of the synthesized peptides were measured on an Agilent 6230 ToF/MS instrument equipped with an ESI injector (Agilent Technologies, Santa Clara, CA, USA). The peptides were dissolved in a mixture of water and ACN containing 0.1% (v/v) TFA. Injection occurred directly into the spray chamber using a syringe pump with flow rates of 10 to 40 µL/min. The spray voltage was used at 4 kV and the desolvation gas was set to 15 psi. All other parameters were optimized for the maximal abundance of $[M+H]^+$.

ChemDraw Professional software version 20.1.1 (Perkin Elmer Informatics, Inc., Waltham, MA, USA) was used for the determination of molar masses and the corresponding mass-to-charge ratios.

Data were analyzed using the MassHunter Workstation Software Version B.08.00 (Agilent Technologies, Santa Clara, CA, USA) and MestReNova version 7.1.2-10008 (Mestrelab Research S. L., Santiago de Compostela, Spain). OriginPro 2023 (OriginLab Corporation, Northampton, MA, USA) was used to generate the depicted spectra.

5.6.2 Determination of the peptide concentration by UV-spectroscopy

All synthesized peptides were *N*-terminally labeled with *o*-aminobenzoic acid (*o*-Abz) to facilitate the determination of the peptide concentration. Therefore, a calibration curve with different concentrations of *o*-Abz-Gly-OH x HCl was recorded in 10 mM phosphate buffer and 6 M GndHCl. The absorbance of *o*-Abz was measured at λ_{max} = 320 nm at pH 7.4 using a quartz SUPRASIL® cuvette (10 mm path length, Hellma® Analytics, Müllheim, Germany) on a Varian Cary 50 UV/Vis spectrophotometer (Varian Medical Systems, Palo Alto, CA, USA). Baseline correction was carried out with spectra measurements containing solely buffer and 6 M GndHCl with pH 7.4.

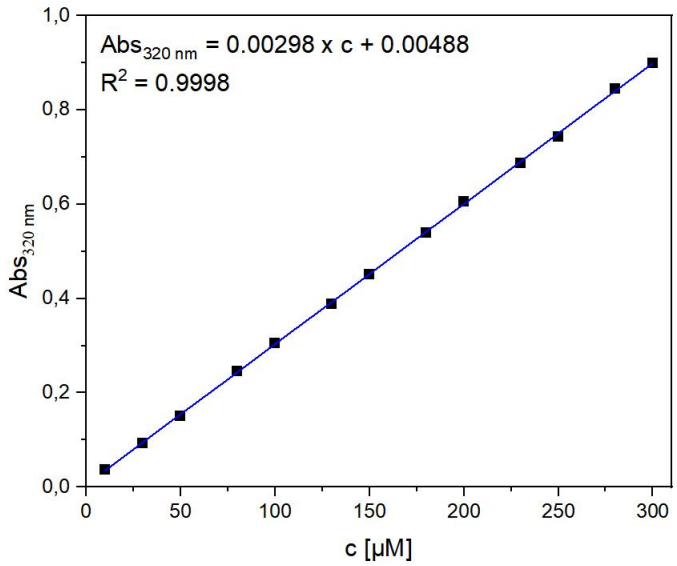

Figure 64: Calibration curve of *o*-Abz-Gly-OH x HCl for the determination of peptide concentrations recorded in 10 mM phosphate buffer and 6 M GdnHCl at pH 7.4.

To determine the concentration of the peptide stock solutions in 1,1,1,3,3,3-hexafluoro-propan-2-ol (HFIP), 10 µM of the stock solution was transferred to an Eppendorf tube. The HFIP was evaporated under a gentle stream of nitrogen, and the peptide was dissolved in 1 mL of 10 mM phosphate buffer and 6 M GndHCl at pH 7.4. The averaged absorption coefficient was subsequently determined by three independent measurements at 320 nm. Using the calibration curve of *o*-Abz-Gly-OH x HCl (Figure 64), conversion of the regression line to c gives the concentration of the peptide stock solution, whilst taking the dilution factor of 100 into account.

5.6.3 Circular dichroism (CD)-spectroscopy

CD-spectroscopic measurements were carried out using a Jasco J-810 spectropolarimeter (JASCO Deutschland GmbH, Pfungstadt, Germany) equipped with a HAAKE WKL recirculating chiller (Haake, Karlsruhe, Germany) and Jasco PTC-423S Peltier type temperature control system (JASCO Deutschland GmbH, Pfungstadt, Germany). The cuvette used had quartz SUPRASIL® material (Hellma® Analytics, Mülheim, Germany) with a 1 mm layer thickness. The peptides were analyzed at 20 µM concentrations for the monomeric peptides and 20 µM total peptide concentration for 1:1 mixtures in 10 mM phosphate buffer at pH 7.4 in the far UV region from 190-240 nm. The data pitch was set to 0.2 nm with a scanning speed of 100 nm min^{-1}. The set response time was 4 s and the used

bandwidth was 1 nm. Thermal denaturation occurred at 222 nm wavelength from 25-100 °C with a heating rate of 1 °C min^{-1} or 3 °C min^{-1}. The coiled-coil assemblies were thermally denatured in 10 mM phosphate buffer at pH 7.4. Chemical denaturation was executed with different concentrations of GndHCl varying from 0.5-6 M. All spectra are the mean of three independent measurements and were normalized to molar ellipticity per residue ($[\theta]$ in 10^3 deg $dmol^{-1}$ cm^2 $residue^{-1}$):

$$[\theta] = \frac{\theta_{obs}}{c \times n \times l \times 10} \quad (5)$$

θ_{obs} corresponds to the measured ellipticity in mdeg, c is the molar concentration in mol L^{-1}, l the path length in cm, and n the number of amide bonds.

The fractional helical content of the peptides (f_H) was calculated using the equation:

$$f_H = \frac{[\theta]_{222\,nm}}{-40000 \times \left(1 - \frac{2.5}{n}\right)} \quad (6)$$

Using the mean residual ellipticity at 222 nm $[\theta]_{222\,nm}$ and n the number of amide bonds.[201]

Data analysis occurred by using either the software J-700 Spectra Manager (JASCO Deutschland GmbH, Pfungstadt, Germany) or JWS-510 J-800 Spectra Manager ver. 2 (JASCO Deutschland GmbH, Pfungstadt, Germany).

Normalization and depiction of the spectra were performed using the program OriginPro 2023 (OriginLab Corporation, Northampton, MA, USA).

5.6.4 Cryogenic-transmission electron microscopy (cryo-TEM)

Peptide mixtures (1 mg/mL) in 10 mM phosphate buffer at pH 7.4 with 4 µL volume were applied to perforated carbon film-covered microscopical 200 mesh grids (R1/4 batch of Quantifoil, MicroTools GmbH, Jena, Germany). The grids used were previously cleaned with chloroform and hydrophilized by 60 s glow discharging at 10 µA in an EMSCOPE SC500. Subsequently, samples were vitrified by automated blotting and plunge freezing using an FEI Vitrobot Mark IV (Thermo Fisher Scientific Inc., Waltham, Massachusetts, USA). Liquid ethane was used as the cryogen. The vitrified samples were then transferred to the autoloader of an FEI TALOS ARCTICA electron microscope (Thermo Fisher Scientific Inc.,

Waltham, MA, USA) equipped with a high-brightness field-emission gun (XFEG) and operated at an acceleration voltage of 200 kV. Photomicrographs were acquired using an FEI Falcon 3 direct electron detector (Thermo Fisher Scientific Inc., Waltham, MA, USA) with an objective aperture of 70 µm at a nominal magnification of 28 000. This corresponds to a calibrated pixel size of 3.75 Å per pixel. The analysis of the average diameter of the *α*-fibers and the creation of the scale bar were performed using ImageJ (Rasband, W.S., ImageJ, U. S. National Institutes of Health, Bethesda, Maryland, USA, https://imagej.nih.gov/ij/, 1997-2018).

5.6.5 Nuclear magnetic resonance (NMR) spectroscopy

All spectra were recorded at 298 K using a Bruker AVANCE III 600 or Bruker AVANCE NEO 500 spectrometer (Billerica, MA, USA) equipped with a TCI triple-resonance cryoprobe. Topspin 4.0 (Bruker, Billerica, MA, USA) was used to process and analyze the generated data. The ^{1}H chemical shifts were referenced to the methyl protons of sodium 3-(trimethylsilyl)propane-1-sulfonate (DSS), and the chemical shifts of ^{13}C and ^{15}N, on the other hand, were referenced indirectly.

5.6.6 Vibrational sum-frequency generation spectroscopy (SFG)

The used SFG spectrometer is a custom-built spectrometer of the working group of Prof. Dr. Braunschweig from the Westfälische Wilhelms-Universität Münster. It uses a Solstice® Ace™ high-energy ultrafast amplifier system (Spectra-Physics®, Milpitas, CA, USA) that generates 70 fs pulses with >7 mJ pulse energy. The pulse energy was split in half through an internal beam splitter to pump a TOPAS Prime (Light Conversion, Vilnius, Lithuania) optical parametric amplifier (OPA) with a subsequent unit for noncollinear difference-frequency generation (NDFG) of the signal and the idler photons of the OPA. This generates mid-infrared (IR) tunable femtosecond pulses with a bandwidth of >300 cm^{-1}. The remainder of energy from the amplifier system experiences spectral narrowing through an etalon filter providing time-asymmetric pulses with a bandwidth of <5 cm^{-1} at 804.1 nm wavelength to yield the visible (VIS) pulse. The angle of incidences of the IR pulse and the VIS pulse are 60° and 55°, respectively, focusing the sample surface with respect to the surface normal. Resulting sum-frequency (SF) photons are collected in a reflection geometry and guided to a Kymera spectrograph (Andor Technology

- Oxford Instruments, Belfast, UK), where they are spectrally dispersed with a 1200 lines/mm grating. Detection of the SF photons occurs with a Newton EMCCD camera (Andor Technology - Oxford Instruments, Belfast, UK).[146,202]

For further details on the construction of the SFG spectrometer see:

J. Phys. Chem. C 2019, 123, 2, 1279-1286.[175]

The glassware used was immersed in a mixture of concentrated sulfuric acid (98%, Rotipuran by Carl Roth GmbH + Co. KG, Karlsruhe, Germany) and Nochromix® (Godax Laboratories Inc., MD, USA) for at least 12 h, then washed thoroughly with deionized water (Millipore), and dried with N_2-gas. Measurements were performed in 30 mm diameter Petri dishes. For this purpose, the peptide solutions were dried in buffer (10 mM phosphate buffer, pH 7.4) after freezing with liquid nitrogen by freeze-drying with an ALPHA 1-2 LD dryer (Christ Gefriertrocknungsanlagen GmbH, Osterode am Harz, Germany) connected to a CHEMISTRY HYBRID PUMP RC 6 (Vacuubrand GmbH + Co KG, Wertheim, Germany). The buffer-dried peptides were then dissolved in ultrapure water (Millipore) for measurements. Peptides containing cysteine were dried without buffer and freshly dissolved with buffer. The total peptide concentration of the measured 1:1 heteroassemblies was 20 µM and monomers were measured at 20 µM concentrations. All peptide solutions (3.5 mL or 5 mL) were equilibrated in the Petri dishes before each measurement so that the peptides could arrange at the air/water interface.

The SF, VIS, and IR beams had either s-, s-, and p- (ssp), or p-, p-, and p- (ppp) polarizations, respectively. The non-resonant contribution from a gold thin film on a Si wafer, which was cleaned in an air-plasma, was used for the normalization of the SFG spectra. For measurements in the amide region in the spectral region of 1100-1750 cm^{-1}, the IR-laser was tuned to four different wavelengths, i.e., 6900 nm, 8100 nm, 9500 nm, and 10300 nm. The thiol region was measured with three IR-wavelengths: 4200 nm, 4400 nm, and 4600 nm.

Spectra were prepared using OriginPro 2023 (OriginLab Corporation, Northampton, MA, USA).

5.6.7 Fourier-transform infrared spectroscopy (FT-IR)

FT-IR spectra were acquired using a Bruker Tensor 27 spectrometer (Billerica, MA, USA) equipped with a liquid nitrogen-cooled MCT photovoltaic detector. The measured samples were in a temperature-controlled, gas-tight IR-cell for liquid samples. It has a volume capacity of about 10 µL and a 50 µm path length and is equipped with CaF_2 windows and a Teflon spacer. The spectral resolution setting was 2 cm^{-1} and baseline correction was performed with Bruker's OPUS 7.8.44 software (Billerica, MA, USA). In each case, -log10(sample spectrum/buffer spectrum) was calculated to obtain the absorption spectra. The subsequent log10 air spectrum was used to subtract the residual from the air so that the air bands near the amide I region landed on the baseline. All spectra measurements and background measurements were scanned with 200 replicates.

All measurements were performed in 10 mM deuterated phosphate buffer and pH 7.4. Peptides were prepared as stock solutions in deuterated buffer at a concentration of 100 µM. The total peptide concentration of the measured 1:1 hetero-assemblies was 200 µM and the monomers were measured at 100 µM concentrations. Spectra were generated with OriginPro 2023 (OriginLab Corporation, Northampton, MA, USA).

5.6.8 Crystallization

Initial crystallization conditions were identified for Accid-pp/Base-pp, Acid-pp/B3β2γ, Acid-CFLE/ B3β2γ, and Acid-ICEF/ B3β2γ by using commercially available screening reagents in a 96-well setup and a Cartesian crystallization robot (Zinsser Analytic, Germany) with the sitting drop vapor diffusion technique. The 96-well screening plates used were Classic Suite (Qiagen, Venlo, Netherlands), Index HR2-144 (Hampton Research, California, USA), Core S26 (Qiagen, Venlo, Netherlands), and The PEGs Suite (Qiagen, Venlo, Netherlands). Peptide solutions were prepared with 10 mM Tris-HCl buffer. Crystallization drops contained 100 nL of crystallization buffer and 100 nL of peptide solution. The appropriate peptide concentration was estimated by the number of clear and precipitated drops, and when necessary, the screens were repeated using a higher or lower peptide concentration. For all assemblies, the optimal peptide

concentration was 15 to 25 mg/mL. All crystallization plates were sealed and incubated at 18 °C.

Optimization screens were performed for multiple hits. The volume of the crystallization drops was increased to 1 µL of crystallization buffer and 1 µL of peptide solution. Conventional systematic variations on the peptide, buffer, and precipitant concentrations were screened, as well as different temperature and pH values. In some cases, different crystallization buffer drop ratios and an additive screen were also tested. In addition, two different microseeding methods were used: streak seeding with a cat whisker and seeding with a seed stock. For crystal freezing, a variety of cryoprotectants were explored.

Conducted optimizations are enlisted for each hetero-assembly:

Table 42: Optimizations performed for Acid-pp/Base-pp.

Original condition: 0.1 M citric acid pH 3.5, 25% (w/v) PEG3350				
Concentration [mg/mL]	Temperature [°C]	Condition A1	Vertical condition variations	Horizontal condition variations
15	18	0.08 M citric acid pH 3.5, 17% (w/v) PEG3350	0.09 M, 0.1 M, 0.11 M, 0.12 M – citric acid	21%, 25%, 29%, 33%, 37% – (w/v) PEG3350
15	4	0.11 M citric acid pH 3.5, 25% (w/v) PEG3350	0.1 M – citric acid	26%, 27%, 28%, 29%, 30% – (w/v) PEG3350
15	18	0.1 M citric acid pH 3.5, 25% (w/v) PEG3350	pH 3.5, pH 3.8 – citric acid	26%, 27%, 28%, 29%, 30% – (w/v) PEG3350
Original condition: 0.1 M sodium acetate trihydrate pH 4.5, 25% (w/v) PEG3350				
Concentration [mg/mL]	Temperature [°C]	Condition A1	Vertical condition variations	Horizontal condition variations
10	18	0.06 M sodium acetate trihydrate pH 4.5, 25% (w/v) PEG3350	0.08 M, 0.1 M, 0.12 M, 0.14 M – sodium acetate trihydrate	20%, 25%, 30%, 35% – (w/v) PEG3350

In addition, an Additive screen (Hampton Research, California, USA) with a 96-well screening plate at 13 mg/mL total peptide concentration for Acid-pp/Base-pp was performed.

Table 43: Optimizations performed for Acid-pp/B3β2γ.

Original condition: 0.1 M sodium/potassium phosphate pH 6.5, 35% (v/v) MPD			
Concentration [mg/mL]	Condition A1	Vertical condition variations	Horizontal condition variations
15	0.05 M sodium/potassium phosphate pH 6.5, 20% (v/v) MPD	0.1 M, 0.15 M – sodium/potassium phosphate	25%, 30%, 35%, 40%, 45% – (v/v) MPD
Original condition: 0.05 M calcium acetate hydrate, 0.1 M imidazole, 20% 2-ethoxyethanol			
Concentration [mg/mL]	Condition A1	Vertical condition variations	Horizontal condition variations
15	0.04 M calcium acetate hydrate, 0.1 M imidazole, 20% 2-ethoxyethanol	0.05 M, 0.06 M – calcium acetate	24%, 28%, 32%, 36%, 40% – 2-ethoxyethanol
Original condition: 0.2 M calcium chloride, 0.1 M HEPES sodium salt pH 7.5, 28% (v/v) PEG400			
Concentration [mg/mL]	Condition A1	Vertical condition variations	Horizontal condition variations
23	0.1 M $CaCl_2$ dihydrate, 0.1 M HEPES pH 7.5, 15% (v/v) PEG400	0.2 M, 0.3 M – $CaCl_2$	18%, 21%, 24%, 27%, 30% – (v/v) PEG400
Original condition: 0.1 M imidazole pH 6.5, 1.0 M sodium acetate			
Concentration [mg/mL]	Condition A1	Vertical condition variations	Horizontal condition variations
10	0.06 M imidazole pH 6.5, 0.6 M sodium acetate	0.08 M, 0.1 M, 0.12 M, 0.14 M – imidazole	0.8 M, 1 M, 1.2 M, 1.4 M – sodium acetate

Table 44: Optimizations performed for Acid-CFLE/B3β2γ.

Original condition: 0.1 M citric acid pH 2.5, 40% (v/v) MPD (final pH 4.0)			
Concentration [mg/mL]	Condition A1	Vertical condition variations	Horizontal condition variations
13	0.1 M citric acid pH 2.0, 25% (v/v) MPD	pH 2.5, pH 3.2, pH 3.8 – citric acid	30%, 35%, 40%, 45%, 50% – (v/v) MPD
Original condition: 0.02 M calcium chloride, 0.1 M sodium acetate pH 4.6, 30% (v/v) MPD			
Concentration [mg/mL]	Condition A1	Vertical condition variations	Horizontal condition variations

10	0.02 M $CaCl_2$ dihydrate, 0.05 M sodium acetate trihydrate pH 4.6, 10% (v/v) MPD	0.1 M, 0.15 M – sodium acetate	15%, 20%, 25%, 30%, 35% – (v/v) MPD
10	0.01 M $CaCl_2$ dihydrate, 0.1 M sodium acetate trihydrate pH 4.6, 10% (v/v) MPD	0.02 M, 0.03 M – $CaCl_2$	15&, 20%, 25%, 30%, 35% – (v/v) MPD

Table 45: Optimizations performed for Acid-ICEF/B3β2γ.

Original condition: 0.2 M ammonium acetate, 0.1 M BIS-TRIS pH 5.5, 45% (v/v) MPD			
Concentration [mg/mL]	Condition A1	Vertical condition variations	Horizontal condition variations
25	0.15 M ammonium acetate, 0.1 M BIS-TRIS pH 5.5, 30% (v/v) MPD	0.2 M, 0.25 M – ammonium acetate	35%, 40%, 45%, 50%, 55% – (v/v) MPD
25	0.2 M ammonium acetate, 0.05 M BIS-TRIS pH 5.5, 30% MPD	0.1 M, 0.15 M – BIS-TRIS	35%, 40%, 45%, 50%, 55% – (v/v) MPD
20	0.2 M ammonium acetate, 0.04 M BIS-TRIS pH 5.5, 22% (v/v) MPD	0.05 M, 0.06 M, 0.07 M – BIS-TRIS	24%, 26%, 28%, 30%, 32% – (v/v) MPD
Original condition: 0.05M Calcium chloride, 0.1M BIS-TRIS pH 6.5, 30% PEG mme 550			
Concentration [mg/mL]	Condition A1	Vertical condition variations	Horizontal condition variations
13	0.04 M $CaCl_2$ dihydrate, 0.1 M BIS-TRIS pH 6.5, 20% PEG-mme 550	0.05 M, 0.06 M – $CaCl_2$	25%, 30% – PEG-mme 550
17	0.01 M $CaCl_2$ dihydrate, 0.1 M BIS-TRIS pH 6.5, 10% PEG-mme 550	0.02 M, 0.03 M, 0.04 M – $CaCl_2$	15%, 20% – PEG-mme 550

Crystals were cryoprotected by brief immersion in a buffer-cryoprotectant mixture before looping. Diffraction was measured at beamline 14.1 of the BESSSY II storage ring (Helmholtz-Zentrum Berlin (HZB), Berlin, Germany).

Additional crystallization conditions were also identified for all systems using commercially available screening reagents with the sitting drop vapor diffusion method. An Oryx-8 robot (Douglas Instruments Limited, Hungerford, UK) and Swissci MRC 96-Well 2-Drop Plates (Molecular Dimensions Ltd, Rotherham, UK)

were used. Applied screening plate reagents were Structure Screen 1 + 2 HT-96 Eco Screen, JCSG Plus™, Morpheus®, PACT Premier™, ProPlex, and SG1™ Screen from Molecular Dimension Ltd (Rotherham, UK). Peptide mixtures contained 1.25 mM of each peptide and were buffered in 0.02 M HEPES at pH 7.8. For the Cys-containing sequences (Acid-CFLE and Acid-ICEF), DTT was added to a final concentration of 10 mM. The crystallization drops contained 0.3 µL of peptide mixture solution and 0.3 µL of precipitant. The volume of screening solution in each well was 50 µL. Finally, the plates were sealed and incubated at 20 °C.

Seeding was performed with seed stocks. One of these stocks contained crystals grown from the ProPlex screen of Acid-CFLE/B3β2γ under condition A12, which were crushed and diluted. Screens conducted with this seed stock were Structure Screen 1 + 2 HT-96 Eco Screen, JCSG Plus™, and Morpheus® for Acid-CFLE/B3β2γ and Acid-ICEF/B3β2γ. These are screens in which MPD is present in certain conditions, apparently leading to crystal growth for the Cys/Phe-motif-containing assemblies, as most of the hits obtained have high MPD concentrations. The same conditions were used for the previous screens. The droplets consisted of 0.3 µL peptide mixture, 0.1 µL seed stock, and 0.4 µL screen solution. Crystals that grew from Structure Screen 1 + 2 HT-96 Eco Screen of Acid-ICEF/B3β2γ under condition A1 were used for a further seeding screen for Acid-ICEF/B3β2γ at 18 mg/mL total peptide concentration.

Optimizing the concentration for Acid-pp/Base-pp and Acid-pp/B3β2γ all six 96-well plate screens were repeated at an elevated concentration of 15 mg/mL.

In general, the hetero-assemblies Acid-pp/Base-pp, Acid-pp/B3β2γ, and Acid-ICEF/B3β2γ appear to prefer higher concentration than that of Acid-CFLE/B3β2γ.

Grown crystals were measured at beamline I04-1 of the Diamond Light Source (Harwell Science and Innovation Campus, Oxfordshire, UK).

Since the Acid-CFLE/B3β2γ hit from the JCSG Plus™ screen at condition H12 resulted in crystals with good diffraction, optimization was set up using the hanging-drop vapor diffusion method to allow additional SAD measurements. The concentration of Acid-CFLE/B3β2γ was not varied in this process.

Table 46: Optimization performed for an analyzed hit of Acid-CFLE/B3β2γ from the JCSG Plus™ screen.

Original condition: 0.2 M ammonium acetate, 0.1 M HEPES pH 7.5, 45% (v/v) MPD		
Condition A1	Vertical condition variations	Horizontal condition variations
0.0 M ammonium acetate, 0.1 M HEPES pH 7.5, 30% (v/v) MPD	0.2 M, 0.4 M, 0.6 M – ammonium acetate	35%, 40%, 45%, 50%, 55% – (v/v) MPD

5.7 Figures and Graphs

Chemical structures and molecules were drawn using ChemDraw Professional software version 20.1.1 (Perkin Elmer Informatics, Inc., Waltham, MA, USA).

Figures of protein and peptide crystal structures were created using the UCSF Chimera package from the Computer Graphics Laboratory, University of California, San Francisco (supported by NIH P41 RR-01081).[203] The structural data with given PDB-codes were taken from the Protein Data Bank (PDB; https://www.rcsb.org). Further illustrations of the generated crystal structure were performed with CCP4mg molecular graphics software (Collaborative Computational Project, Number 4. 1994).[204,205]

NMR spectra were illustrated using TopSpin 4.2.0 (Bruker, Billerica, MA, USA).

Depicted diagrams, graphs, chromatograms, and mass spectra were generated with OriginPro 2023 (OriginLab Corporation, Northampton, MA, USA).

6. Literature

(1) Barlow, D. J.; Thornton, J. M. Helix Geometry in Proteins. *J Mol Biol* **1988**, *201* (3), 601–619. https://doi.org/10.1016/0022-2836(88)90641-9.

(2) Raj, M.; Bullock, B. N.; Arora, P. S. Plucking the High Hanging Fruit: A Systematic Approach for Targeting Protein-Protein Interactions. *Bioorg Med Chem* **2013**, *21* (14), 4051–4057. https://doi.org/10.1016/j.bmc.2012.11.023.

(3) Stites, W. E. Protein-Protein Interactions: Interface Structure, Binding Thermodynamics, and Mutational Analysis. *Chem Rev* **1997**, *97* (5), 1233–1250. https://doi.org/10.1021/cr960387h.

(4) Keskin, O.; Gursoy, A.; Ma, B.; Nussinov, R. Principles of Protein-Protein Interactions: What Are the Preferred Ways for Proteins to Interact? *Chem Rev* **2008**, *108* (4), 1225–1244. https://doi.org/10.1021/cr040409x.

(5) Muttenthaler, M.; King, G. F.; Adams, D. J.; Alewood, P. F. Trends in Peptide Drug Discovery. *Nat Rev Drug Discov* **2021**, *20*, 309–325. https://doi.org/10.1038/s41573-020-00135-8.

(6) Erak, M.; Bellmann-Sickert, K.; Els-Heindl, S.; Beck-Sickinger, A. G. Peptide Chemistry Toolbox – Transforming Natural Peptides into Peptide Therapeutics. *Bioorg Med Chem* **2018**, *26* (10), 2759–2765. https://doi.org/10.1016/j.bmc.2018.01.012.

(7) Du, M.; Xu, Z.; Chen, H.; Fan, F.; Shi, P.; Wu, D. Food-Derived Osteogenic Peptides towards Osteoporosis. In *Biologically Active Peptides: From Basic Science to Applications for Human Health*; Elsevier, 2021; pp 665–688. https://doi.org/10.1016/B978-0-12-821389-6.00027-3.

(8) Mimmi, S.; Maisano, D.; Quinto, I.; Iaccino, E. Phage Display: An Overview in Context to Drug Discovery. *Trends Pharmacol Sci* **2019**, *40* (2), 87–91. https://doi.org/10.1016/j.tips.2018.12.005.

(9) Passioura, T.; Katoh, T.; Goto, Y.; Suga, H. Selection-Based Discovery of Druglike Macrocyclic Peptides. *Annu Rev Biochem* **2014**, *83*, 727–752. https://doi.org/10.1146/annurev-biochem-060713-035456.

(10) Skowron, K. J.; Speltz, T. E.; Moore, T. W. Recent Structural Advances in Constrained Helical Peptides. *Med Res Rev* **2019**, *39* (2), 749–770. https://doi.org/10.1002/med.21540.

(11) Chung, C. W.; Hann, M. M. Targeting Protein-Protein Interactions Perspective. In *Structural Biology in Drug Discovery: Methods, Techniques, and Practices*; Renaud, J.-P., Ed.; WILEY, 2020; pp 479–502. https://doi.org/10.1002/9781118681121.ch20.

(12) Edwards, T. A.; Wilson, A. J. Helix-Mediated Protein-Protein Interactions as Targets for Intervention Using Foldamers. *Amino Acids* **2011**, *41* (3), 743–754. https://doi.org/10.1007/s00726-011-0880-8.

(13) Guarracino, D. A.; Arora, P. S. Making Strides in Peptide-Based Therapeutics. *Chem Biol* **2009**, *16* (9), 919–920. https://doi.org/10.1016/j.chembiol.2009.09.005.

(14) Boyle, A. L.; Woolfson, D. N. De Novo Designed Peptides for Biological Applications. *Chem Soc Rev* **2011**, *40* (8), 4295–4306. https://doi.org/10.1039/c0cs00152j.

(15) Ramachandran, G. N.; Sasisekharan, V. Conformation of Polypeptides and Proteins. *Adv Protein Chem* **1968**, *23*, 283–437. https://doi.org/10.1016/S0065-3233(08)60402-7.

(16) Lehninger, A. L.; Nelson, D. L.; Cox, M. M. *Lehninger Principles of Biochemistry*, Fourth Edi.; W. H. Freeman & Co.: New York, 2004.

(17) Kaplan, J.; DeGrado, W. F. De Novo Design of Catalytic Proteins. *Proceedings of the National Academy of Sciences* **2004**, *101* (32), 11566–11570. https://doi.org/10.1073/pnas.0404387101.

(18) Chakrabartty, A.; Baldwin, R. L. Stability of α-Helices. *Adv Protein Chem* **1995**, *46*, 141–176. https://doi.org/10.1016/S0065-3233(08)60334-4.

(19) Lupas, A. N.; Bassler, J. Coiled Coils – A Model System for the 21st Century. *Trends Biochem Sci* **2017**, *42* (2), 130–140. https://doi.org/10.1016/j.tibs.2016.10.007.

(20) Crick, F. H. C. The Packing of α-Helices: Simple Coiled-Coils. *Acta Crystallogr* **1953**, *6* (8), 689–697. https://doi.org/10.1107/s0365110x53001964.

(21) Pauling, L.; Corey, R. B. Compound Helical Configurations of Polypeptide Chains: Structure of Proteins of the α-Keratin Type. *Nature* **1953**, *171* (4341), 59–61. https://doi.org/https://doi.org/10.1038/171059a0.

(22) Astbury, W. T.; Reed, R.; Spark, L. C. An X-Ray and Electron Microscope Study of Tropomyosin. *Biochemical Journal* **1948**, *43* (2), 282–287. https://doi.org/10.1042/bj0430282.

(23) Lupas, A. Coiled Coils: New Structures and New Functions. *Trends Biochem Sci* **1996**, *21* (10), 375–382. https://doi.org/10.1016/S0968-0004(96)10052-9.

(24) Woolfson, D. N. The Design of Coiled-Coil Structures and Assemblies. *Adv Protein Chem* **2005**, *70*, 79–112. https://doi.org/10.1016/S0065-3233(05)70004-8.

(25) Woolfson, D. N. Coiled-Coil Design: Updated and Upgraded. In *Fibrous Proteins: Structures and Mechanisms. Subcellular Biochemistry*; Springer, 2017; Vol. 82, pp 35–61. https://doi.org/10.1007/978-3-319-49674-0.

(26) Mason, J. M.; Arndt, K. M. Coiled Coil Domains: Stability, Specificity, and Biological Implications. *ChemBioChem* **2004**, *5* (2), 170–176. https://doi.org/10.1002/cbic.200300781.

(27) Rhys, G. G.; Wood, C. W.; Lang, E. J. M.; Mulholland, A. J.; Brady, R. L.; Thomson, A. R.; Woolfson, D. N. Maintaining and Breaking Symmetry in Homomeric Coiled-Coil Assemblies. *Nat Commun* **2018**, *9* (4132), 1–12. https://doi.org/10.1038/s41467-018-06391-y.

(28) Burkhard, P.; Meier, M.; Lustig, A. Design of a Minimal Protein Oligomerization Domain by a Structural Approach. *Protein Science* **2000**, *9* (12), 2294–2301. https://doi.org/10.1110/ps.9.12.2294.

(29) Kohn, W. D.; Mant, C. T.; Hodges, R. S. α-Helical Protein Assembly Motifs. *J. Biol. Chem.* **1997**, *272* (5), 2583–2586. https://doi.org/10.1074/jbc.272.5.2583.

(30) Yu, Y. B. Coiled-Coils: Stability, Specificity, and Drug Delivery Potential. *Adv Drug Deliv Rev* **2002**, *54*, 1113–1129. https://doi.org/10.1016/S0169-409X(02)00058-3.

(31) Pagel, K.; Koksch, B. Following Polypeptide Folding and Assembly with Conformational Switches. *Curr. Opin. Chem. Biol.* December 2008, pp 730–739. https://doi.org/10.1016/j.cbpa.2008.09.005.

(32) Wagschal, K.; Tripet, B.; Mant, C.; Hodges, R. S.; Lavigne, P. The Role of Position a in Determining the Stability and Oligomerization State of α-Helical Coiled Coils: 20 Amino Acid Stability Coefficients in the Hydrophobic Core of Proteins. *Protein Science* **2008**, *8* (11), 2312–2329. https://doi.org/10.1110/ps.8.11.2312.

(33) Tripet, B.; Wagschal, K.; Lavigne, P.; Mant, C. T.; Hodges, R. S. Effects of Side-Chain Characteristics on Stability and Oligomerization State of a de Novo-Designed Model Coiled-Coil: 20 Amino Acid Substitutions in Position "d." *J Mol Biol* **2000**, *300* (2), 377–402. https://doi.org/10.1006/jmbi.2000.3866.

(34) Fletcher, J. M.; Boyle, A. L.; Bruning, M.; Bartlett, Sg. J.; Vincent, T. L.; Zaccai, N. R.; Armstrong, C. T.; Bromley, E. H. C.; Booth, P. J.; Brady, R. L.; Thomson, A. R.; Woolfson, D. N. A Basis Set of de Novo Coiled-Coil Peptide Oligomers for Rational Protein Design and Synthetic Biology. *ACS Synth Biol* **2012**, *1* (6), 240–250. https://doi.org/10.1021/sb300028q.

(35) Harbury, P. B.; Zhang, T.; Kim, P. S.; Alber, T. A Switch Between Two-, Three-, and Four-Stranded Coiled Coils in GCN4 Leucine Zipper Mutants. *Science (1979)* **1993**, *262* (5138), 1401–1407. https://doi.org/10.1126/science.8248779.

(36) Truebestein, L.; Leonard, T. A. Coiled-Coils: The Long and Short of It. *BioEssays* **2016**, *38* (9), 903–916. https://doi.org/10.1002/bies.201600062.

(37) Koronakis, V.; Sharff, A.; Koronakis, E.; Luisi, B.; Hughes, C. Crystal Structure of the Bacterial Membrane Protein TolC Central to Multidrug Efflux and Protein Export. *Nature* **2000**, *405*, 914–919. https://doi.org/10.1038/35016007.

(38) Lupas, A. N.; Gruber, M. The Structure of α-Helical Coiled Coils. *Adv Protein Chem* **2005**, *70*, 37–78. https://doi.org/10.1016/S0065-3233(04)70003-0.

(39) Brown, J. H.; Cohen, C.; Parry, D. A. D. Heptad Breaks in α-Helical Coiled Coils: Stutters and Stammers. *Proteins: Structure, Function and Genetics* **1996**, *26* (2), 134–145. https://doi.org/10.1002/(SICI)1097-0134(199610)26:2<134::AID-PROT3>3.0.CO;2-G.

(40) Parry, D. A. D. Fibrinogen: A Preliminary Analysis of the Amino Acid Sequences of the Portions of the α, β and γ-Chains Postulated to Form the Interdomainal Link Between Globular Regions of the Molecule. *J. Mol. Biol.* **1978**, *120* (4), 545–551. https://doi.org/10.1016/0022-2836(78)90353-4.

(41) Cohen, C.; Parry, D. A. D. α-Helical Coiled Coils and Bundles: How to Design an α-helical Protein. *Proteins: Structure, Function, and Bioinformatics* **1990**, *7* (1), 1–15. https://doi.org/10.1002/prot.340070102.

(42) Zhou, N. E.; Kay, C. M.; Hodges, R. S. Synthetic Model Proteins. Positional Effects of Interchain Hydrophobic Interactions on Stability of Two-Stranded α-Helical Coiled-Coils. *Journal of Biological Chemistry* **1992**, *267* (4), 2664–2670. https://doi.org/10.1016/s0021-9258(18)45932-7.

(43) Hill, R. B.; Raleigh, D. P.; Lombardi, A.; Degrado, W. F. De Novo Design of Helical Bundles as Models for Understanding Protein Folding and Function. *Acc Chem Res* **2000**, *33* (11), 745–754. https://doi.org/10.1021/ar970004h.

(44) Appella, D. H.; Christianson, L. A.; Karle, I. L.; Powell, D. R.; Gellman, S. H. β-Peptide Foldamers: Robust Helix Formation in a New Family of β-Amino Acid Oligomers. *J. Am. Chem. Soc.* **1996**, *118* (51), 13071–13072. https://doi.org/10.1021/ja963290l.

(45) Cussol, L.; Mauran-Ambrosino, L.; Buratto, J.; Belorusova, A. Y.; Neuville, M.; Osz, J.; Fribourg, S.; Fremaux, J.; Dolain, C.; Goudreau, S. R.; Rochel,

N.; Guichard, G. Structural Basis for α-Helix Mimicry and Inhibition of Protein–Protein Interactions with Oligourea Foldamers. *Angewandte Chemie - International Edition* **2021**, *60* (5), 2296–2303. https://doi.org/10.1002/anie.202008992.

(46) Shin, Y. H.; Yang, H. Exploration of α/β/γ-Peptidomimetics Design for BH3 Helical Domains. *Chemical Communications* **2022**, *58* (7), 945–948. https://doi.org/10.1039/d1cc05758h.

(47) Yokoo, H.; Misawa, T.; Demizu, Y. De Novo Design of Cell-Penetrating Foldamers. *Chemical Record* **2020**, *20* (9), 912–921. https://doi.org/10.1002/tcr.202000047.

(48) Oba, M. Cell-Penetrating Peptide Foldamers: Drug-Delivery Tools. *ChemBioChem* **2019**, *20* (16), 2041–2045. https://doi.org/10.1002/cbic.201900204.

(49) Hirano, M.; Saito, C.; Goto, C.; Yokoo, H.; Kawano, R.; Misawa, T.; Demizu, Y. Rational Design of Helix-Stabilized Antimicrobial Peptide Foldamers Containing α,α-Disubstituted Amino Acids or Side-Chain Stapling. *Chempluschem* **2020**, *85* (12), 2731–2736. https://doi.org/10.1002/cplu.202000749.

(50) Hamuro, Y.; Schneider, J. P.; DeGrado, W. F. De Novo Design of Antibacterial β-Peptides. *J Am Chem Soc* **1999**, *121* (51), 12200–12201. https://doi.org/10.1021/ja992728p.

(51) Tew, G. N.; Scott, R. W.; Klein, M. L.; Degrado, W. F. De Novo Design of Antimicrobial Polymers, Foldamers, and Small Molecules: From Discovery to Practical Applications. *Acc Chem Res* **2010**, *43* (1), 30–39. https://doi.org/10.1021/ar900036b.

(52) Oh, B. C.; Yoon, E.; Gong, J.; Kim, J.; Driver, R. W.; Kim, Y.; Kim, W. Y.; Lee, H. S. Morphology Transformation of Foldamer Assemblies Triggered by Single Oxygen Atom on Critical Residue Switch. *Small* **2021**, *17* (36). https://doi.org/10.1002/smll.202102525.

(53) Kato, T. Foldamer. In *Cell-penetrating peptides: Design, Development and Applications*; Oba, M., Demizu, Y., Eds.; Wiley-VCH GmbH: Weinheim, Germany, 2022; pp 79–107.

(54) Pasco, M.; Dolain, C.; Guichard, G. Foldamers in Medicinal Chemistry. In *Comprehensive Supramolecular Chemistry II*; Elsevier Inc., 2017; Vol. 5, pp 89–125. https://doi.org/10.1016/B978-0-12-409547-2.12565-X.

(55) Horne, W. S.; Price, J. L.; Keck, J. L.; Gellman, S. H. Helix Bundle Quaternary Structure from α/β-Peptide Foldamers. *J Am Chem Soc* **2007**, *129* (14), 4178–4180. https://doi.org/10.1021/ja070396f.

(56) Fortuna, P.; Twarda-Clapa, A.; Skalniak, L.; Ożga, K.; Holak, T. A.; Berlicki, Ł. Systematic 'Foldamerization' of Peptide Inhibiting P53-MDM2/X Interactions by the Incorporation of Trans- or Cis-2-Aminocyclopentanecarboxylic Acid Residues. *Eur J Med Chem* **2020**, *208* (112814), 1–8. https://doi.org/10.1016/j.ejmech.2020.112814.

(57) Nyakatura, E. K.; Mortier, J.; Radtke, V. S.; Wieczorek, S.; Rezaei Araghi, R.; Baldauf, C.; Wolber, G.; Koksch, B. β- and γ-Amino Acids at α-Helical Interfaces: Toward the Formation of Highly Stable Foldameric Coiled Coils. *ACS Med Chem Lett* **2014**, *5* (12), 1300–1303. https://doi.org/10.1021/ml500361c.

(58) Seebach, D.; Beck, A. K.; Bierbaum, D. J. The World of β- and γ-Peptides Comprised of Homologated Proteinogenic Amino Acids and Other Components. *Chem Biodivers* **2004**, *1* (8), 1111–1239. https://doi.org/doi.org/10.1002/cbdv.200490087.

(59) Abele, S.; Seebach, D. Preparation of Achiral and of Enantiopure Geminally Disubstituted β- Amino Acids for β-Peptide Synthesis. *European J Org Chem* **2000**, *2000* (1), 1–15. https://doi.org/10.1002/(SICI)1099-0690(200001)2000:1<1::AID-EJOC1>3.0.CO;2-6.

(60) Ordóñez, M.; Cativiela, C.; Romero-Estudillo, I. An Update on the Stereoselective Synthesis of γ-Amino Acids. *Tetrahedron Asymmetry* **2016**, *27* (20–21), 999–1055. https://doi.org/10.1016/j.tetasy.2016.08.011.

(61) Brenner, M.; Seebach, D. Synthesis and CD Spectra in MeCN, MeOH, and H2O of γ-Oligopeptides with Hydroxy Groups on the Backbone. *Helv Chim Acta* **2001**, *84* (5), 1181–1189. https://doi.org/10.1002/1522-2675(20010516)84:5<1181::AID-HLCA1181>3.0.CO;2-0.

(62) Lee, H. S.; Park, J. S.; Kim, B. M.; Gellman, S. H. Efficient Synthesis of Enantiomerically Pure β 2-Amino Acids via Chiral Isoxazolidinones. *J. Org. Chem.* **2003**, *68* (4), 1575–1578. https://doi.org/10.1021/jo026738b.

(63) Gnad, F.; Poleschak, M.; Reiser, O. Stereoselective Synthesis of Novel Conformationally Restricted β- and γ-Amino Acids. *Tetrahedron Lett* **2004**, *45* (22), 4277–4280. https://doi.org/10.1016/j.tetlet.2004.04.013.

(64) Dexter, C. S.; Jackson, R. F. W.; Elliott, J. Synthesis of Enantiomerically Pure β- and γ-Amino Acid Derivatives Using Functionalized Organozinc Reagents. *J. Org. Chem.* **1999**, *64* (20), 7579–7585. https://doi.org/10.1021/jo990941y.

(65) Hintermann, T.; Gademann, K.; Jaun, B.; Seebach, D. γ-Peptides Forming More Stable Secondary Structures than α-Peptides: Synthesis and Helical NMR-Solution Structure of the γ-Hexapeptide Analog of H-(Val-Ala-Leu)2-OH. *Helv Chim Acta* **1998**, *81* (5), 983–1002. https://doi.org/10.1002/hlca.19980810514.

(66) Süssmuth, R. D.; Mainz, A. Nonribosomal Peptide Synthesis - Principles and Prospects. *Angew. Chem. Int. Ed.* **2017**, *56* (14), 3770–3821. https://doi.org/10.1002/anie.201609079.

(67) Kleinkauf, H.; Von Dohren, H. A Nonribosomal System of Peptide Biosynthesis. *Eur. J. Biochem* **1996**, *236* (2), 335–351. https://doi.org/10.1111/j.1432-1033.1996.00335.x.

(68) Katoh, T.; Suga, H. Development of Bioactive Foldamers Using Ribosomally Synthesized Nonstandard Peptide Libraries. *Bull. Chem. Soc. Jpn.* **2021**, *94* (2), 549–557. https://doi.org/10.1246/BCSJ.20200326.

(69) Orwa, J. A.; Govaerts, C.; Busson, R.; Roets, E.; Van Schepdael, A.; Hoogmartens, J. Isolation and Structural Characterization of Polymyxin B

Components. *J Chromatogr A* **2001**, *912* (2), 369–373. https://doi.org/10.1016/S0021-9673(01)00585-4.

(70) Kitagawa, I.; Kobayashi, M.; Lee, N. K.; Shibuya, H.; Kawata, Y.; Sakiyama, F. Structure of Theonellapeptolide ID, A New Bioactive Peptolide from an Okinawan Marine Sponge, Theonella SP. (Theonelliae). *Chem Pharm Bull (Tokyo)* **1986**, *34* (6), 2664–2667.

(71) Vasudev, P. G.; Chatterjee, S.; Narayanaswamy, S.; Padmanabhan, B. Structural Chemistry of Peptides Containing Backbone Expanded Amino Acid Residues: Conformational Features of β, γ, and Hybrid Peptides. *Chem Rev* **2011**, *111* (2), 657–687. https://doi.org/10.1021/cr100100x.

(72) Kritzer, J. A.; Tirado-Rives, J.; Hart, S. A.; Lear, J. D.; Jorgensen, W. L.; Schepartz, A. Relationship between Side Chain Structure and 14-Helix Stability of β 3-Peptides in Water. *J Am Chem Soc* **2005**, *127* (1), 167–178. https://doi.org/10.1021/ja0459375.

(73) Lee, H. L.; Syud, F. A.; Wang, X.; Gellman, S. H. Diversity in Short β-Peptide 12-Helices: High-Resolution Structural Analysis in Aqueous Solution of a Hexamer Containing Sulfonylated Pyrrolidine Residues. *J. Am. Chem. Soc.* **2001**, *123* (31), 7721–7722. https://doi.org/10.1021/ja010734r.

(74) Kaur, K.; Sprules, T.; Soliman, W.; Beleid, R.; Ahmed, S. Right-Handed 14-Helix in β 3-Peptides from L-Aspartic Acid Monomers. *Biochim Biophys Acta Proteins Proteom* **2008**, *1784* (4), 658–665. https://doi.org/10.1016/j.bbapap.2008.01.009.

(75) Shin, S.; Lee, M.; Guzei, I. A.; Kang, Y. K.; Choi, S. H. 12/10-Helical β-Peptide with Dynamic Folding Propensity: Coexistence of Right- and Left-Handed Helices in an Enantiomeric Foldamer. *J Am Chem Soc* **2016**, *138* (40), 13390–13395. https://doi.org/10.1021/jacs.6b08235.

(76) Sharma, G. V. M.; Yadav, T. A.; Choudhary, M.; Kunwar, A. C. Design of β-Amino Acid with Backbone-Side Chain Interactions: Stabilization of 14/15-Helix in α/β-Peptides. *J. Org. Chem.* **2012**, *77* (16), 6834–6848. https://doi.org/10.1021/jo300865d.

(77) Srinivasulu, G.; Kiran Kumar, S.; Sharma, G. V. M.; Kunwar, A. C. 11/9-Mixed Helices in the α/β-Peptides Derived from Alternating α- and β-Amino Acids with Proteinogenic Side Chains. *J. Org. Chem.* **2006**, *71* (22), 8395–8400. https://doi.org/10.1021/jo0612980.

(78) Grison, C. M.; Robin, S.; Aitken, D. J. 13-Helix Folding of a β/γ-Peptide Manifold Designed from a "Minimal-Constraint" Blueprint. *Chem. Commun.* **2016**, *52* (50), 7802–7805. https://doi.org/10.1039/c6cc02142e.

(79) Choi, S. H.; Guzei, I. A.; Spencer, L. C.; Gellman, S. H. Crystallographic Characterization of 12-Helical Secondary Structure in β-Peptides Containing Side Chain Groups. *J Am Chem Soc* **2010**, *132* (39), 13879–13885. https://doi.org/10.1021/ja1062532.

(80) Crisma, M.; Formaggio, F.; Moretto, A.; Toniolo, C. Peptide Helices Based on α-Amino Acids. *Biopolymers - Peptide Science* **2006**, *84* (1), 3–12. https://doi.org/10.1002/bip.20357.

(81) Sharma, G. V. M.; Reddy, N. Y.; Ravi, R.; Sreenivas, B.; Sridhar, G.; Chatterjee, D.; Kunwar, A. C.; Hofmann, H. J. Synthesis of C-Linked Carbo-β 2-Amino Acids and β 2-Peptides: Design of New Motifs for Left-Handed 12/10- and 10/12-Mixed Helices. *Org Biomol Chem* **2012**, *10* (46), 9191–9203. https://doi.org/10.1039/c2ob26615f.

(82) Rueping, M.; Schreiber, J. V.; Lelais, G.; Jaun, B.; Seebach, D. Mixed β 2/β 3-Hexapeptides and β 2/β 3-Nonapeptides Folding to (P)-Helices with Alternating Twelve- and Ten-Membered Hydrogen-Bonded Rings. *Helv Chim Acta* **2002**, *85* (9), 2577–2593. https://doi.org/10.1002/1522-2675(200209)85:9<2577::AID-HLCA2577>3.0.CO;2-D.

(83) Schmitt, M. A.; Choi, S. H.; Guzei, I. A.; Gellman, S. H. Residue Requirements for Helical Folding in Short α/β-Peptides: Crystallographic Characterization of the 11-Helix in an Optimized Sequence. *J Am Chem Soc* **2005**, *127* (38), 13130–13131. https://doi.org/10.1021/ja0536163.

(84) Sharma, G. V. M.; Jadhav, V. B.; Ramakrishna, K. V. S.; Jayaprakash, P.; Narsimulu, K.; Subash, V.; Kunwar, A. C. 12/10- and 11/13-Mixed Helices in α/γ- and β/γ- Hybrid Peptides Containing C-Linked Carbo-γ-Amino Acids with

Alternating α- and β-Amino Acids. *J Am Chem Soc* **2006**, *128* (45), 14657–14668. https://doi.org/10.1021/ja064875a.

(85) Guo, L.; Zhang, W.; Reidenbach, A. G.; Giuliano, M. W.; Guzei, I. A.; Spencer, L. C.; Gellman, S. H. Characteristic Structural Parameters for the γ-Peptide 14-Helix: Importance of Subunit Preorganization. *Angew. Chem. Int. Ed.* **2011**, *50* (26), 5843–5846. https://doi.org/10.1002/anie.201101301.

(86) Hanessian, S.; Luo, X.; Schaum, R.; Michnick, S. Design of Secondary Structures in Unnatural Peptides: Stable Helical γ- Tetra-, Hexa-, and Octapeptides and Consequences of α-Substitution [27]. *J Am Chem Soc* **1998**, *120* (33), 8569–8570. https://doi.org/10.1021/ja9814671.

(87) Mathieu, L.; Legrand, B.; Deng, C.; Vezenkov, L.; Wenger, E.; Didierjean, C.; Amblard, M.; Averlant-Petit, M. C.; Masurier, N.; Lisowski, V.; Martinez, J.; Maillard, L. T. Helical Oligomers of Thiazole-Based γ-Amino Acids: Synthesis and Structural Studies. *Angew. Chem. Int. Ed.* **2013**, *52* (23), 6006–6010. https://doi.org/10.1002/anie.201302106.

(88) Sharma, G. V. M.; Jayaprakash, P.; Narsimulu, K.; Ravi Sankar, A.; Ravinder Reddy, K.; Radha Krishna, P.; Kunwar, A. C. A Left-Handed 9-Helix in γ-Peptides: Synthesis and Conformational Studies of Oligomers with Dipeptide Repeats of C-Linked Carbo- γ 4-Amino Acids and γ-Aminobutyric Acid. *Angew. Chem. Int. Ed.* **2006**, *45* (18), 2944–2947. https://doi.org/10.1002/anie.200504380.

(89) Reddy, M. M. B.; Basuroy, K.; Aravinda, S.; Balaram, P. Crystallographic Characterization of the α,γ C12 Helix in Hybrid Peptide Sequences. *J. Pept. Sci.* **2016**, *22* (8), 504–510. https://doi.org/10.1002/psc.2896.

(90) Jadhav, S. V.; Bandyopadhyay, A.; Gopi, H. N. Protein Secondary Structure Mimetics: Crystal Conformations of α/γ 4-Hybrid Peptide12-Helices with Proteinogenic Side Chains and Their Analogy with α- And β-Peptide Helices. *Org Biomol Chem* **2013**, *11* (3), 509–514. https://doi.org/10.1039/c2ob26805a.

(91) Vasudev, P. G.; Chatterjee, S.; Ananda, K.; Shamala, N.; Balaram, P. Hybrid αγ Polypeptides: Structural Characterization of a C12/C10 Helix with

Alternating Hydrogen-Bond Polarity. *Angew. Chem.* **2008**, *120* (34), 6530–6532. https://doi.org/10.1002/ange.200801665.

(92) Bouillère, F.; Thétiot-Laurent, S.; Kouklovsky, C.; Alezra, V. Foldamers Containing γ-Amino Acid Residues or Their Analogues: Structural Features and Applications. *Amino Acids* **2011**, *41* (3), 687–707. https://doi.org/10.1007/s00726-011-0893-3.

(93) Price, J. L.; Horne, W. S.; Gellman, S. H. Structural Consequences of β-Amino Acid Preorganization in a Self-Assembling α/β-Peptide: Fundamental Studies of Foldameric Helix Bundles. *J Am Chem Soc* **2010**, *132* (35), 12378–12387. https://doi.org/10.1021/ja103543s.

(94) O'Shea, E. K.; Rutkowski, R.; Kim, P. S. Evidence That the Leucine Zipper Is a Coiled Coil. *Science (1979)* **1989**, *243* (4890), 538–542. https://doi.org/10.1126/science.2911757.

(95) O'Shea, E. K.; Klemm, J. D.; Kim, P. S.; Alber, T. X-Ray Structure of the GCN4 Leucine Zipper, a Two-Stranded, Parallel Coiled Coil. *Science (1979)* **1991**, *254* (5031), 539–544. https://doi.org/10.1126/science.1948029.

(96) Giuliano, M. W.; Horne, W. S.; Gellman, S. H. An α/β-Peptide Helix Bundle with a Pure B3-Amino Acid Core and a Distinctive Quaternary Structure. *J Am Chem Soc* **2009**, *131* (29), 9860–9861. https://doi.org/10.1021/ja8099294.

(97) Horne, W. S.; Price, J. L.; Gellman, S. H. Interplay among Side Chain Sequence, Backbone Composition, and Residue Rigidification in Polypeptide Folding and Assembly. *PNAS July* **2008**, *8*, 9151–9156. https://doi.org/10.1073/pnas.0801135105.

(98) Araghi, R. R.; Jäckel, C.; Cölfen, H.; Salwiczek, M.; Vçlkel, A.; Wagner, S. C.; Wieczorek, S.; Baldauf, C.; Koksch, B. A β/γ Motif to Mimic α-Helical Turns in Proteins. *ChemBioChem* **2010**, *11* (3), 335–339. https://doi.org/10.1002/cbic.200900700.

(99) Baldauf, C.; Günther, R.; Hofmann, H. J. Helix Formation in α,γ- and β,γ-Hybrid Peptides: Theoretical Insights into Mimicry of α- and β-Peptides. *J. Org. Chem.* **2006**, *71* (3), 1200–1208. https://doi.org/10.1021/jo052340e.

(100) Rezaei Araghi, R.; Baldauf, C.; Gerling, U. I. M.; Cadicamo, C. D.; Koksch, B. A Systematic Study of Fundamentals in α-Helical Coiled Coil Mimicry by Alternating Sequences of β- And γ-Amino Acids. *Amino Acids* **2011**, *41* (3), 733–742. https://doi.org/10.1007/s00726-011-0941-z.

(101) Araghi, R. R.; Mahrenholz, C. C.; Volkmer, R.; Koksch, B. Investigation of the Network of Preferred Interactions in an Artificial Coiled-Coil Association Using the Peptide Array Technique. *Beilstein Journal of Organic Chemistry* **2012**, *8*, 640–649. https://doi.org/10.3762/bjoc.8.71.

(102) Nyakatura, E. K.; Rezaei Araghi, R.; Mortier, J.; Wieczorek, S.; Baldauf, C.; Wolber, G.; Koksch, B. An Unusual Interstrand H-Bond Stabilizes the Heteroassembly of Helical Aβγ-Chimeras with Natural Peptides. *ACS Chem Biol* **2014**, *9* (3), 613–616. https://doi.org/10.1021/cb4007979.

(103) Smith, G. P. Filamentous Fusion Phage: Novel Expression Vectors That Display Cloned Antigens on the Virion Surface. *Science (1979)* **1985**, *228* (4705), 1315–1317. https://doi.org/10.1126/science.4001944.

(104) *https://www.nobelprize.org/uploads/2018/10/advanced-chemistryprize-2018.pdf (last access: 04/20/2023).*

(105) Pilsl, L. K. A.; Reiser, O. α/β-Peptide Foldamers: State of the Art. *Amino Acids* **2011**, *41* (3), 709–718. https://doi.org/10.1007/s00726-011-0894-2.

(106) Hintermann, T.; Seebach, D. The Biological Stability of β-Peptides: No Interactions between α-and β-Peptidic Structures? *Chimia (Aarau)* **1997**, *51* (5), 244–247. https://doi.org/10.2533/chimia.1997.244.

(107) Yokoo, H.; Hirano, M.; Misawa, T.; Demizu, Y. Helical Antimicrobial Peptide Foldamers Containing Non-Proteinogenic Amino Acids. *ChemMedChem* **2021**, *16* (8), 1226–1233. https://doi.org/10.1002/cmdc.202000940.

(108) Araghi, R. R.; Koksch, B. A Helix-Forming αβγ-Chimeric Peptide with Catalytic Activity: A Hybrid Peptide Ligase. *Chem. Commun.* **2011**, *47* (12), 3544–3546. https://doi.org/10.1039/c0cc03760e.

(109) Kritzer, J. A.; Lear, J. D.; Hodsdon, M. E.; Schepartz, A. Helical β-Peptide Inhibitors of the P53-HDM2 Interaction. *J Am Chem Soc* **2004**, *126* (31), 9468–9469. https://doi.org/10.1021/ja031625a.

(110) Chène, P. Inhibiting the P53-MDM2 Interaction: An Important Target for Cancer Therapy. *Nat Rev Cancer* **2003**, *3* (2), 102–109. https://doi.org/10.1038/nrc991.

(111) Grison, C. M.; Miles, J. A.; Robin, S.; Wilson, A. J.; Aitken, D. J. An α-Helix-Mimicking 12,13-Helix: Designed α/β/γ-Foldamers as Selective Inhibitors of Protein-Protein Interactions. *Angewandte Chemie* **2016**, *128* (37), 11262–11266. https://doi.org/10.1002/ange.201604517.

(112) Lessene, G.; Czabotar, P. E.; Colman, P. M. BCL-2 Family Antagonists for Cancer Therapy. *Nat Rev Drug Discov* **2008**, *7* (12), 989–1000. https://doi.org/10.1038/nrd2658.

(113) Sadowsky, J. D.; Murray, J. K.; Tomita, Y.; Gellman, S. H. Exploration of Backbone Space in Foldamers Containing α- and β-Amino Acid Residues: Developing Protease-Resistant Oligomers That Bind Tightly to the BH3-Recognition Cleft of Bcl-XL. *ChemBioChem* **2007**, *8* (8), 903–916. https://doi.org/10.1002/cbic.200600546.

(114) Sadowsky, J. D.; Schmitt, M. A.; Lee, H. S.; Umezawa, N.; Wang, S.; Tomita, Y.; Gellman, S. H. Chimeric (α/β + α)-Peptide Ligands for the BH3-Recognition Cleft of Bcl-XL: Critical Role of the Molecular Scaffold in Protein Surface Recognition. *J Am Chem Soc* **2005**, *127* (34), 11966–11968. https://doi.org/10.1021/ja053678t.

(115) Sadowsky, J. D.; Fairlie, W. D.; Hadley, E. B.; Lee, H. S.; Umezawa, N.; Nikolovska-Coleska, Z.; Wang, S.; Huang, D. C. S.; Tomita, Y.; Gellman, S. H. (α/β + α)-Peptide Antagonists of BH3 Domain/Bcl-x L Recognition: Toward General Strategies for Foldamer-Based Inhibition of Protein-Protein

Interactions. *J Am Chem Soc* **2007**, *129* (1), 139–154. https://doi.org/10.1021/ja0662523.

(116) Boersma, M. D.; Haase, H. S.; Peterson-Kaufman, K. J.; Lee, E. F.; Clarke, O. B.; Colman, P. M.; Smith, B. J.; Horne, W. S.; Fairlie, W. D.; Gellman, S. H. Evaluation of Diverse α/β-Backbone Patterns for Functional α-Helix Mimicry: Analogues of the Bim BH3 Domain. *J Am Chem Soc* **2012**, *134* (1), 315–323. https://doi.org/10.1021/ja207148m.

(117) Horne, W. S.; Boersma, M. D.; Windsor, M. A.; Gellman, S. H. Sequence-Based Design of α/β-Peptide Foldamers That Mimic BH3 Domains. *Angew. Chem. Int. Ed.* **2008**, *47* (15), 2853–2856. https://doi.org/10.1002/anie.200705315.

(118) Lee, E. F.; Smith, B. J.; Horne, W. S.; Mayer, K. N.; Evangelista, M.; Colman, P. M.; Gellman, S. H.; Fairlie, W. D. Structural Basis of Bcl-x L Recognition by a BH3-Mimetic α/β-Peptide Generated by Sequence-Based Design. *ChemBioChem* **2011**, *12* (13), 2025–2032. https://doi.org/10.1002/cbic.201100314.

(119) Stephens, O. M.; Kim, S.; Welch, B. D.; Hodsdon, M. E.; Kay, M. S.; Schepartz, A. Inhibiting HIV Fusion with a β-Peptide Foldamer. *J Am Chem Soc* **2005**, *127*, 13126–13127. https://doi.org/10.1021/ja053444.

(120) Johnson, L. M.; Mortenson, D. E.; Yun, H. G.; Horne, W. S.; Ketas, T. J.; Lu, M.; Moore, J. P.; Gellman, S. H. Enhancement of α-Helix Mimicry by an α/β-Peptide Foldamer via Incorporation of a Dense Ionic Side-Chain Array. *J Am Chem Soc* **2012**, *134* (17), 7317–7320. https://doi.org/10.1021/ja302428d.

(121) Johnson, L. M.; Horne, W. S.; Gellman, S. H. Broad Distribution of Energetically Important Contacts across an Extended Protein Interface. *J Am Chem Soc* **2011**, *133* (26), 10038–10041. https://doi.org/10.1021/ja203358t.

(122) Matthews, T.; Salgo, M.; Greenberg, M.; Chung, J.; DeMasi, R.; Bolognesi, D. Enfuvirtide: The First Therapy to Inhibit the Entry of HIV-1 into Host CD4 Lymphocytes. *Nat Rev Drug Discov* **2004**, *3* (3), 215–225. https://doi.org/10.1038/nrd1331.

(123) English, E. P.; Chumanov, R. S.; Gellman, S. H.; Compton, T. Rational Development of β-Peptide Inhibitors of Human Cytomegalovirus Entry. *J. Biol. Chem.* **2006**, *281* (5), 2661–2667. https://doi.org/10.1074/jbc.M508485200.

(124) Dennison, S. R.; Wallace, J.; Harris, F.; Phoenix, D. A. Amphiphilic α-Helical Antimicrobial Peptides and Their Structure/Function Relationships. *Protein Pept Lett* **2005**, *12* (1), 31–39. https://doi.org/10.2174/0929866053406084.

(125) Liu, D.; DeGrado, W. F. De Novo Design, Synthesis, and Characterization of Antimicrobial β-Peptides. *J Am Chem Soc* **2001**, *123* (31), 7553–7559. https://doi.org/10.1021/ja0107475.

(126) Porter, E. A.; Wang, X.; Lee, H.-S.; Weisblum, B.; Gellman, S. H. Non-Haemolytic β-Amino-Acid Oligomers. *Nature* **2000**, *404*, 565. https://doi.org/10.1038/35007145.

(127) Arvidsson, P. I.; Ryder, N. S.; Weiss, H. M.; Hook, D. F.; Escalante, J.; Seebach, D. Exploring the Antibacterial and Hemolytic Activity of Shorter- and Longer-Chain β-, α ,β-, and γ-Peptides, and of β-Peptides from β 2-3-Aza- and β 3-2-Methylidene-Amino Bearing Proteinogenic Side Chains - A Survey. *Chem Biodivers* **2005**, *2* (3), 401–420. https://doi.org/10.1002/cbdv.200590020.

(128) Albanesi, D.; Martín, M.; Trajtenberg, F.; Mansilla, M. C.; Haouz, A.; Alzari, P. M.; De Mendoza, D.; Buschiazzo, A.; Greenberg, E. P. Structural Plasticity and Catalysis Regulation of a Thermosensor Histidine Kinase. *PNAS* **2009**, *106* (38), 16185–16190. https://doi.org/10.1073/pnas.0906699106.

(129) Möglich, A.; Ayers, R. A.; Moffat, K. Structure and Signaling Mechanism of Per-ARNT-Sim Domains. *Structure* **2009**, *17* (10), 1282–1294. https://doi.org/10.1016/j.str.2009.08.011.

(130) Dong, G.; Medkova, M.; Novick, P.; Reinisch, K. M. A Catalytic Coiled Coil: Structural Insights into the Activation of the Rab GTPase Sec4p by Sec2p. *Mol Cell* **2007**, *25* (3), 455–462. https://doi.org/10.1016/j.molcel.2007.01.013.

(131) Zhang, R.; Epstein, H. F. Homodimerization through Coiled-Coil Regions Enhances Activity of the Myotonic Dystrophy Protein Kinase. *FEBS Lett* **2003**, *546* (2–3), 281–287. https://doi.org/10.1016/S0014-5793(03)00601-X.

(132) Dawson, P. E.; Muir, T. W.; Clark-Lewis, I.; Kent, S. B. H. Synthesis of Proteins by Native Chemical Ligation. *Science (1979)* **1994**, *266* (5186), 776–779. https://doi.org/10.1126/science.7973629.

(133) Richert, M. E.; Gochev, G. G.; Braunschweig, B. Specific Ion Effects of Trivalent Cations on the Structure and Charging State of β-Lactoglobulin Adsorption Layers. *Langmuir* **2019**, *35* (35), 11299–11307. https://doi.org/10.1021/acs.langmuir.9b01803.

(134) Li, X.; Roiaz, M.; Pramhaas, V.; Rameshan, C.; Rupprechter, G. Polarization-Dependent SFG Spectroscopy of Near Ambient Pressure CO Adsorption on Pt(111) and Pd(111) Revisited. *Top Catal* **2018**, *61* (9–11), 751–762. https://doi.org/10.1007/s11244-018-0949-7.

(135) Shen, Y. R. Surface Properties Probed by Second-Harmonic and Sum-Frequency Generation. *Nature* **1989**, *337*, 519–525. https://doi.org/10.1038/337519a0.

(136) Miyamae, T.; Yokoyama, H.; Han, S.; Ishizone, T. Surface Characterization of Block Copolymers with Water-Soluble Block by Using Sum-Frequency Generation Spectroscopy. *e-Journal of Surface Science and Nanotechnology* **2006**, *4*, 515–520. https://doi.org/10.1380/ejssnt.2006.515.

(137) Morsbach, S.; Gonella, G.; Mailänder, V.; Wegner, S.; Wu, S.; Weidner, T.; Berger, R.; Koynov, K.; Vollmer, D.; Encinas, N.; Kuan, S. L.; Bereau, T.; Kremer, K.; Weil, T.; Bonn, M.; Butt, H. J.; Landfester, K. Engineering Proteins at Interfaces: From Complementary Characterization to Material Surfaces with Designed Functions. *Angew. Chem. Int. Ed.* **2018**, *57* (39), 12626–12648. https://doi.org/10.1002/anie.201712448.

(138) Hirose, C.; Akamatsu, N.; Domen, K. Formulas for the Analysis of Surface Sum-Frequency Generation Spectrum by CH Stretching Modes of Methyl and Methylene Groups. *J Chem Phys* **1992**, *96* (2), 997–1004. https://doi.org/10.1063/1.462120.

(139) Zhu, X. D.; Suhr, H.; Shen, Y. R. Surface Vibrational Spectroscopy by Infrared-Visible Sum Frequency Generation. *Phys. Rev. B* **1987**, *35* (6), 3047–3050. https://doi.org/10.1103/PhysRevB.35.3047.

(140) Moad, A. J.; Simpson, G. J. A Unified Treatment of Selection Rules and Symmetry Relations for Sum-Frequency and Second Harmonic Spectroscopies. *J. Phys. Chem. B* **2004**, *108* (11), 3548–3562. https://doi.org/10.1021/jp035362i.

(141) Gonella, G.; Lütgebaucks, C.; De Beer, A. G. F.; Roke, S. Second Harmonic and Sum-Frequency Generation from Aqueous Interfaces Is Modulated by Interference. *J. Phys. Chem. C* **2016**, *120* (17), 9165–9173. https://doi.org/10.1021/acs.jpcc.5b12453.

(142) Ohno, P. E.; Wang, H. F.; Geiger, F. M. Second-Order Spectral Lineshapes from Charged Interfaces. *Nat Commun* **2017**, *8* (1). https://doi.org/10.1038/s41467-017-01088-0.

(143) Tyrode, E.; Corkery, R. Charging of Carboxylic Acid Monolayers with Monovalent Ions at Low Ionic Strengths: Molecular Insight Revealed by Vibrational Sum Frequency Spectroscopy. *J. Phys. Chem. C* **2018**, *122* (50), 28775–28786. https://doi.org/10.1021/acs.jpcc.8b09505.

(144) Vanselous, H.; Petersen, P. B. Extending the Capabilities of Heterodyne-Detected Sum-Frequency Generation Spectroscopy: Probing Any Interface in Any Polarization Combination. *J. Phys. Chem. C* **2016**, *120* (15), 8175–8184. https://doi.org/10.1021/acs.jpcc.6b01252.

(145) Nihonyanagi, S.; Yamaguchi, S.; Tahara, T. Direct Evidence for Orientational Flip-Flop of Water Molecules at Charged Interfaces: A Heterodyne-Detected Vibrational Sum Frequency Generation Study. *J. Chem. Phys.* **2009**, *130* (20), 204704–204705. https://doi.org/10.1063/1.3135147.

(146) Schnurbus, M.; Hardt, M.; Steinforth, P.; Carrascosa-Tejedor, J.; Winnall, S.; Gutfreund, P.; Schönhoff, M.; Campbell, R. A.; Braunschweig, B. Responsive Material and Interfacial Properties through Remote Control of Polyelectrolyte–Surfactant Mixtures. *ACS Appl Mater Interfaces* **2022**, *14* (3), 4656–4667. https://doi.org/10.1021/acsami.1c18934.

(147) Ataka, K.; Kottke, T.; Heberle, J. Thinner, Smaller, Faster: IR Techniques to Probe the Functionality of Biological and Biomimetic Systems. *Angew. Chem. Int. Ed.* **2010**, *49* (32), 5416–5424. https://doi.org/10.1002/anie.200907114.

(148) Hosseinpour, S.; Roeters, S. J.; Bonn, M.; Peukert, W.; Woutersen, S.; Weidner, T. Structure and Dynamics of Interfacial Peptides and Proteins from Vibrational Sum-Frequency Generation Spectroscopy. *Chem Rev* **2020**, *120* (7), 3420–3465. https://doi.org/10.1021/acs.chemrev.9b00410.

(149) Watry, M. R.; Richmond, G. L. Orientation and Conformation of Amino Acids in Monolayers Adsorbed at an Oil/Water Interface as Determined by Vibrational Sum-Frequency Spectroscopy. *J. Phys. Chem. B* **2002**, *106* (48), 12517–12523. https://doi.org/10.1021/jp021469e.

(150) Mermut, O.; Phillips, D. C.; York, R. L.; McCrea, K. R.; Ward, R. S.; Somorjai, G. A. In Situ Adsorption Studies of a 14-Amino Acid Leucine-Lysine Peptide onto Hydrophobic Polystyrene and Hydrophilic Silica Surfaces Using Quartz Crystal Microbalance, Atomic Force Microscopy, and Sum Frequency Generation Vibrational Spectroscopy. *J Am Chem Soc* **2006**, *128* (11), 3598–3607. https://doi.org/10.1021/ja056031h.

(151) Schmüser, L.; Roeters, S.; Lutz, H.; Woutersen, S.; Bonn, M.; Weidner, T. Determination of Absolute Orientation of Protein α-Helices at Interfaces Using Phase-Resolved Sum Frequency Generation Spectroscopy. *J. Phys. Chem. Lett.* **2017**, *8* (13), 3101–3105. https://doi.org/10.1021/acs.jpclett.7b01059.

(152) Pagel, K.; Wagner, S. C.; Samedov, K.; Von Berlepsch, H.; Böttcher, C.; Koksch, B. Random Coils, β-Sheet Ribbons, and α-Helical Fibers: One Peptide Adopting Three Different Secondary Structures at Will. *J Am Chem Soc* **2006**, *128* (7), 2196–2197. https://doi.org/10.1021/ja057450h.

(153) Pandya, M. J.; Spooner, G. M.; Sunde, M.; Thorpe, J. R.; Rodger, A.; Woolfson, D. N. Sticky-End Assembly of a Designed Peptide Fiber Provides Insight into Protein Fibrillogenesis. *Biochemistry* **2000**, *39* (30), 8728–8734. https://doi.org/10.1021/bi000246g.

(154) Araghi, R. R. α-Helical Coiled Coil Mimicry by Alternating Sequences of β- and γ-Amino Acids. *Dissertation, Freie Universität Berlin*. 2011.

(155) Szefczyk, M.; Szulc, N.; Gąsior-Głogowska, M.; Modrak-Wójcik, A.; Bzowska, A.; Majstrzyk, W.; Taube, M.; Kozak, M.; Gotszalk, T.; Rudzińska-Szostak, E.; Berlicki, Ł. Hierarchical Approach for the Rational Construction of Helix-Containing Nanofibrils Using α,β-Peptides. *Nanoscale* **2021**, *13* (7), 4000–4015. https://doi.org/10.1039/d0nr04313c.

(156) Hartmann, M. D.; Ridderbusch, O.; Zeth, K.; Albrecht, R.; Testa, O.; Woolfson, D. N.; Sauer, G.; Dunin-Horkawicz, S.; Lupas, A. N.; Alvarez, B. H. A Coiled-Coil Motif That Sequesters Ions to the Hydrophobic Core. *PNAS* **2009**, *106* (40), 16950–16955. https://doi.org/10.1073/pnas.0907256106.

(157) Whitson, S. R.; LeStourgeon, W. M.; Krezel, A. M. Solution Structure of the Symmetric Coiled Coil Tetramer Formed by the Oligomerization Domain of HnRNP C: Implications for Biological Function. *J Mol Biol* **2005**, *350* (2), 319–337. https://doi.org/10.1016/j.jmb.2005.05.002.

(158) Lindhout, D. A.; Litowski, J. R.; Mercier, P.; Hodges, R. S.; Sykes, B. D. NMR Solution Structure of a Highly Stable de Novo Heterodimeric Coiled-Coil. *Biopolymers* **2004**, *75* (5), 367–375. https://doi.org/10.1002/bip.20150.

(159) O'Donoghue, S. I.; Nigles, M. *Structure Computation and Dynamics in Protein NMR*; Rama Krishna, N., Berliner, L. J., Eds.; Biological Magnetic Resonance: New York, 1999; Vol. 17.

(160) Dames, S. A.; Kammerer, R. A.; Wiltscheck, R.; Engel, J.; Alexandrescu, A. T. NMR Structure of a Parallel Homotrimeric Coiled Coil. *Nat Struct Mol Biol* **1998**, *5* (8), 687–691. https://doi.org/10.1038/90444.

(161) Pasco, M.; Dolain, C.; Guichard, G. Foldamers. In *Supramolecular Chemistry in Water*; Kubik, S., Ed.; Wiley-VCH Verlag GmbH & Co. KGaA, 2019; pp 337–374.

(162) McInteer, B. B. Isotope Separation by Distillation: Design of a Carbon-13 Plant. *Sep Sci Technol* **1980**, *15* (3), 491–508. https://doi.org/10.1080/01496398008068494.

(163) Raun, W. R.; Johnson, G. V.; Westerman, R. L. Fertilizer Nitrogen Recovery in Long-Term Continuous Winter Wheat. *Soil Sci. Soc. Am. J.* **1999**, *63* (3), 645–650. https://doi.org/10.2136/sssaj1999.03615995006300030030x.

(164) Lindhout, D. A.; Thiessen, A.; Schieve, D.; Sykes, B. D. High-Yield Expression of Isotopically Labeled Peptides for Use in NMR Studies. *Protein Science* **2003**, *12* (8), 1786–1791. https://doi.org/10.1110/ps.0376003.

(165) Susi, H.; Byler, D. M. *[13] Resolution-Enhanced Fourier Transform Infrared Spectroscopy of Enzymes*; Hirs, C. H. W., Timashef, S. N., Eds.; Academic Press, 1986; Vol. 130. https://doi.org/10.1016/0076-6879(86)30015-6.

(166) Barth, A. Infrared Spectroscopy of Proteins. *Biochim Biophys Acta Bioenerg* **2007**, *1767* (9), 1073–1101. https://doi.org/10.1016/j.bbabio.2007.06.004.

(167) Yang, H.; Yang, S.; Kong, J.; Dong, A.; Yu, S. Obtaining Information about Protein Secondary Structures in Aqueous Solution Using Fourier Transform IR Spectroscopy. *Nat Protoc* **2015**, *10* (3), 382–396. https://doi.org/10.1038/nprot.2015.024.

(168) Lau, S. Y. M.; Taneja, A. K.; Hodges, R. S. Synthesis of a Model Protein of Defined Secondary and Quaternary Structure. Effect of Chain Length on the Stabilization and Formation of Two-Stranded α-Helical Coiled-Coils. *J. Biol. Chem.* **1984**, *259* (21), 13253–13261. https://doi.org/10.1016/s0021-9258(18)90686-1.

(169) Surewicz, W. K.; Mantsch, H. H.; Chapman, D. Determination of Protein Secondary Structure by Fourier Transform Infrared Spectroscopy: A Critical Assessment. *Biochemistry* **1993**, *32* (2), 389–394. https://doi.org/10.1021/bi00053a001.

(170) Valenti, L. E.; Paci, M. B.; De Pauli, C. P.; Giacomelli, C. E. Infrared Study of Trifluoroacetic Acid Unpurified Synthetic Peptides in Aqueous Solution: Trifluoroacetic Acid Removal and Band Assignment. *Anal Biochem* **2011**, *410* (1), 118–123. https://doi.org/10.1016/j.ab.2010.11.006.

(171) Alben, J. O.; Bare, G. H. Ligand-Dependent Heme-Protein Interactions in Human Hemoglobin Studied by Fourier Transform Infrared Spectroscopy. *J.*

Biol. Chem. **1980**, *255* (9), 3892–3897. https://doi.org/10.1016/S0021-9258(19)85609-0.

(172) Dong, A.; Caughey, W. S. [9] Infrared Methods for Study of Hemoglobin Reactions and Structures. In *Methods in Enzymology*; Everse, J., Vandegriff, K. D., Winslow, R. M., Eds.; Academic Press, 1994; Vol. 232, pp 139–175. https://doi.org/10.1016/0076-6879(94)32047-0.

(173) Alben, J. O.; Bare, G. H.; Bromberg, P. A. Sulphydryl Groups as a New Molecular Probe at the A1 B1 Interface in Haemoglobin Using Fourier Transform Infrared Spectroscopy. *Nature* **1974**, *252*, 736–738. https://doi.org/10.1038/252736a0.

(174) Mielcarek, A.; Dołęga, A. Weak Hydrogen Bonding Interaction S-H⋯O=C Studied by FT-IR Spectroscopy and DFT Calculations. *J Mol Struct* **2016**, *1103*, 217–223. https://doi.org/10.1016/j.molstruc.2015.09.032.

(175) Garciá Rey, N.; Weißenborn, E.; Schulze-Zachau, F.; Gochev, G.; Braunschweig, B. Quantifying Double-Layer Potentials at Liquid-Gas Interfaces from Vibrational Sum-Frequency Generation. *J. Phys. Chem. C* **2019**, *123* (2), 1279–1286. https://doi.org/10.1021/acs.jpcc.8b10097.

(176) Wensien, M.; von Pappenheim, F. R.; Funk, L. M.; Kloskowski, P.; Curth, U.; Diederichsen, U.; Uranga, J.; Ye, J.; Fang, P.; Pan, K. T.; Urlaub, H.; Mata, R. A.; Sautner, V.; Tittmann, K. A Lysine–Cysteine Redox Switch with an NOS Bridge Regulates Enzyme Function. *Nature* **2021**, *593* (7859), 460–464. https://doi.org/10.1038/s41586-021-03513-3.

(177) El Antri, S.; Sire, O.; Alpert, B. A Fourier Transform Infrared Study of Oxyhemoglobin in Aqueous Solution. *Chem.Phys. Lett.* **1989**, *161* (1), 47–49. https://doi.org/10.1016/S0009-2614(89)87029-0.

(178) Burton, A. J.; Thomas, F.; Agnew, C.; Hudson, K. L.; Halford, S. E.; Brady, R. L.; Woolfson, D. N. Accessibility, Reactivity, and Selectivity of Side Chains within a Channel of de Novo Peptide Assembly. *J Am Chem Soc* **2013**, *135* (34), 12524–12527. https://doi.org/10.1021/ja4053027.

(179) Tamogami, J.; Kikukawa, T.; Ohkawa, K.; Ohsawa, N.; Nara, T.; Demura, M.; Miyauchi, S.; Kimura-Someya, T.; Shirouzu, M.; Yokoyama, S.; Shimono, K.; Kamo, N. Interhelical Interactions between D92 and C218 in the Cytoplasmic Domain Regulate Proton Uptake upon N-Decay in the Proton Transport of Acetabularia Rhodopsin II. *J Photochem Photobiol B* **2018**, *183*, 35–45. https://doi.org/10.1016/j.jphotobiol.2018.04.012.

(180) Gray, T. M.; Matthews, B. W. Intrahelical Hydrogen Bonding of Serine, Threonine and Cysteine Residues Within α-Helices and Its Relevance to Membrane-Bound Proteins. *J Mol Biol* **1984**, *175* (1), 75–81. https://doi.org/10.1016/0022-2836(84)90446-7.

(181) Gregoret, L. M.; Rader, S. D.; Fletterick, R. J.; Cohen, F. E. Hydrogen Bonds Involving Sulfur Atoms in Proteins. *Proteins: Structure, Function, and Bioinformatics* **1991**, *9* (2), 99–107. https://doi.org/10.1002/prot.340090204.

(182) McPherson, A.; Gavira, J. A. Introduction to Protein Crystallization. *Acta Crystallogr F Struct Biol Commun* **2014**, *70* (1), 2–20. https://doi.org/10.1107/S2053230X13033141.

(183) Zalewski, J. K.; Heber, S.; Mo, J. H.; O'conor, K.; Hildebrand, J. D.; Vandemark, A. P. Combining Wet and Dry Lab Techniques to Guide the Crystallization of Large Coiled-Coil Containing Proteins. *Journal of Visualized Experiments* **2017**, *2017* (119). https://doi.org/10.3791/54886.

(184) Gordy, W.; Shields, H. Electron Spin Resonance Studies of Radiation Damage to Proteins. *Radiat Res* **1958**, *9* (6), 611–625. https://doi.org/10.2307/3570707.

(185) Garman, E. F. Radiation Damage in Macromolecular Crystallography: What Is It and Why Should We Care? *Acta Crystallogr D Biol Crystallogr* **2010**, *66* (4), 339–351. https://doi.org/10.1107/S0907444910008656.

(186) Grum, V. L.; Li, D.; MacDonald, R. I.; Mondragó, A. Structures of Two Repeats of Spectrin Suggest Models of Flexibility. *Cell* **1999**, *98*, 523–535. https://doi.org/10.1016/S0092-8674(00)81980-7.

(187) Lorenzo, D. N.; Edwards, R. J.; Slavutsky, A. L. Spectrins: Molecular Organizers and Targets of Neurological Disorders. *Nature Reviews Neuroscience*. Springer Nature April 1, 2023, pp 195–212. https://doi.org/10.1038/s41583-022-00674-6.

(188) Choi, H. J.; Weis, W. I. Crystal Structure of a Rigid Four-Spectrin-Repeat Fragment of the Human Desmoplakin Plakin Domain. *J Mol Biol* **2011**, *409* (5), 800–812. https://doi.org/10.1016/j.jmb.2011.04.046.

(189) Pascual, J.; Pfuhl, M.; Rivas, G.; Pastore, A.; Saraste, M. The Spectrin Repeat Folds into a Three-Helix Bundle in Solution. *FEBS Lett* **1996**, *383* (3), 201–207. https://doi.org/10.1016/0014-5793(96)00251-7.

(190) Kemp, G.; Nilsson, O. B.; Tian, P.; Best, R. B.; Von Heijne, G. Cotranslational Folding Cooperativity of Contiguous Domains of α-Spectrin. *PNAS* **2020**, *117* (25), 14119–14126. https://doi.org/10.1073/pnas.1909683117/-/DCSupplemental.

(191) Pascual, J.; Pfuhl, M.; Walther, D.; Saraste, M.; Nilges, M. Solution Structure of the Spectrin Repeat: A Left-Handed Antiparallel Triple-Helical Coiled-Coil. *J. Mol. Biol.* **1997**, *273*, 740–751. https://doi.org/10.1006/jmbi.1997.1344.

(192) Woody, R. W. Circular Dichroism Spectrum of Peptides in the Poly(Pro)II Conformation. *J Am Chem Soc* **2009**, *131* (23), 8234–8245. https://doi.org/10.1021/ja901218m.

(193) Serpa, J. J.; Parker, C. E.; Petrotchenko, E. V.; Han, J.; Pana, J.; Borchers, C. H. Mass Spectrometry-Based Structural Proteomics. *Eur. J. of Mass Spectrom.* **2012**, *18* (2), 251–267. https://doi.org/10.1255/ejms.1178.

(194) Campos-Olivas, R. NMR Screening and Hit Validation in Fragment Based Drug Discovery. *Curr Top Med Chem* **2011**, *11* (1), 43–67. https://doi.org/10.2174/156802611793611887.

(195) Moreau, V. H.; Valente, A. P.; Almeida, F. C. L. Prediction of the Amount of Secondary Structure of Proteins Using Unassigned NMR Spectra: A Tool for Target Selection in Structural Proteomics. *Genet Mol Biol* **2006**, *29* (4), 762–770. https://doi.org/10.1590/S1415-47572006000400030.

(196) Siegal, G.; Hollander, J. G. Target Immobilization and NMR Screening of Fragments in Early Drug Discovery. *Curr Top Med Chem* **2009**, *9* (18), 1736–1745. https://doi.org/10.2174/156802609790102400.

(197) Zheng, T. T.; Boyle, A.; Robson Marsden, H.; Valdink, D.; Martelli, G.; Raap, J.; Kros, A. Probing Coiled-Coil Assembly by Paramagnetic NMR Spectroscopy. *Org Biomol Chem* **2015**, *13* (4), 1159–1168. https://doi.org/10.1039/c4ob02125h.

(198) Finkelstein, H. Darstellung Organischer Jodide Aus Den Entsprechenden Bromiden Und Chloriden. *Berichte der deutschen chemischen Gesellschaft* **1910**, *43* (2), 1528–1532. https://doi.org/10.1002/cber.19100430257.

(199) Gude, M.; Ryf, J.; White, P. D. An Accurate Method for the Quantitation of Fmoc-Derivatized Solid Phase Supports. *Letters in Peptide Science* **2003**, *9*, 203–206. https://doi.org/10.1023/A:1024148619149.

(200) *Sigma Aldrich, "Peptide Resin Loading Protocols" - "FMOC LOADING TEST" can be found under https://www.sigmaaldrich.com/DE/en/technical-documents/technical-article/chemistry-and-synthesis/peptide-synthesis/peptide-resin-loading (last access: 03/30/2023)*.

(201) Chen, Y.-H.; Yang, J. T.; Chau, K. H. Determination of the Helix and ß Form of Proteins in Aqueous Solution by Circular Dichroism. *Biochemistry* **1973**, *13* (16), 3350–3359. https://doi.org/10.1021/bi00713a027.

(202) Glikman, D.; García Rey, N.; Richert, M.; Meister, K.; Braunschweig, B. PH Effects on the Molecular Structure and Charging State of β-Escin Biosurfactants at the Air-Water Interface. *J Colloid Interface Sci* **2022**, *607*, 1754–1761. https://doi.org/10.1016/j.jcis.2021.09.086.

(203) Pettersen, E. F.; Goddard, T. D.; Huang, C. C.; Couch, G. S.; Greenblatt, D. M.; Meng, E. C.; Ferrin, T. E. UCSF Chimera - A Visualization System for Exploratory Research and Analysis. *J. Comput. Chem.* **2004**, *25*, 1605–1612. https://doi.org/10.1002/jcc.20084.

(204) McNicholas, S.; Potterton, E.; Wilson, K. S.; Noble, M. E. M. Presenting Your Structures: The CCP4mg Molecular-Graphics Software. *Acta Crystallogr D*

Biol Crystallogr **2011**, *67* (4), 386–394. https://doi.org/10.1107/S0907444911007281.

(205) Winn, M. D.; Ballard, C. C.; Cowtan, K. D.; Dodson, E. J.; Emsley, P.; Evans, P. R.; Keegan, R. M.; Krissinel, E. B.; Leslie, A. G. W.; McCoy, A.; McNicholas, S. J.; Murshudov, G. N.; Pannu, N. S.; Potterton, E. A.; Powell, H. R.; Read, R. J.; Vagin, A.; Wilson, K. S. Overview of the CCP4 Suite and Current Developments. *Acta Crystallogr D Biol Crystallogr* **2011**, *67* (4), 235–242. https://doi.org/10.1107/S0907444910045749.

7. Appendix

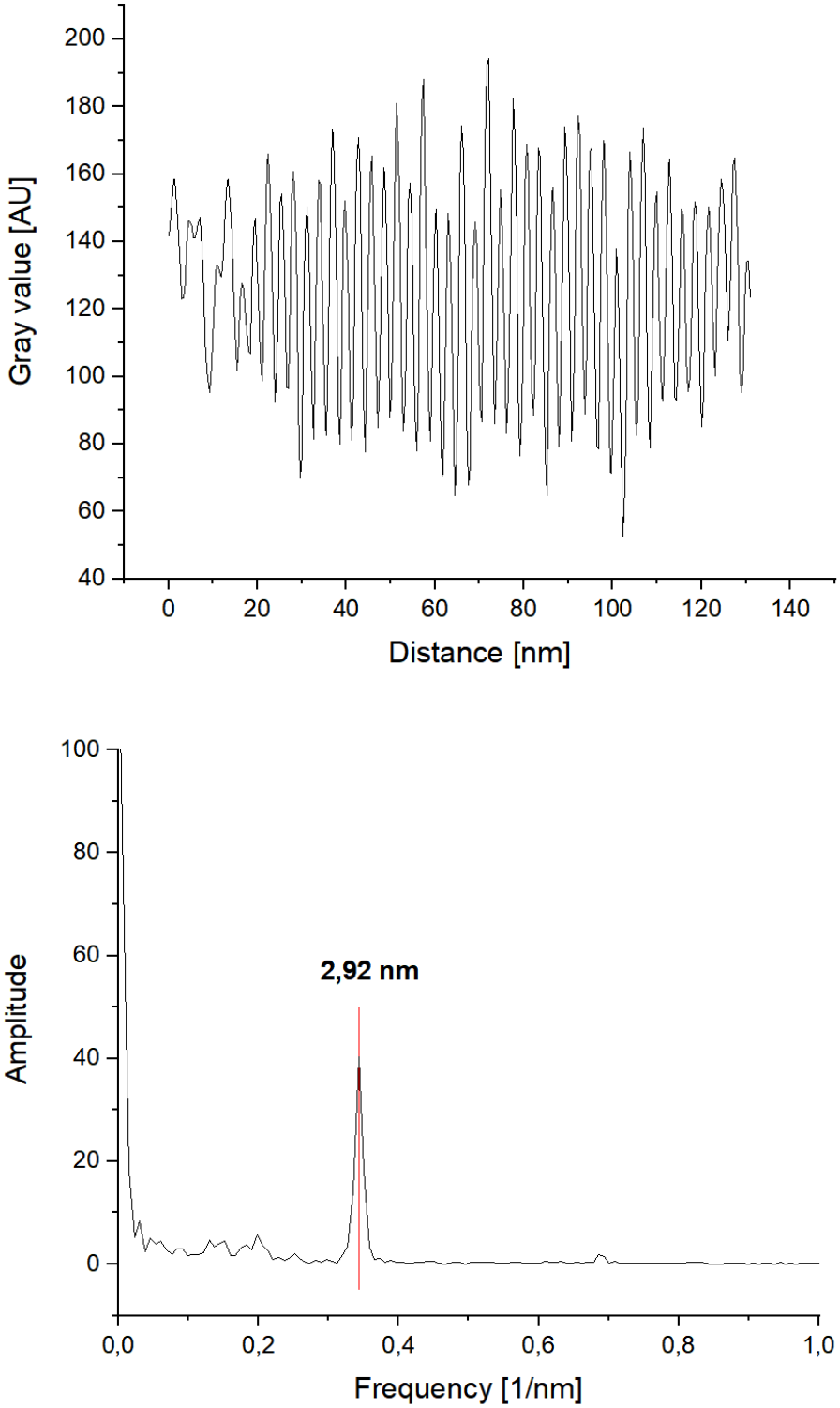

Figure 65: First light-to-dark plot for the average diameter determination of crystalline Acid-CFLE/B3β2γ during cryo-TEM (1 mg/mL total peptide concentration of equimolar peptide mixture in 10 mM phosphate buffer at pH 7.4).

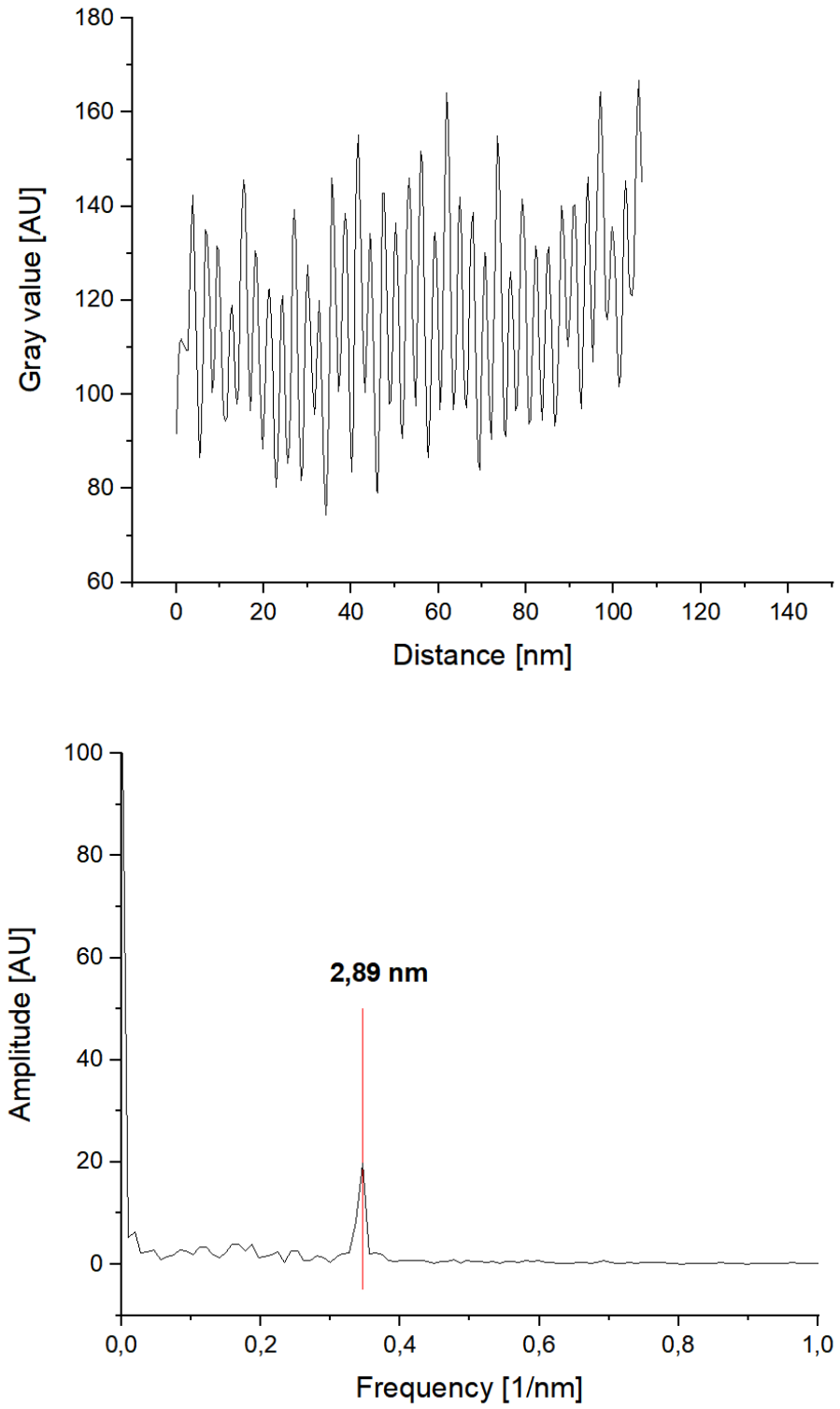

Figure 66: Second light-to-dark plot for the average diameter determination of crystalline Acid-CFLE/B3β2γ during cryo-TEM (1 mg/mL total peptide concentration of equimolar peptide mixture in 10 mM phosphate buffer at pH 7.4).

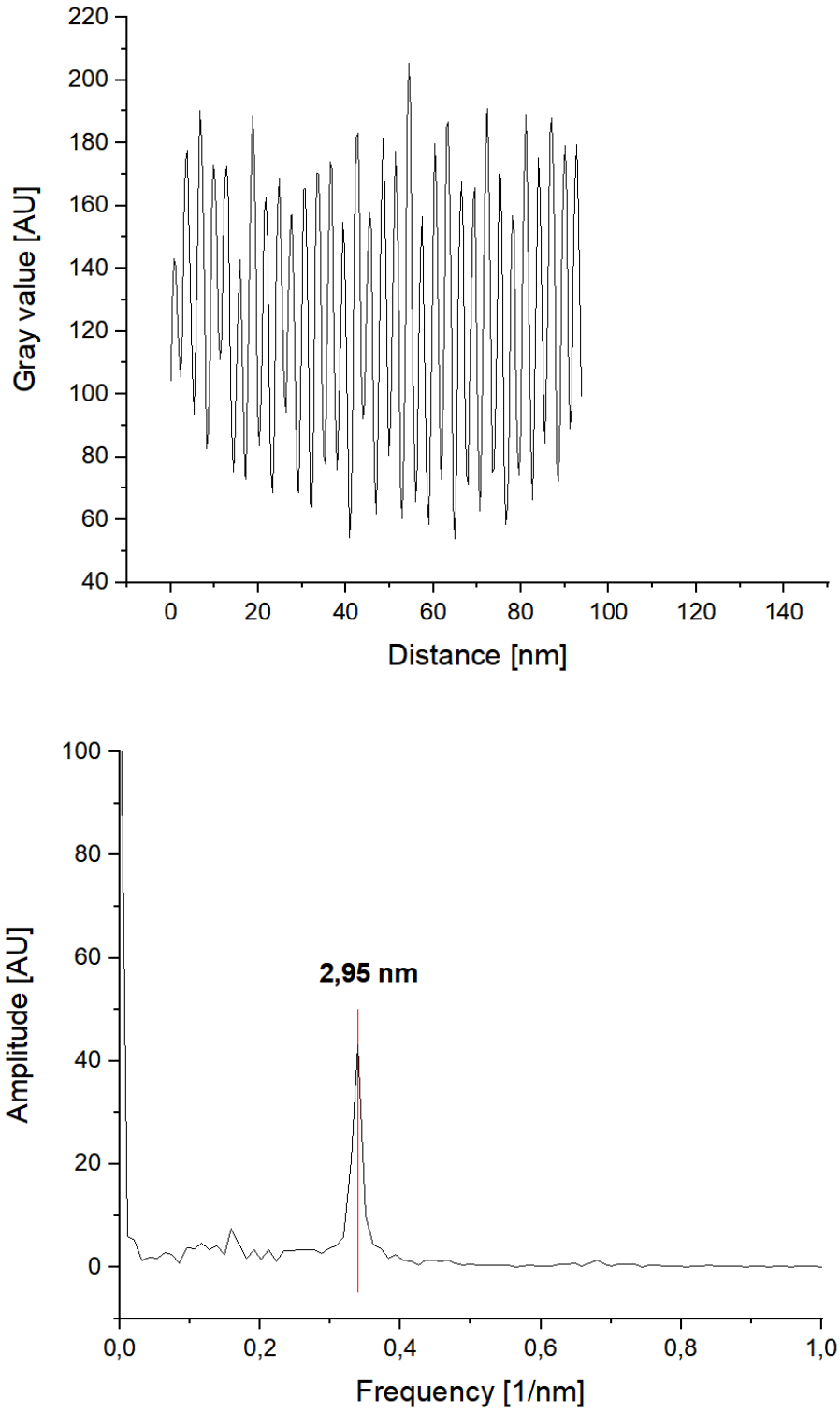

Figure 67: Third light-to-dark plot for the average diameter determination of crystalline Acid-CFLE/B3β2γ during cryo-TEM (1 mg/mL total peptide concentration of equimolar peptide mixture in 10 mM phosphate buffer at pH 7.4).

Table 47: SFG fitting results for w5 at minimum 2500 cm^{-1} to 2600 cm^{-1} maximum in the thiol region.

System	second order electric susceptibility $\chi^{(2)}$	Wavelength [cm^{-1}]	Amplitude
Acid-ICEF	0.018476	2560.9247	0.037979
Acid-ICEF/Base-pp	0.23116	2558.9536	0.020992
Acid-ICEF/B3β2γ	0.12112	2563.2111	0.030036
Acid-I*m*CEF	0.012829	2552.7321	0.014708
Acid-I*m*CEF/B3β2γ	0.16186	2593.7899	0
Acid-ranICEF	0.040971	2554.0769	0.012822
Acid-ranICEF/B3β2γ	0.11392	2560.2527	0.02855
Acid-CFLE	0.031872	2552.726	0.029817
Acid-CFLE/B3β2γ	0.10281	2566.2729	0.029559
Acid-*m*CFLE/B3β2γ	0.095613	2558.7835	3.2605×10^{-10}

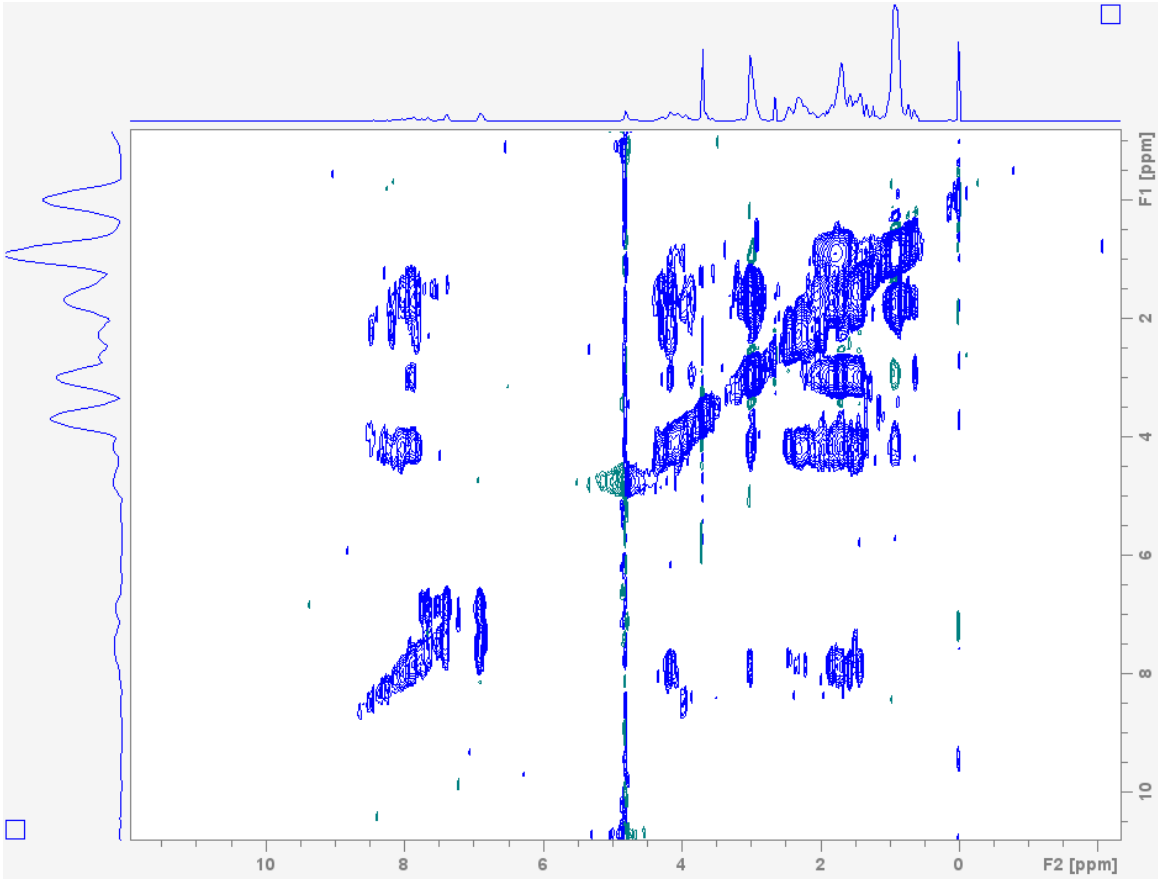

Figure 68: ^{1}H-^{1}H-TOCSY of Base-pp (2.6 mg) in NMR buffer containing 100 mM phosphate buffer at pH 7.4, 20 mM potassium fluoride (KF), 0.1 mM sodium trimethylsilylpropanesulfonate (DSS), 4 mM sodium azide (NaN3) and 5% deuterated water (D2O). Measurement was performed at 298 K and referenced to DSS.

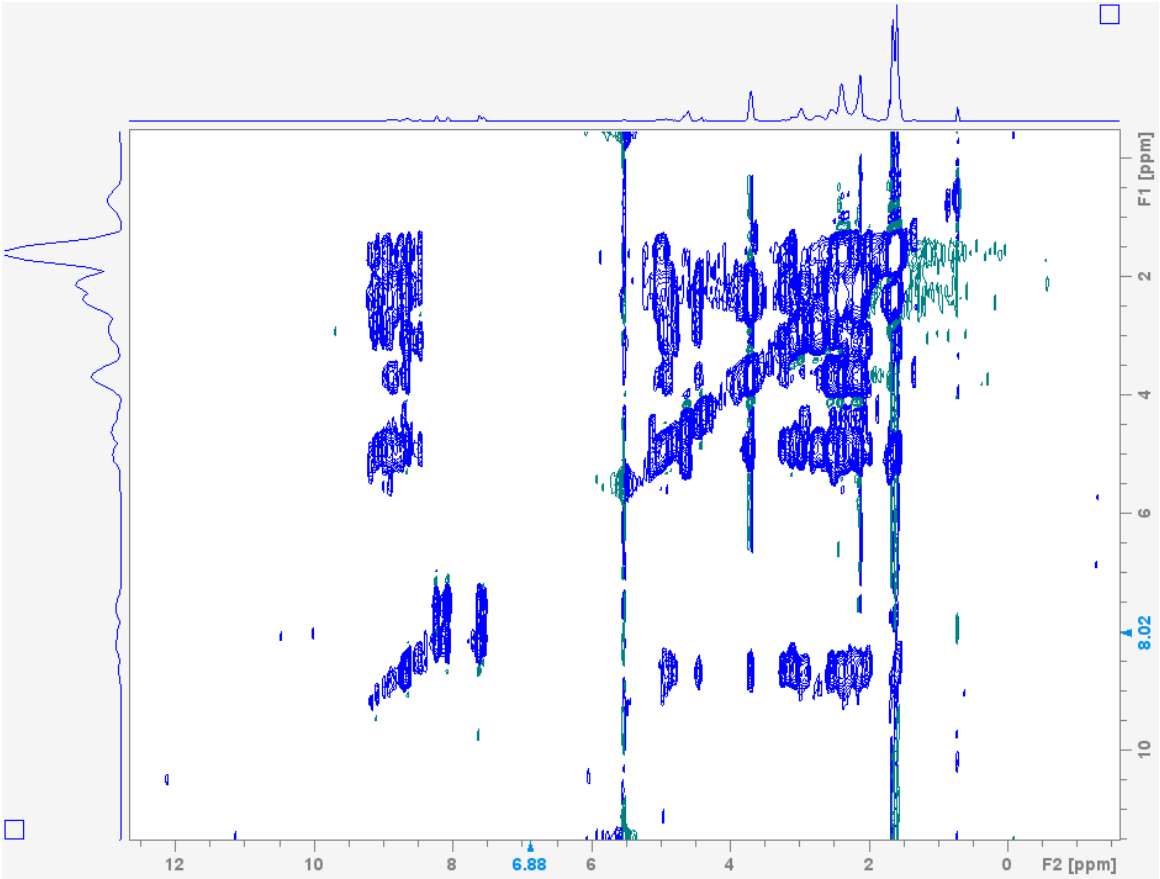

Figure 69: ^{1}H-^{1}H-TOCSY of B3β2γ (1.6 mg) in NMR buffer containing 100 mM phosphate buffer at pH 7.4, 20 mM potassium fluoride (KF), 0.1 mM sodium trimethylsilylpropanesulfonate (DSS), 4 mM sodium azide (NaN3) and 5% deuterated water (D2O). Measurement was performed at 298 K and referenced to DSS.

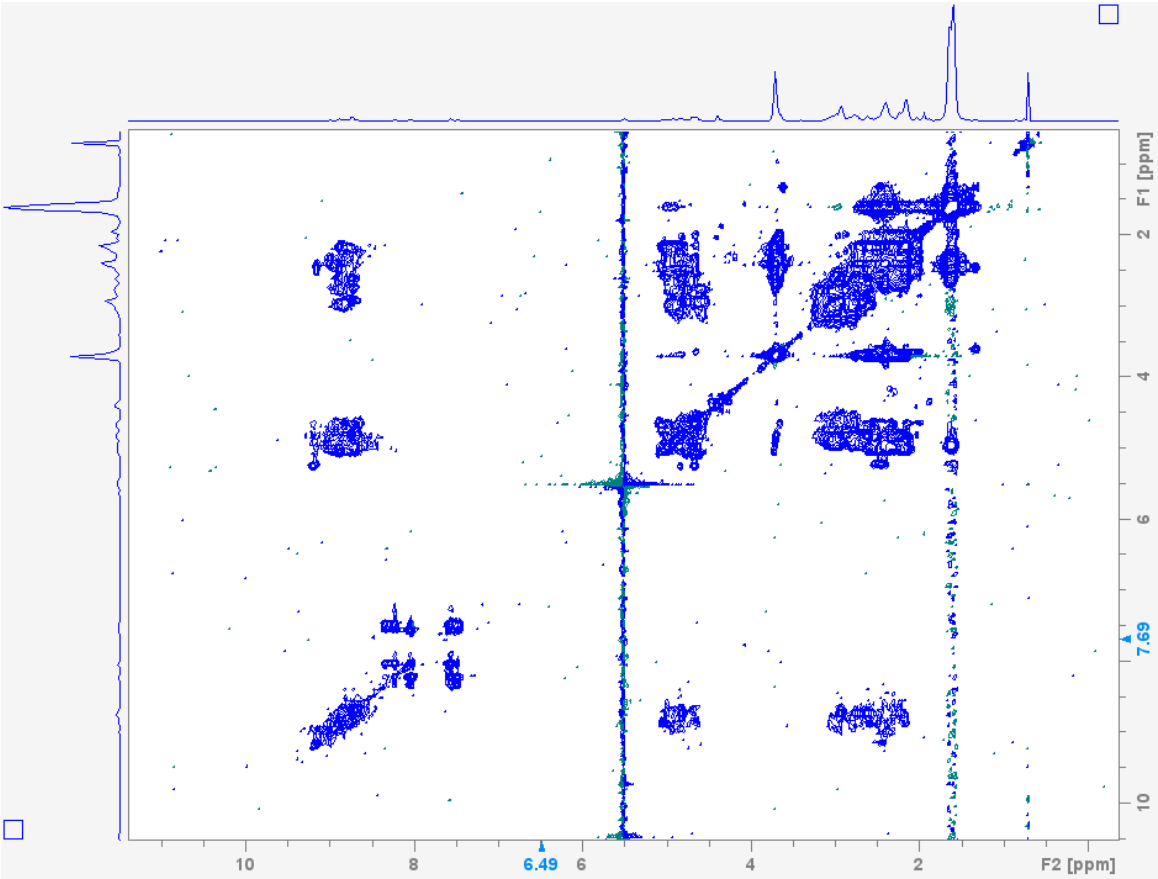

Figure 70: ^{1}H-^{1}H-TOCSY of Acid-pp (1.9 mg) in NMR buffer containing 100 mM phosphate buffer at pH 7.4, 20 mM potassium fluoride (KF), 0.1 mM sodium trimethylsilylpropanesulfonate (DSS), 4 mM sodium azide (NaN3) and 5% deuterated water (D2O). Measurement was performed at 298 K and referenced to DSS.

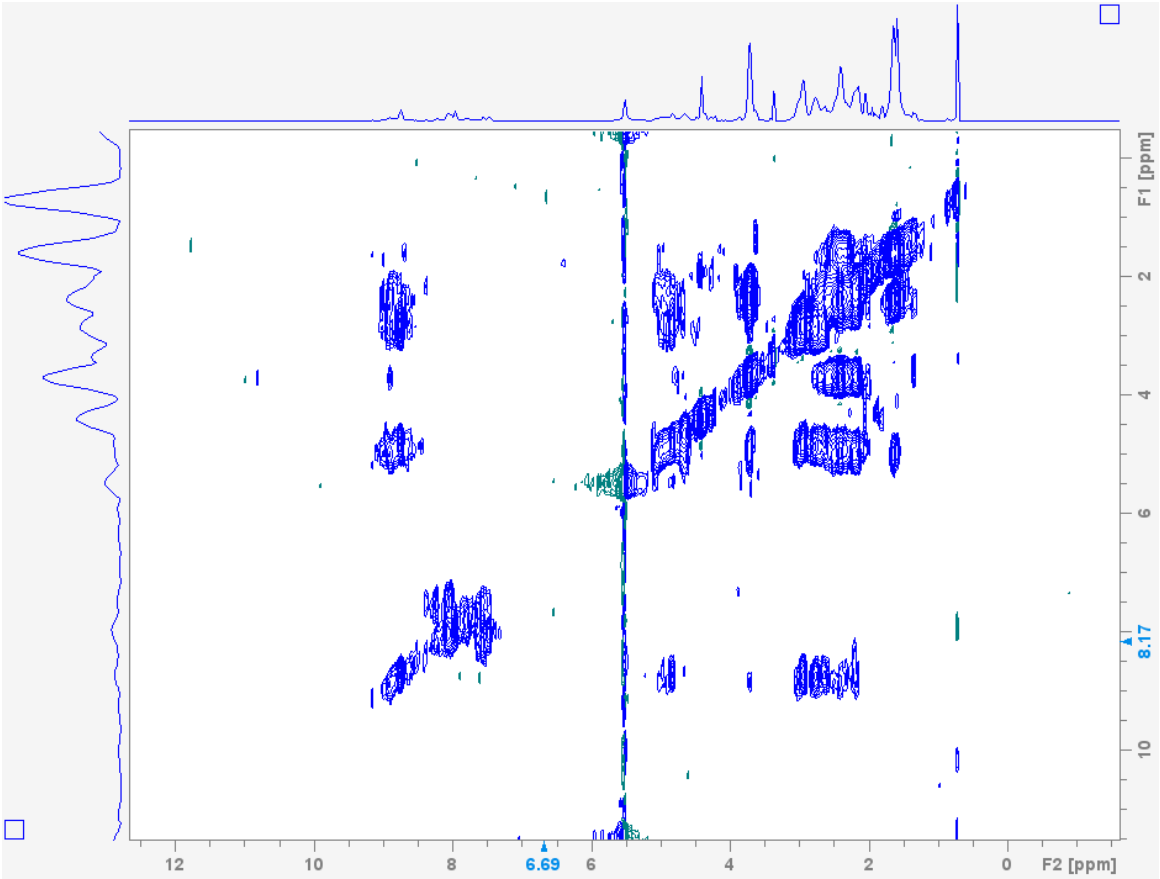

Figure 71: ^{1}H-^{1}H-TOCSY of Acid-CFLE (1.4 mg) in NMR buffer containing 100 mM phosphate buffer at pH 7.4, 20 mM potassium fluoride (KF), 0.1 mM sodium trimethylsilylpropanesulfonate (DSS), 4 mM sodium azide (NaN3) and 5% deuterated water (D2O). Measurement was performed at 298 K and referenced to DSS.

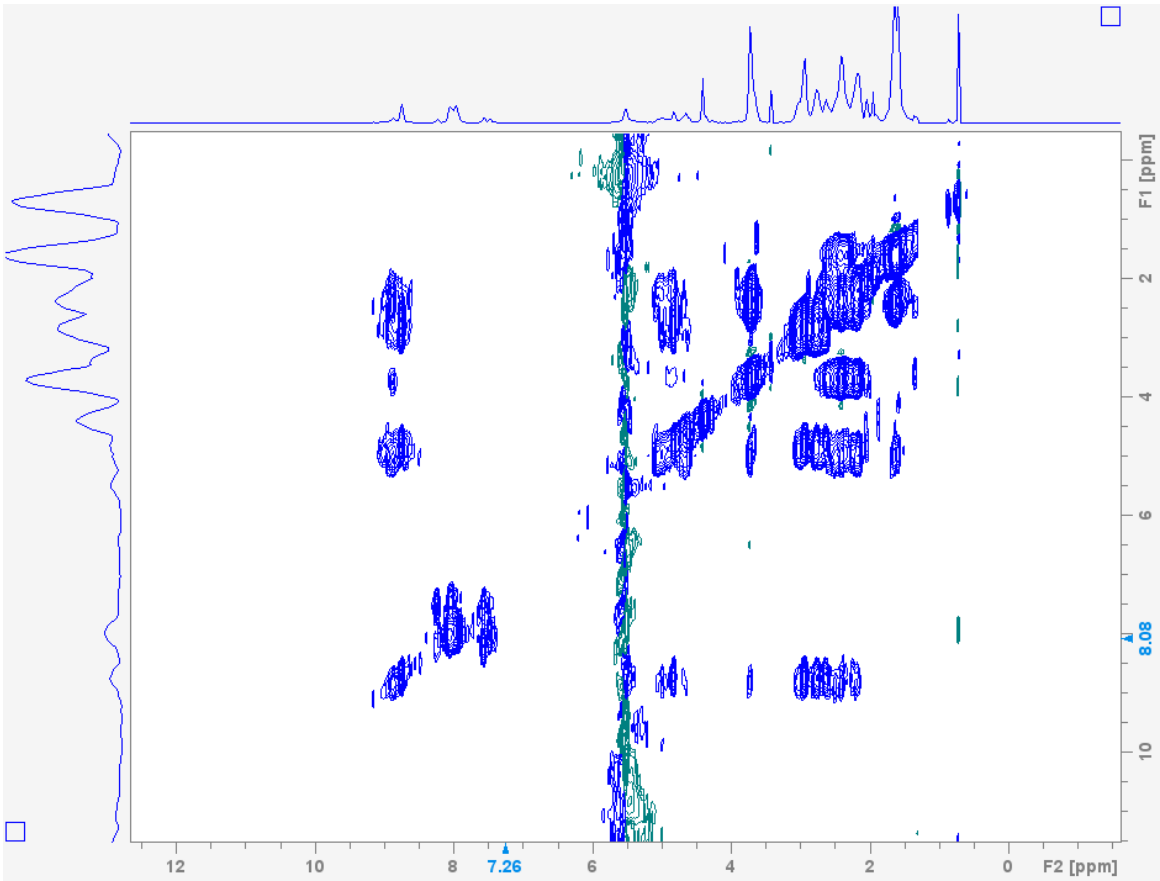

Figure 72: ^{1}H-^{1}H-TOCSY of Acid-ICEF (2.4 mg) in NMR buffer containing 100 mM phosphate buffer at pH 7.4, 20 mM potassium fluoride (KF), 0.1 mM sodium trimethylsilylpropanesulfonate (DSS), 4 mM sodium azide (NaN3) and 5% deuterated water (D2O). Measurement was performed at 298 K and referenced to DSS.

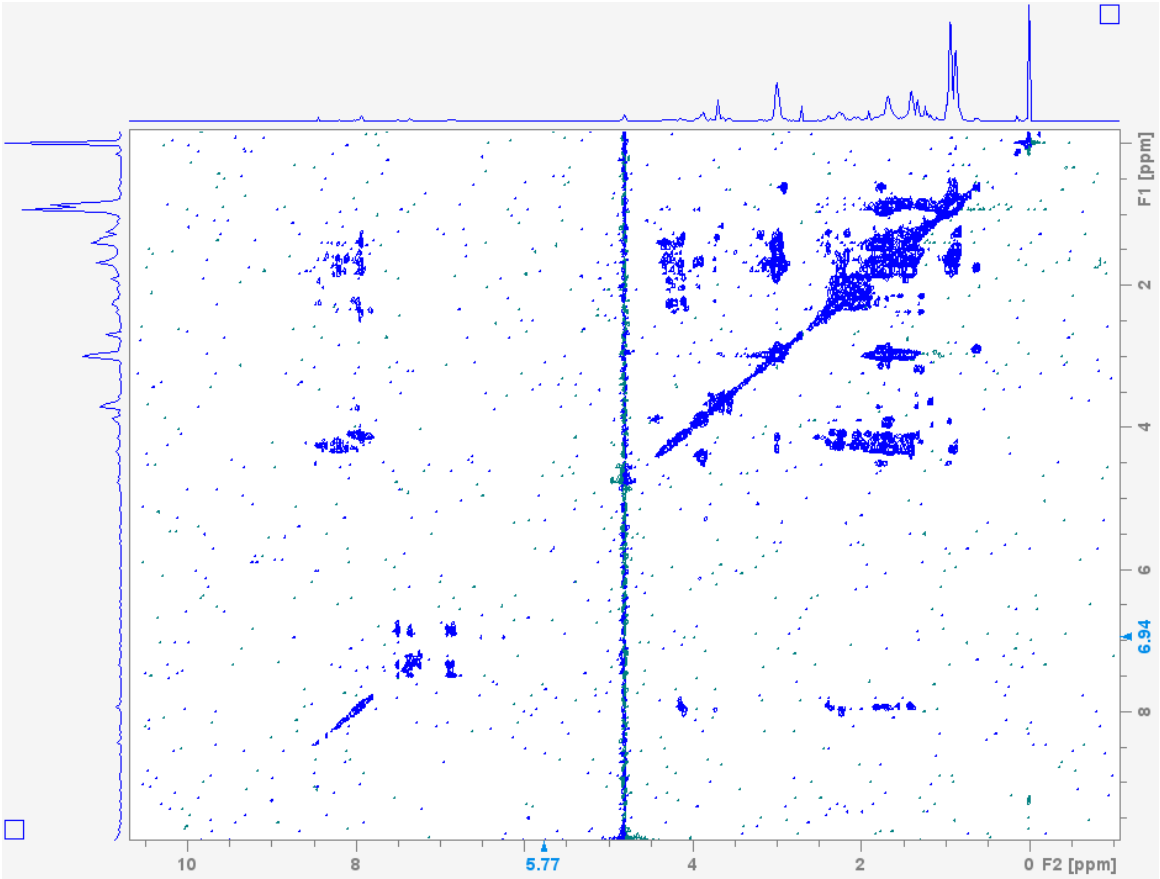

Figure 73: ^{1}H-^{1}H-TOCSY of Acid-pp/B3β2γ (338 µM) in NMR buffer containing 100 mM phosphate buffer at pH 7.4, 20 mM potassium fluoride (KF), 0.1 mM sodium trimethylsilylpropanesulfonate (DSS), 4 mM sodium azide (NaN3) and 5% deuterated water (D2O). Measurement was performed at 298 K and referenced to DSS.

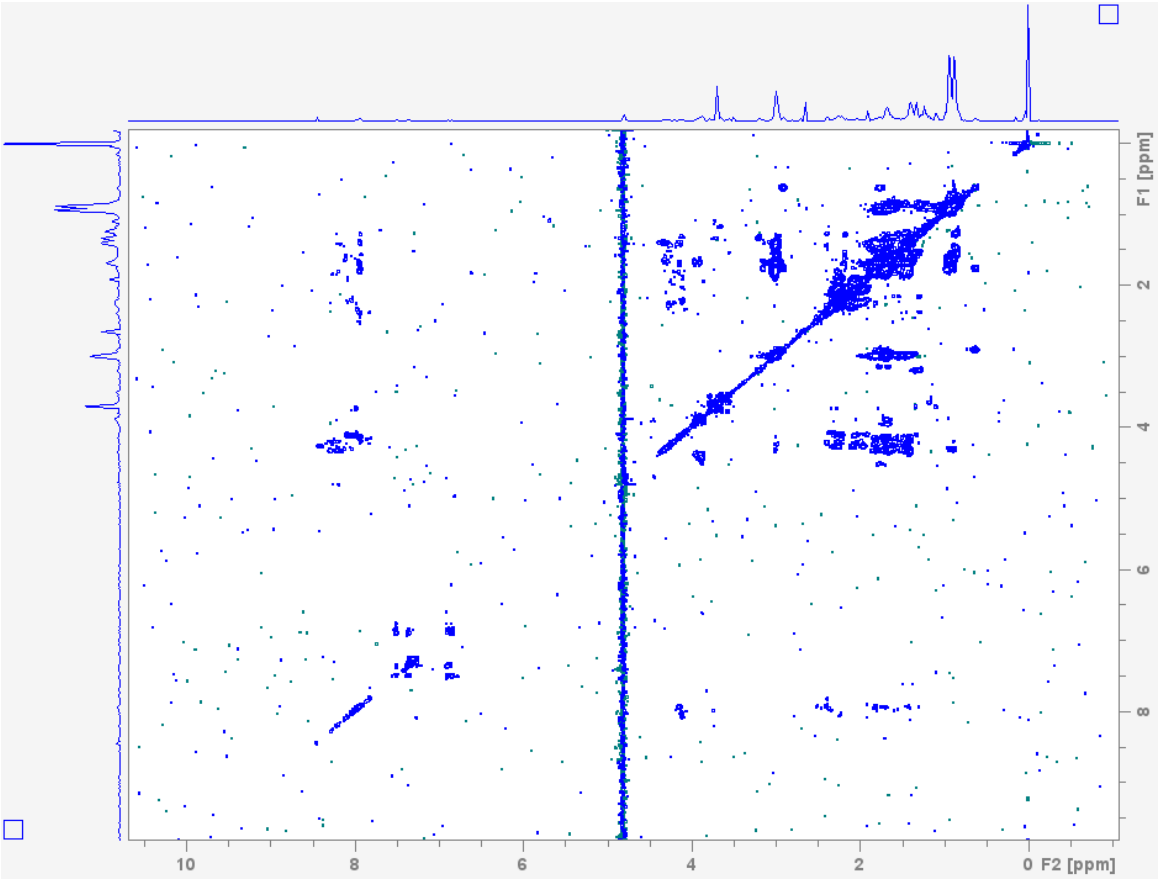

Figure 74: ^{1}H-^{1}H-TOCSY of Acid-CFLE/B3β2γ (305 µM) in NMR buffer containing 100 mM phosphate buffer at pH 7.4, 20 mM potassium fluoride (KF), 0.1 mM sodium trimethylsilylpropanesulfonate (DSS), 4 mM sodium azide (NaN3) and 5% deuterated water (D2O). Measurement was performed at 298 K and referenced to DSS.

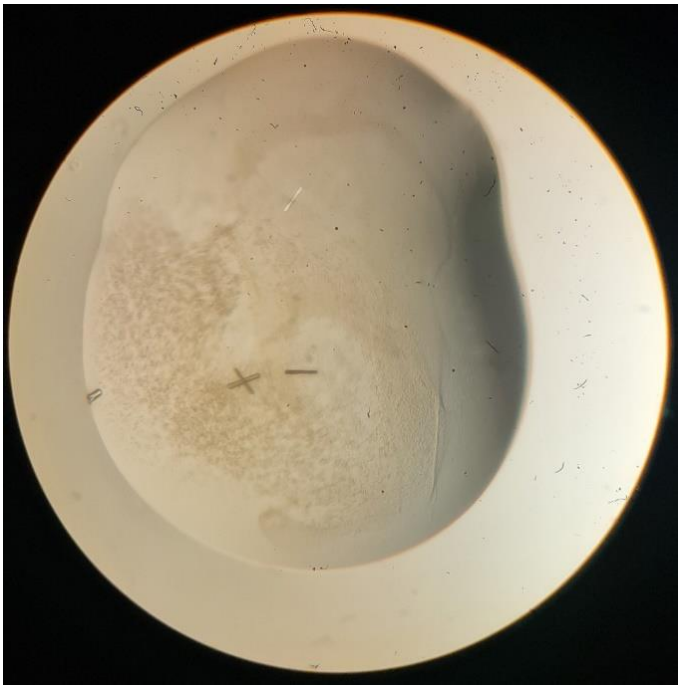

Figure 75: Acid-CFLE/B3β2γ, screening hit in G2 Classic 1; 0.2 M $CaCl_2$, 0.1 M HEPES sodium salt pH 7.5, 28% (v/v) PEG400.

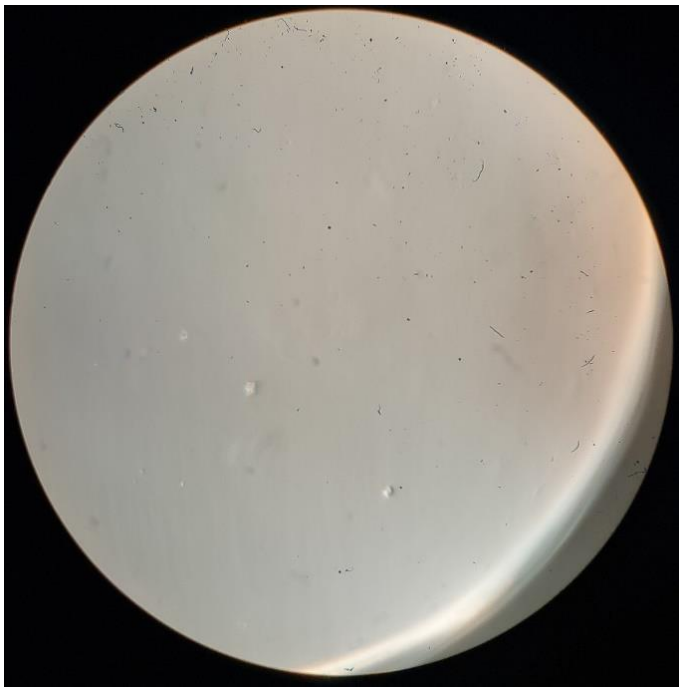

Figure 76: Acid-ICEF/B3β2γ, screening hit in B7 Index 2; 0.2 M ammonium acetate, 0.1 M BIS-TRIS pH 5.5, 45% (v/v) MPD.

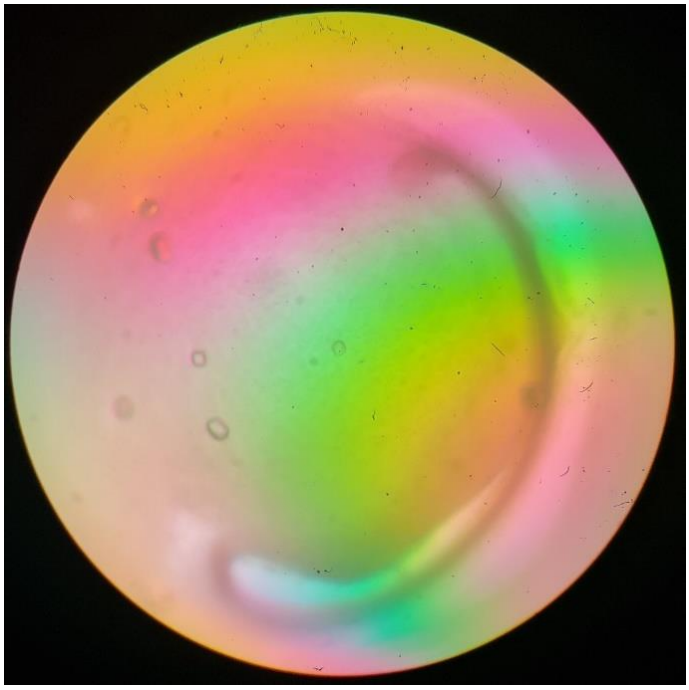

Figure 77: Acid-pp/Base-pp; hit derived from optimization: 0.14 M citric acid pH 3.5, 21% PEG3350, 15 mg/mL total peptide concentration (original condition: H5 Index 2; 0.1 M citric acid pH 3.5, 25% (w/v) PEG3350).

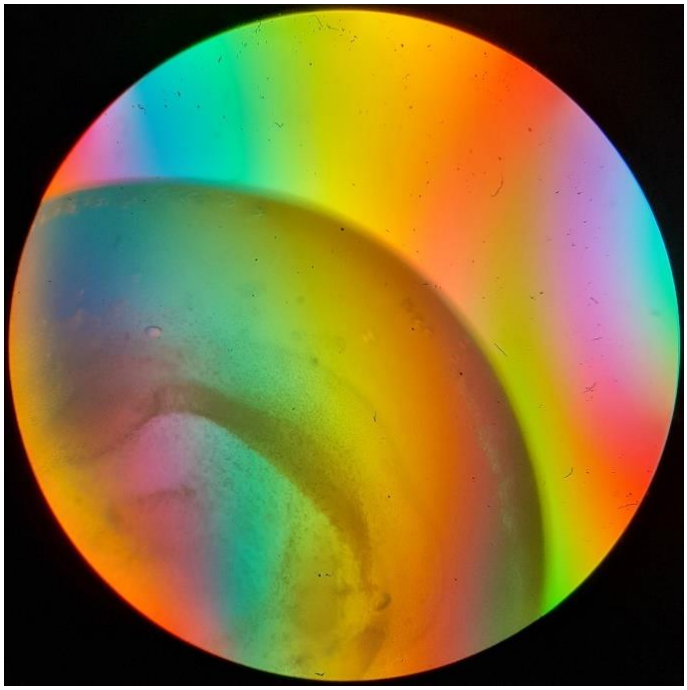

Figure 78: Acid-pp/Base-pp; hit derived from optimization: 0.14 M citric acid pH 3.5, 25% PEG3350, 15 mg/mL total peptide concentration (original condition: H5 Index 2; 0.1 M citric acid pH 3.5, 25% (w/v) PEG3350). The crystals are crowded on the side of the drop.

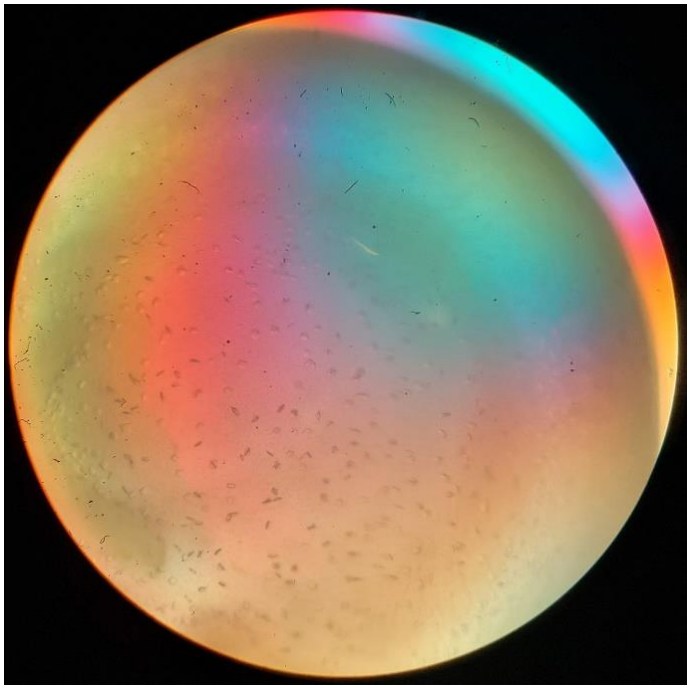

Figure 79: Acid-pp/Base-pp; hit derived from optimization: 0.11 M citric acid pH 3.5, 33% PEG3350, 15 mg/mL total peptide concentration (original condition: H5 Index 2; 0.1 M citric acid pH 3.5, 25% (w/v) PEG3350).

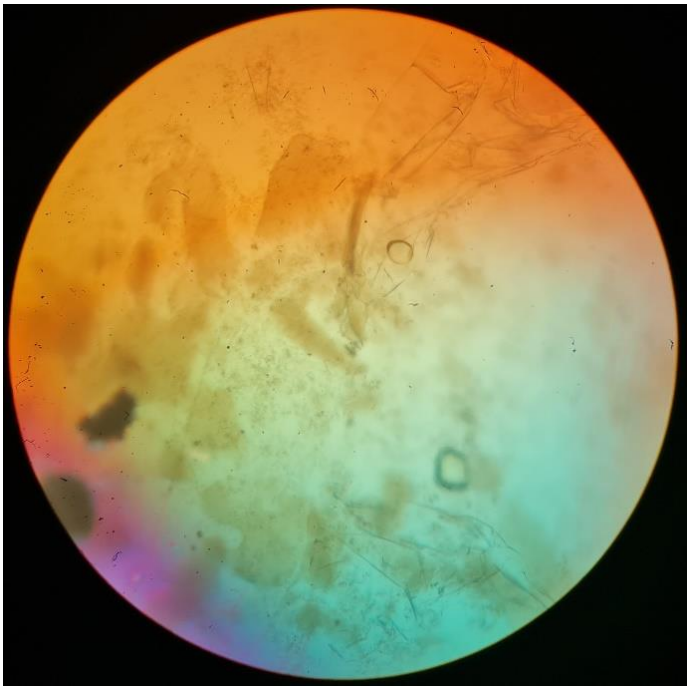

Figure 80: Acid-pp/Base-pp; hit derived from optimization: 0.1 M citric acid pH 3.5, 25% PEG3350, 15 mg/mL total peptide concentration (original condition: H5 Index 2; 0.1 M citric acid pH 3.5, 25% (w/v) PEG3350). The grown crystals are larger, but appear “gnawed”.

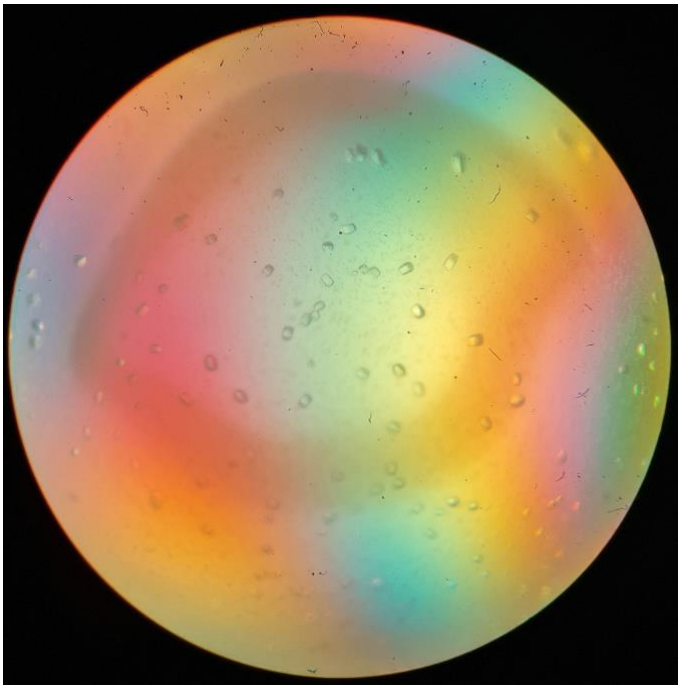

Figure 81: Acid-pp/Base-pp; hit derived from optimization: 0.1 M citric acid pH 3.5, 25% PEG3350, 15 mg/mL total peptide concentration (original condition: H5 Index 2; 0.1 M citric acid pH 3.5, 25% (w/v) PEG3350).

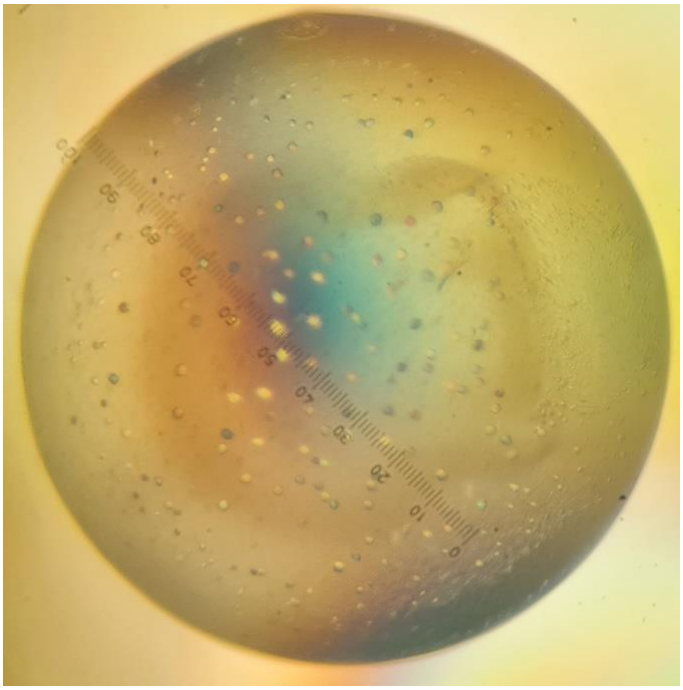

Figure 82: Acid-pp/Base-pp; hit derived from optimization: 0.11 M citric acid pH 3.5, 25% PEG3350, 15 mg/mL total peptide concentration (original condition: H5 Index 2; 0.1 M citric acid pH 3.5, 25% (w/v) PEG3350) at 4 °C.

Figure 83: Acid-pp/Base-pp; hit derived from optimization: 0.1 M citric acid pH 3.5, 25% PEG3350, 15 mg/mL total peptide concentration (original condition: H5 Index 2; 0.1 M citric acid pH 3.5, 25% (w/v) PEG3350) at 4 °C.

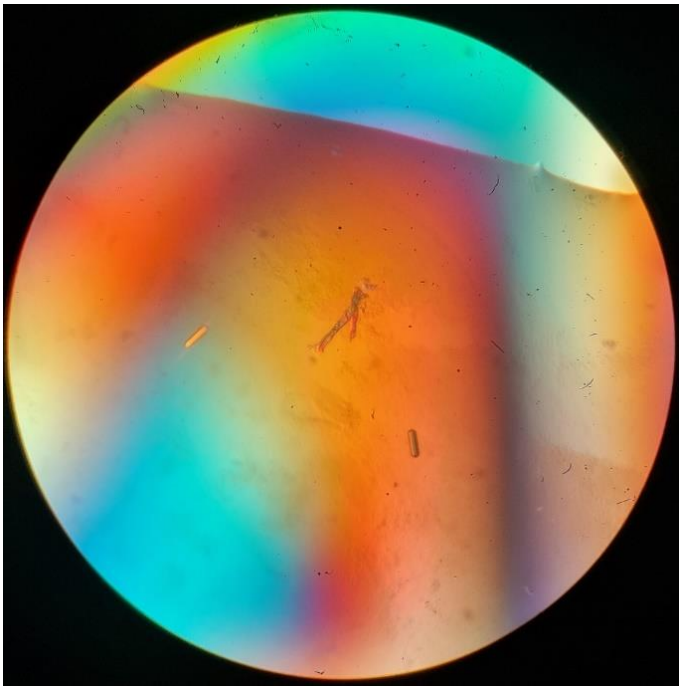

Figure 84: Acid-pp/B3β2γ; hit derived from optimization: 0.5 M $CaCl_2$ dihydrate, 0.1 M HEPES pH 7.5, 21% PEG400, 23 mg/mL total peptide concentration (original condition: G2 Classic 1; 0.2 M $CaCl_2$, 0.1 M HEPES sodium salt pH 7.5, 28% (v/v) PEG400).

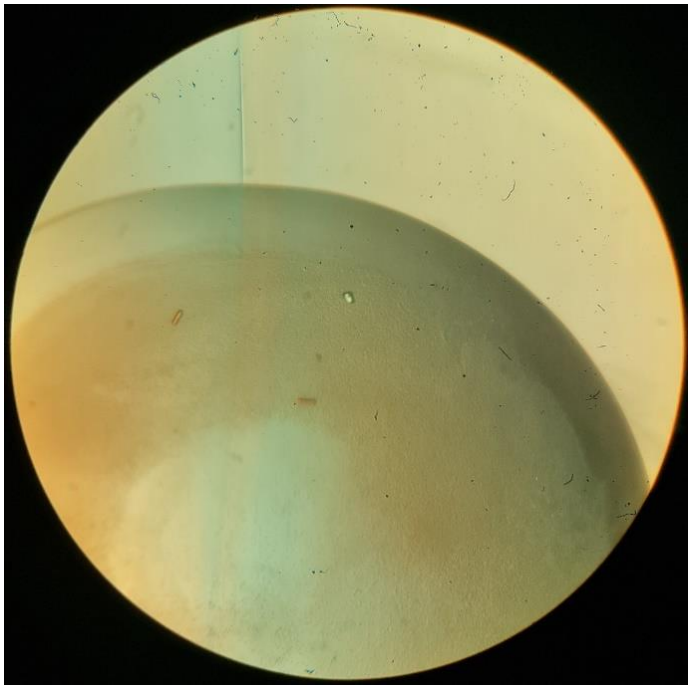

Figure 85: Acid-pp/B3β2γ; hit derived from optimization: 0.1 M $CaCl_2$ dihydrate, 0.1 M HEPES pH 7.5, 27% PEG400, 23 mg/mL total peptide concentration (original condition: G2 Classic 1; 0.2 M $CaCl_2$, 0.1 M HEPES sodium salt pH 7.5, 28% (v/v) PEG400).

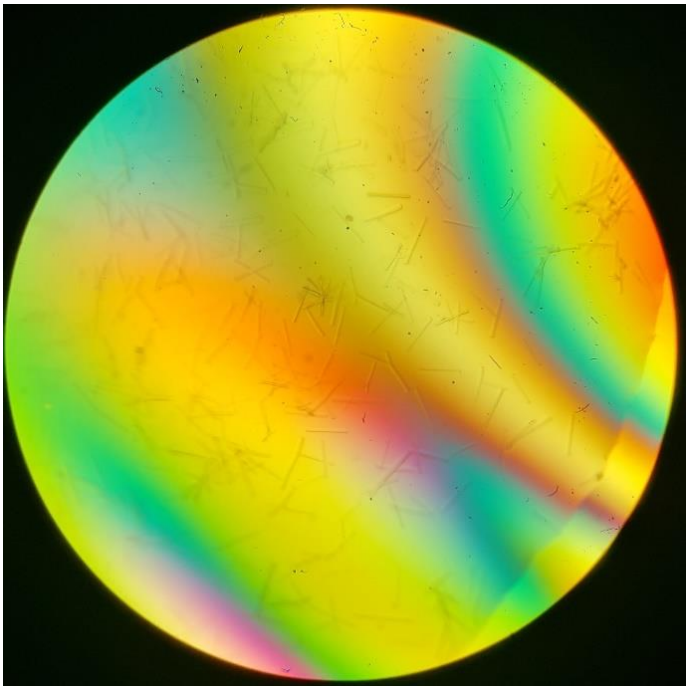

Figure 86: Acid-CFLE/B3β2γ; hit derived from optimization: 0.05 M $CaCl_2$ dihydrate, 0.1 M sodium acetate trihydrate pH 4.6, 30% MPD, 10 mg/mL total peptide concentration (original condition: B3 Classic 1; 0.02 M $CaCl_2$, 0.1 M sodium acetate pH 4.6, 30% (v/v) MPD).

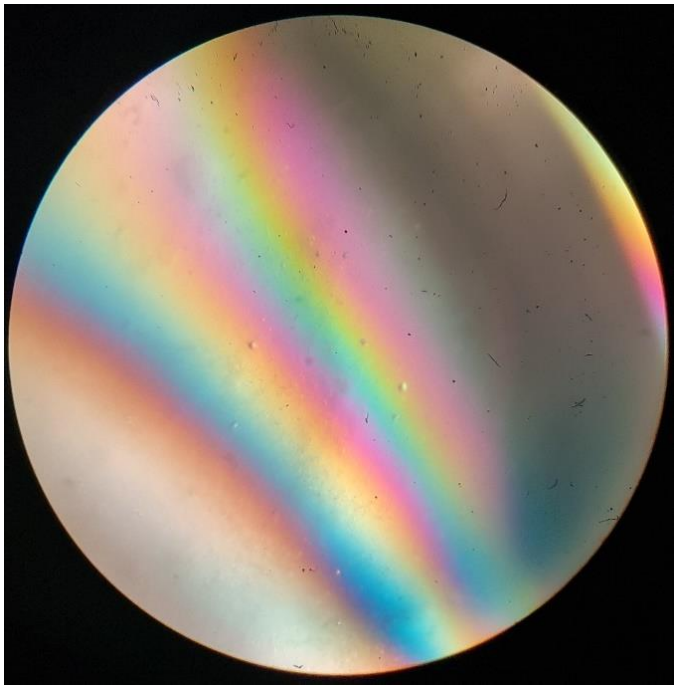

Figure 87: Acid-ICEF/B3β2γ; hit derived from optimization: 0.02 M $CaCl_2$ dihydrate, 0.1 M BIS-TRIS buffer pH 6.5, 15% PEG-mme 550, 17 mg/mL total peptide concentration (original condition: F7 Index 2; 0.05 M $CaCl_2$, 0.1 M BIS-TRIS buffer pH 6.5, 30% PEG-mme 550).

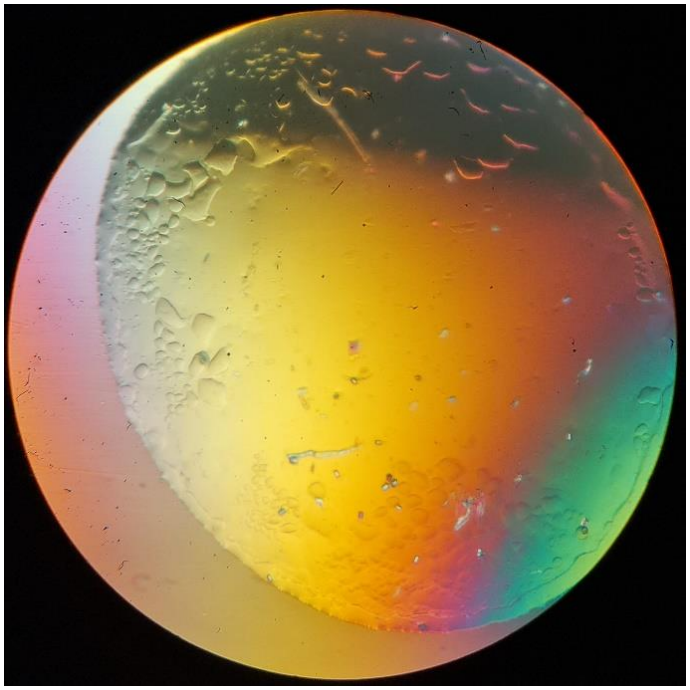

Figure 88: Acid-ICEF/B3β2γ; hit derived from optimization: 0.35 M ammonium acetate, 0.1 M BIS-TRIS buffer pH 5.5, 35% MPD, 25 mg/mL total peptide concentration (original condition: B7 Index 2; 0.2 M ammonium acetate, 0.1 M BIS-TRIS buffer pH 5.5, 45% (v/v) MPD). Phase separation visible.

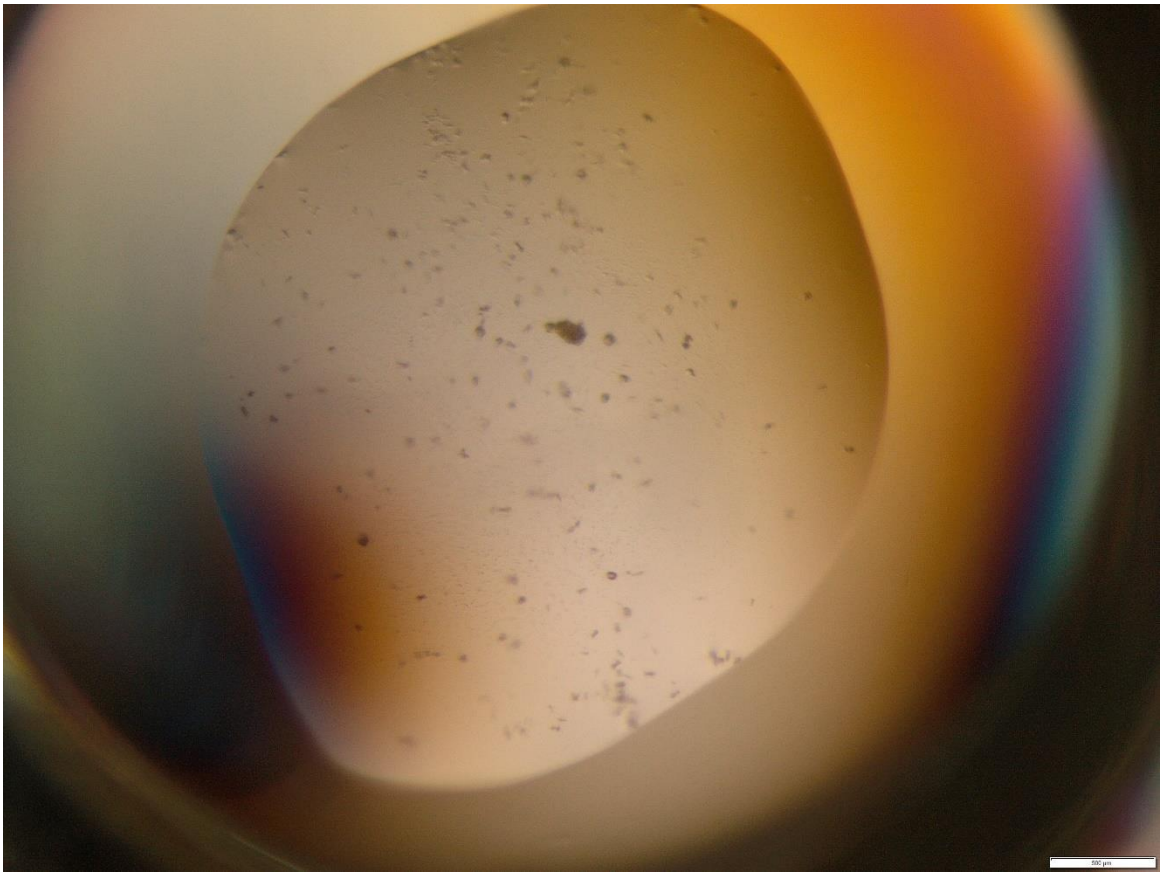

Figure 89: Acid-pp/Base-pp; original hit from H2 of Structure Screen 1 + 2: 0.1 M cadmium chloride hemi(pentahydrate), 0.1 M sodium acetate pH 4.6, 30% (v/v) PEG400. The scale bar in the bottom right corner corresponds to 500 µm.

Figure 90: Acid-CFLE/B3β2γ; original hit from D8 of JCSG Plus™: 0.1 M Tris pH 8.0, 40% (v/v) MPD. The scale bar in the bottom right corner corresponds to 500 µm.

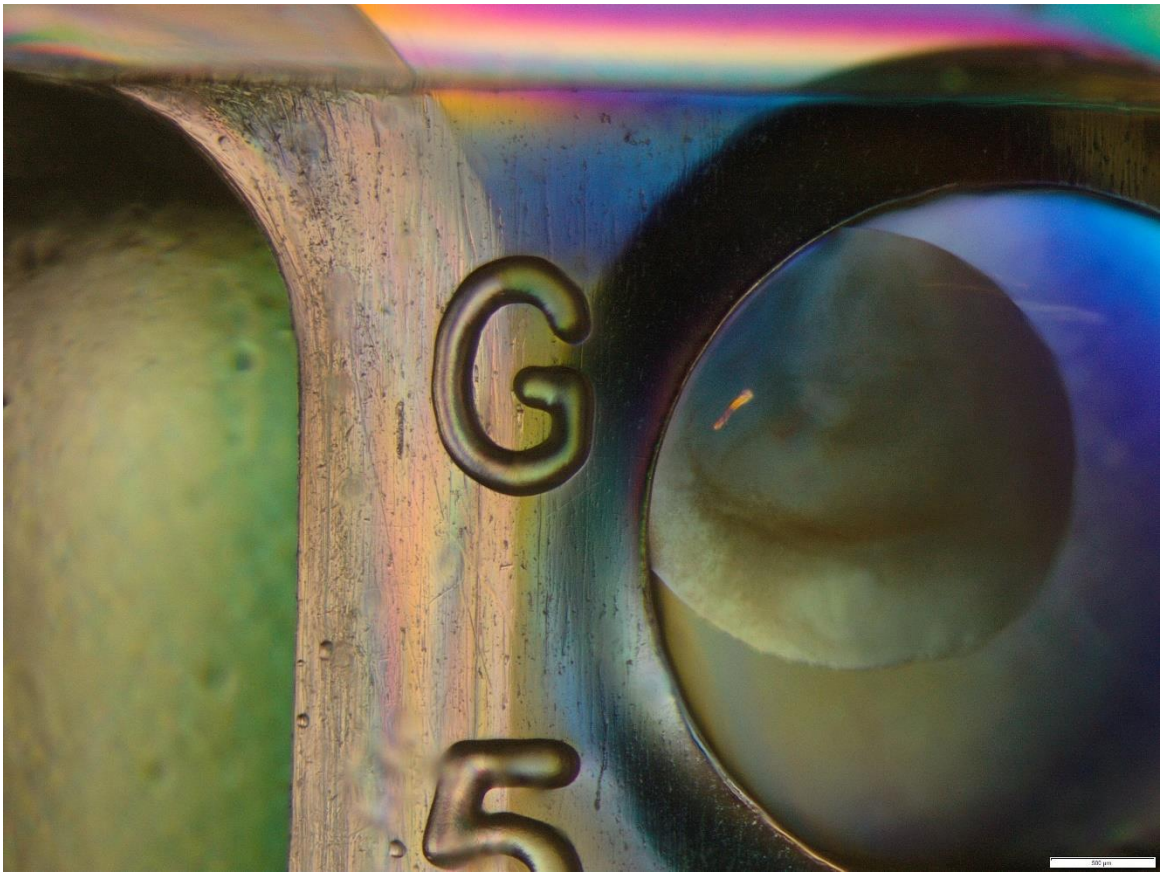

Figure 91: Acid-CFLE/B3β2γ; original hit from G5 of JCSG Plus™: 0.2 M cobalt(II) chloride hexahydrate, 0.005 M cadmium chloride hemi(pentahydrate), 0.005 M magnesium chloride hexahydrate, 0.005 M nickel(II) chloride hexahydrate. The scale bar in the bottom right corner corresponds to 500 µm.

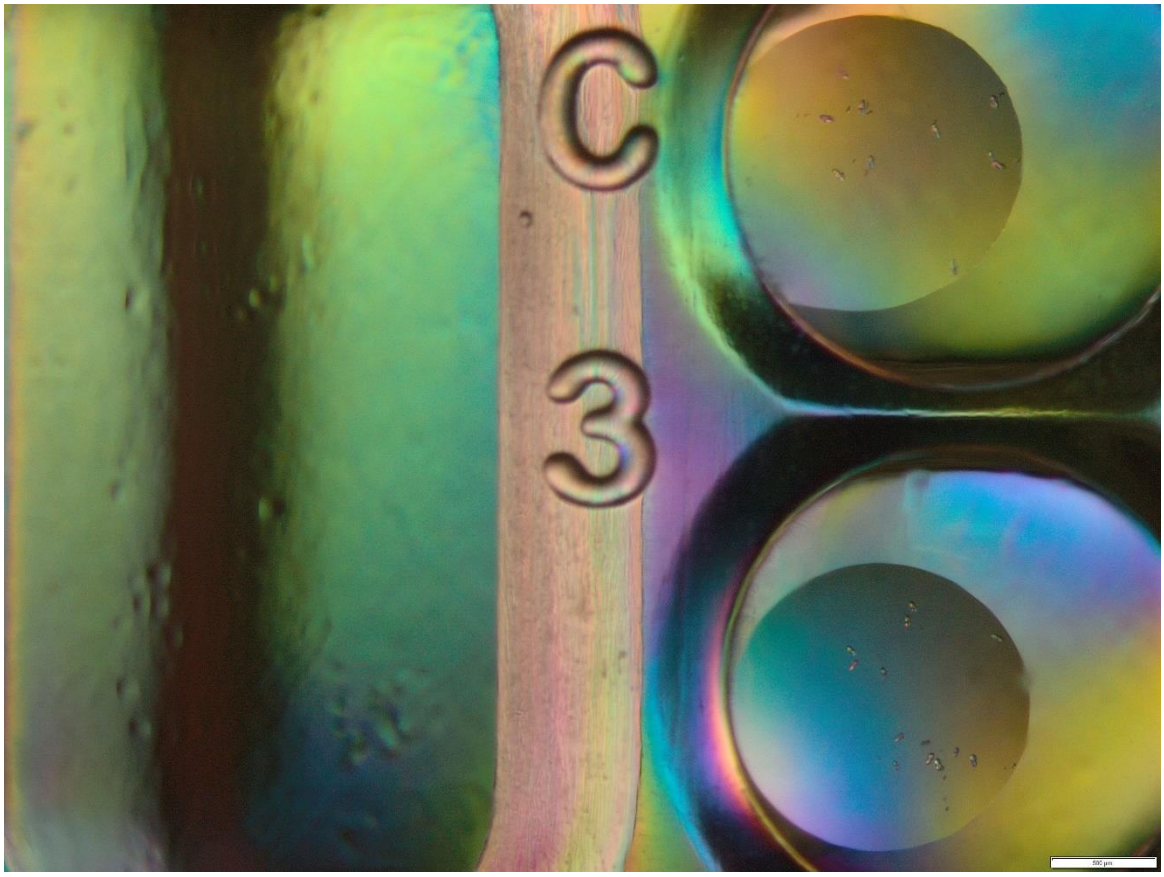

Figure 92: Acid-CFLE/B3β2γ (top) and Acid-ICEF/B3β2γ (bottom); original hit from C3 of Structure Screen 1 + 2: 1.5 M lithium sulfate, 0.1 M sodium HEPES pH 7.5. The scale bar in the bottom right corner corresponds to 500 µm.

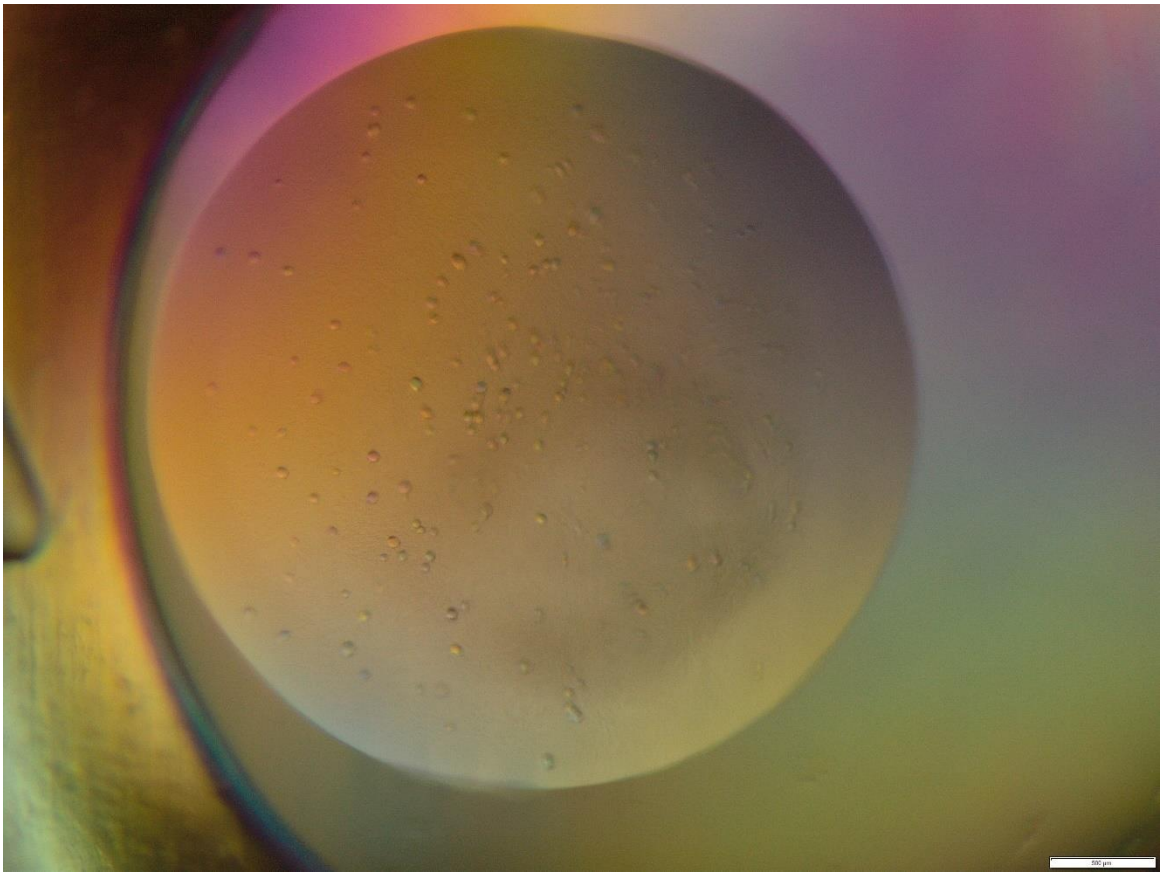

Figure 93: Acid-CFLE/B3β2γ; original hit from A12 of ProPlex screen: 0.2 M sodium acetate trihydrate, 0.1 M sodium citrate pH 5.5, 5% (w/v) PEG4000. These crystals were used for the seeding experiments. The scale bar in the bottom right corner corresponds to 500 µm.

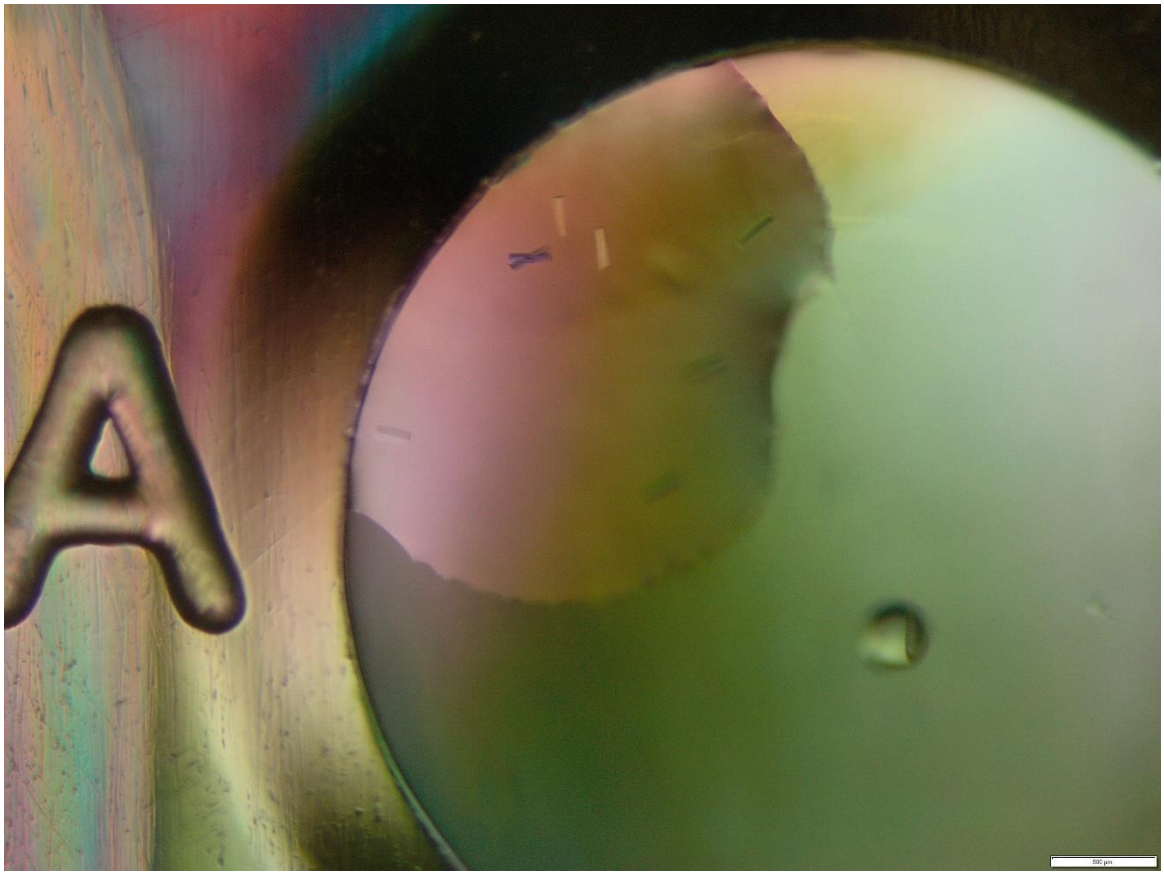

Figure 94: Acid-CFLE/B3β2γ; screening hit obtained through microseeding. A4 from JCSG Plus™ screen: 0.02 M $CaCl_2$ dihydrate, 0.1 M sodium acetate pH 4.6, 30% (v/v) MPD. The scale bar in the bottom right corner corresponds to 500 µm.

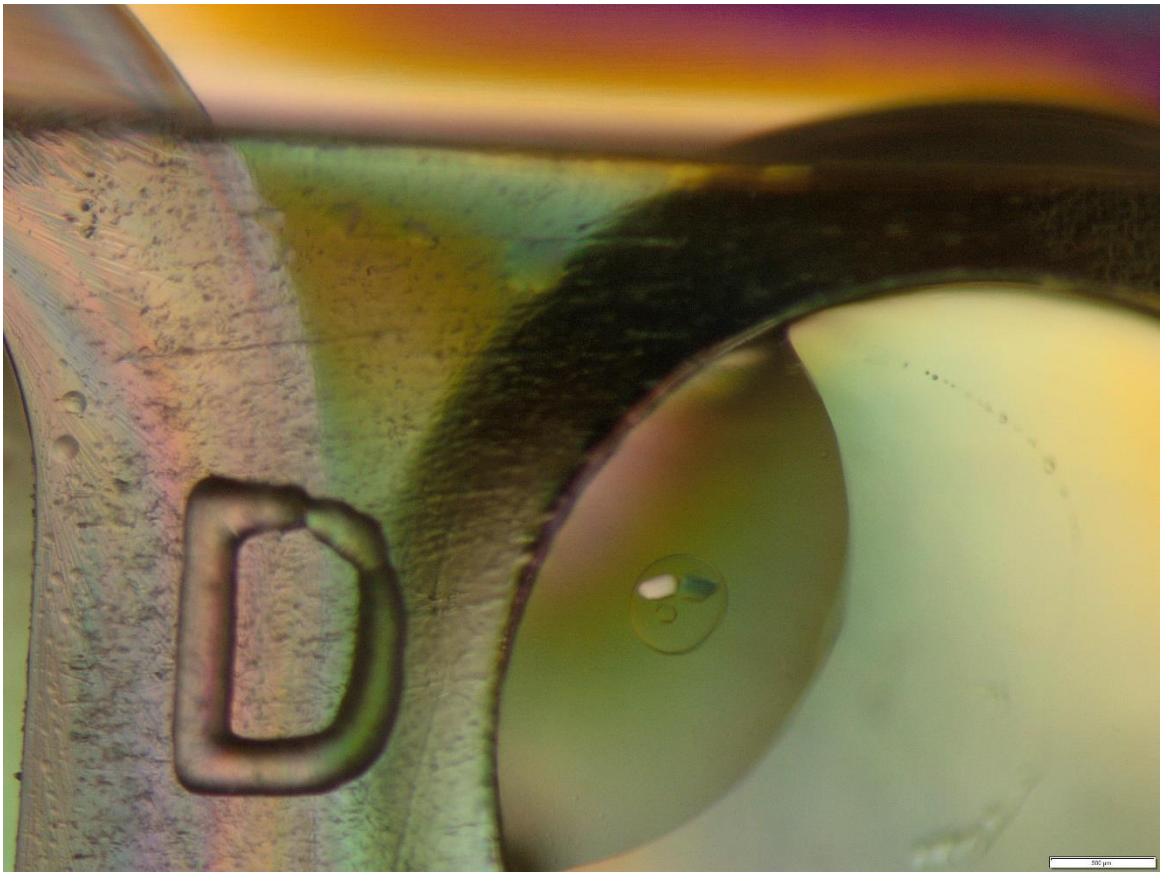

Figure 95: Acid-CFLE/B3β2γ; screening hit obtained through microseeding. D5 from JCSG Plus™ screen: 0.1 M HEPES pH 7.5, 70% (v/v) MPD. The scale bar in the bottom right corner corresponds to 500 µm.

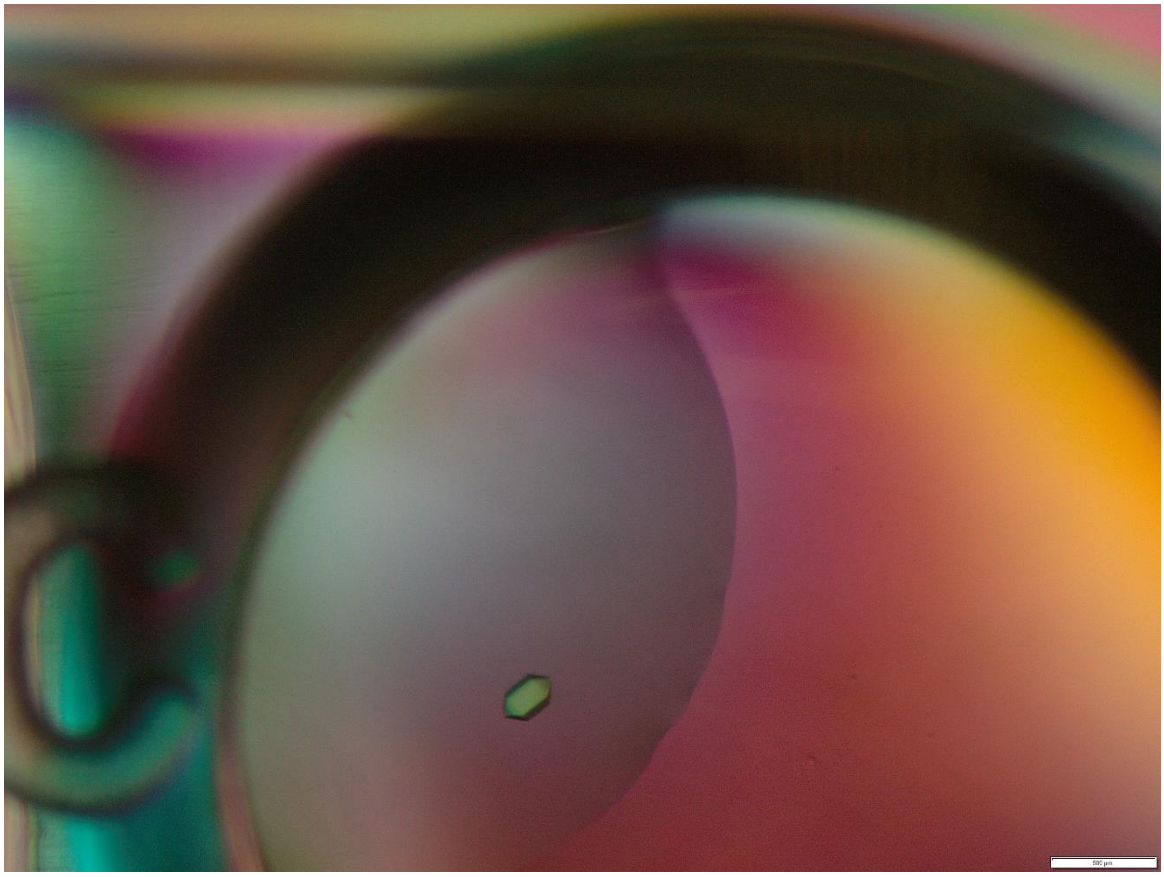

Figure 96: Acid-CFLE/B3β2γ; screening hit obtained through microseeding: C12 from Structure Screen 1 + 2: 0.2 M ammonium acetate, 0.1 M Tris pH 8.5, 30% (v/v) 2-Propanol. The scale bar in the bottom right corner corresponds to 500 µm.

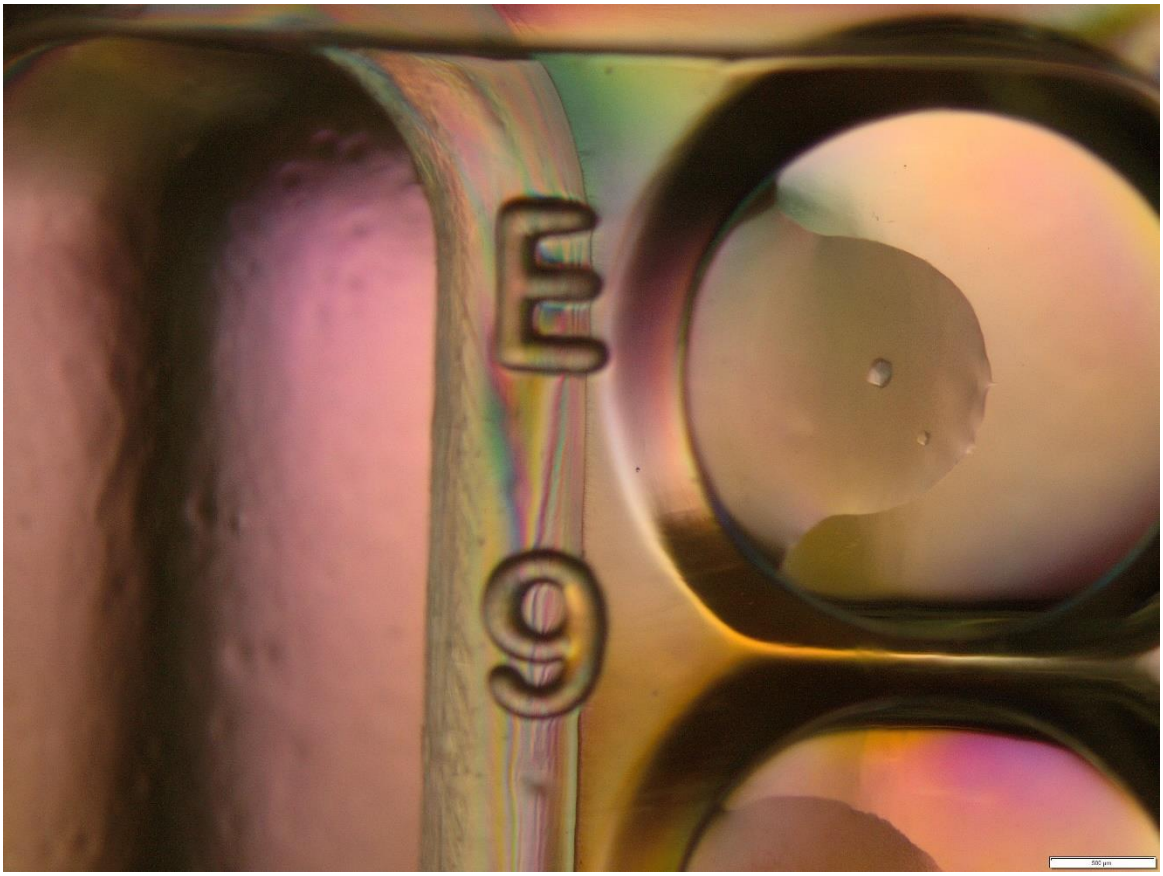

Figure 97: Acid-CFLE/B3β2γ; screening hit obtained through microseeding: E9 of Structure Screen 1 + 2: 0.1 M Tris pH 8.5, 20% (v/v) Ethanol. The scale bar in the bottom right corner corresponds to 500 µm.

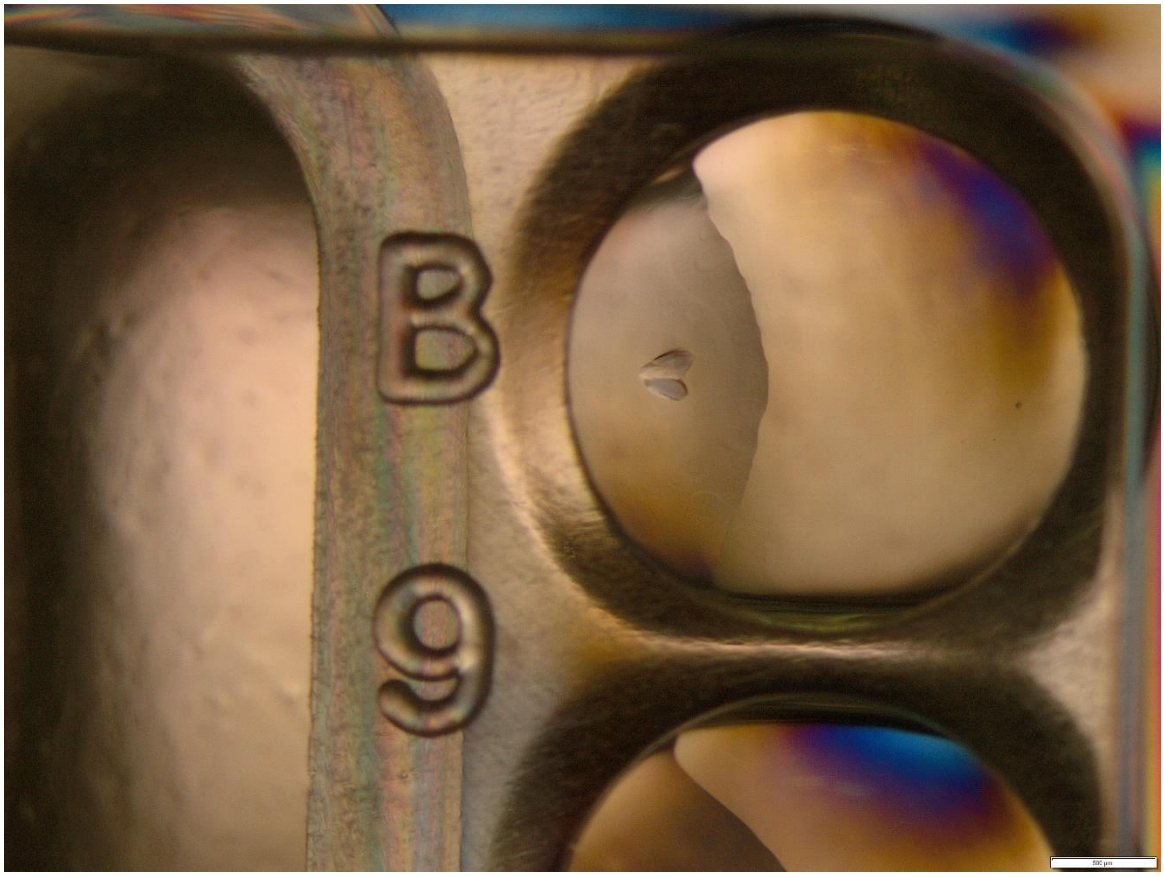

Figure 98: Acid-CFLE/B3β2γ; screening hit obtained through microseeding: B9 of Structure Screen 1 + 2: 0.2 M sodium citrate tribasic dihydrate, 0.1 M sodium HEPES pH 7.5, 30% (v/v) MPD. The scale bar in the bottom right corner corresponds to 500 µm.

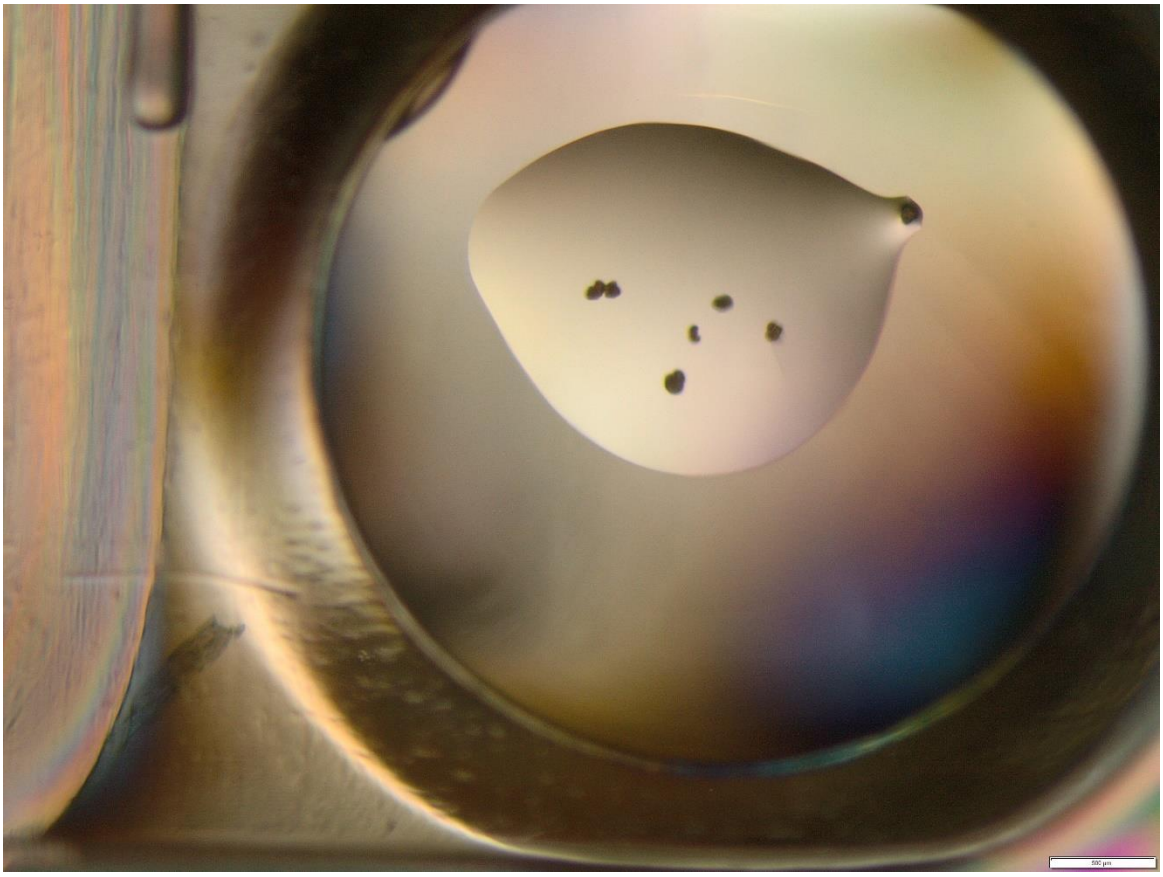

Figure 99: Acid-ICEF/B3β2γ; screening hit obtained through microseeding (cross-seeding with Acid-CFLE/B3β2γ from A12 of ProPlex screen): A1 of Structure Screen 1 + 2: 0.02 M $CaCl_2$ dihydrate, 0.1 M sodium acetate pH 4.6, 30% (v/v) MPD. The scale bar in the bottom right corner corresponds to 500 µm.